New Phthalimide-based Sensors for Chiral and Achiral Anions and Peroxides

Inaugural-Dissertation

Zur Erlangung des Doktorgrades

der Mathematisch-Naturwissenschaftlichen Fakultät

der Universität zu Köln

vorgelegt von

Yrene Hortencia Díaz Pérez

aus Caracas

(Venezuela)

Köln 2009

For my Parents and Claus Miara

Acknowledgements

Explanation

This work was performed from October 2006 to December 2009 under the supervision of Prof. Dr. Axel G. Griesbeck at the Department of Chemistry, Institute of Organic Chemistry, University of Cologne.

In the experimental part names in the format **pydr[number]** refer to the enumeration in the lab-journal.

Abbreviations

^{1}H NMR	Proton Nuclear Magnetic Resonance Spectroscopy
^{13}C NMR	Carbon Nuclear Magnetic Resonance Spectroscopy
Abs.	Absorption
Ar.	Aromatic
ACN/CH$_3$CN	Acetonitrile
b.p.	Boiling point (°C)
cat.	Catalyst
Cbz	Carbonylbenzyloxy
CL	Chemoluminescence
CT	Charge transfer
n-Bu	*n*-Butyl
t-Bu	*t*-Butyl
d	Doublet
dd	Doublet of Doublet
DA	Diels-Alder
DABCO	1,4-Diazabicyclo[2,2,2]octane
DBU	1,8-Diazabicyclo[5.4.0]undec-7-ene
DCC	Dicyclohexylcarbodiimide
DCM	Dichlormethan
DMAP	*N,N*-Dimethylaminopyridine
DMBA	*N,N*-Dimethyl(phenyl)methanamine
1,2-DMB	1,2-Dimethoxybenzene
1,3-DMB	1,3-Dimethoxybenzene
1,4-DMB	1,4-Dimethoxybenzene
DMBA	*N,N*-dimethyl(phenyl)methanamine
DMPAA	2-(3,4-dimethoxyphenyl)acetic acid
DMSO	Dimethylsulfoxide
Em.	Emission

equiv.	Equivalent
eq.	Equation
E_s	Singlet energy
EtOAc	Ethylacetate
EtOH	Ethanol
Et_3N	Trimethylamine
Exc.	Excitation
F	Fluorescence intensity
FRET	Fluorescence Resonance Energy Transfer
GC/MS	Coupled gas chromatography-mass spectrometry
GP	General procedure
h	Hour
HMQC	Heteronuclear Multiple-Quantum Coherence Experiment
HOMO	Highest Occupied Molecular Orbital
HRMs	High Resolution Mass Spectrometry
IC	Internal conversion
ICT	Internal Charge Transfer
IR	Infrared spectrum
ISC	Intersystem Crossing
J	Coupling constant (Hz)
K_D	Stern-Volmer constant
k_q	Bimolecular quenching constant
K_{CT}	Constant of CT complex
k_F	Fluorescence rate constant
LUMO	Lowest Unoccupied Molecular Orbital
MeOH	Methanol
M	Molar concentration
m	Multiplet
min.	Minute
mmol	Milli mole
M.p.	Melting Point
MPAA	2-(4-methoxyphenyl)acetic acid
MS	Mass Spectrometry
NMP	N-methyl-2-pyrrolidinone
NMR	Nuclear Magnetic Resonance
ns	Nano second (10^{-9} s)
PET	Photoinduced Electron Transfer

Q	Quencher
q	Quartet
RET	Resonance Electron Trensfer
R_f	Rate of flow (retention factor)
r.t.	Room Temperature
s	Second or singlet (in NMR)
S_0	Singlet ground state
S_1	First excited singlet state
T	Temperature
T_1	First excited triplet state
TBA	Tetrabutylammonium
t	Triplet
THF	Tetrahydrofuran
TLC	Thin-layer Chromatography
TSA	*p*-Toluenesulfonic acid
UV	Ultraviolet
UV-vis	Ultraviolet visible
λ	Wavelength
ε	Molar extinction coefficient
μ	Micro (10^{-6})
τ	Lifetime
*	Excited state
Φ_f	Fluorescence Quantum Yield

Abstract

The first part of this work describes the synthesis of fluorescent and non-fluorescent phthalimide derivatives *via* straightforward synthetic routes, including multicomponent reactions (MCRs) (scheme 1-a), and aromatic substitutions and reductions (scheme 1-b).
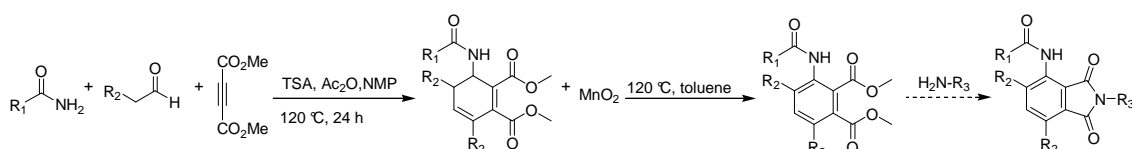
a.-

b.-
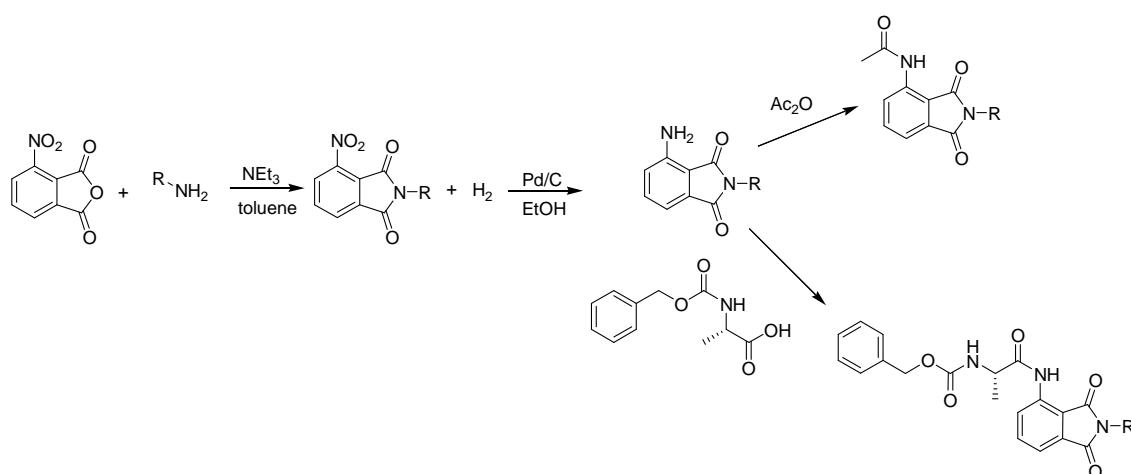
Scheme 1

In the second part the synthesis of new *photocages* based on aminophthalimide-serine was carried out and the fluorescence quenching behaviour of these *photocages* was investigated (scheme 2)
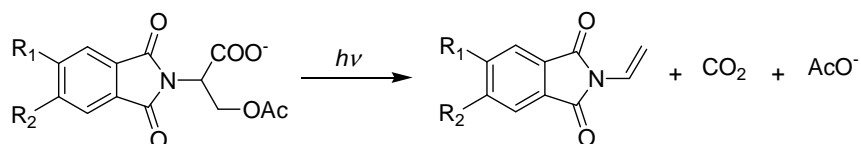
Scheme 2

In order to obtain new chiral sensors for achiral and chiral anion recognition the fluorescent sensors **107**, **109-112** were synthesized in the third part of this work. The syntheses are based on urea-activated phthalimides with stereogenic centers that were synthesized using an efficient procedure involving a Curtius rearrangement (scheme 3).
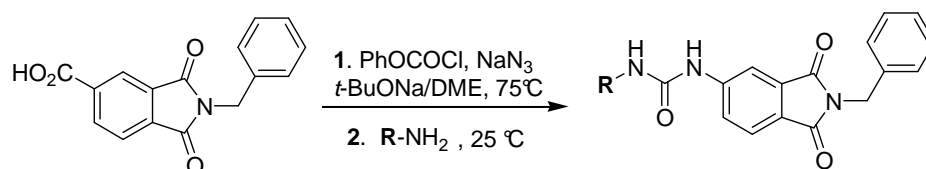
Scheme 3

The non-fluorescent sensor **123** based on a thiourea-activated phthalimide with a stereogenic center was synthesized following a synthetic route involving five steps each of which could be performed with good yields (scheme 4).
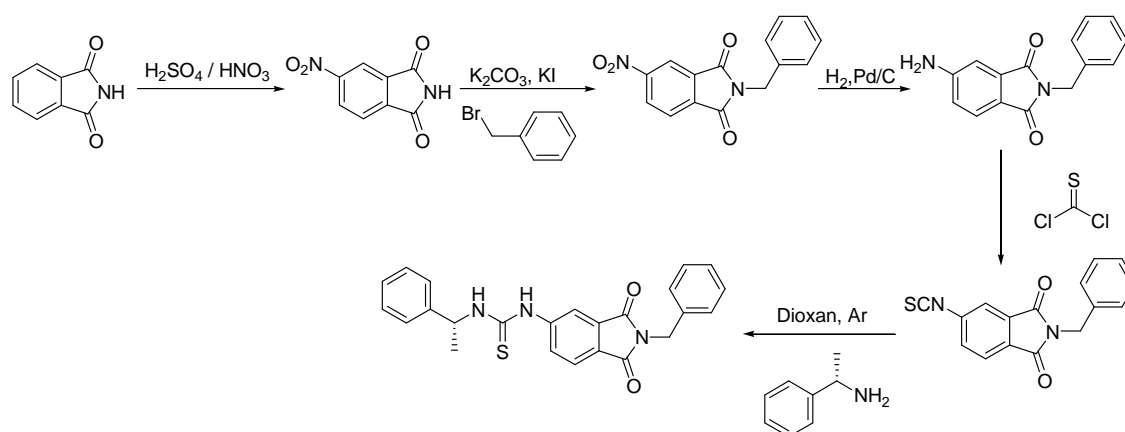
Scheme 4

This work demonstrates the capability of a new series of fluorescent and non-fluorescent chiral sensors obtained through the previously described synthetic routes to recognize achiral and chiral anions and peroxides.

Photophysical properties of the sensors such as absorption (abs), excitation (exc), emission (em) wavelengths (λ), Stokes shifts, singlet energies (E_s), fluorescence lifetimes (τ_F), quantum fluorescence yields (Φ_F) and fluorescence rate constants (k_F) were determined in several solvents in order to compare the solvent effects on the different photophysical properties of the sensor.

The recognition of the achiral and chiral anions was performed through absorption, fluorescence and ^{1}H NMR experiments. To consolidate the experimental results, theoretical calculations based on DFT methods at B31YP/6-31G* level were carried out.

Recognition of peroxides was conducted by fluorescence experiments before and after irradiation of the sensor–peroxide solutions at 350 nm.
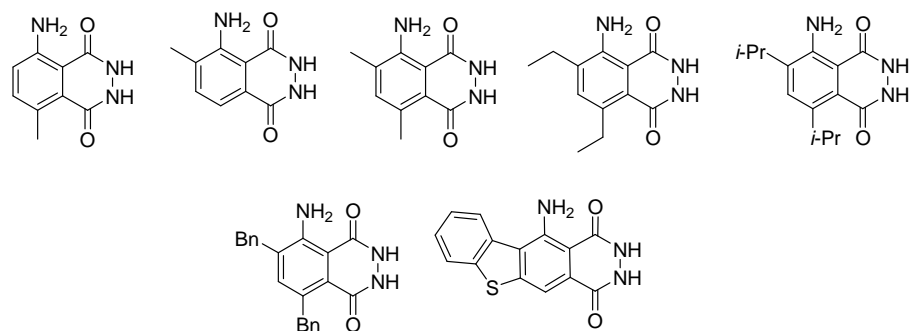
Scheme 5

In the last part of this thesis the photophysical properties of luminol derivatives were compared with the parent luminol. Furthermore, comparative studies of the chemoluminescence efficiency of these luminol derivatives were carried out (scheme 5).

Kurzzusammenfassung

Im ersten Teil dieser Arbeit wurden verschiedene fluoreszierende und nicht-fluoreszierende Phthalimidderivate über vergleichsweise einfache synthetische Routen hergestellt. Eine der verwendeten Routen verlief über eine Multikomponeten-Reaktion (MCR, Abbildung 1-a). Davon abgesehen, wurden überwiegend aromatische Substitution und Reduktionen eingesetzt (Abbildung 1-b).
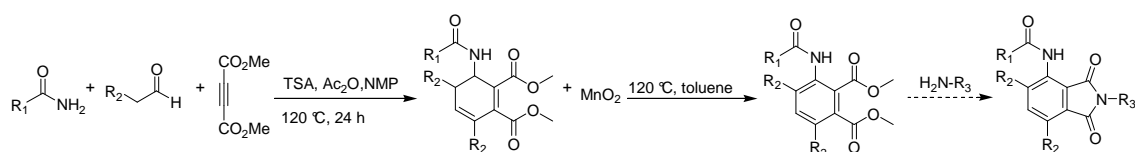
a.-

b.-
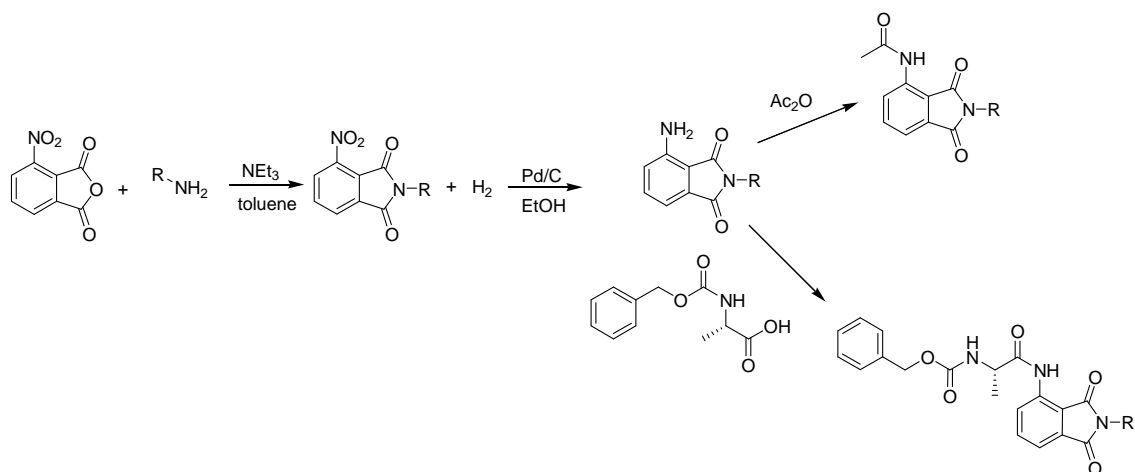
Abbildung 1

Im zweiten Teil der Arbeit wurde eine Synthese für neue Aminophthalimid-Serin Systeme, die als sogenannte *photocages* eingesetzt werden konnten, entwickelt und durchgeführt. Für diese *photocages* wurden eine Reihe von Fluoreszenzlöschungs-Experimenten durchgeführt (Abbildung 2).
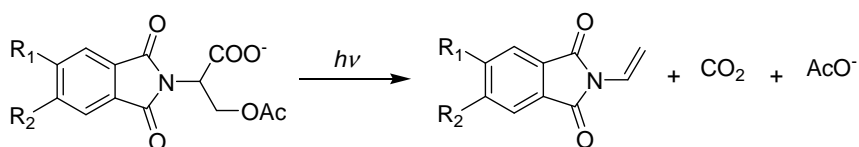
Abbildung 2

Neue chirale Sensoren **107**, **109**-**112** für die Erkennung von achiralen und chiralen Anionen wurden im dritten Teil dieser Arbeit synthetisiert und untersucht. Die verwendete Synthese

zielte auf Harnstoff-aktivierte Phthalimide mit einem stereogenenen Zentrum, die unter Anwendung einer effizienten Methode (Curtius-Umlagerung) hergestellt wurden (Abbildung 3).
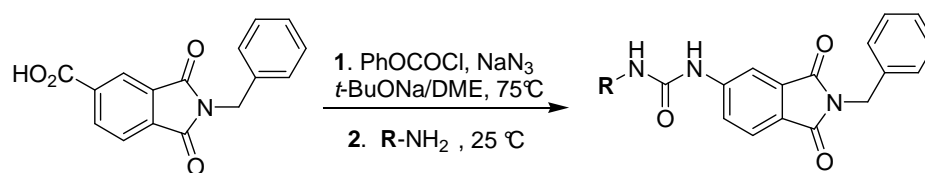
Abbildung 3

Der nicht fluoreszierende Sensor **123** basiert auf einem über Thioharnstoff aktivierten Phtalimid mit einem stereogenen Zentrum und wurde durch Fünfstufensynthese in guten Ausbeuten hergestellt (Abbildung 4).
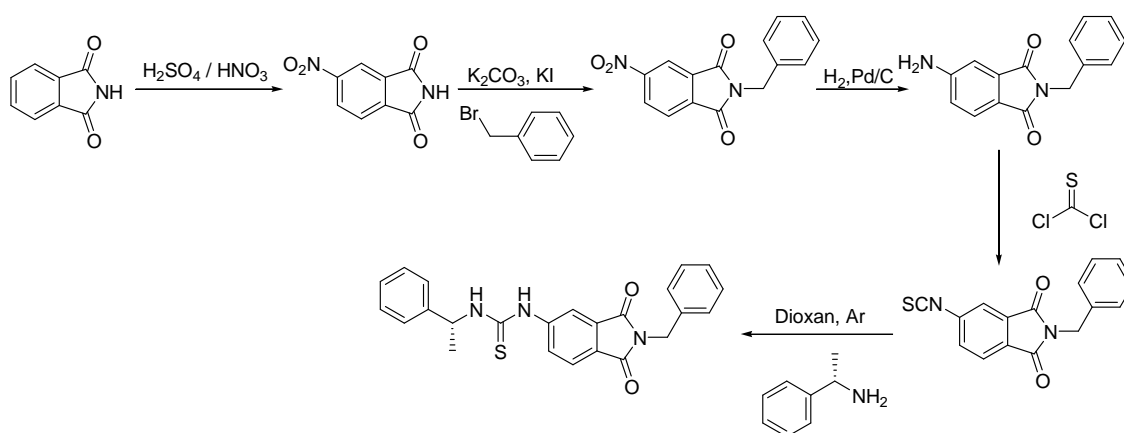
Abbildung 4

In der vorliegenden Arbeit wurde das Potential dieser neuen fluoreszierenden und nicht fluoreszierenden chiralen Sensoren für chirale und achirale Anionen und Peroxide untersucht.

Die photophysikalischen Eigenschaften der Sensoren wie Absorption (abs), Anregung (exc), Wellenlänge (λ), Stokes-Verschiebung, Singulett Energie (E_s), Fluoreszenz-Lebensdauer (τ_F), Fluoreszenz-Quantenausbeute (Φ_F) and Fluoreszenz-Geschwindigkeits-konstante (k_F) wurden in verschiedenen Lösungsmitteln gemessen, um Lösungsmitteleffekte auf die verschiedenen photophysikalischen Eigenschaften der Sensoren zu vergleichen.

Die Erkennung von achiralen und chiralen Anionen wurde über Absorption, Fluoreszenz und ^{1}H-NMR Experimente bestimmt. Um die experimentellen Ergebnisse zu stützen, wurden DFT-theoretische Berechnungen auf B31YP/6-31G* Niveau durchgeführt.

Die Erkennung der Peroxide wurde durch Fluoreszenzexperimente vor und nach der Belichtung von Sensor-Peroxid Proben bei 350 nm durchgeführt.
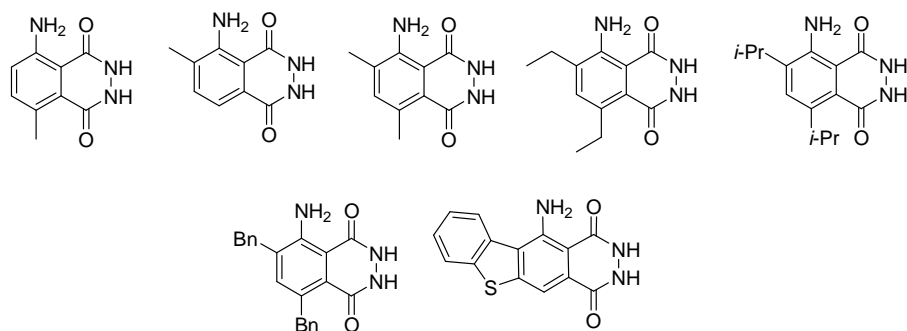
Abbildung 5

Der letzte Teil der Arbeit behandelt die Untersuchung der photophysikalischen Eigenschaften von Luminol-Derivaten und vergleicht diese mit denen des Grundkörpers Luminol. Dazu wurde unter anderem eine vergleichenden Studie der Chemolumineszenzeffizienz dieser Luminol-Derivate durchgeführt (Abbildung 5).

CONTENT

1 Introduction

1.1 Electronic States

A full understanding of photochemical reactions requires an appreciation of the nature and properties of electronically excited states. Quantum mechanical concepts are invaluable in the analysis of the behavior of electronically excited molecules and can be used to rationalize experimental observations despite the approximations involved.

Each electron in a molecule carries a spin angular momentum with a spin quantum number s = 1/2. A point charge moving in a Coulomb field gives rise to a magnetic moment which, in the presence of a magnetic field, may take up one of two orientations. The magnetic moment may be aligned in the direction of the lines of force of the applied magnetic field or opposed to it, giving rise to two different energy states of the electron. A transition between the two energy levels corresponding to these states involves a change of alignment of the electron magnetic moment and is the basis of electron spin resonance.

The term electron spin refers to the alignment of the electron magnetic moment with respect to an imaginary magnetic field. If no field is present, there can be no splitting in the electron spin energy levels but the individual moments will still be present and will still dictate how the electrons interact with each other and with the nucleus.

The total spin angular momentum possessed by a many-electron atom or molecule is represented by the total spin quantum number S, which may be calculated as the vector sum of all the individual contributions from each electron. Two electrons, each possessing $s = 1/2$, may be present with their spins parallel or opposed. If the spins are opposed the total quantum number S is zero. If the electron spins are parallel the total quantum number S is 1/2 + 1/2 = 1. The spin multiplicity gives the number of states expected in the presence of an applied magnetic field and is given by 2S+1. Thus, a molecule with all electrons spin-paired (which will be the case for the ground electronic state of most organic molecules) possesses $S = 0$ and a spin multiplicity of 1. Such an electronic state is referred to as a singlet state. The combination of ground state and singlet state is abbreviated by the symbol S_0. [1]

The Pauli Exclusion Principle states that two electrons in an atom can not have the same set of four quantum numbers. This restriction requires that no more than two electrons can fit in one orbital; furthermore, the two must have opposed spin states. [2]

It is common to present these different spin states by a simplified molecular energy level diagram to which the appropriate labels are attached. An example of such a state diagram is illustrated in figure 1 for a generalized unsaturated hydrocarbon.
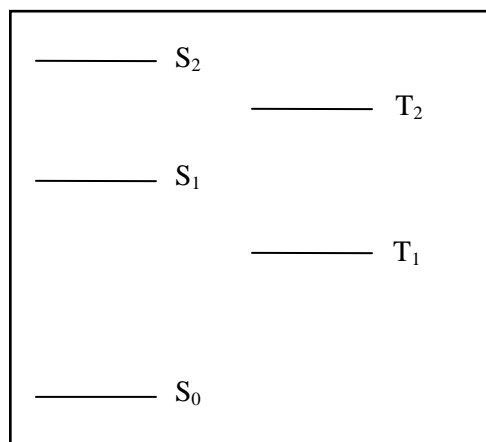
Figure 1: General state diagram of the (relative) energy of the lowest vibrational level

The excited T_1 state is indicated to have an energy lower than that of the excited S_1 state. This lowering of the T_1 state energy is due to spin correlation. It is a consequence of the operation of the Pauli principle, and is summarized by Hund´s rule [1] of maximum multiplicity. Even in the present situation where the two unpaired electrons occupy different orbitals, there is a minimum energy of electron-electron repulsion when their spins are parallel. This repulsion energy will determine the energy difference between the excited and singlet state and will depend on the extent of space between the orbitals involved.

1.2 Energy level diagrams for photoluminescent molecules (Jablonski Diagram)

Excitation of molecules are initiated by absorption of two modes of radiation, one centered around the wavelength λ_1 ($S_0 \rightarrow S_1$), and the second around a shorter wavelength λ_2 ($S_0 \rightarrow S_2$).

What happens to an electronically excited molecule that does not undergo some kind of chemical reaction? The molecule cannot persist in an excited state indefinitely, since it represents a situation unstable with respect to the ground state. Electron de-excitation must occur somehow, the excess energy being released as thermal or radiative energy. Transitions involving the de-excitation of electronically excited states that do not involve the emission of radiation are called nonradiative transitions.

The emitted radiation is called *fluorescence* if it originates in the de-excitation of an excited state that has the same spin multiplicity as the ground state, and the emission is called

phosphorescence if it originates from the de-excitation of an excited state of spin multiplicity different from that of the ground state (for example, $T_1 \ldots S_0$).

We can use the state diagram in figure 1 and indicate all the possible transitions that may occur between different energy levels. The result (figure 2) is called a Jablonski diagram.
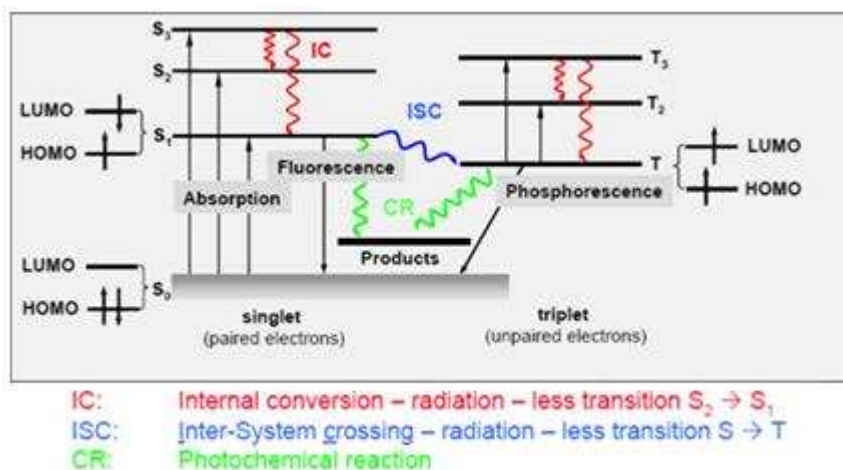
Figure 2: Jablonski Diagram [3]

Radiative transitions are "vertical" transitions and involve a change in the total energy of the molecule due to the absorption and emission of a photon. Nonradiative transitions are "horizontal" transitions and involve conversion from one state to another at a constant energy. A conversion between states of the same spin multiplicity is called *internal conversion* (IC) and for states of different spin multiplicity the term *intersystem crossing* (ISC) is used. In the solution phase the excess vibrational energy is rapidly removed by collisions with solvent molecules, a process sometimes referred to as *vibrational relaxation* (VR).

1.3 The Franck-Condon principle, absorption and emission spectra

The Franck-Condon principle states for the classical electronic transition of a vibrating molecule:

"Since electronic motions are much faster than nuclear motion, electronic transitions occur most favorably when the nuclear structure of the initial and final state are most similar".

The conversion of electronic energy into vibrational energy may be the rate determining step in an electronic transition between states of different nuclear geometries. A description of the Franck-Condon principle would be that (a) for radiative transitions, nuclei *geometries* do not change during the time it takes for a photon to "hit", "be absorbed" and cause an electron to jump; and (b) for nonradiative transitions, nuclear *motions* do not change during the time it

takes an electron to jump from one orbital to another. Figure 3 shows the potential energy curves of the possible Franck-Condon transition.

Absorption and emission spectra are not sharp lines with respect to the frequency ν of the absorbed or emitted light of the equation $\Delta E = h\nu$ from the postulate that only one electron is excited or de-excited in an individual absorption or emission event.

In a set of molecules, an electronic transition is not as "pure" as it is in a single atom or molecule. This is due to the fact that, in order to describe the electronic states of a molecule, the motions of nuclei relative to one another (e.g. vibrations, rotations, collisions) must be considered. The sharp line or band which characterizes atomic transitions is replaced by a set of closely spaced lines in molecular absorption which may be only partially resolved or even completely unresolved. For organic molecules in solution - i.e. our case - this latter situation is common.

In analogy to absorption, the most probable emissions will be those which occur vertically. In contrast to absorption, the equilibrium separation of the ground state potential-energy curve minimum is smaller than that of the excited state curve, so that the most probable vertical transitions produce an elongated ground state, while absorption produces a compressed excited state immediately after transition. [4]
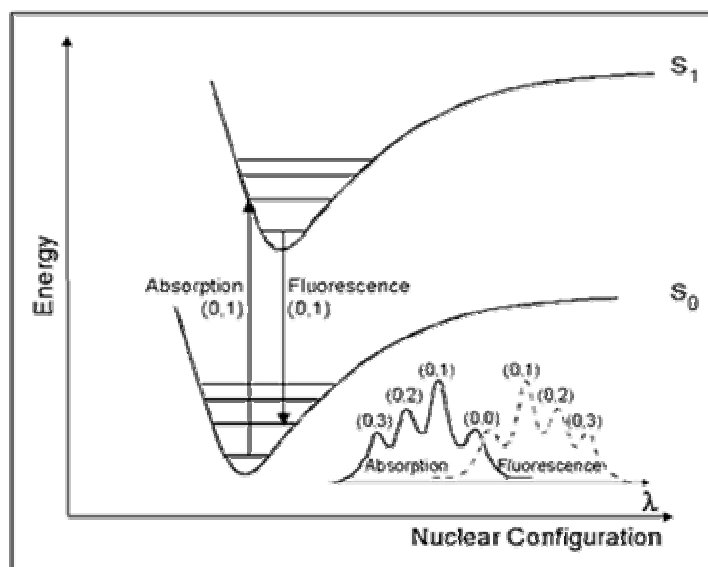
Figure 3: Franck-Condon diagram [5]

1.4 Fluorescence

The electron in the excited orbital is paired (by opposite spin) to the second electron in the ground state orbital. Consequently, return to the ground state is spin allowed and occurs rapidly

by emission of a photon. The emission rates of fluorescence are typically 10^8 s^{-1}, so that a typical fluorescence lifetime is close to 10 ns. [6]

Some typical fluorescent substance (fluorophores) are quinine, fluorescein, rhodamine B, pyridine 1 etc, as shown in figure 4. The first observation of fluorescence from a quinine solution in sunlight was reported by Sir John Frederick William Herschel in 1845. [6],[7] The experiment consisted of a observation of a glass of tonic water that was exposed to sunlight; a faint blue glow is frequently visible at the surface. The quinine in tonic water is excited by the ultraviolet light from the sun. Upon return to the ground state the quinine emits blue light with a wavelength near 450 nm. Due to this discovery, quinine was responsible for stimulating the development of the first spectrofluorometers that appeared in the 1950s.
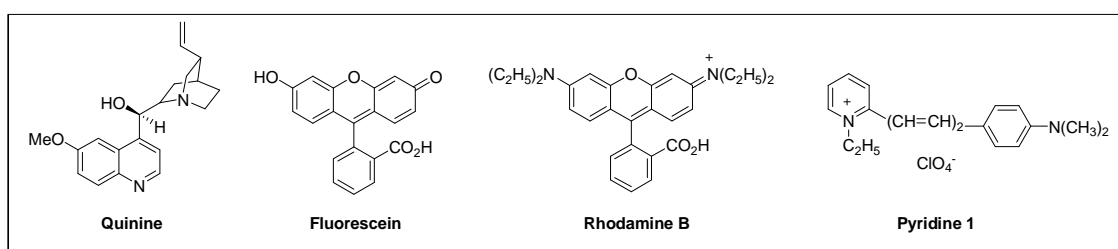
Figure 4: Typical fluorescent compounds

Other fluorophores are encountered in daily life like fluorescein and rhodamine. Polynuclear aromatic hydrocarbons, such as anthracene and perylene, are also fluorescent, and the emission from such species is used for environmental monitoring of oil pollution. Pyridine 1 and rhodamine are frequently used in dye lasers.

The most intense and useful fluorescence is found in compounds containing aromatic functional groups with low energy $\pi \rightarrow \pi^*$ transition levels. Compounds containing aliphatic and alicyclic carbonyl structures or highly conjugated double bond structures may also exhibit fluorescence, but the number of these is small compared to the number of existing aromatic system. Another group which can fluorescence in solution are the unsubstituted aromatic hydrocarbon, the quantum efficiency usually increasing with the number of the rings and their degree of condensation.

The simple heterocycles, such as pyridine, furane, thiophene and pyrrole (figure 5) do not exhibit fluorescence, on the other hand, fused ring structures ordinarily do. Fluorescence is observed for compounds like quinoline, isoquinoline, and indole.
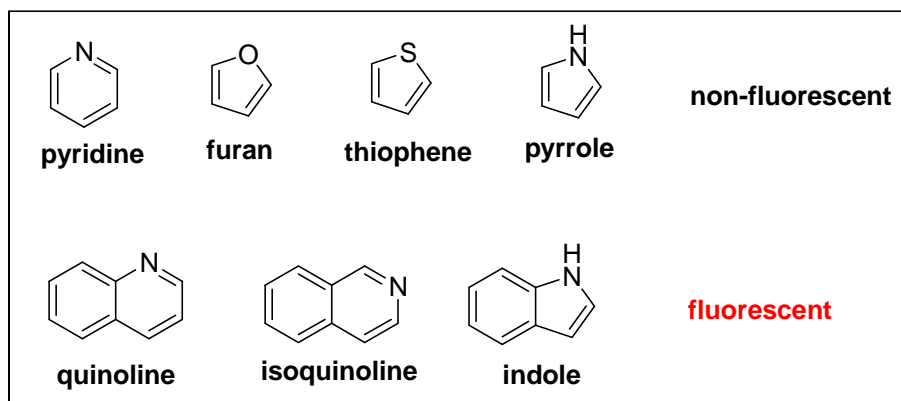
Figure 5: Fluorescent and non-fluorescent molecules

The influence of halogen substitution is striking: the decrease in fluorescence with increasing atomic number of the halogen is thought to be in part due to the heavy atom effect, which increases the probability for intersystem crossing to the triplet state because of large spin-orbit coupling contribution. [2]

Substitution of a carboxylic acid or carbonyl group on an aromatic ring generally inhibits fluorescence. In these compounds, the energy of the n, π^* transition is less than that of the π, π^* transitions.[2]

1.4.1 Characteristic of fluorescence emission

A fluorescence emission spectrum is a plot of the fluorescence intensity *vs.* wavelength (nm) or wavenumber (cm^{-1}). Emission spectra are dependent on the chemical structure of the fluorophore and the solvent in which it is dissolved. Another important feature of fluorescence is its highly sensitive detection. Fluorescence has some more general characteristics that will be describe in the following sections.

The Stokes Shift

The energy of emission is generally lower than that of absorption, and thus, fluorescence occurs at lower energies or longer wavelengths. [6] This shift in wavelength to a lower frequency is called the *Stokes shift* (figure 6).
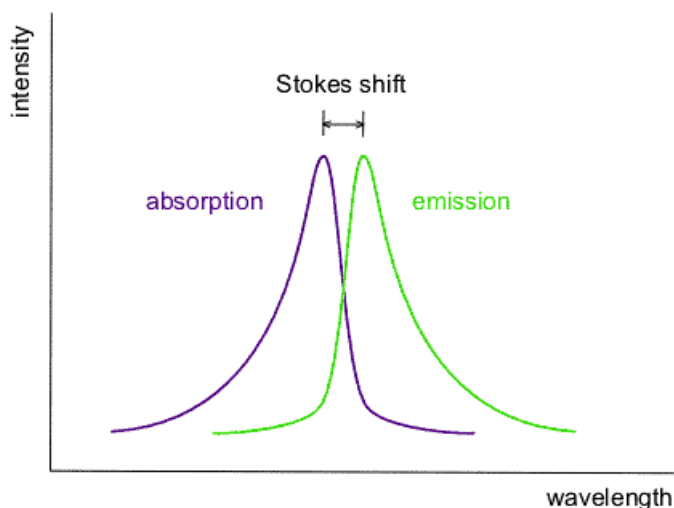
Figure 6: Absorption and emission spectra, Stokes shift [8]

Emission spectra are typically independent of the excitation wavelength

The same fluorescence emission spectrum is generally observed irrespectivly of the excitation wavelength (Kasha´s rule).[9],[6] Upon excitation into higher electronic and vibrational levels, the excess energy is quickly dissipated, leaving the fluorophore in the lowest vibrational level of S_1. Because of this rapid relaxation (about 10^{-12} s), emission spectra are usually independent of the excitation wavelength.

There are exceptions, such as fluorophores that exist in two ionization states, each of which display distinct absorption and emission spectra. Also, some molecules are known to emit from the S_2 level, but such emissions are rare and generally not observed in biological molecules. [6]

Effect of pH on Fluorescence

The wavelength and the emission intensity are likely to be different for the ionized and nonionized forms of the compounds, if they have acidic or basic substituents which are pH-dependent. For example, aniline has several resonance forms while the anilinium ion has only one. This resonance form leads to a more stable first excited state; fluorescence in the ultraviolet region is the consequence.

Experiments with pH-sensors have been used for the detection of end points in acid/base titrations. Changes in acid or base dissociation constants with excitation are common and occasionally as large as four to five orders of magnitude. [2]

Effect of solvent polarity

The effects of solvent polarity are one origin of the Stokes shift. Figure 7 shows a plot of emission spectra of 4-dimethylamino-4´-nitrostilbene (DNS) in solvents of increasing polarity.
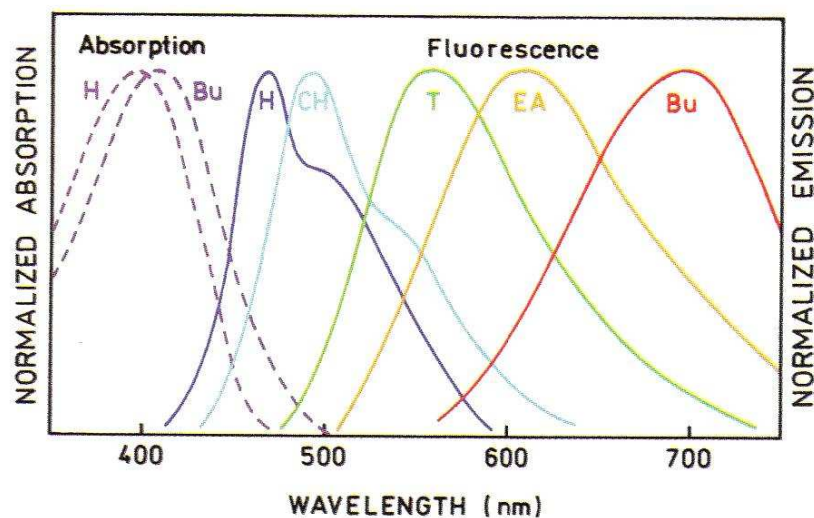
Figure 7: Emission spectra of DNS in H, hexane; CH, cyclohexane; T, toluene; EA, ethyl acetate; Bu, n-butanol [6]

Emission from fluorophores generally takes place at longer wavelengths than those at which absorption occurs. This loss of energy is due to a variety of dynamic processes that occur following light absorption. Figure 8 shows the Jablonski diagram for fluorescence with solvent relaxation.

Solvent effects shift the emission to even lower energies due to stabilization of the excited state by polar solvent molecules. In general, only fluorophores that are polar themselves display a large sensitivity to solvent polarity. Nonpolar molecules, such as unsubstituted aromatic hydrocarbons, are much less sensitive towards solvent polarity.
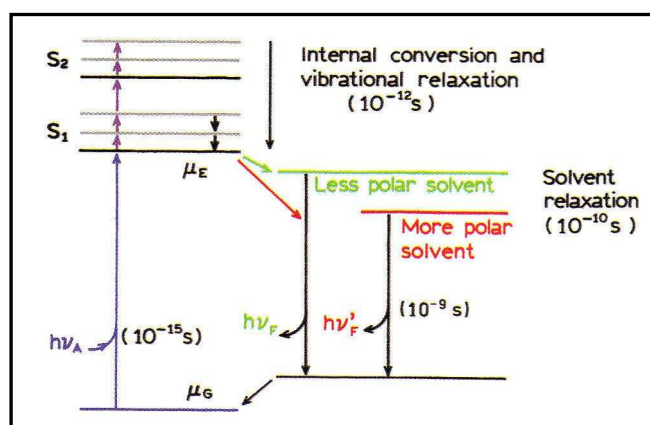
Figure 8: Jablonski diagram for fluorescence with solvent relaxation [6]

1.4.2 Fluorescence quenching

Fluorescence quenching refers to any process that decreases the fluorescence intensity of a sample. Various processes of molecular interactions can result in quenching, for example:

- Excited state reactions (chemical quenching)

- Molecular rearrangements (chemical quenching)

- Energy transfer (physical quenching)

- Ground state complex formation (static quenching)

- Collisional quenching (dynamic quenching)

In this opportunity two of the molecular interactions will be discussed, collisional or dynamic quenching and the ground state complex formation or static quenching.

Collisional quenching

Collisional quenching occurs when the excited state fluorophore is deactivated upon contact with some other molecule in solution, which is called quencher. The Jablonski diagram figure 9 illustrates this process and fluorescence resonance energy transfer (FRET).
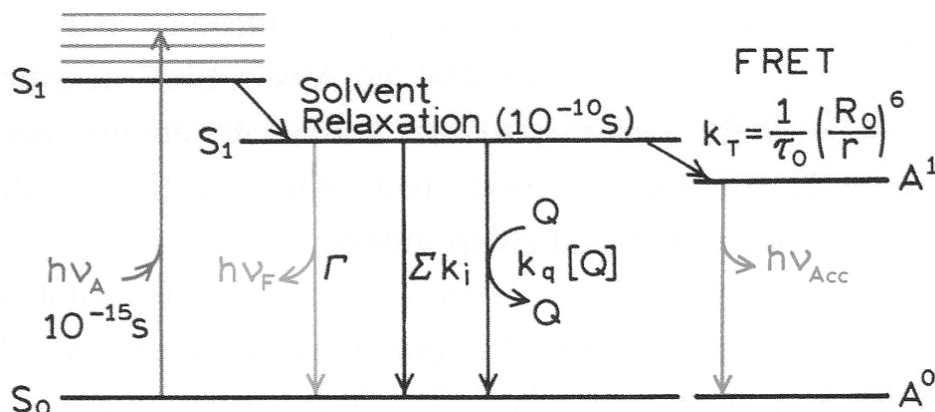
Figure 9: Jablonski diagram with solvent relaxation and energy transfer (FRET) [6]

For collisional quenching the fluorophore is returned to the ground state during a diffusive encounter with the quencher. The molecule is not chemically altered in the process.

The decrease of intensity in this process is described by the Stern-Volmer equation (**1**):

$$\mathbf{F_0 / F = 1 + K\,[Q] = 1 + k_q \tau_0\,[Q]} \tag{1}$$

In this equation F_0 is the emission intensity of the fluorophor without quencher, F is the emission intensity with quencher, K is the Stern-Volmer quenching constant, k_q is the bimolecular quenching constant, τ_0 is the unquenched lifetime, and [Q] is the quenching concentration.

The Stern-Volmer quenching constant K indicates the sensitivity of the fluorophore to a quencher. A linear Stern-Volmer plot is generally indicative of a single class of fluorophores, all

equally accessible to the quencher. It is important to recognize that observation of a linear Stern-Volmer plot does not prove that collisional quenching of fluorescence has occurred.

Static quenching

Static quenching can occur as a result of the formation of a nonfluorescent ground state complex between the fluorophore and the quencher. When this complex absorbs light it immediately returns to the ground state without emission of a photon.

Static quenching is described by equation **2**:

$$\mathbf{F_0 / F = 1 + \mathit{K_s} [\mathit{Q}]} \tag{2}$$

Note that the dependency of F_0 / F on [Q] is linear, which is identical to the observed for dynamic quenching (eq. 1), except that the quenching constant is now the association constant.

The measurement of fluorescence lifetimes is the most definitive method to distinguish static and dynamic quenching. For static quenching $\tau_0 / \tau = 1$, in contrast to dynamic quenching $F_0 / F = \tau_0 / \tau$ well as shown in figure 10.
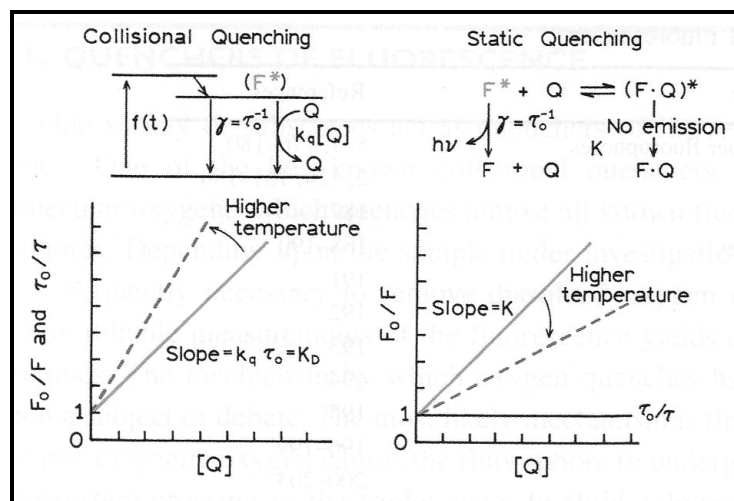
Figure 10: Comparision of dynamic and static quenching [6]

Both quenching processes can also be distinguished by their differing dependence on temperature and viscosity. Higher temperatures result in faster diffusion and hence large amounts of collisional quenching. Higher temperatures will typically result in the dissociation of weakly bound complexes, and hence smaller amounts of static quenching.

The absorption spectrum of the fluorophor is, on careful examination, one additional method to distinguish between static and dynamic quenching. Collisional quenching only affects the excited states of the fluorophore, and thus no changes in the absorption spectra are expected. In contrast, ground state complex formation will frequently result in perturbation of the absorption spectrum of the fluorophore.

Combined dynamic and static quenching

It is possible that the fluorophore can be quenched both by collisions and by complex formation with the same quencher.

The Stern-Volmer plot is an upward curvature, concave towards the *y*-axis. The Stern-Volmer equation is modified to second order in [*Q*] (eq. 3), which accounts for the upward curvature observed when both static and dynamic quenching occur for the same fluorophore.

$$\mathbf{F_0 / F = 1 + (K_D + K_S)\,[Q] + K_D\,K_S\,[Q]^2} \qquad \textbf{(3)}$$

The dynamic component can generally be selected to compare the magnitude of the expected diffusion- controlled value of the solution, by the temperature or viscosity dependence of the values or from other available informations about the sample.

1.4.3 Resonance energy transfer (RET)

There is a process that causes a decrease in the fluorescence intensity of the donor and transfers the energy to an acceptor. This process is called resonance energy transfer (RET) and it can be considered a quenching process. The acceptor can be fluorescent or nonfluorescent, but in both cases the fluorescence intensity of the initially excited molecule is decreased.

Figure 11 shows that the fluorophore initially has two electrons in the highest-occupied (HO) molecular orbital. Absorption of light results in elevation of one electron to the lowest-unoccupied (LU) orbital.
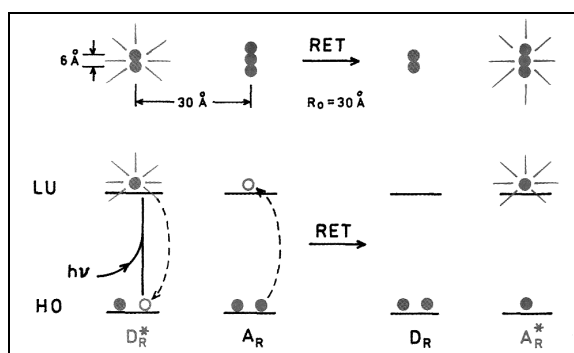
Figure 11: Molecular orbital schematic for resonance energy transfer. The top row the size of fluorophores relative to the Föster distance R_0 [6]

When RET occurs, the electron in the excited donor (D_R^*) returns to the ground state. Simultaneously an electron in the acceptor (A_R) goes into a higher excited-state orbital. If the acceptor is fluorescent it may then emit. If the acceptor is nonfluorescent the energy is dissipated as heat.

The important point is that quenching is due to short-range interactions between F and Q, shown in figure 12, and RET is due to long-range dipolar interactions between D_R^* and A_R.

The rate of energy transfer is given by eq. **4**

$$k_T\,(r) = 1\,/\,\tau_D\,(R_0\,/\,r)^6 \tag{4}$$

where τ_D is the donor lifetime in the absence of the acceptor, r is the center-to-center distance between D_R and A_R, and R_0 is the Förster distance.

The rate of quenching depends on the extent of interaction between the electron clouds in F and Q. The rate depends on the distance according to eq. **5**

$$K_E\,(r) = A\,\exp\,[\text{-}\beta\,(r\,\text{-}\,r_o)] \tag{5}$$

where r is the center-to-center distance between F and Q and r_c is the distance of the closest approach at molecular contact. A is expected to have a value near 10^{13} s^{-1} and finally β is typically near 1 Å^{-1}. This equation does not include the effect of diffusion on quenching and only describes the effect of distance on quenching but does not reveal the mechanisms of quenching.
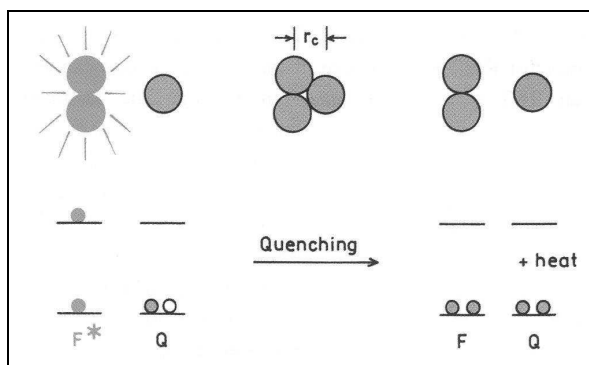
Figure 12: Schematic of fluorescence quenching [6]

1.4.4 Mechanisms of quenching

There are at least three different mechanisms for singlet quenching:

1. Intersystem crossing (ISC) or the heavy atom effect

2. Electron exchange or Dexter interactions

3. Photoinduced electron transfer

The quenching process can occur by combination of these mechanisms.[6]

Intersystem crossing

ISC is a process in which the spin of an excited electron is reversed wich results in a change of the multiplicity of the molecules results. This process is most common in molecules that contain heavy atoms (the heavy atom effect). Apparently spin-orbital interactions become large in the presence of such atoms and a change in spin is thus more favorable. The presence of paramagnetic species such as molecular oxygen in solution also enhances intersystem crossing and consequently decreases fluorescence, [2] as shown in figure 13.
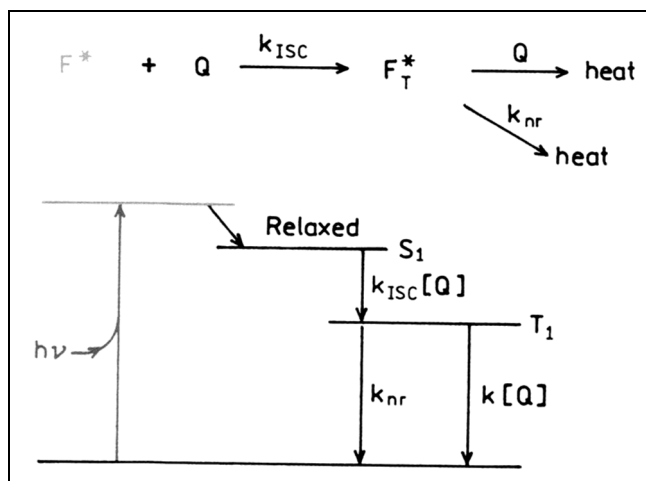
Figure 13: Quenching by intersystem crossing [6]

Electron exchange

This interaction occurs between a donor D_E and an acceptor A_E, where E indicates electron exchange. The excited donor has an electron in the LU orbital. This electron is transferred to the HO orbital of the acceptor, so the acceptor is left in an excited state.
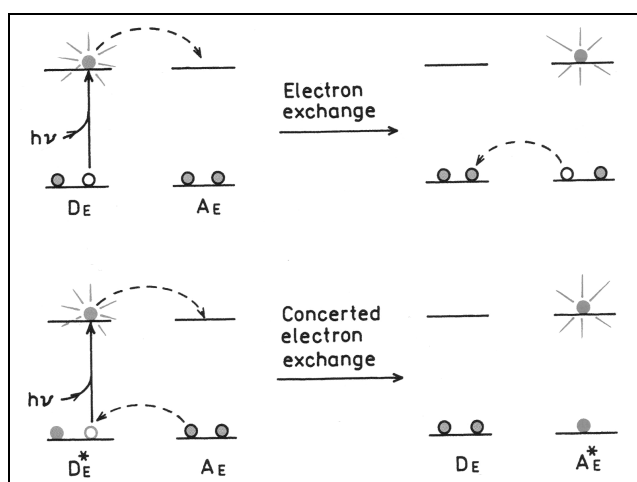
Figure 14: Schematic for stepwise (top) or concerted (bottom) electron exchange [6]

At the same time or in a subsequent step an electron from the acceptor HO undergoes electron back transfer to the donor HO. Electron exchange is similar to RET because the energy is transferred to an acceptor. Figure 14 shows a schematic view for the electron exchange quenching.

Photoinduced electron transfer

In photoinduced electron transfer (PET) a complex is formed between the electron donor D_P and the electron acceptor A_p, yielding $D_p^+A_p^-$. This charge transfer complex can return to the ground state without emission of a photon, but in some cases exciplex emission is observed. Finally, the extra electron of the acceptor is returned to the electron donor. Figure 15 shows the molecular orbital diagram for photoinduced electron transfer.
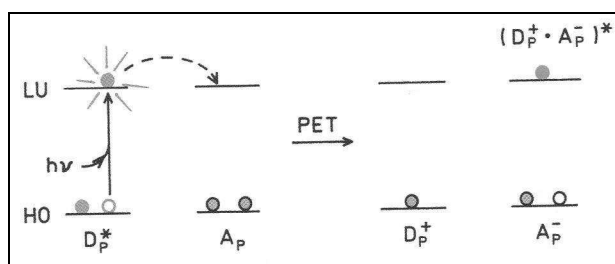
Figure 15: Molecular orbital schematic for photoinduced electron transfer [6]

PET quenching can also occur by electron transfer from the excited fluorophore to the quencher. In PET the terms donor and acceptor do not classify which species is initially in the excited state. This is the difference from RET, where the fluorophore is always the donor.

1.5   *Fluorescence lifetimes and quantum yields*

The singlet *lifetime* determinates the time available for the fluorophore to interact with a substrate or diffuse in its environment, and hence the information available from its emission. The lifetime of the excited state is defined by the average time wich the molecule spends in the excited state. Generally, fluorescenece lifetimes are between 100 ps and 10 ns. [6]

Quantum yield of fluorescence is the number of emitted photons relative to the number of absorbed photons. [6] For a highly fluorescent molecule such as fluorescein, the quantum yield under several conditions approaches unity. Species that do not fluoresce have quantum yield that approach zero. [2]

1.6   Fluorescence sensing

The design of fluorescent sensors has attracted considerable interest due to its importance to analytical chemistry, clinical biochemistry, medicine, industrial and environmental chemistry etc. Numerous chemical and biochemical analytes can be detected by fluorescence methods: cations, anions, neutral molecules and gases. [10]

Fluorescence sensors are more sensitive than absorption sensors (colorimetric sensors) because the light absorbance is measured as the difference in intensity between light passing through the reference and the sample. In fluorescence the intensity is measured directly, without comparison with a reference beam. [6]

Fluorescence sensing requires a change in a spectral property in response to the analyte. Changes can occur in the fluorescence intensity, excitation spectrum, emission spectrum, anisotropy, or lifetime of the sensing probe. [6]

In a fluorescence sensing approach, the fluorophore is the *signaling* species, i.e. it acts as a signal transducer that converts the information in the presence of an analyte (guest) into an optical signal expressed as the changes in the photophysical characteristics of the fluorophore. [10] The receptor recognizes the guest and a behaviour change in the fluorescence signal is produced (figure 16).
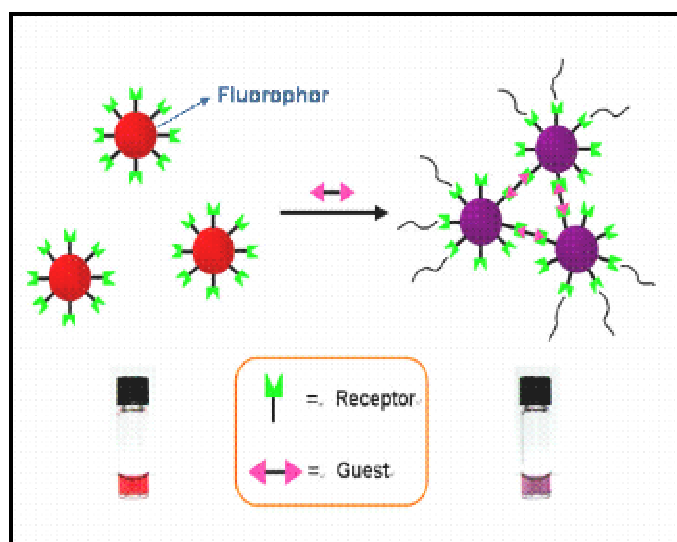
Figure 16: Principle of fluorescence sensing

1.6.1 Mechanisms of sensing

There is a variety of signaling mechanisms the simplest mechanism is collisional quenching, where the fluorophor is quenched by the analyte. Static quenching can also be used for sensing but the lifetime does not change. [6] Other mechanisms have been described such as ground state

charge transfer, [11a,b] photoinduced electron transfer (PET), [11c,g] excimer / exciplex formation, [12] intramolecular charge transfer [11g],[13] and excited-state proton transfer.[14] Resonance energy transfer (RET) is perhaps the most general and valuable phenomenon for fluorescence sensors.[6]

Due to the mechanisms of sensing fluorescent sensors can be classified in three classes: [10]

- Class 1: fluorophores that undergo quenching upon collision with an analyte (*e.g.* O_2, Cl^-).

- Class 2: fluorophores that can reversibly bind an analyte. If the analyte is a proton, the term *fluorescent pH indicator* is often used. If the analyte is an ion, the term *fluorescent chelating agent* is appropriate. Fluorescence can either be quenched upon binding (CEQ type: Chelation Enhancement of Quenching), or enhanced (CEF type: Chelation Enhancement of Fluorescence). In other cases, the compound is said to be *fluorgenic* (e.g. 8-hydroxyquinoline (oxime)).

- Class 3: fluorophore linked, via a spacer or not, to a receptor. The design of such sensors, which are based on molecule or ion recognition by the receptor, requires special care in order to fulfill the criteria of affinity and selectivity. These aspects are revelant to the field of *supramolecular chemistry*. The changes in photophysical properties of the fluorophore upon interaction with the bound analyte are due to the perturbation by the latter of photoinduced processes such as electron transfer, charge transfer, energy transfer, excimer / exciplex formation or disappearance etc.

In this work it was tried to approach achiral and chiral anions, cations and peroxides-sensors.

1.6.2 Cations sensing

Detecting cations is of great interest for different areas such as chemistry, biology or medicine. Sodium, potassium, magnesium and calcium are involved in biological processes such as the transmission of nerve impulses, muscle contraction, regulation of cell activity, etc. Zinc is an essential component of many enzymes; it plays a major role in enzyme regulation, gene expression, neurotransmission, etc.

On the other hand, there are some metal ions toxic to organisms (mercury, cadmium, etc.), and early detection in the environment is desirable. Aluminum is also potentially toxic: it is probably at the origin of some diseases such as osteomalacia, anemia, neurodegenerytive or bone diseases. Control of aluminum content of is thus necessary in the production of agricultural goods as well as in the pharmaceutical industry.[10]

Colorimetric determination of cations based on changes in color on complexation by dye reagents started to be popular a long time ago, especially in the case of alkaline earth metals ions, which are efficiently chelated by agents of the EDTA type. Sine fluorimetric techniques are more sensitive than photometric ones, numerous fluorogenic chelating reagents were studied and applied to practical cases.

Fluorescent molecular sensors of the EDTA type exhibit high selectivity for calcium with respect to other ions present in cells. In the late 1960s Crown ethers and cryptands were discovered [10] and opened up new possibilities for cation recognition with improvement of selectivity, especially for alkali metal ions.

Fluorescent sensors emerged some years later with the design of a fluoroionophore. The ionophore moiety has been recognized by the fluorophore, this experienced changes in its fluorescence properties due to binding between ionophore and fluorophore.

The stability of a complex between ionophore and fluorophore depends on many factors: nature of cation, nature of solvent, temperature, ionic strength and in some cases also pH.

The connection between the ionophore and the fluorophore is very important in aspects of sensing design, bearing in mind the search for the strongest perturbation of the photophysical properties of the fluorophore by the cation. The ionophore may be linked to the fluorophore via a spacer, but in many cases some atoms or groups participating in the complexation belong to the fluorophore. Therefore, the selectivity of binding often results from the whole structure involving both signaling and recognition moieties.

Fluorescence sensors of cations will be presented in the following part. The recognition of the cation can be explained by different mechanisms.

Stanculescu and coworkers [15] used tetrandrine (6,6´,7,12-tetramethoxy-2,2´-dimethyl-berbaman; TET; figure 17) as fluorescent sensor. They characterized the binding properties of TET as host towards alkaline and alkaline earth metals, engaged in a molecular recognition process. The recognition has been studied by UV-*vis* and fluorescence spectroscopy.

After titration of TET with Na^+, K^+, Mg^{2+} and Ca^+, changes in the absorbance of TET were observed in the region of 300-325 nm, where TET starts to absorb with the derived spectra slightly shifted. These aspects lead to the conclusion that TET selectively complexes Ca^{2+} and Mg^{2+} ions which can be classificated as hard acids.
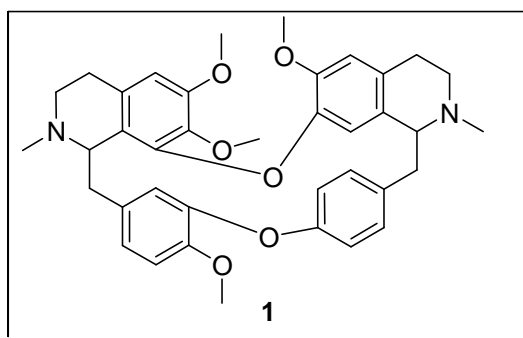
Figure 17: 6,6´,7,12-Tetramethoxy-2,2´-dimethyl-berbaman; TET (1)

The fluorescence emission showed a hypsochromic shift (~6 nm) upon addition of Ca^{2+}, accompanied by a 1.5- fold fluorescence enhancement. The blue shift and the increase in fluoresecence intensity are attributed to Ca^{2+} binding to TET which results in a more rigid structure of the ligand after complexation. The fluorescence enhancement may happen due to the suppression of the intramolecular phothoinduced electron transfer (PET) from the oxygen ion pairs. Another explanations is that the metal binding alters the rate of one or more relaxation processes from the excited state: radiative decay, internal conversion (IC) or intersystem crossing (ISC).

Zinc is one of the most important transition metal ions found in nature, where it has multiple roles in both extra- and intra-cellular functions. Gunnlaugsson and coworkers [16] were active in the development of supramolecular luminescent chemosensors for zinc and other ions and molecules. In this case they chose to use 4-amino-1,8-naphthalimide (figure 18) as a photostable fluorophore reporter in designing **2** , as it absorbs in the visible region and emits in the green, with Stokes shift of *ca*.100 nm. Importantly, **2** does not respond to Ca^{2+} and Mg^{2+}, or many other transition metal ions.
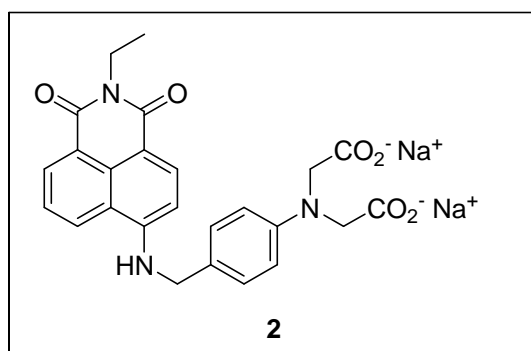
Figure 18: 4-amino-1,8-naphthalimide (2)

The ability of **2** to detect Zn^{2+} and other physiologically and non-physiogically relevant cations was carried out at pH 7.4 by monitoring the changes in the absorption and emission spectra. The absorption spectra of **2** showed a broad band in the visible region between 370 and

510 nm with λ_{max} at *ca.* 442 nm (logε = 4.28) which was assigned to an internal charge transfer excited state (ICT). No significant changes were seen in the absorption spectra upon a spectroscopic pH titration from pH 2-12.

The enhancement in the fluorescence emission at pH 7.4 upon addition of $ZnCl_2$ is due to the binding of the Zn^{+2} to the carboxylates of the imidodiacetate and the aromatic nitrogen moiety. In particular, the latter interactions increase the oxidation potential of the receptor with comitant reduction in the receptor´s ability to quench the fluorescence of the naphthalimide moiety *via* PET, in the same way as for H^+ above. Other experiments with different divalent and monovalent cations confirmed the selectivity of **2** towards Zn^{2+}.

Detection of Cu^{2+} ions is important for environmental and biological systems. However, the selectivity for Cu^{2+} over other ions, such as Pb^{2+}, and Fe^{3+}, is not very satisfactory in some cases [17]. So, development of new Cu^{2+} selective turn-on fluorescence sensors is still important and necessary. Li and coworkers [17] synthesized a new fluorescent sensors based on calix[4]arene **3** and **4** (figure 19) bearing four iminoquinoline subunits on the upper rim, which showed a remarkable enhanced fluorescent intensity in the presence of Cu^{2+} ions and a high selectivity towards Cu^{2+} ions over a wide range of tested metal ions in acetronitrile.
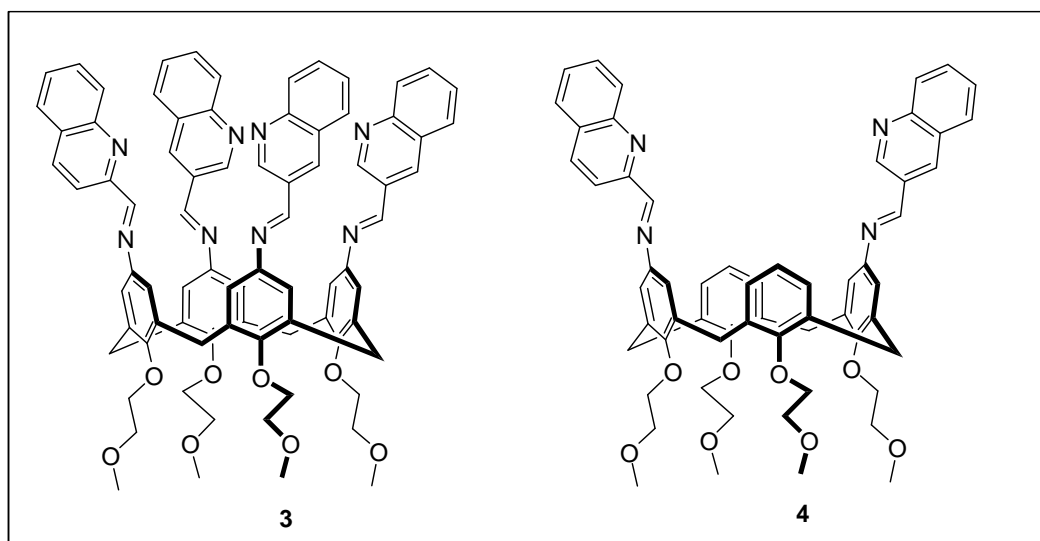
Figure 19: Calix[4]arene derivates 3 and 4

The fluorescence titration of **3** with Cu^{2+} showed an increase of the emission intensity of about 1200-fold when the concentration of Cu^{2+} was increased up to 11 x 10^{-5} M. The association constant (K_{ass}) was determined to be 3.67 x 10^7 M^{-1}, which indicates a high affinity of **3** to Cu^{2+}.

Similar to **3**, the fluorescence enhancement of **4** in the presence on Cu^{2+} could also be observed, but it is obviously less than that of **3** induced by Cu^{2+} in the same conditions. The

association constant (K_{ass}) of the 1:1 complex **4**-Cu^{2+} was calculated to be 3.7 x 10^5 M^{-1}, which is only about one-hundredth of that of the 1:1 complex [**3**-Cu^{2+}]. These results indicated that tetraiminoquinoline derived calix[4]arene **3** might have a preorganized and multi-coordinated complexing site for Cu^{2+} ions.

For rationalizing the observed fluorescenece enhancement, two factors may be considered. First, the low fluorescence intensity of **3** in CH_3CN in the absence of Cu^{2+} ions may be attributed to a radiationless channel from the $n\pi^*$ state of the emission of the quinoline group by the lone-pair electron of the imine nitrogen atom (PET). When a Cu^{2+} ion coordinates with the ion pair of the imino and quinoline nitrogens, the energy of the $n\pi^*$ state is raised so that the $\pi\pi^*$ state of the emission of the quinoline group becomes the lowest excited state, leading to a substantial increase in fluorescence intensity (PET). Secondary, Cu^{2+} binding to **3** induces its conformation restriction, which could also result in the increased fluorescence intensity.

Lanthanide ions are known to show long-lived spectrally distinct fluorescence or phosphorescence. Lifetimes are generally in the order of several hundreds of microseconds to milliseconds for visible-light-emitting Eu(III) and Tb(III). These long lifetimes, caused by parity-forbidden transition resulting from 4f orbitals and characteristic linelike emmission spectra have triggered the application of lanthanides for the development of luminescent materials, chemosensors and luminescent labels. Oueslati and coworkers [18] were interested in calix[4]azacrowns with aminopolyamide bridges. These compounds contain amide and amine functionalities, both known for their capability to bind lanthanide ions via interaction with C=O oxygen atoms and amine nitrogen atoms.
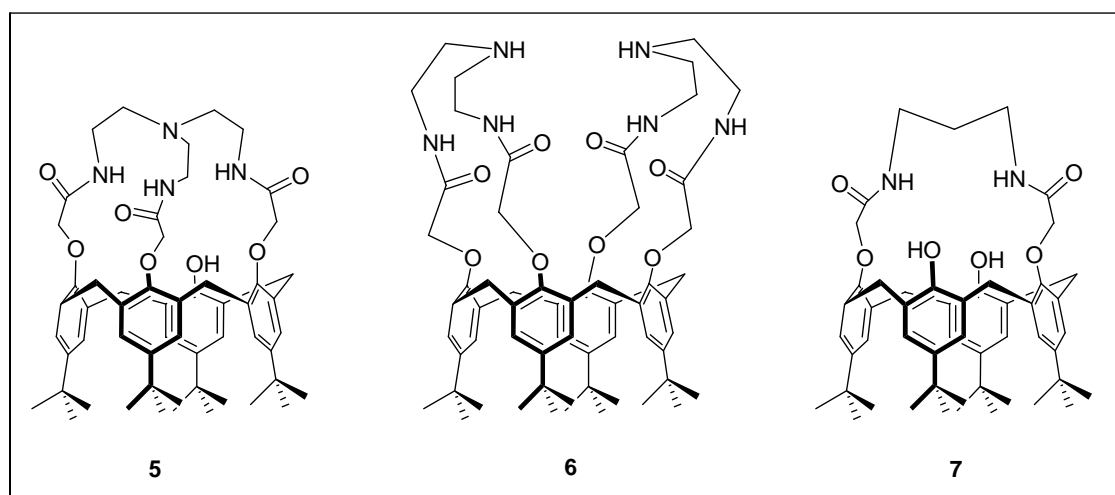
Figure 20: Calix[4]azacrown derivates 5, 6 and 7

They used **5** and **6** for the complexation of lanthanide ions such as Eu^{3+}, Tb^{3+}, Nd^{3+}, Er^{3+}, La^{3+}, which was investigated by UV-*vis*, fluorescence spectroscopy and ^1H NMR.

The UV absorption spectra of **5** and **6** upon addition of lanthanide triflates showed significant changes, albeit dependent on the ligand structure. The observed changes indicated the formation of at least two different complexes. The complex stability constant in the form log β_{ij} values were calculated by analysis of the absorption spectra and are summarized in table 1.

Table 1: Stability Constants (log β_{ij}) of Lanthanide Complexes with 5 in acetonitrile.

Metal	R^a	Log $\beta_{ij}{}^b$
Eu (III)	1:1	4.69 ± 0.32
	1:2	9.52 ± 0.01
Tb (III)	1:1	5.67 ± 0.30
	1:2	10.66 ± 0.70
Nd (III)	1:1	5.71 ± 0.02
	1:2	10.66 ± 0.70
Er (III)	1:1	4.94 ± 0.30
	1:2	10.54 ± 0.02
La (III)	1:1	6.01 ± 0.20
	1:2	9.80 ± 0.20

[a] Metal-to ligand ratio. [b] Determined by absorption spectroscopy : T = 298 K, [5] = 6.89 10^{-5} M.

This data has to be interpreted with caution, since the small changes in the UV spectra did not allow a sufficiently accurate determination of complex stability constants.

The fluorescence of **5** was enhanced upon lanthanide complexation and other experiments were carried out to prove that the mechanism involves the amine nitrogen in the fluorescence enhancement of **5**. PET from the electron-donating tertiary amine to the aromatic moieties of the calixarene, which is switched off upon involvement of nitrogen lone pair in metal complexation and can be assumed to be the transduction mechanism. This conclusion is supported by strong fluorescence quenching (90%) of **5** to that of **7** as verified by the quantum yield and lifetime measurements. [18]

Compound **6** showed strong fluorescence quenching as a result of lanthanide ion complexation. With the control experiment of trifluoroacetic acid no significant changes of the fluorescence was observed, similar situation for **7**. This is surprising since **6** also contains electron-donating secondary amine groups on the bridges, albeit weaker than the tertiary amine group in **5**. The blocking of PET upon lanthanide complexation, which would result in an enhancement of the fluorescence, seems to be of minor importance compared to other effects which lead to fluorescence quenching, for instance the participation of accelerated intersystem crossing (ISC) due to lanthanides as heavy atoms.

In summary, for ligand **5** complexation outside the ionophoric cavity is assumed, the more flexible ligand **6** should be able to accommodate the lanthanide ion inside the cavity.

Fluorescein and related derivates have been widely employed as signaling basis for molecular imaging and chemosensing applications, including the detection of metal ions like

K^+, Mg^{2+}, Zn^{2+}, Cd^{2+}, Pb^{2+} and Hg^{2+}. Choi and coworkers [19] reported the selective chemodosimetric (chemodosimeters detect an analyte trough a highly selective and usually irreversible chemical reaction) between the dosimeter molecule and the target analyte leadind to an observable signal, in which an accumulative effect is directly related to the analyte concentration [20] Hg^{2+} signaling behavior of simply structured fluorescein derivates (scheme 1). Dichlorofluorescein and its methyl ester derivate showed pronounced Hg^{2+} selective chromogenic and fluorogenic signaling behaviors in aqueous environment *via* selective mercuration of the 4´,5´-position of the xanthene moiety.
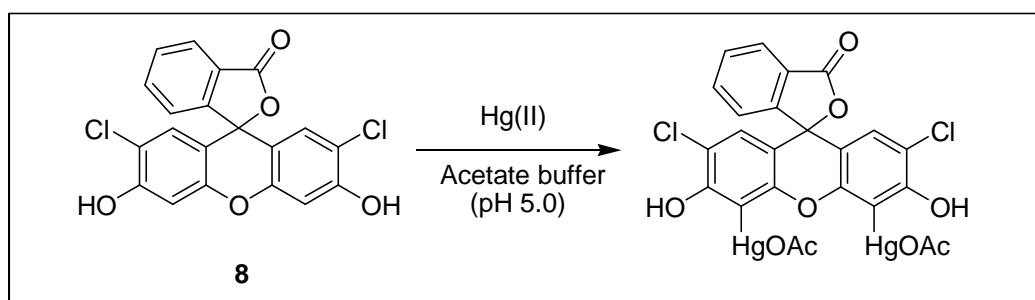
Scheme 1: Dichlorofluorescein derivate (8) with Hg^{2+}

The absorption bands at 475 and 505 nm of **8** upon treatment with Hg^{2+} ions were gradually decreased and red-shifted to 483 and 533 nm. The color of the solution changed from yellowish green to orange. Other metal ions induced some variation in absorbance without significantly changing the absorption maximum. The ratio of A_{533}/A_{483} was 1.02 for Hg^{2+} ions and varied in a limited range from 0.058 (Ni^{2+}) to 0.085 (Ag^+) for the other metal ions.

The characteristic fluorescence spectrum of **8** was effectively quenched upon treatment with Hg^{2+} ions. The quenching efficiency can be expressed by the ratio of I_0/I at 528 nm (I_0 and I represent the fluorescence intensity of **8** in the absence and in the presence of metals ions, respectively); I_0/I was greater than 1900 for Hg^{2+} ions. Other metal ions did not induce noticeable changes in the fluorescence emission of **8**.
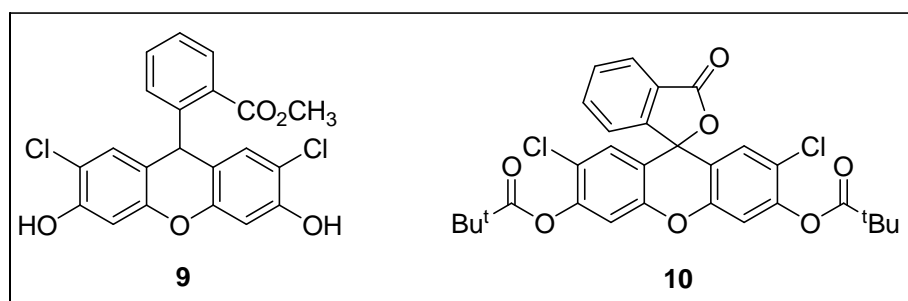
Figure 21: Derivates of dichlorofluorescein

Methyl ester **9** (figure 21) exihibited similar chromogenic and fluorogenic behaviors to **8**, the absorption band was red-shifted ($\Delta\lambda = 35$ nm), and fluorescence was exclusively and efficiently quenched by Hg^{2+} ions (I_0/I at 534 nm = 501). However, compound **9** showed somewhat less sensitive Hg^{2+} signaling than **8**. In contrast, the response of the pivaloyl derivate **10**, which could not be mercurated on the xanthene moiety, were insignificant, highlighting the importance of the phenolic moieties of the xanthene in the signaling process.

1.6.3 Anions sensing

Anions play an important role in chemical and biological processes. Many anions act as nucleophiles, bases, redox agents or transfer catalysts. [10] Most enzymes bind anions as either substrates or cofactors. The chloride ion is of special interest because it is crucial in several phases of human biology and in disease regulation. Moreover, it is of great interest to detect anionic molecule pollutants such as nitrate and phosphates in ground water. [10]

Anions such as organic phosphates and even fluoride are harmful to the environment and consequently to humans. The ability to selectively detect these anions in environmental samples has become a dramatic necessity as organophosphates are components of nerve agents [21] and fluoride is associated with nerve gases and the refinement of uranium used to nuclear weapons manufacture. [22]

The design of selective anion molecular sensors with optical or electrochemical detection is thus of major interest, however it has received much less attention than molecular sensors for cations.

A typical fluorescent sensor for anions is generally built through a modular approach, by either covalently or noncovalently attaching an appropriate photoactive fluorophore to the receptor with an affinity for the desired substrate. Following the receptor-anion interaction, an appropriate signaling process must take place.

The fluorescent mechanisms used in the signaling process for anion sensing are generally photoinduced electron transfer (PET), excited-state proton transfer, excimer/exciplex formation, metal-to-ligand charge transfer, and modulation of efficiency of interchromophore energy transfer. [23]

There are many fluorescence sensors for halide ions (except F⁻) that are based on dynamic quenching of a dye (fluorophor). In particular, the determination of chloride anions in living cells is done according to this principle. Some halide ion sensors are given in figure 22.
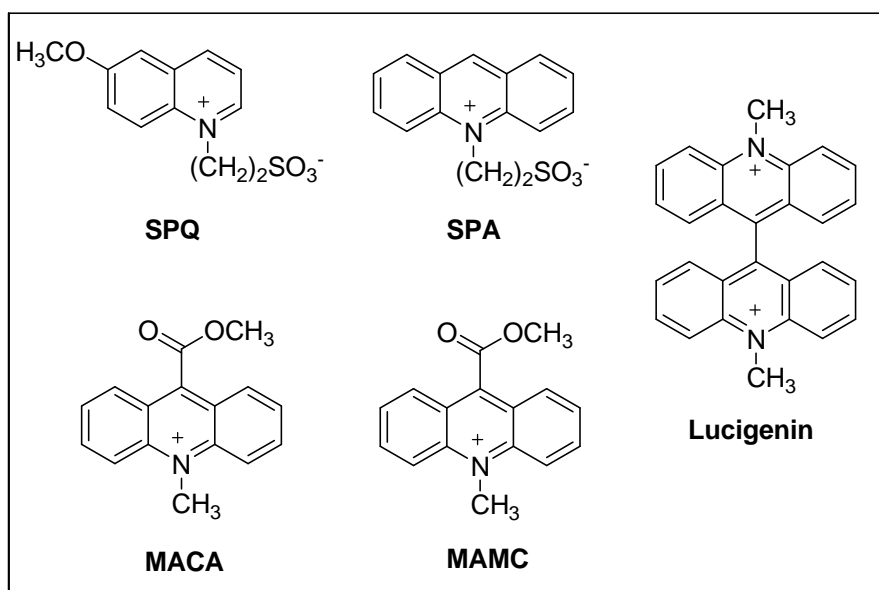
Figure 22: Various halide ion sensors

Their lack of selectivity is shown by the Stern-Volmer constants in table 2. For instance 6-methoxy- *N*-(3-sulfopropyl)quinolinium (SPQ) is mainly used as Cl^- sensitive fluorescent indicator, but its fluorescence is also quenched by several other anions (I^-, Br^- and SCN^-, but not by NO_3^-). [24]

Table 2: Stern-Vollmer constants (M^{-1}) of halide molecular sensors in aqueous solutions.

Compound	Cl^-	Br^-	I^-	SCN^-
SPQ	118	175	276	211
SPA	5	224	307	255
Lucigenin	390	585	750	590
MACA	225	480	550	480
MAMC	160	250	267	283

Abbreviations: SPQ: 6-methoxy-N-(sulfopropyl)quinolinium; SPA: N-(sulfopropyl)acridinium; lucigenin: bis-N-methylacridinium nitrate; MACA: 10-methylacridinium-9-carboxamide; MAMC: N-methylacridinium-9-methyl carboxylate.

For F^- recognition the diprotonated form of hexadecyltetramethylsapphyrin is used that contains a pentaaza macrocyclic core as shown in figure 23. The selectivity for fluoride ions was found to be high in methanol (stability constants of the complex $\sim 10^5$) with respect to chloride and bromide (stability constants $\leq 10^2$).
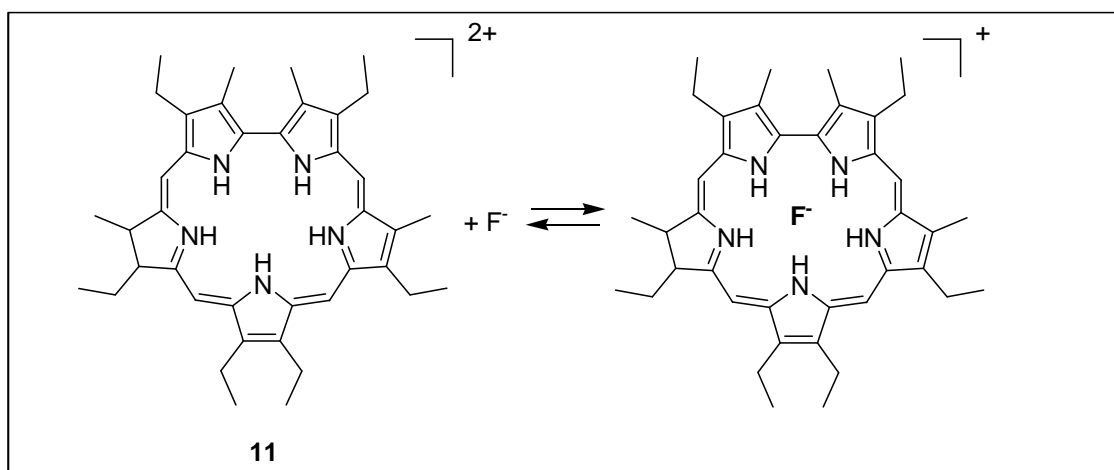
Figure 23: Selective sensor (11) for fluoride ions

This selectivity can be explained by the fact that F⁻ (ionic radius ~ 1.19 Å) can be accommodated within the sapphyrin cavity to form a 1:1 complex with the anion in the plane of the sapphyrin, whereas Cl⁻ and Br⁻ are too large (ionic radii 1.67 and 1.82 Å respectively) and form an out-of-plane ion paired complex. [25]

Phosphate anions have attracted much attention because of their biological relevance. Anthrylpolyamine conjugate probes can recognize phosphate groups due to photoinduced electron transfer from the unprotonated amino group to anthracene, but it is dependent of the pH on the fluorescence sensor. At pH 6, a fraction of 70% of **12** exists as a triprotonated form, the nitrogen atom close to the anthracene moiety being unprotonated. This fraction has a very low fluorescence emission.
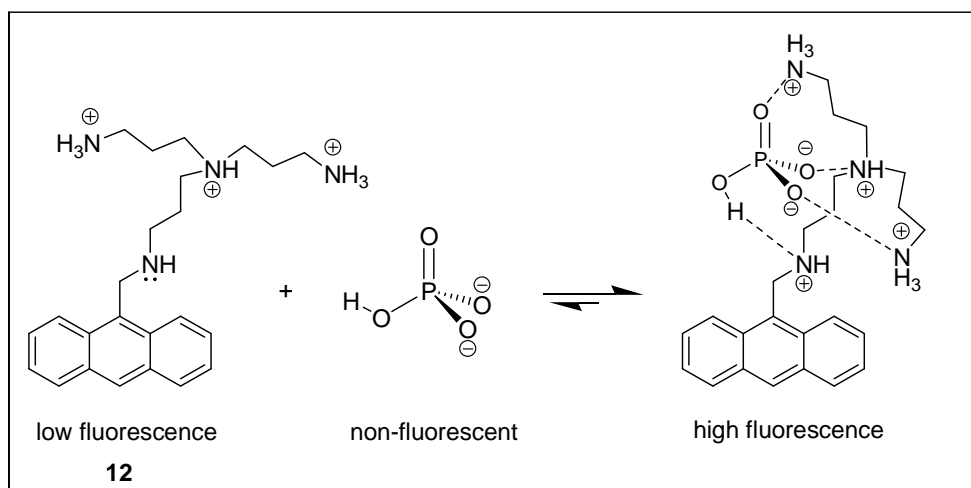
Figure 24: Selective sensor (12) for phosphate anions

The monohydrogenophosphate whose three oxygen atoms interact with the three positive charges (tri-cation of the amine groups); the remaining phosphate OH group is in a favorable

position to undergo intracomplex proton transfer to the unprotonated amino group, which eliminates intramolecular quenching. The result of this binding is a drastic enhancement of fluorescence emission of the complex. This fluorescence sensor can also bind ATP, citrate and sulfate but the stability of the complex is low. [26] The mechanism is shown in figure 24.

The development of neutral charge chemosensors involves the criteria of PET sensing using the *fluorophore-spacer-receptor model*. In function of this criterion Gunnlaugsson and coworkers [27] synthesized a neutral charge chemosensor through the combination of anthracene as chromophore and thiourae as electroneutral anion receptor. The different chemosensors are shown in figure 25.
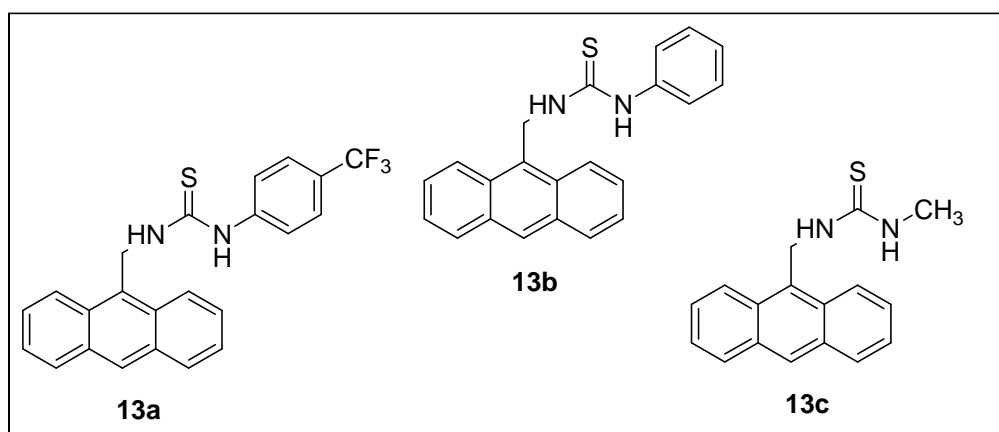
Figure 25: Anthracene derivates used as fluorescence sensors (13 a-c)

Anthracene fluorescence emission is selectively quenched upon titration with AcO^-, $H_2PO_4^-$ and F^- but not by Cl^- or Br^- in DMSO. Of the three chemosensors, **13a** was expected to show the strongest binding due to this effect and **13c** the least.

The fluorescence emission spectra of 1-((anthracen-10-yl)methyl)-3-(4-(trifluoromethyl) phenyl)thiourea (**13a**) when titrated with AcO^- in DMSO displayed typical PET behaviour. Upon adittion of the AcO^-, the maximum emission intensity decreased with no other spectral changes being observed. Similar emission and absorption effects were observed for 1-((anthracen-10-yl)methyl)-3-phenylthiourea (**13b**) and 1-((anthracen-10-yl)methyl)-3-methyl-thiourea (**13c**).

When the fluorescence titrations of **13a-c** were carried out in other solvents such as CH_3CN, CH_3CO_2Et or THF, the emission was also quenched upon adittion of AcO^- but the degree of quenching was somewhat smaller. In EtOH, wich is a higly competitive hydrogen bonding solvent, no binding was observed between the **13a** and AcO^-. Furthemore, no exciplex emission could be observed in any of these solvents.

The simple fluorescent PET anion chemosensors **13a-c** show ideal PET sensing behaviour upon ion recognition, only fluorescence emission is *switched off*.

In order to investigate the selectivity and sensitivity of the sensor towards biologically important anions, Gunnlaugsson and coworkers [27] carried out a series of titrations using TBA salts of F⁻, Cl⁻, Br⁻ and $H_2PO_4^-$ in DMSO. In the case of $H_2PO_4^-$ and F⁻ the fluorescence emission was quenched by *ca.* 50 ($\Phi_F = 0.0156$) and 90% ($\Phi_F = 0.0011$) respectively (at 443 nm), but for Cl⁻ and Br⁻ a minor quenching process was observed ($< 7\%$), ruling out a quenching by the heavy atom effect.

Gunnlaugsson and coworkers [27] proposed that the rate of electron transfer from the HOMO of the thiourea-anion complex to the anthracene excited state, upon anion recognition *i.e*, the reduction potential of the thiourea is increased causing PET to become competitively more viable, which causes the fluorescence emission to be quenched. The fluorescence emission spectra of **13a** when titrated with AcO⁻ in DMSO displayed typical PET behavior, the intensity of the bands at 443, 419 and 397 nm decreased gradually with no other changes being observed.

Another reason why the detection of F⁻ is important is the over-accumulation of fluorides in the bones can be toxic, which is. Lee and coworkers [23] synthesized a fluorescent anion sensor (figure 26), based on a biaryl-thiourea system, which shows a fluorescent emission enhancement by conformational restriction upon hydrogen bond-mediated complexation of F⁻.
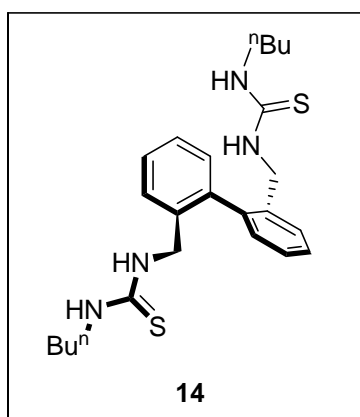
Figure 26: Fluorescence anion sensor 14

The anion (as TBA salts) recognition was investigated in CH_3Cl. In the absence of anions, the maximum of the emission spectrum of **14** is characterized at 379 nm. The presence of F⁻ resulted in a fluorescence enhancement at 356 nm. The dependence of the intensity at 356 nm on the concentration of F⁻ strongly suggests that two kinds of complexes are formed.

As the complex A is formed, **14** shows fluorescence enhancement *via* conformational restriction. Then, as complex B is formed, a decrease in the fluorescence intensity takes place by the loss of conformational restriction induced by complex A, this mechanism is shown in

scheme 2. For complex A the association constant is calculated to be 1.08×10^4 M^{-2} and for complex B to be 2.28×10^7 M^{-2}.
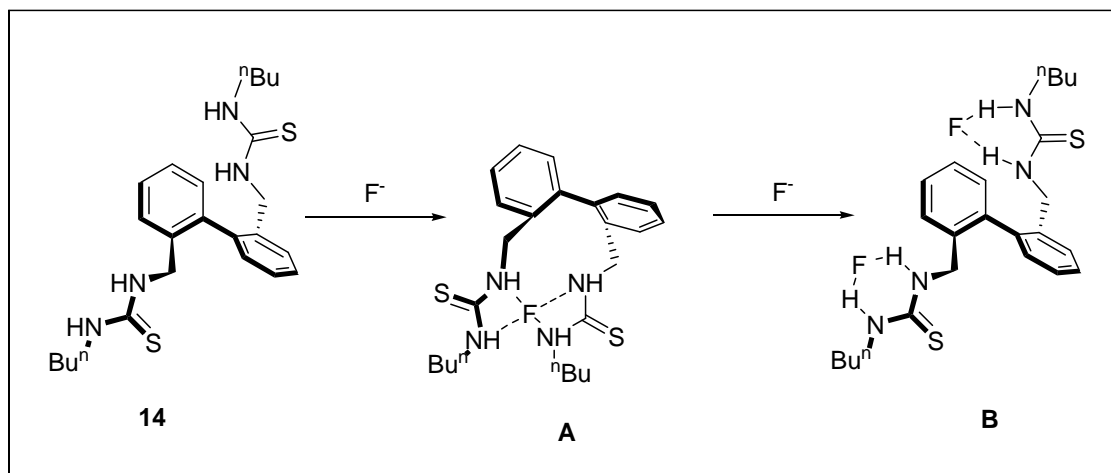
Scheme 2: Proposed mechanism for the complexation of 14 with fluoride ions

The fluorescence titration of **14** with $H_2PO_4^-$, $CH_3CO_2^-$, HSO_4^-, Cl^- and Br^- only shows broad emission enhancement around 470 nm. This result indicates that even though these anions interact with thiourea groups, they do not necessarily form a complex with **14** like complex A. Thus, fluorescence enhancement at 356 nm via conformation restriction was not detected.

The fluoride anion$^-$ exhibits a stronger basicity than other anions, and should exhibit a more effective hydrogen bonding interaction with the thiourea groups comprising the binding site. The fluorescent sensor shows fluorescence emission enhancement by conformational restriction upon hydrogen-bond mediated complexation of fluoride ions.

Zhang and coworkers [28] observed a red-shifted fluorescence emission in 3-hydroxyl-2-naphthanilide (**15**) in acetonitrile and drastically enhanced of the fluorescence intensity upon addition of anions such as F^-, AcO^- and $H_2PO_4^-$, with the enhancement depending on anion basicity (figure 27).
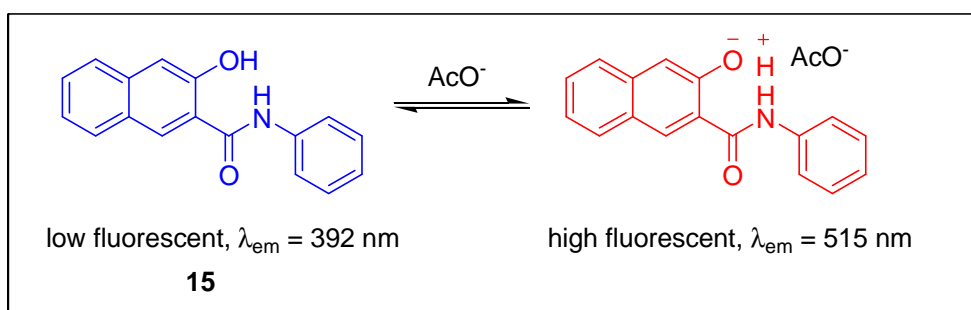
Figure 27: Proposed mechanism of fluorescence sensor 15 for the recognition of AcO$^-$

The reason why **15** was used for this experiment as fluorescent sensor was mainly based on the fact that:

- **15** contains both OH and amide NH groups that are well known to be involved in anion-binding in nature and extensively employed in developing anion receptors and sensors.

- The aciditiy of phenolic OH and aromatic amino NH protons is drastically enhanced upon photoexcitation and therefore an excited-state intermolecular ESPT channel might be opened upon anion binding.

After monitoring the fluorescence spectra of **15** in acetonitrile in the presence of anions such as F^-, AcO^-, $H_2PO_4^-$, Cl^-, Br^- and ClO_4^- (as TBA salts) it was found that, whereas **15** emitted only short wavelength fluorescence at 392 nm (λ_{ex} = 300 nm) with a very low fluorescence quantum yield ($\Phi \sim 10^{-4}$) in CH_3CN, a new substantially red-shifted emission appeared at 515 nm upon addition of F^- and was dramatically enhanced with increasing F^- concentration. The color of the solution changed to yellow and returned to colorless when a protic solvent such as methanol or water was introduced, suggesting that the interaction between **15** and F^- was hydrogen bonding, likely at the amide NH and phenol OH sites.

Other anions such as AcO^-, $H_2PO_4^-$ and Cl^- were found to induce similar variations in both absorption and fluorescence spectra with magnitudes that depended on the anion´s basicity, whereas Br^- and ClO_4^- hardly induced any changes. The association constants (K_{ass}) between **15** and the anions were fitted from nonlinear regressions and the data listed in table 3 shows higher binding affinity to and more efficient fluorescence enhancement by F^- than for other anions. This is because of its high charge density and small size which enables it to be a strong hydrogen bonding acceptor that shows interaction with phenol or amide derivates containing only a single hydrogen bonding donor group.

Table 3: Association constants (K_{ass} M^{-1}) for anions with 15 in acetonitrile from absorption (422 nm) and fluorescence (λ_{em} = 515 nm, λ_{ex} = 377 nm) titrations [a]

Anion	K_{ass} (abs.)	K_{ass} (flu.)
Br^-, ClO_4^-	na [b]	na [b]
Cl^-	$(2.73 \pm 1.14) \times 10^3$	$(1.00 \pm 0.16) \times 10^3$
$H_2PO_4^-$	$(1.13 \pm 0.06) \times 10^4$	$(1.20 \pm 0.08) \times 10^4$
AcO^-	$(5.94 \pm 0.39) \times 10^5$	$(4.43 \pm 1.08) \times 10^5$
F^-	$> 10^6$ [c]	$> 10^6$ [c]

[a] Anions exist as their TBA salts. [b] Not available because of the minor spectral change. [c] Too high to be accurately determined.

Zhang and coworkers [28] demonstrated a simple fluorescent sensor for anions following the excited-state intermolecular proton transfer (ESPT) signaling mechanism.

Fluorescent sensor **16**, 1,8-bis(phenylureido)naphthalene and analog **17**, 2,3-bis(phenyl-ureido)naphthalene (figure 28) were synthesized from diaminonaphthalene and phenyl isocyanate by Xu and coworkers.[29] They reported that these novel fluorescent sensors for fluoride yield increased fluorescence upon binding to fluoride. Other halide ions cause slight decreases in fluorescence emission when interaction with the sensor molecule takes place.
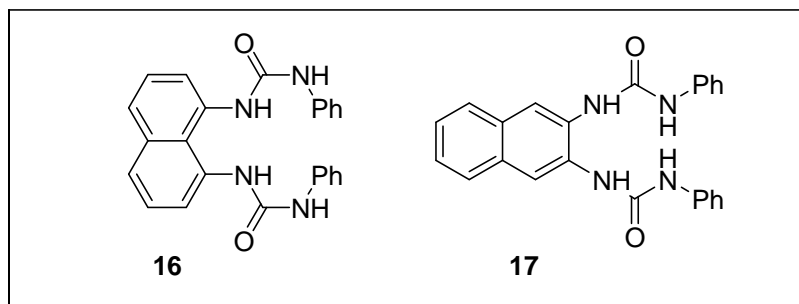
Figure 28: Structure of sensor 16 and 17

The binding constant for fluoride (1:1) with **16** was determined to be 73.650 M^{-1}. The binding constants for chloride, bromide and iodide were found to be 690.345 and 76 M^{-1} respectively.

Fluorescent experiments with **17** indicated quenching effects with all four halides. The sensors **16** and **17** have the same functional groups but different location of the two urea groups, so the different response to halides must result from different relative positions of the urea groups. Due to computer modeling, Xu and coworkers [29] found that upon binding of fluoride, the molecule becomes more planar, which likely contributes to the increased fluorescence. The chloride, bromide and iodide complexes do not exhibit the same degree of planarity. Furthermore, these large ions have a much weaker binding afinity and are good fluorescence quenchers, which may offset any increase in fluorescence due to geometry changes.

Gunnlaugsoon and coworkers [30] presented "second generation" PET anion sensors. These sensors are built up in a *receptor-space-fluorophore-spacer-receptor* manner. The two anion receptors are connected in a linear fashion *via* the two spacers to an anthracene fluorophore through the 9 and 10 positions. This design was realized for two thiourea based fluorescent sensors **18**-1 and **18**-2 and the urea analogue **18**-3, that is shown in figure 29.

The ground and excited state properties of **18**-3 were investigated in DMSO. The anion recognition was evaluated using ^{1}H NMR as well as absorption and fluorescence spectroscopy. For sensors **18**-3 the emission was *switched off* upon titration with various anions. For simple anions such as acetate or fluoride, the recognition was shown to occur through hydrogen

bonding of the corresponding anion to the receptors. This gave rise to only minor changes in the absorption spectra, but caused significant changes in the fluorescence emission spectrum, which was substantially (70-95%) quenched. These results corroborated the PET quenching of the anthracene excited state upon anion recognition, due to hydrogen bonding between the thiourea or urea protons and the anions. Fluorescence emission changes upon recognition of simple anions such as AcO^- and $H_2PO_4^-$ were monitored in function of anion concentration. Gunnlaugsson and coworkers demonstrated that the recognition was due to the formation of a 1:2 binding between the sensors and the anions. For halides such as Cl^- and Br^- no significant fluorescence changes occurred. However, for F^- the emission was almost fully quenched after addition of only one equivalent of the anion.
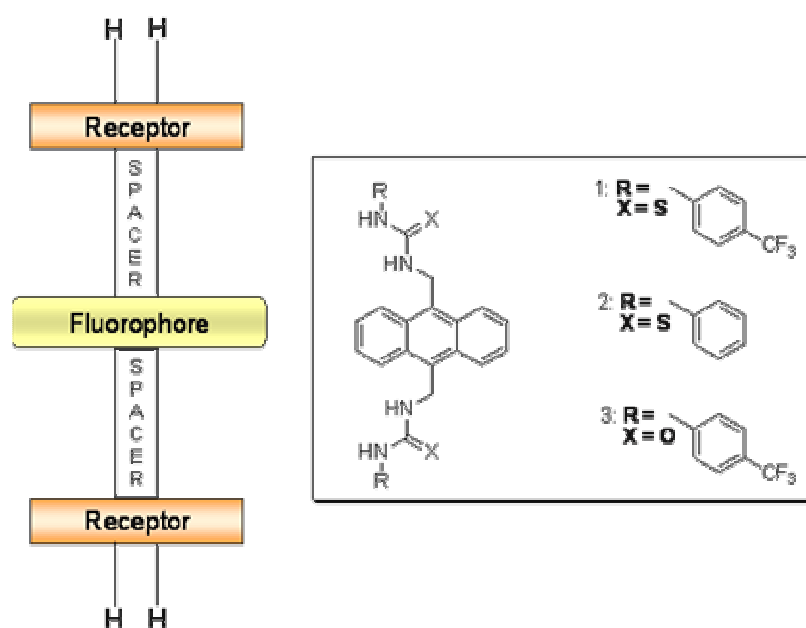
Figure 29: The *receptor-spacer-fluorophore-spacer-receptor* model used and the corresponding sensor 18 (1-3)

For all of the anions, the quenching contributed to enhanced efficiency of PET from the receptor to the excited state of the fluorophor.

The recognition of bis-anions such as pyrophosphate, malonate and glutarate was also demonstrated. For the first two of these anions, the sensing was shown to have a 1:1 stoichiometry, whereas for glutarate the binding was most likely 1:2 for **18**-**1** and **18-2**. However, for the urea based sensor **18-3**, the binding was found to be 1:1 for all the bis-anions. The binding (1:1 and 1:2) was observed to depend on the length of the spacer separating the two carboxylate moieties and the nature of the receptor. The binding constants are summarized in table 4.

Table 4: Binding constants of the proposed 1:1 binding to 18-1, 18-2, and 18-3 [a,b].

Anion	Sensor 18-1	Sensor 18-2	Sensor 18-3
F⁻	4.13	3.03	3.30
Pyrophosphate	3.40	3.07	2.72
Malonate	2.34	3.15	2.66
Glutarate	3.74	3.27	3.77

[a] All measured in DMSO at room temperature and repeated 2 or more times. Using data from different wavelengths gave, on all occasions, the same binding constant within 5-10% error. [b] Determined using the equation: $\log [(I_{max} - I_F)/ (I_F - I_{max})] = \log [anion] - \log\beta$.

By modulation of the electronic structure of the receptor, the sensitivity of the recognition process could be modified; *e.g.* compound **18-1** bearing the trifluoromethyl substituent (figure 29), showed stronger binding to the anion and to the bis-anions than **18-2**, which only possesses a simple phenyl moiety.

It is known that the ICT photophysics and emissions are highly dependent of the electron donor / acceptor strength and in many cases dual fluorescence can been observed from the ICT fluorophores. Wen and coworkers [31] have been investigating possibilities to employ the ICT photophysics of *p*-dimethylaminobenzonitrile (DMABN) and analogues molecules in constructing anion receptors. They showed that for *p*-dimethylaminobenzoamide, *N*-(p-dimethylamino-benzoyl)thiourea and *N*-(p-dimethylaminobenzoamido)thiourea, in which the anion binding sites incorporated in the electron acceptors are amide and thiourea, respectively, the ICT dual fluorescence was sensitive to the presence of anions such as AcO⁻, F⁻, $H_2PO_4^-$, HSO_4^-, Br⁻ and Cl⁻.

The binding constants are listed in table 5. The binding constants ranging from 10^4 to 10^6 M^{-1} varied in the order of F⁻ > AcO⁻ > $H_2PO_4^-$ >> HSO_4^-, Br⁻, Cl⁻. With the same anion, the binding constants varied in the order of DGTU < DGTU-*p*-Cl < DGTU-*m*-Br < DGTU-*p*-CF₃ < DGTU-*p*-CN (figure 30), as expected from the increasing acidity of the thioureido –NH protons.

Table 5: Binding constants (K_{ass}) of anions with DGTU-Rs in acetonitrile from absorption (344 nm) and fluorescence (ICT / LE) titrations. [a]

Flu. sensor	F⁻-K_{ass}(abs)[b], 10^5 M^{-1}	AcO⁻K_{ass}(abs)[b], 10^5 M^{-1}	F⁻-K_{ass}(flu)[c], 10^4 M^{-1}	AcO⁻-K_{ass}(flu)[c], 10^4 M^{-1}
H	0.12 ± 0.02	nd [d]	0.22 ± 0.03	nd [d]
p-Cl	0.18 ± 0.03	nd [d]	0.40 ± 0.04	nd [d]
m-Br	0.24 ± 0.03	nd [d]	4.73 ± 0.55	1.33 ± 0.11
m-CF₃	1.47 ± 0.32	1.58 ± 0.14	9.74 ± 1.57	1.95 ± 0.36
p-CN	25.8 ± 7.1	3.60 ± 0.80	16.8 ± 5.2	8.41 ± 1.55

[a] Anions exits in their TBA salts. [b] Binding constants obtained from absorption titration. [c] Binding constants obtained from fluorescence titration. [d] Not determined because of minor spectral change that did not allow an accurate evaluation of binding constant. This was also the case for other anions examined such as $H_2PO_4^-$, HSO_4^-, Br⁻, and Cl⁻.
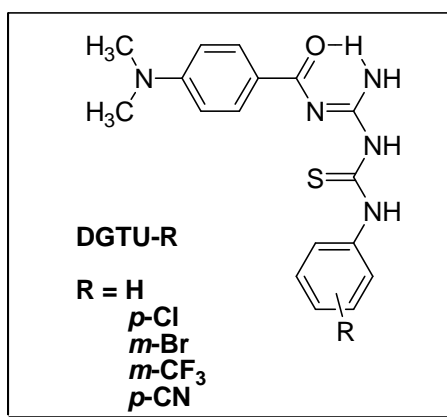
Figure 30: Molecular structures of DGTU-Rs 19

By substitution at the phenylthiourea moiety it was observed that the substituent electronic effect could be efficiently transmitted to the CT fluorophore and hence influenced its CT dual fluorescence.

The recognition of the anions involved a blue-shift in the CT emission and a decrease in the CT to LE (locally excited state) intensity ratio.

Fabbrizzi and coworkers [32] compared the H-bond donor tendencies of urea and thiourea and verified the occurrence of deprotonation processes in the presence of certain basic anions such as halides and carboxylates in DMSO solution. They used a phthalimide substituent as fluorophor. The phthalimide substituent has been appended at the urea or thiourea subunit in order to provide an optical signal for the occurrence of the receptor-anion interaction. The fluorescent sensor is shown in figure 31.
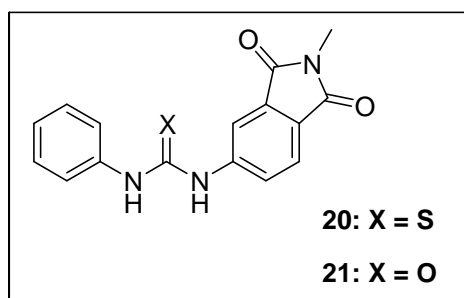
Figure 31: Fluorescence sensors based on thiourea 20 and urea 21 receptors

This study was performed via UV-*vis* and ^{1}H NMR tritration experiments in DMSO solution. It was found that two consecutive equilibria take place in solution, involving the neutral receptor LH and the anion X$^-$:

$$LH + X\text{-} \rightleftharpoons [LH\cdots X]\text{-} \tag{6}$$

$$[LH\cdots X]^- + X^- \rightleftharpoons L^- + [HX_2]^- \tag{7}$$
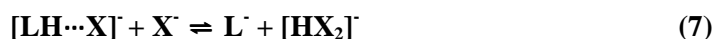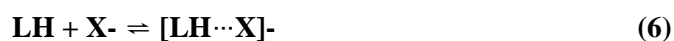
The first equilibrium (eq. 6) resulted in a more or less stable H-bond complex for all investigated anions. The second equilibrium (eq.7) is related to both the intrinsic acidity of HL and the stability of $[HX_2]^-$. The table shows that the receptor **21**, containing the less acidic urea subunit, undergoes the protonation and HX release only in the presence of F^-, to form the very stable $[HF_2]^-$ self-complex. On the other hand, the more acidic thiourea containing receptor **20** undergoes deprotonation in the presence of a greater number of anions, the value of the binding constants decreasing with stability of the self complex $[HX_2]$: $F^- > AcO^- > H_2PO_4^-$.

Table 6: Log$K$ values for the interaction of receptors 20 and 21 with the anions in DMSO solution at 25 °C.

Receptor	Equilibrium	F^-	AcO^-	$C_6H_5CO_2^-$	$H_2PO_4^-$	Cl^-
20	$LH + X^- \rightleftharpoons [LH \cdots X]^-$	5.7	6.02	5.77	5.44	4.88
	$[LH \cdots X]^- + X^- \rightleftharpoons L^- + [HX_2]^-$	5.5	3.23	3.36	0.55	—
21	$LH + X^- \rightleftharpoons [LH \cdots X]^-$	4.86	4.63	4.18	4.47	4.38
	$[LH \cdots X]^- + X^- \rightleftharpoons L^- + [HX_2]^-$	1.83	—	—	—	—

In summary the more acidic receptor **21** forms, with a given anion, a more stable complex than the less acidic receptor 22. This behavior is consistent with the view of hydrogen bonding as an incipient proton transfer from the receptor to the anion; where the more acidic the receptor, the stronger the H-bond with anion.

Chen and coworkers [33] designed and synthesized a series of fluorescent sensors integrating both an amide and a pyrrole functionality for anion-recognition and sensing. The recognition and sensing have been investigated through changes in the UV-*vis* and fluorescence spectra in the presence of anions. The mechanism for the reaction between the fluorescent sensors and the anions has been further explored by ^{1}H NMR titration experiments.

The fluorescent sensors are shown in figure 32. The authors were prepared by condensation of pyrrol-2-carbonyl chloride with the corresponding aryldiamine in CH_2Cl_2.

The anion sensing was carried out with 11 different anions (CN^-, F^-, Cl^-, Br^-, I^-, NO_3^-, OH^-, AcO^-, $H_2PO_4^-$, HSO_4^- and ClO_4^-) with all fluorescent sensors.

Fluorescent sensor **22** displays colorimetric and fluorescent responses only to OH^-, F^- and CN^-. **23** exhibited a strong response to CN^- and somewhat weakes responses to OH^-, AcO^- and $H_2PO_4^-$ in CH_3CN solution.

Addition of CN^-, OH^-, F^-, AcO^- and $H_2PO_4^-$ to **24** produced a color change from colorless to orange-red. Except for F^-, which apparently displays multiple equilibria in solution, a new band developed at around 480 nm on addition of CN^-, OH^-, AcO^- or $H_2PO_4^-$.

The spectrometric titrations of **25** and **26** with anions were carried out in DMSO solution because of the solubility issue. **25** and **26** responded only to CN^-, OH^-, F^-, and AcO^- to produce a color change from red to purple for **25** and colorless to pale yellow for **26**.
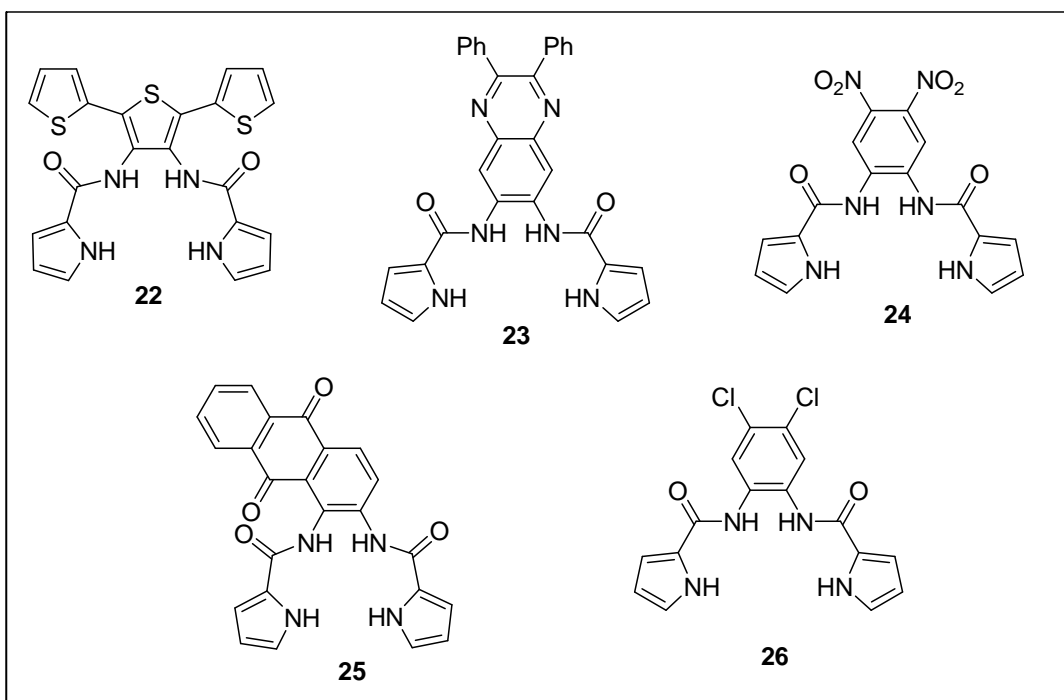
Figure 32: Fluorescent sensors 22-26

The formation of hydrogen-bonded complexes apparently exerts very little perturbation of the electron density distribution and thus, the absorption and fluorescence spectra show almost no or very little changes compared with the ^{1}H NMR spectra. The observations of a red shift in both absorption and fluorescence spectra generally imply that neat proton transfer occurs from the acidic amide NH group to the anion.

Cyanide is a nucleophilic anion, its addition on the **22**, **25** and **26** produced the deprotonation of the acidic NH group on this fluorescent sensors, addition of cyanide resulted in nucleophilic addition on the electron-deficient amide carbonyl group in the fluorescent sensors **23** and **24**.

The strong electron-withdrawing nature of the NO_2 or quinoxaline functionality renders the amide groups highly electron-deficient and susceptible to the nucleophilic addition by cyanide to the carbonyl groups along with a higher acidity of the amine groups. Nucleophilic attac of the cyanide in the vicinity of the amide carbonyl groups induces the potential hydrogen-bonding. The next figure shows the reaction of cyanide with **24**.
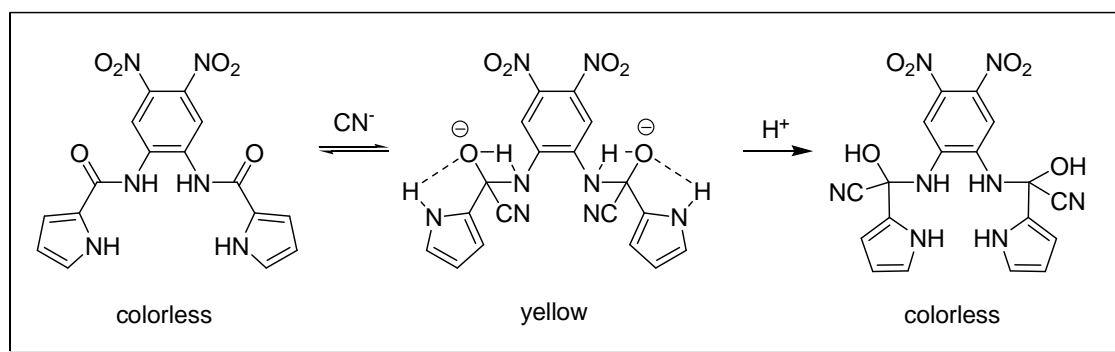
Scheme 3: Proposed cyanohydrin formation fronm reaction of probe 24 and cyanide

1.6.4 **Chiral recognition**

It is well known that chemical properties and biological activity of chiral compounds are strongly dependent on the absolute configuration; each enantiomer may have different pharmacological properties in terms of activity, potency, toxicity, transport mechanisms and metabolitic route. [34]

The development of artificial chiral receptors, which show properties of chiral recognition and chiral catalysis, has attracted considerable attention, because recognition and catalysis are fundamental characteristics of biochemical systems, and could contribute to the development of pharmaceuticals, enantioselective sensors, catalysts, enzyme models and other molecular devices.[35]

27a: R = CH₃, n = 2
27b: R = PhCH₂, n = 2
27c: R = CH₃, n = 3
27d: R = PhCH₂, n = 3
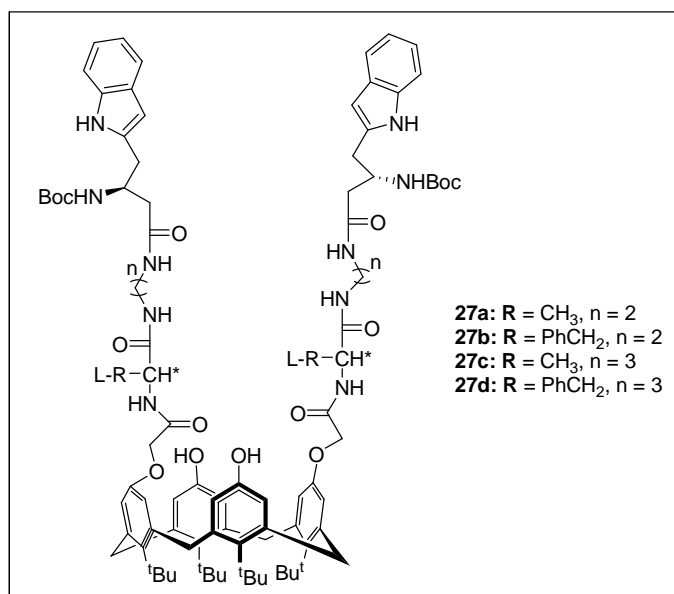
Figure 33: Fluorescent sensors 27a-d

Qing and coworkers [36] reported four two-armed chiral calix[4]arenes derivates (figure 33) bearing *L*-tryptophan units, which exhibit highly sensitive fluorescence response to

phenylglycinol and can discriminate phenylglycinol from phenylalaninol quickly trough the apparent difference in the fluorescence titration. They also have a good enantioselective recognition abilities towards phenylglycinol.

The authors observed a rapid increase of the fluorescence emission upon the addition of (*R*)-phenylglycinol, while the fluorescent intensity of **27d** at 456 nm showed an enhancement of about 800% with addition of 6.0 equiv. of guest molecule. The addition of (*R*)-phenylalaninol did not induce fluorescence enhancement. The intensity of **27d** at 450 nm only increased about 35% with the same amounts equiv. of the guest.

For the complex of 1:1 stoichiometry, an association constant K_{ass} can be calculated by using the following equation

$$I/I_0 = 1 + \frac{I_{\lim}/I_0 - 1}{2}\left[1 + \frac{C_A}{C_H} + \frac{1}{K_a C_H} - \sqrt{\left(1 + \frac{C_A}{C_H} + \frac{1}{K_a C_H}\right)^2 - 4\frac{C_A}{C_H}}\right] \quad (8)$$

where *I* represents the fluorescence intensity, and C_H and C_G are the corresponding concentrations of host and guest, respectively. C_0 is the initial concentration of the host. The association constants (K_{ass}) and correlation coefficients (R) obtained by non-linear least-squares analysis of *I* versus C_H and C_G are listed in table 7. The association constant of **27d** with (*R*)-phenylglycinol was 564.5 M^{-1}, while that of **27d** (*R*)-phenylalaninol was 91.2 M^{-1}, which demonstrated that **27d** has a good recognition ability between phenylglycinol and phenylalaninol.

Table 7: Association constants (K_{ass}) and enantioselectivities K_R/K_S of receptors 27a-d with *R/S*- phenylglycinol (Phegly) and *R/S*- phenylalaninol (Phe-ala) guest in CH_3CN and CH_3Cl at 25 °C.[a]

Guest	Receptor 27a		Receptor 27b		Receptor 27c		Receptor 27d	
	K_{ass} (dm³ mol⁻¹)[b]	K_R/K_S	K_{ass} (dm³ mol⁻¹)[b]	K_R/K_S	K_{ass} (dm³ mol⁻¹)[b]	K_R/K_S	K_{ass} (dm³ mol⁻¹)[b]	K_R/K_S
(*R*)-Phe-gly[c]	88.5 ±10.6	2.54	110.8± 10.6	0.77	145.7 ± 12.3	0.44	564.5 ± 51.5	2.00
(*S*)-Phe-gly[c]	34.9 ± 3.9		144.1 ± 4.5		331.2 ± 28.7		281.8 ± 23.4	
(*R*)-Phe-ala[d]	10.3 ± 1.5	1.98	18.6 ± 4.2	0.94	51.3 ± 9.8	0.41	91.2 ± 13.7	0.81
(*S*)-Phe-ala[d]	5.2 ± 0.8		19.7 ± 3.8		124.0 ±13.5		112.0 ± 9.8	
(*R*)-Phe-gly[e]	15.6 ± 2.4	2.44	16.8 ± 2.6	1.18	24.7 ± 3.5	0.17	223.4 ± 35.2	2.73
(*S*)-Phe-gly[e]	6.4 ± 1.3		14.2 ± 2.0		141.3 ± 3.5		81.9 ± 10.5	
(*R*)-Phe-ala[f]	5.7 ± 1.1	2.28	11.7 ± 1.9	1.43	27.3 ± 3.8	0.76	48.3 ± 6.3	1.63
(*S*)-Phe-ala[f]	2.5 ± 0.6		8.2 ± 1.2		35.6 ± 4.6		29.7 ± 2.9	

[a] The association constants of receptors 27a-d with R/S- phenylglycinol (Phegly) and R/S- phenylalaninol (Phe-ala) in DMSO were too small to be reliable. [b] The values were calculated based on the change of the fluorescence spectra. [c] R/S- phenylglycinol (Phegly) in CH_3CN. [d] R/S- phenylalaninol (Phe-ala) in CH_3CN. [e] R/S- phenylglycinol (Phegly) in CH_3Cl. [f] R/S- phenyl-alaninol (Phe-ala) in CH_3Cl.

The reason of this selective recognition may be that the two indole rings of **27d** are in close proximity and an intramolecular excimer is formed through the interaction of one indole in the excited state with the other indole in the ground state. When the phenylglycinol is added, the π–π stacking between the aromatic ring of phenylglycinol and the indole rings of receptor promoted energy transfer from the excited fluorophore to the other one in the ground state and an enhancement of fluorescence is observed.

Phenylalaninol could not induce such fluorescence enhancement probably because the aromatic ring of phenylalaninol is incapable of forming effective π–π stacking with the indole rings of the receptors molecule to promote the energy transfer between the two fluorophores. Such differences in the fluorescent response also prove that the π–π stacking is the most important factor in the fluorescence response upon complexation between the host and amino alcohol.

The receptors **27c** and **27d** exhibited better fluorescent response than the receptors **27a** and **27b**, which may be because the receptors **27c** and **27d** have a much more flexible structure compared with **27a** and **27b**. The flexible structures could enable the two indole rings to approach to closer proximity promote the energy transfer process more easily.

Solvent comparison experiments demonstrated that CH_3CN was the most effective solvent to detect the concentration of amino alcohol and to carry out the chemical recognition process.

Amino acids and their derivates are important components of chemical and biological systems and their recognition, in particular chiral recognition attracts considerable interest. Many examples in literature show that thiourea as receptors is able to form stable complexes with anions, some of them also exhibit good enantioselective recognition abilities towards various amino acid derivates. [37]

Qing and coworkers [37] synthesized three linear thioureas as anion receptors (**28-30**) from amino acids. Their bonding properties with various chiral *N*-protected amino acid anions have been examined by using UV-vis and fluorescence titration experiments in DMSO (figure 34).

Receptor **28** exhibited upon addition of the *N*-Boc-*L*-Ala anion a gradual decrease of the absorption maximum (at 360 nm) with red shift (about 10 nm) and a new absorption peak at 482 nm. The new absorption suggested the formation of a complex between **28** and *N*-Boc-*L*-Ala. Similar phenomena were observed when *N*-Boc-*D*-Ala was added to the solution of receptor **28**.

There are differences in the absorbance spectra and the color of the solution indicates that **28** has a good enantioselective recognition ability towards the *N*-Boc-D/*L*-Ala anions. In addition the association constants (K_{ass}) are different, which corresponds to moderate enantioselectivity ($K_{ass}(L)/K_{ass}(D)$) of 2.7.
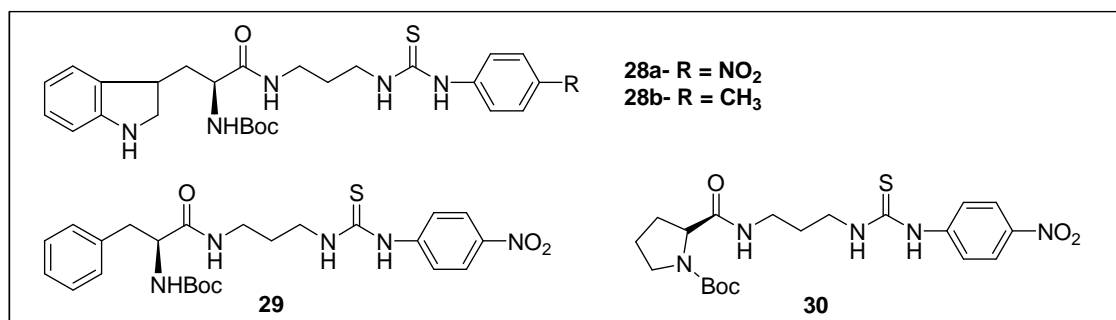
Figure 34: Fluorescent sensors 28a-b, 29 and 30

The fluorescence emission (λ_{ex} = 295 nm; λ_{em} = 347 nm) of the receptor **28a** in the presence of the *N*-Boc-*D*-Ala or *N*-Boc-*L*-Ala anion in DMSO increases gradually. The result is a nonlinear curve that confirms the interaction between receptor **28a** and *N*-Boc-*D*-Ala to form a 1:1 complex. The data of these chiral recognitions systems is summarized in table 8.

Comparative UV-vis and fluorescence experiments were performed to explore whether receptors **29** and **30** have the similar recognition abilities.

Table 8: Association constants (K_{ass}) and enantioselectivities K_D/K_L of receptor 28a with
***D/L*-monocarboxylate in DMSO at 25 °C.**

Guest[a]	K_{ass} (dm^3 mol^{-1})[b,c]	K_D/K_L
N-Boc-*L*-Ala	192.7 ± 6.1	
N-Boc-*D*-Ala	519.7 ± 13.4	2.70
N-Ac-*L*-Ala	79.9 ± 8.6	
N-Ac-*D*-Ala	578.3 ± 31.5	7.24
N-Bz-*L*-Ala	[d]	
N-Bz-*D*-Ala	[d]	
N-Boc-*L*-Phe	347.2 ± 24.1	
N-Boc-*D*-Phe	83.3 ± 8.8	0.24
L-mandelate	303.7 ± 8.9	
D-mandelate	619.5 ± 13.8	2.04
L-phenylglicine	(1.52 ± 0.07) x 10^3	
D-phenylglycine	(4.62 ± 0.24) x 10^3	3.04

[a] The anions were used as their tetrabutylammonium salts. The amino groups of the amino acid were protected by *tert*-butylcarbonate, acetyl or benzoyl respectively.[b] The data were calculated from UV-vis titration in DMSO. [c] All error values were obtained by results of nonlinear curve fitting, the correlation coefficient (*R*) of nonlinear curve; fitting is over 0.99. [d] Reliable association constants could not be obtained due to the too small change in the UV-vis spectra.

Receptor **28a** was developed to give strong hydrogen bonding to anions, which could rise to colorimetric changes upon anion recognition; the 4-nitro-phenyl moiety is part of amidothiourea

anion receptor moiety, giving rise to an internal charge transfer (ICT) absorption band in the absorption spectra.

In the absence of anions, the photoinduced electron transfer (PET) process between the indole group and weak electron withdrawing amide substituents results in a decreasing fluorescence intensity. When the anions were added to the solution, the interaction of the anion with receptor unit could erase this specific PET progress and induce fluorescence recovery. Therefore, anion induced fluorescence enhancement was observed.

Huang and coworkers [34] reported two chiral fluorescent receptors **31a** and **31b** (figure 35) bearing anthracene, amino acid and thiourea units, which were conveniently synthesized in a few steps and in good yields. Their enantioselective recognition of malete, aspartate and glutamate were studied by fluorescence emission, UV-vis absorption in DMSO solution, and ^{1}H NMR spectra.
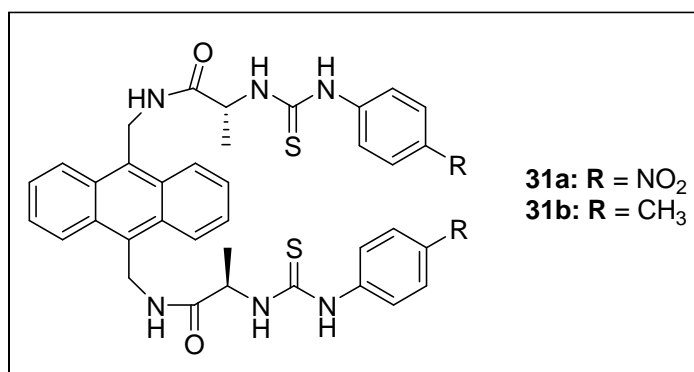
Figure 35: Fluorescent sensor 31a-b

The recognition of *L*-malate in DMSO with the fluorescent sensor **31a** showed a decrease of the fluorescence emission intensity at 429 nm, while it was enhanced at 538 nm, when gradually increasing the concentration of the anions. The dual fluorescence peaks may be due to the locally excited (LE) state and charge transfer (CT) state in equilibrium.

When the receptor binds anions, hydrogen bonds are formed leading to the corresponding complexes. Therefore, formed electron density in the supramolecular system is increased to enhance the charge-transfer interactions between the electron-rich donor nitrogen of the thiourea units and the electron-deficient *p*-nitophenyl moieties.

The changes in fluorescence emission and UV-vis spectra with different concentrations of *D*-malate were similar. Addition of *L*-malate to a solution of **31a** led the same effect but weaker compound to *D*-malate. The quenching efficiencies ($\Delta I_L / \Delta I_D = 1.67$) indicated that the receptor **31a** has a good enantioselective recognition ability for *D/L*-malate. In addition, the association contants (K_{ass}) are different; the association constant of **31a** with *L*-malate is 3.62 x 10^4 M^{-1},

while that of **31a** with *D*-malate is 3.75 x 10^3 M^{-1}, thus the enantioselectivity ($K_{ass}(L)$ / $K_{ass}(D)$) is 9.65 for malate. These obvious changes in fluorescence and UV-vis spectra show that **31a** has an excellent chiral recognition ability towards the enantiomers of malate. The corresponding association constants (K_{ass}) of interaction between host and guest are listed in table 9.

Table 9: Association constants (K_{ass}) of 31a and 31b with the chiral dicarboxylate anions in DMSO.

Guest	Receptor 31a		Receptor 31b	
	K_{ass} (M)$^{-1b}$	K_I/K_D	K_{ass} (M)$^{-1b}$	K_I/K_D
L-malate	(3.62 ± 0.25^c) x 10^4		(5.18 ± 0.26^c) x 10^3	
D-malate	(3.75 ± 0.33^c) x 10^3	9.65	(2.38 ± 0.32^c) x 10^3	2.18
L-aspartate	(2.90 ± 0.17^c) x 10^4		(9.91 ± 0.17^c) x 10^3	
D-aspartate	$(5.11 \pm 0..24^c)$ x 10^3	5.68	(2.45 ± 0.23^c) x 10^3	4.04
L-glutamate	(1.78 ± 0.48^c) x 10^4		(6.13 ± 0.15^c) x 10^3	
D-glutamate	(8.24 ± 0.33^c) x 10^3	2.16	(2.50 ± 0.34^c) x 10^3	2.45

[a] The anions were used as their tetrabutylamonium salts. [b] The data were calculated from results of fluorescence titrations in DMSO. [c] All error values were obtained by results of nonlinear curve fitting.

When *D/L*-malate interacts with the receptor of **31b**, a PET process is involved. Fluorescence quenching and the changes in the absorption spectra of the anthracene moiety confirms that the PET process occurs with anion binding.

The value of the association constant of **31b** with *L*-malate is 5.18 x 10^3 M^{-1}, while that of **31b** with *D*-malate is 2.38 x 10^3 M^{-1}, which corresponds to a *L/D*-selectivity ($K_{ass}(L)$ / $K_{ass}(D)$) of 2.18.

The variations of fluorescence emission and absorption spectra of **31b** in the presence of *D/L*-aspartate and glutamate were similar to that observed for **31b** with *D/L*-malate, which implies that the PET process occurred with anion binding. All results are summarized in table 9.

The steric effect of the receptors, structural complementarity with guests, and multiple hydrogen bonding may be responsible for the enantioselective recognition. Sensitive fluorescent response and good enantioselctive recognition ability reveals that **31a** can be used as fluorescent chemosensor for malate.

In addition Huang and coworkers [38] reported four chiral fluorescent sensors **32a-d** containing thiourea and amine groups. Their enantioselective recognition towards α-phenylglycine and phenylglycinol in DMSO was studied by fluorescence emission and UV-vis absorption spectra.
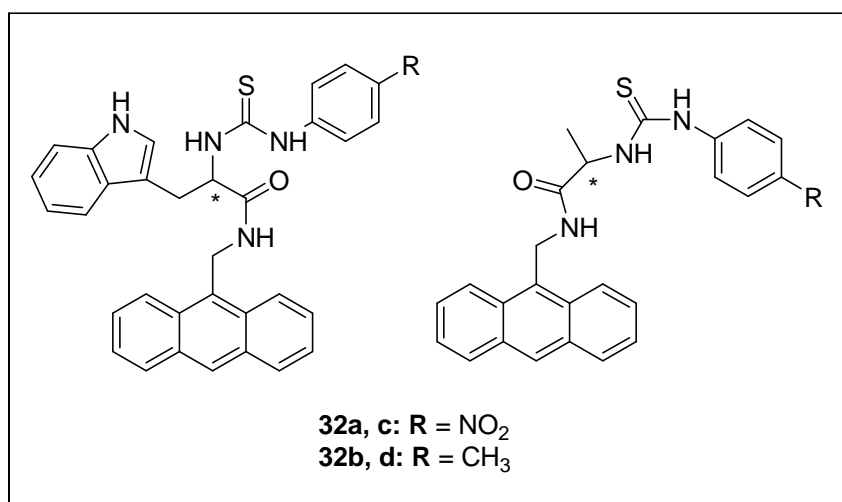
Figure 36: Fluorescent sensor 32a-d

At higher concentrations of *D/L*-phenylglycine, the fluorescence emission intensity gradually increased which indicates a complexation between **32a** and the anions. In the absence of anions, the photoinduced electron transfer PET process between the anthracene group and the weak electron-withdrawing amide substituents might result in decreased fluorescence intensity. Upon addition of anions, the interaction between the anion with the NH-group of thiourea and indole could diminish the PET progress to induce fluorescence retrieval. Therefore, anion-induced fluorescence enhancement was observed.

The different increasing efficiencies ($\Delta I_L / \Delta I_D = 1.8$) indicate that receptor **32a** has a good enantioselectivitve recognition ability between *L/D*-α-phenylglycine. The UV-vis spectra show a gradual decrease of the absorption intensity at 370 nm and a new absorption band at 475 nm upon decreasing the concentration of *L/D*-α-phenylglycine. This can be explained by expansion of the conjugative system as a result of an intermolecular charge transfer (ICT) process. An isosbestic point at 393 nm was observed, indicating the formation of a host-guest complex. Similar but smaller variations in the fluorescence and absorption spectra were observed when **32a** interacted with *L/D*-phenylglycinol. The data for all anions with the fluorescent sensor are summarized in table 10.

The association contants of **32a** and **32c** are always much higher compared to **32b** and **32d** with the corresponding anions. The results demonstrated that the introduction of an electron-withdrawing substituent (NO_2) enhances the acidity of NH group of thiourea, which provides an effective intramolecular charge transfer and enhances the hydrogen bond ability.

Table 10: Association constants (K_{ass}) and enantioselectivities (K_L/K_D) for the complexation of receptors 32a-d with *L/D*-phenylglycine (Phegly) and phenylglycinol (Pho) in DMSO at 25 °C.

Guest	Receptor 32a		Receptor 32b		Receptor 32c		Receptor 32d	
	K_{ass} (M)$^{-1a,b}$	K_L/K_D	K_{ass} (M)$^{-1a,b}$	K_L/K_D	K_{ass} (M)$^{-1a,b}$	K_L/K_D	K_{ass} (M)$^{-1a,b}$	K_L/K_D
L-Phegly[c]	$(2.96 \pm 0.16) \times 10^4$	5.63	$(8.12 \pm 0.15) \times 10^3$	2.49	$(1.83 \pm 0.13) \times 10^4$	3.53	$(3.86 \pm 0.25) \times 10^2$	2.10
D-Phegly	$(5.26 \pm 0.25) \times 10^3$		$(3.26 \pm 0.32) \times 10^3$		$(5.18 \pm 0.19) \times 10^3$		$(1.84 \pm 0.12) \times 10^2$	
L- Pho	$(4.85 \pm 0.02) \times 10^3$	4.29	$(3.32 \pm 0.16) \times 10^2$	2.17	$(3.10 \pm 0.41) \times 10^3$	3.38	$-^d$	
D- Pho	$(1.13 \pm 0.12) \times 10^3$		$(1.53 \pm 0.21) \times 10^2$		$(9.17 \pm 0.32) \times 10^2$		$-^d$	

[a] The data were calculated from results of fluorescence titrations in DMSO. [b] All error values were obtained by the results of nonlinear curve fitting. [c] The anions were used as their tetrabutylammonium salts. [d] The change of fluorescence spectra is minor, so the association constants can not be calculated.

Liu and coworkers [39] reported the synthesis of 1,8-bis(3-*tert*-butyl-9-acridyl)naphthalene *N,N*-dioxide, **33** (figure 37) from 3-*tert*-butylaniline and 2-chlorobenzoic acid in five steps with 29% overal yield. The product was used for fluorescence and absorption chiral recognition of amino alcohols. The capacity of these chemosensors for enantioselective recognition of amino acids, carboxylic acids and other chiral hydrogen bond donors has been attributed to the flexibility of the cofacial heteroaryl rings in 1,8-diheteroarylnaphthalenes with the naphthalene framework. The torsion angle can change over a range of 50°, in particular upon binding to a guest molecule.
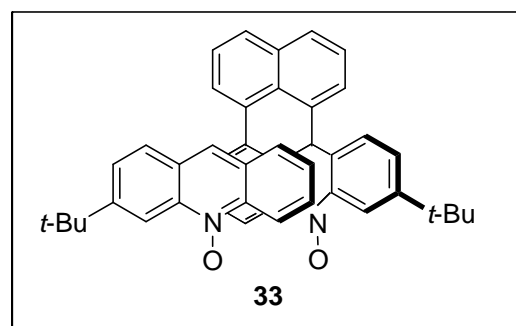

Figure 37: Fluorescent sensor 33

The fluorescence emission is increased by stoichiometric amounts of Sc(OTf)$_3$ but this is not the case in the presence of other metals ions, such as Cu(OTf)$_2$, Zn(OTf)$_2$, Yb(OTf)$_3$, Sn(OTf)$_2$, and In(OTf)$_2$. The authors realized that the fluorescence emission of the scandium *N,N´*- dioxide complex at 588 nm disappeared upon addition of amino alcohols such as alaninol.

The titration of alaninol or other amino alcohols to the Sc[(+)-**33**]$_2$ would result in the replacement of the first *N,N´*-dioxide ligand from the metal center by *D/L*- alaninol and generate the respective diastereomeric complex. Because the ligand exchange proceeds via diastereoisomeric scandium complex intermediates, one enantiomer of alaninol was expected to

be more effective in displacing *D*-alaninol than *L*-alaninol. As a result, the fluorescence signal of the *N,N′*-dioxide-derivate scandium complex could be exploited for sensing purposes.

Chiral recognition requires multiple-point interaction. [40] Chi and coworkers [41] developed a mono boronic acid by using an additional interaction, *i.e*. hydrogen bonding. This compound showed enantioselectivity towards mono α-hydroxyl acids. Using this concept the authors reported two photoinduced electron transfer (PET) chiral sensors **34** and **35** (figure 38).
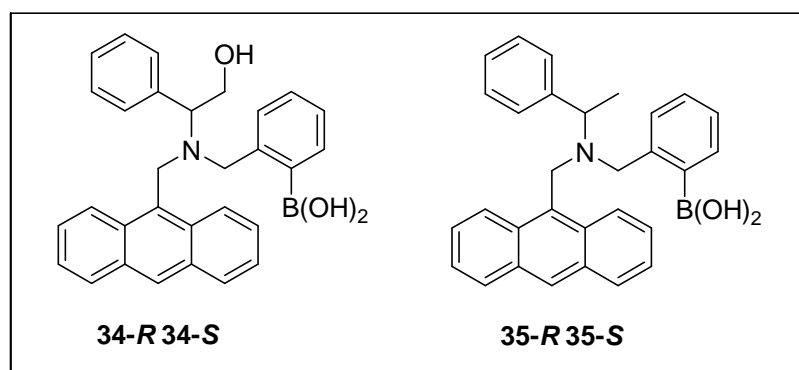

34-*R* 34-*S*   **35-*R* 35-*S***

Figure 38: Chiral fluorescent sensors 34 and 35

Enantioselective fluorescence enhancement was observed for **34-*S***. An association constant (K_{ass}) of 5.04×10^3 M^{-1} was observed for *D*-mandelic acid, versus K_{ass} of 2.77×10^3 M^{-1} for *L*-mandelic acid, which corresponds to *D/L*-selectivity ($K_{ass}(D) / K_{ass}(L)$) of 1.8 for mandelic acid. A mirror effect was observed for the **34-*R*** with the pair *D/L*- mandelic acid and the selectivity was $K_{ass}(L) / K_{ass}(D) = 2.7$. Chemosensor **35** is not enantioselective for mandelic acid.

The authors inferred that the hydroxyl group in **34** is essential for the enantioselectivity, because this additional intramolecular hydrogen bond increases the enantioselectivity.

For lactic acids, the enantioselective recognition is more challenging because the methyl group is less bulky than the phenyl group in mandelic acid, and the minor steric hindrance may attenuate the enantioselectivity. However, the titration of *D/L*-lactatic acid into **34** shows selectivity in a factor of 2.8 of *D*-lactic acid over *L*-lactic acid. With **35**, no enantioselectivity was found.

The recognition of **34** and **35** toward chiral acids is summarized in table 11.

Table 11: Association constants (K_{ass}) and enantioselectivities K_D/K_L of sensors D/L- 34 and 35 with α-hydroxy acids.

Guest	Receptor D-34		Receptor L-34		Receptor D-35		Receptor L-35	
	K_{ass}(M)$^{-1a}$	K_D/K_l	K_{ass} (M)$^{-1a}$	K_D/K_l	K_{ass} (M)$^{-1a}$	K_D/K_l	K_{ass} (M)$^{-1a,}$	K_D/K_l
D-mandelic acid	$(2.11 \pm 0.15) \times 10^3$	2.66	$(5.04 \pm 0.77) \times 10^3$	0.54	$(4.20 \pm 0.02) \times 10^4$	1.03	$(4.29 \pm 0.03) \times 10^4$	1.04
L-mandelic acid	$(6.62 \pm 0.64) \times 10^3$		$(2.77 \pm 0.57) \times 10^3$		$(4.34 \pm 0.02) \times 10^4$		$(4.49 \pm 0.03) \times 10^4$	
D- lactic acid	$(4.46 \pm 0.57) \times 10^2$	2.35	$(1.26 \pm 0.21) \times 10^3$	0.37	$(1.63 \pm 0.07) \times 10^4$	0.83	$(1.74 \pm 0.08) \times 10^4$	0.80
L- lactic acid	$(1.05 \pm 0.14) \times 10^3$		$(4.72 \pm 0.82) \times 10^2$		$(1.36 \pm 0.07) \times 10^4$		$(1.40 \pm 0.07) \times 10^4$	
D-tartaric acid	$(8.51 \pm 0.13) \times 10^3$	0.92	$(8.88 \pm 0.40) \times 10^3$	0.94	$(3.25 \pm 0.14) \times 10^4$	0.99	$(3.35 \pm 0.12) \times 10^4$	0.96
L-tartaric acid	$(7.90 \pm 0.37) \times 10^3$		$(8.42 \pm 0.31) \times 10^3$		$(3.24 \pm 0.12) \times 10^4$		$(3.22 \pm 0.14) \times 10^4$	

[a] Constant determined by fitting a 1:1 binding model I/I_0.

The enantioselectivity of **34** towards chiral mono α-hydroxy acids may be result of the additional hydrogen binding of the hydroxyl group to the boron center. Recognition of **34** in aqueous solution was carried out, but no enantioselectivity was found.

1.6.5 Hydrogen peroxide recognition

Hydrogen peroxide (H_2O_2) is an essential oxygen metabolite in living systems and increasing evidence supports its role as a messenger in cellular signal transduction. However, overproduction of H_2O_2 and other reactive oxygen species (ROS) from the mitochondrial electron transport chain leads to oxidative stress and the subsequent functional decline of organ system. Accumulation of oxidative damage over time is connected to debilitating human diseases where age is a risk factor, including Alzheimer´s and related neurodegenerative diseases, as well as cardiovascular disorders and cancer.[42]

In industry hydrogen peroxide it also an important product, the current global production of hydrogen peroxide is *ca*. 2.1 x 10^6 ton per year. It is used in many areas including the bleaching of wood pulp and paper, the treatment of industrial wastewaters and effluent, in food and pharmaceuticals industry as a bleach and disinfectant.

The limit for inhalation of H_2O_2 vapor is set to 1 ppm and the concentration levels over 7 ppm are known to cause lung irritation. The high concentration of H_2O_2 in aqueous solutions that are commonly used in industry (greater than 10% w/v) is very oxidizing and corrosive upon contact, causing severe burns to mucus membranes, gastrointestinal mucosa, skin and eyes. [43]

Above roughly 70% concentration, hydrogen peroxide can give off vapor that can detonate above 70 °C (158 °F) at normal atmospheric pressure. [44]

Detection and analysis of explosive materials and formulations has become an integral part of national and global security. The lack of robust low-power portable detection devices for the rapid on-site screening of both common and suspicious chemicals, materials, cargo and persons, has driven the need for improved sensor devices, such as photoluminescence sensors. However, improvised peroxide explosives are not detectable by these technologies. [45]

The following part will present some new approaches for the detection of H_2O_2.

Chang and coworkers [46] designed a cellpermeable optical probe for H_2O_2 using 3´,6´-bis(pinacolatoboron)fluoran **36** (scheme 4). This specific dye contains arylborante groups, which were converted into phenols upon interaction with the peroxide. This compound is nonfluorescent under physiological conditions (pH = 7) and does not absorb in the visible spectral range due to its lactone form. Exposure to H_2O_2 causes the hydrolytic deprotection of the boronate functions and generates the open colored fluorescein. This gradually leads to an increase in fluorescence intensity at around 510 nm when excited at 450 nm. They evaluated the probe in living cells and confirmed that the compound responds to H_2O_2 in the micromolar range.
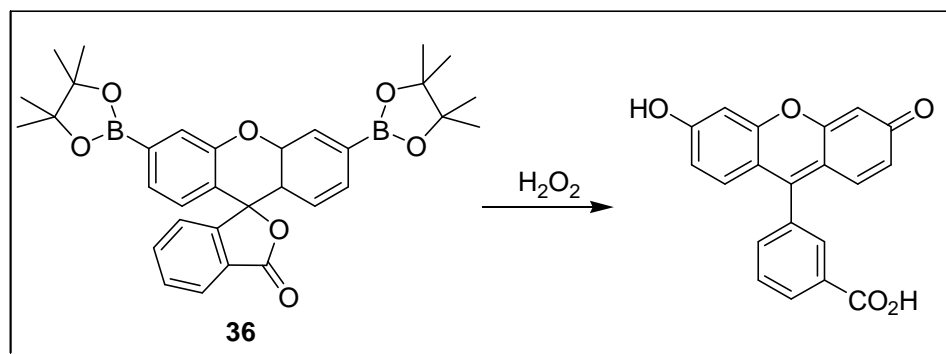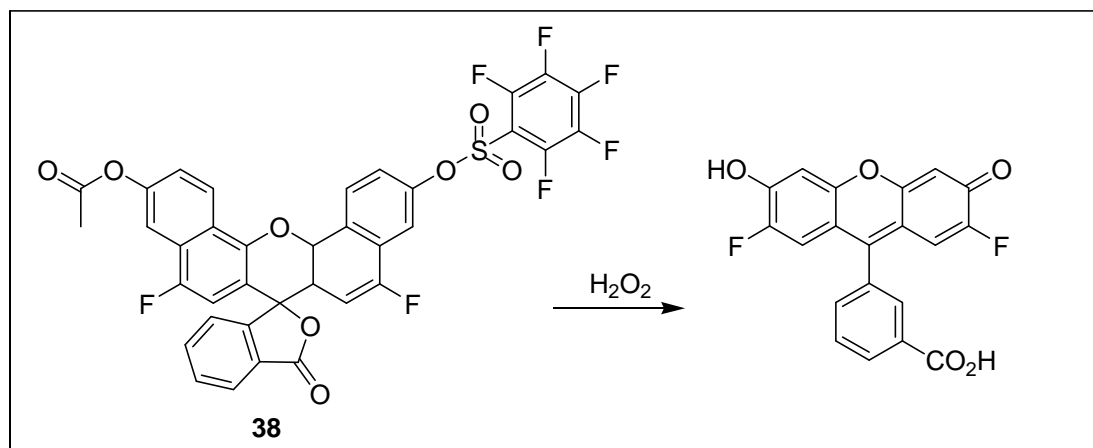
Scheme 4: Raction between 36 and hydrogen peroxide

Xu and coworkers [46] synthesized naphthofluorescein disulfonate with the aim to shift the absorbance and fluorescence into the near infrared spectral range and to enhance sensitivity. The initial dye is a colourless lactone, and a hydrolytic deprotection of the naphthofluorescein disulfonate **37** (scheme 5) by H_2O_2 causes the formation of a coloured and fluorescent naphthofluorescein with a fluorescence maximum at 662 nm (excitation at 602 nm). It exhibited good selectivity also in the presence of interfering species such as ascorbic acid, glutathione, hypochloride or hydroxyl radical and could be applied for monitoring nanomolar concentrations of H_2O_2 in living cells.
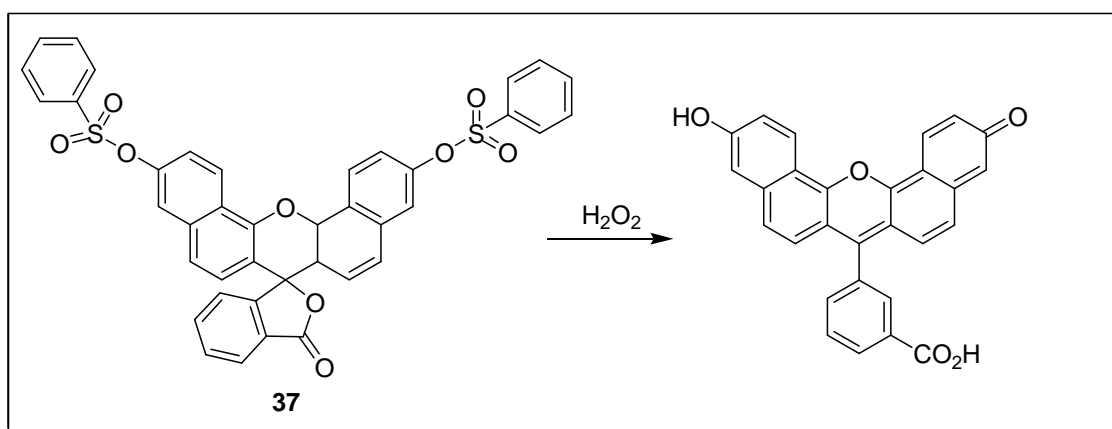

Scheme 5: Reaction between 37 and hydrogen peroxide

Maeda and coworkers [46] reported the synthesis of comparable fluorescein derivates with chloro- and fluoro substituents e.g.compound **38** (scheme 6) and observed similar selectivity (5 pmol to 90 nmol hydrogen peroxide), albeit the fluorescence increases at around 514 nm when excited at 492 nm.

**Scheme 6: Reaction between 38 and hydrogen peroxide**

RPF1 presents a single absorption band at 420 nm, with blue-colored fluorescence from a corresponding emission band at 464 nm. The spectral date is consistent with minimal FRET from the coumarin donor to the closed form of the colorless fluoran acceptor. Upon treatment with H_2O_2, excitation at 420 nm produces a bright green-colored fluorescence. The resulting emission spectrum possesses one major band centered at 517 nm with a minor band at 461 nm, consistent with increased FRET from the coumarin donor to the open form of the colored fluorescein acceptor. The fluorescence response is accompanied by concomitant growth of a visible wavelength absorption band characteristic for fluorescein, and high-resolution mass spectrometry confirms that pedant fluorescein is generated from the reaction between RPF1 and H_2O_2.
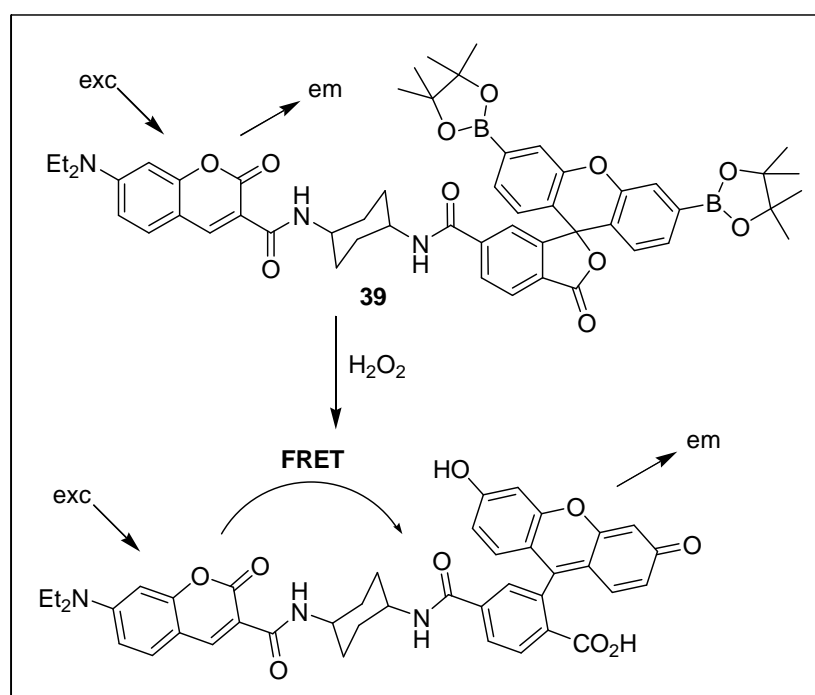
Scheme 7: Activation of Ratio-Peroxyfluor-1, RPF-1 or 39

This FRET-based reagent features good selectivity for H_2O_2 over competing ROS (reactive oxygen species) as well as visible wavelength excitation and emission profiles to minimize damage and autofluorescence from biological samples.

Mills and coworkers [43] prepared a dye ion-pair complex of tris(2,2´-bipyridyl)-ruthenium(II)ditetraphenylborate, $[Ru(bpy)_3{}^{2+}(Ph_4B^-)_2]$ to improve the detection of H_2O_2. This recognition was carried out by recording the UV-vis and fluorescence spectra.

$$H_2O_2 + 2Ru(bpy)_3{}^{2+} \rightarrow 2Ru(bpy)_3{}^{3+} + 2\ OH^-$$
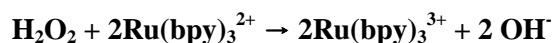
The main feature of this system is the one-pot formulation of a coating ink that, when dried, forms an active, single-layer, fluorescence-based H_2O_2 sensor capable of detecting H_2O_2 over the range 0.01-1 M.

1.7 Phthalimides as chromophore

The photopysical properties of phthalimides have been intensively studied over the last decades. Phthalimides show a relatively unstructured UV absorption spectra with absorption maxima around 220 nm (π, π^*) and 295 nm (n, π^*), respectively. The fluorescence properties are sensitive to solvent polarity and in protic solvents, also to hydrogen bonding. In general, phthalimides show a broad structureless phosphorescence centered around 450 nm with a triplet lifetime between $\tau_p = 0.7\text{-}1.06$ s at -196 °C and between 2 and 10 µs at room temperature in the absence of oxygen. Quantum yields of phosphorescence were measured in the range of $\Phi_p = 0.3 - 0.7$. The order of the excited states of phthalimides has been controversially discussed. The level of the (n, π) triplet state is either slightly below or above the lowest singlet state which accounts for the high intersystem crossing rates. [47]

4-Amino-*N*-methylphthalimide (4-AMP) (figure 39:) fluorophore has been described as convenient solvatochromic fluorescent dye because of its high fluorescence quantum yield, sensitivity of the fluorescence parameters to the added reagents and surounding environment and electron-deficient nature. [48]
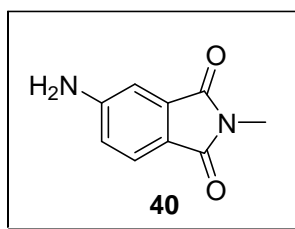

Figure 39: 4-Amino-*N*-methylphthalimide (40)

Recently, Fabbrizzi and coworkers [32] have used urea / thiourea-phthalimide derivates as chemosensors, where binding tendencies of the sensor towards anions were investigated by UV-vis and ^{1}H NMR titration. More recently, Samanta and coworkers [48] have studied the behavior of an amido-phthalimide derivate in the absence / presence of halide ions, suggesting that F$^-$ induces deprotonation of the urea moiety of the sensor system as a signaling mechanism.
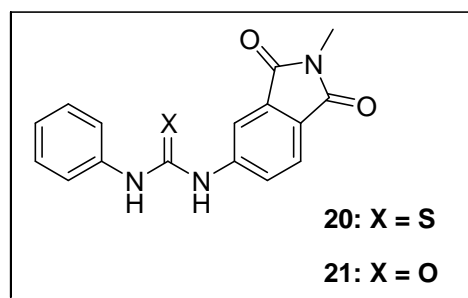

Figure 40: Fluorescence sensors base on thioure 20 and urea 21 receptors

1.8 Multicomponent reactions

The usual procedure for the synthesis of organic compounds is the stepwise formation of the individual bonds in the target molecule. Multicomponent reactions (MCRs) would be a much more efficient route to the target compounds as they offer significant advantages over stepwise procedures, especially with respect to environmental sustainability, practicability and atom efficiency. Compared to stepwise procedures, the most evident benefit of multicomponent reactions lies in the inherent formation of several bonds in one operation without isolation of the intermediates, changing the reaction conditions or addition of any further reagents. [49]
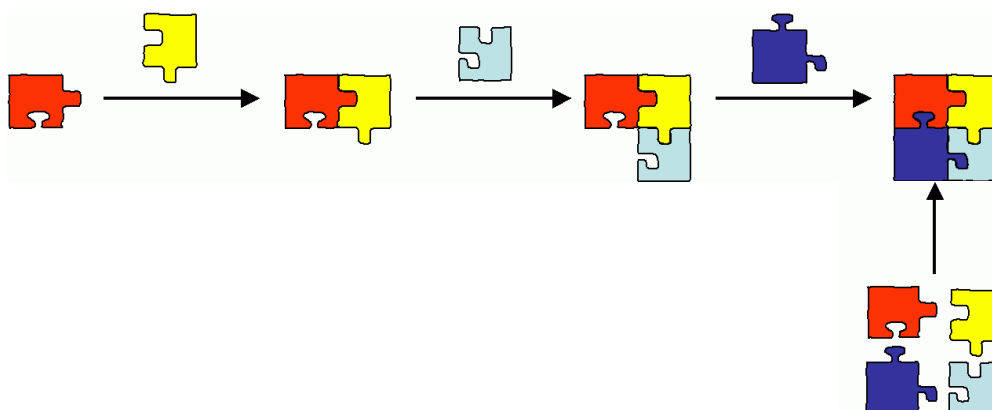

Figure 41: Chemistry jigsaws: Multi-step (top) or multicomponent (bottom) assembly of the same compound

Prominent examples of MCRs are the Strecker reaction, the Hantzsch pyrrole synthesis, the Biginelli synthesis of dihydropyrimidines, the Mannich reaction, and the Ugi MCR. [49]

The Diels-Alder reaction is one of the most powerful tools in the synthesis of complex organic molecules by virtue of its versatility atom-economy and stereocontrol. Therefore, it establishes a favourable transformation in efficient organic synthesis. MCRs based on Diels-Alder chemistry have highly efficient one-pot methodologies. [50]

Beller and coworkers [49] discovered a new multicomponent methodology in which **a**mides and **a**ldehydes react with **d**ienophiles (**AAD** reaction) to give a large variety of 1-acyl-amino-2-cyclohexene derivates. The AAD reaction involves 1-(*N*-acylamino)-1,3-butadienes as key intermediates, which are generated in the initial condensation step and subsequently trapped by dienophiles in a Diels-Alder reaction (scheme 8).
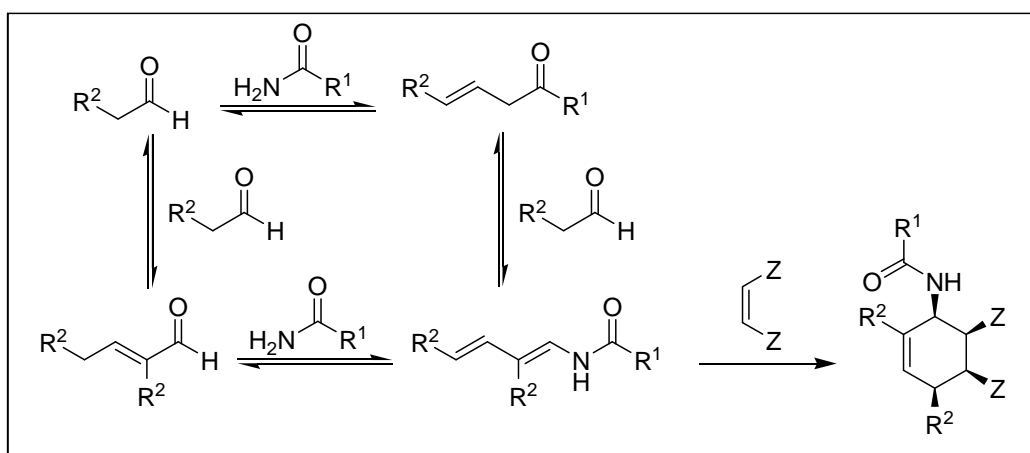

Scheme 8: Three-component coupling reaction of amides, aldehydes and dienophiles

The following part presents MCRs employing simple aldehydes, carboxamides and electron-deficient dienophiles.

1.8.1 One-pot reactions with dienophilic acetylendicarboxylates

The application of highly electron-deficient dialkyl acetylenedicarboxylates as dienophiles affordes 1-acylaminocyclohexa-2,4-diene derivates via the typical condensation Diels-Alder reaction sequences in good yields, as shown in table 6. Jacobi *et al*. obtained adducts that via concomitant double bond shift give a conjugated diene moiety (scheme 7). The double bond migration is subjected to thermodynamic control and thereby promoted the formation of the more stable *trans* isomer.[50]
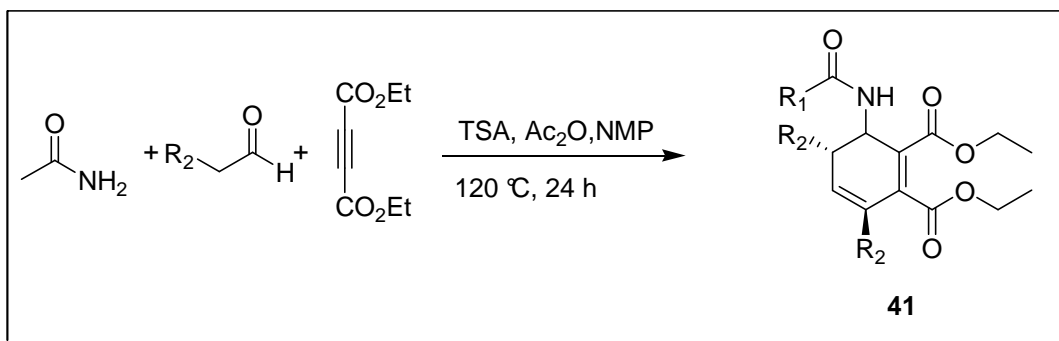
Scheme 9: One-pot reaction of aldehydes, carboxamides and diethyl acetylendicarboxylate

Table 12: Substituent of the one-pot reaction of aldhydes, carboxamides and diethyl acetylenedicarboxylate and the yield of each reaction

R^1	R^2	Yield (%)
Me	Me	69
Me	Et	84
Me	*i*-Pr	74

## 1.8.2 One-pot reactions with dienophilic maleimide and methyl maleimide

In general, the synthesis of 4-(*N*-acetylamino)-5,7-dimethyl-1,3-dioxo-*cis*-2,3,3a,4,7,7a-hexahydro-1H-isoindole (**42**) can be realized via two different routes that are shown in scheme 10. The target compound **42** is accessible *via* a one-pot protocol which obviates the need for intermediate workup and purification procedures.
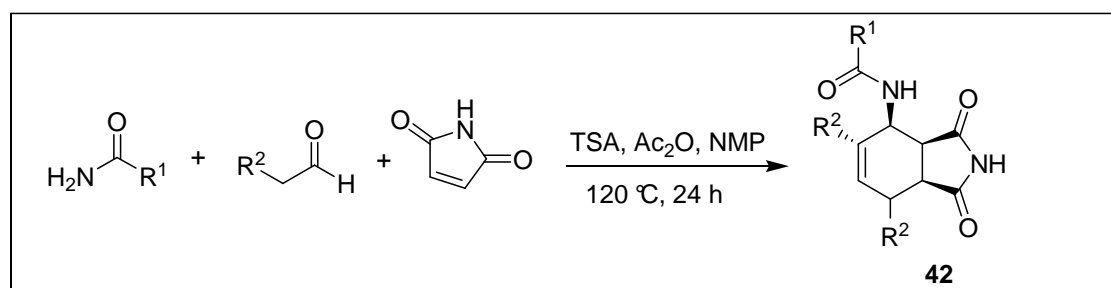
Scheme 10: One-pot synthesis of Diels-Alder aducct

The multicomponent route indeed afforded (**42**) in excellent yields. With more than the twice yield, this one-pot approach outperforms the two-step route in efficiency as well as in simplicity and involves nearly quantitative formation of intermediate aminodiene.

The combination of the MCRs of *O*-benzyl carbamate, aldehydes and maleimide as dienophilic produces the precursor of luminol derivates (scheme 11)
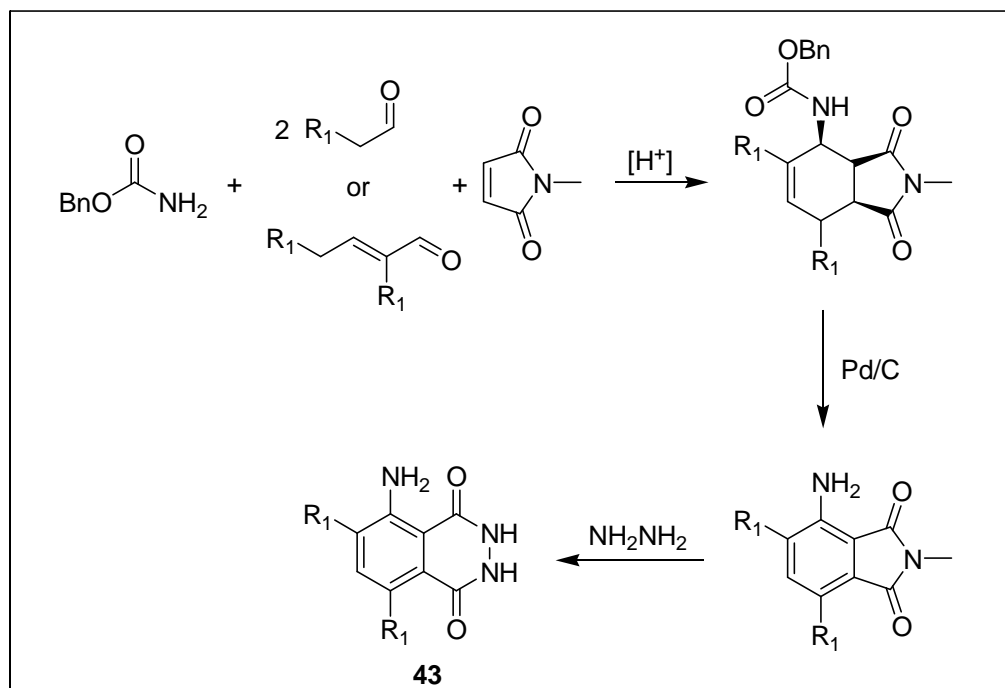
**Scheme 11: Three-step synthesis of substituted luminol derivates**

A palladium catalyzed aromatization of the three-component coupling products (product of the MCRs), which is based on a new intramolecular transfer hydrogenation reaction produces deprotection-aromatization of the MCRs products and allows the synthesis of polysubstituted anilines with diverse substitution patterns. [51] With the 3-aminophthalimide and its derivates (product of the deprotection-aromatization) different luminol derivates were synthesized by the reaction with hydrazine. [51]

1.9 Chemoluminescence

The number of chemical reactions that produce chemoluminescence is small, thus limiting this procedure to a relatively small number of species. Nevertheless, some of the compounds that do react to give chemoluminescence are important components in nature.

Chemoluminescence is produced when a chemical reaction yields an electronically excited species which emits light as it returns to its ground state. Chemoluminescence reactions are encountered in a number of biological systems, where the process is often termed bioluminescence.

Over a century ago, it was discovered that several relatively simple organic compounds also are capable of exhibiting chemoluminescence. The simplest type of reaction of such compounds to produce chemoluminescence can be formulated as

$$A + B \rightarrow C^* + D$$

$$C^* \rightarrow C + h\nu$$
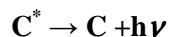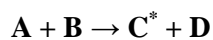
Were C^* represents the excited state of the species C. Most chemoluminescence reactions are considerably more complicated than it is suggested by the foregoing equations.[2]

Since the discovery of luminol (5-amino-2,3-dihydro-1,4-phthalazinedione) by Albrecht in 1928, much effort has been expended in an attempt to understand the mechanisms of phthal-hydrazide chemoluminescence and to uncover the factors governing the efficiency of light production.[52]

Luminol has been observed to produce chemoluminescence at a wavelength of 425 nm under many conditions. The chemoluminescence of luminol is now being used widely as analytical tool for many laboratory and environmental applications, including immunoassay, monitoring of metabolic pathways, detection of free radicals, analysis of a variety of trace metals, and detection of other inorganic substances. [53]

The detection of Fe^{2+} by chemoluminescence was first described as an analytical tool by Seitz and Hercules. The development of methods for practical and sensitive measurements of Fe^{2+} was carried out by O´Suvillan and coworkers and King and coworkers. Unlike methods developed for other trace metals, many of which rely upon the use of H_2O_2 as an oxidizing agent, Fe^{2+} can produce strong chemoluminescence with luminol in the presence of O_2 only. [53]

The chemoluminescence method has the following advantages:

- high sensitivity

- the measurements can be made extremely rapidly

- no chemical treatment of the sample is required prior to analysis

- it is relatively insensitive to interference from other trace metals

- it can distinguish between Fe^{2+} and Fe^{3+} oxidation states.

The mechanism *via* which the oxidation of luminol leads to chemoluminescence is not easy to understand. However, well-controlled experimentation by Merényi *et al* has isolated many of the mechanism through which luminol chemoluminescence can proceed. Similarly, the mechanism via which Fe^{2+} induces chemoluminescence in luminol is not adequately reported,

despite multiple studies examining the influence of different factors such as pH, buffer and organic ligands in the presence and absence of H_2O_2. [53]

Other authors suppose that the chemoluminescence intensity of the system is directly related to the Fe^{2+} concentration, without giving detailed consideration to the mechanism involved. This is problematic because the concentration of free radicals in solution for a given Fe^{2+} concentration may differ depending on the initial Fe^{2+} concentration. Thus, the calibrated value of chemoluminescence intensity for a particular Fe^{2+} may depend on the starting concentration of Fe^{2+} used during calibration, even if the medium used in calibration is identical to the sample.

The interference with the chemoluminescence based detection of Fe^{2+} by organic material has been attributed to three potential sources:

- scavenging of radical intermediates in the luminol oxidation process

- complexation of free Fe^{2+}

- re-absorption of the chemoluminescence light.

Rose and coworkers [53] clarified the mechanism of luminol chemoluminescence in the Fe^{2+}-O_2 system and identified existing agent(s) of luminol oxidation. In summary, the possible mechanism for this chemoluminescence system is shown in scheme 12. [53]
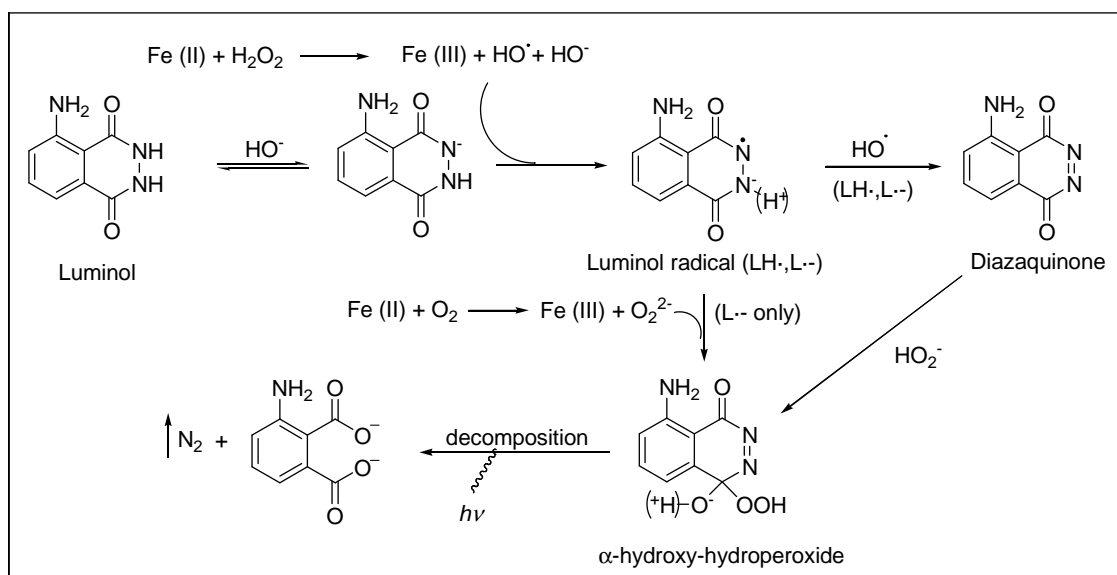
Scheme 12: Possible chemoluminescence mechanism of luminol with Fe^{2+} and hydrogen peroxide

Luminol chemoluminescence is initiated by the one electron oxidation of luminol to luminol radical anions by strong oxidants including horseradish peroxidase, metals such as cobalt, copper and iron and organic complexes of these metals. Despite a huge number of studies, the mechanism of the process leading to enhancement or inhibition of luminol chemoluminescence

is still not fully understood. However, Uzu and coworkers [54] studied in dicopper complexes because it has been reported that H_2O_2 is formed concurrently with quinone formation catalyzed by dicopper complex. The dicopper complex catalyzes both the reduction of dissolved O_2 and the following oxidation of luminol with H_2O_2 to yield efficient chemoluminescence (scheme 13).
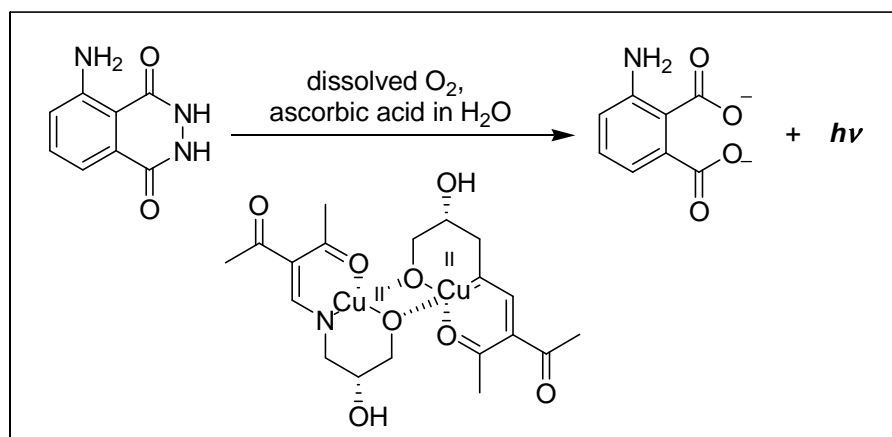
Scheme 13: Mechanism of luminol oxidation through dicopper complex

Numerous methods like Cu^{2+}, Fe^{2+}, Co^{2+} have also been used as redox-active compounds in the luminol chemoluminescence. [55]

2 Aim of the work

Detecting cations, achiral and chiral anions and hydrogen peroxide is of great interest for many fields of science, such as chemistry, biology and medical science. In the last decades much effort has been put into the research on the synthesis of a new generation of sensors that are able to recognize these analytes.

One approach to detect these analytes is the use of fluorescent sensors. Typically these sensors are more sensitive than absorption sensors (colorimetric sensors) as the signal can be detected directly and does not have to be compared to a reference beam. Different studies show that interaction between analyte and sensor through hydrogen bonding is a powerful tool due to the strong binding of the formed complexes. Furthermore, the resulting change in the electronic structure can possibly change the fluorescence properties of the fluorophor.

In the last years significant reactions and characteristics of phthalimide derivatives have been intensively studied and reported by our research group. The high fluorescence quantum yield makes phthalimides attractive fluorophores.

Taking in account these factors, the aim of this work was to synthesize new fluorescent sensors based on phthalimide derivatives to recognized cations, achiral and chiral anions and hydrogen peroxide. The recognition was to be based on hydrogen bonding interaction or metal coordination.

In the last part of this work the interest was focused on the study of photophysical properties and the chemoluminescence efficiency of a series of new luminol derivatives. Luminol as parent motif has been known for decades for its robust chemoluminescent behavior in the presence of oxidants. Therefore, structural analogs can lead to practical applications as analytical probe for metal ions, oxidants or anions.

3 Results and Discussion

3.1 Synthesis of nitro- and amino-substituted phthalimide derivatives from benzylamine

In order to develop new fluorescence sensors based on phthalimide derivativess, a synthetic route *via* the reaction between 3-nitrophthalic anhydride and benzylamine was developed. Heating under azeotropic conditions with a catalytic amount of triethylamine led to the formation of the expected product 2-benzyl-4-nitroisoindoline-1,3-dione (**46**) (*N*-benzyl-3-nitro-phthalimide) in 85 % isolated yield.[56]

In the next step 2-benzyl-4-nitroisoindoline-1,3-dione was reduced with catalytic amounts of Pd/C under H_2-atmosphere in EtOH, giving the product 4-amino-2-benzylisoindoline-1,3-dione (**47**) which was the precursor for other syntheses (scheme 14).[57]
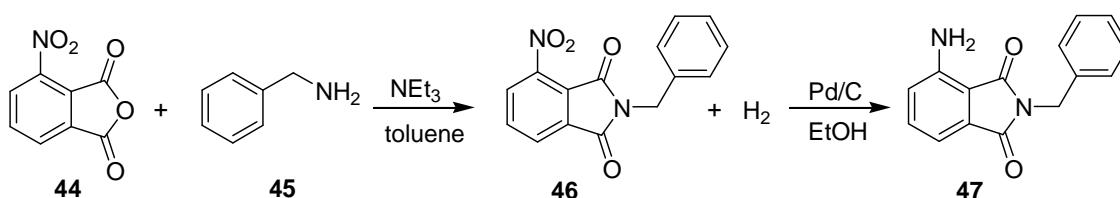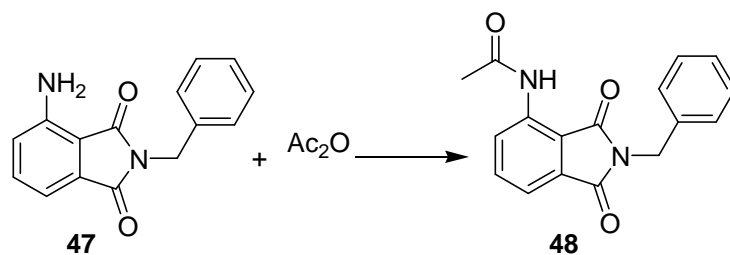

Scheme 14

Product **47** was isolated in 82 % yield and characterized by NMR and IR-spectroscopy. The N-H stretch bands was observed at 3472 (m) and 3351 (m) cm^{-1}.

## 3.2 Synthesis of phathalimide derivativess from 4-amino-2-benzylisoindoline-1,3-dione

Compound **47** was acetylated to give *N*-(2-benzyl-1,3-dioxoisoindolin-4-yl)acetamide (**48**). IR-spectroscopy showed the change of the NH_2 signal (two bands at 3472 and 3351 cm^{-1}) to a NHAc-group (one band at 3346 cm^{-1} with minor intensity, due to hydrogen bonding). Compound **48** was then used for preliminary fluorescence experiments as well as a starting material **47** (scheme 15).

Other syntheses were carried out in order to produce chiral carbamates and chiral ureas based on phthalimide derivate **47.** Unfortunately, the majority of attempts were not successful. One possible reason may be that the amine group in position 3 of the aromatic ring is less reactive towards an electrophilic attack than the one in position 4. This low reactivity may be due to hydrogen bonding between the carbonyl group of the indole moiety and the amine to form a stable 6-membered ring.

Scheme 15

The coupling reaction was carried out with DCC in dry CH_2Cl_2 and the progress of this reaction was monitored by TLC. After two days a new product was observed and isolated. The product benzyl (*S*)-1-(2-benzyl-1,3-dioxoisoindolin-4-ylcarbamoyl)ethylcarbamate (**50**) was characterized by ^{1}H NMR only. Due to the low yield of this synthesis (35 %), not enough substance was present for other characterizations methods. For time reasons it was not possible to repeat this reaction or purify the target molecule (scheme 16).
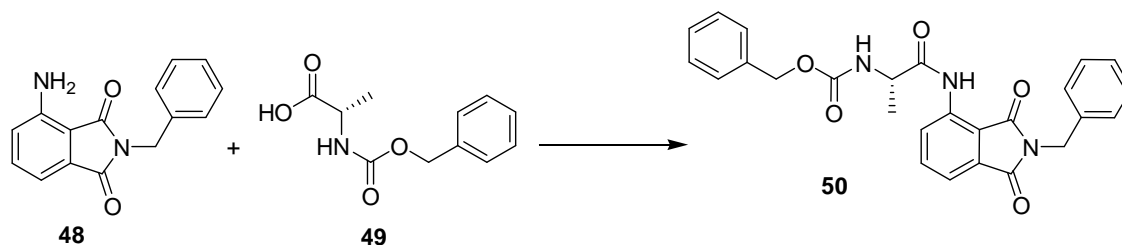
Scheme 16

This synthetic route that uses the coupling between the amine group and an amino acid establishes an easy access to new interesting chiral fluorescence sensors. The method has to be optimized for a higher yield.
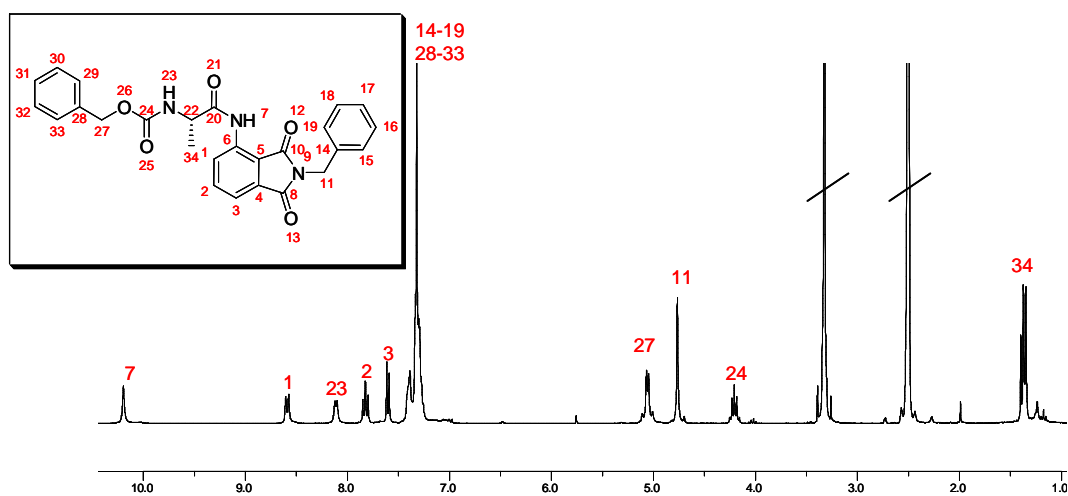
**Figure 42: ^{1}H NMR spectrum of the isolated product 50**

We used the synthetic route shown in part 3.1 to obtain other phthalimide derivatives such as the compounds presented in the following chapter.

3.3 Synthesis of nitro-, amino-substituted phthalimide derivatives from 2,2-Diphenylhydrazine

The reaction between 3-nitrophthalic anhydride and 2,2-diphenylhydrazine was carried out by heating the two starting materials in the presence of catalytic amounts of triethylamine (azeotropic conditions). The expected product 2-(diphenylamino)-4-nitroisoindoline-1,3-dione (**52**) was obtained in 70 % yield.[56]

In the next step, compound **52** was reduced with catalytic amounts of Pd/C under H_2 atmosphere in EtOH and the product 2-(diphenylamino)-4-aminoisoindoline-1,3-dione (**53**) was isolated in 67 % yield.

This synthetic route for the synthesis of nitro-, amino-substituted phthalimide-derivatives is a simple method that, in general, gives good yields. The purification of the products was carried out by crystallization and by column chromatography.
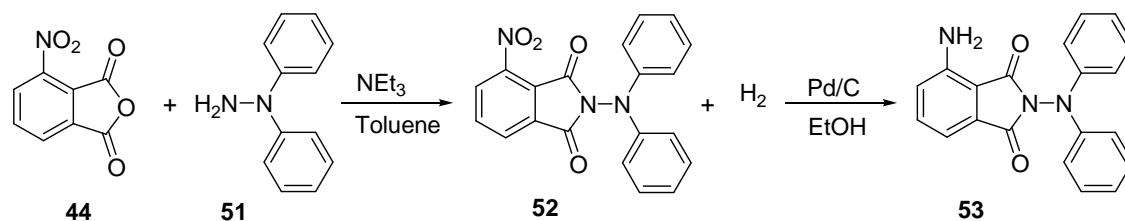
Scheme 17

Products **47**, **48** and **53** were characterized directly and used for different fluorescence experiments such as the deactivation and activation of the fluorescence emission through addition of molecular quenchers or metal ions. In the following part, the results of this fluorescence experiments are presented.

3.4 Quenching study of amino- and acetamido-substituted phthalimide derivatives

Fluorescence quenching studies of products **47** and **48** were conducted with different molecular quenchers which are shown in figure 43. The concentration of the quencher was adjusted at 0.3 M and of the fluorophor at 1mM. The excitation and emission slits were set to 2.5 nm. Equivalents of quencher were added into the quartz cells that contained the fluorophor. The fluorescence spectrum was measured directly after each addition step.
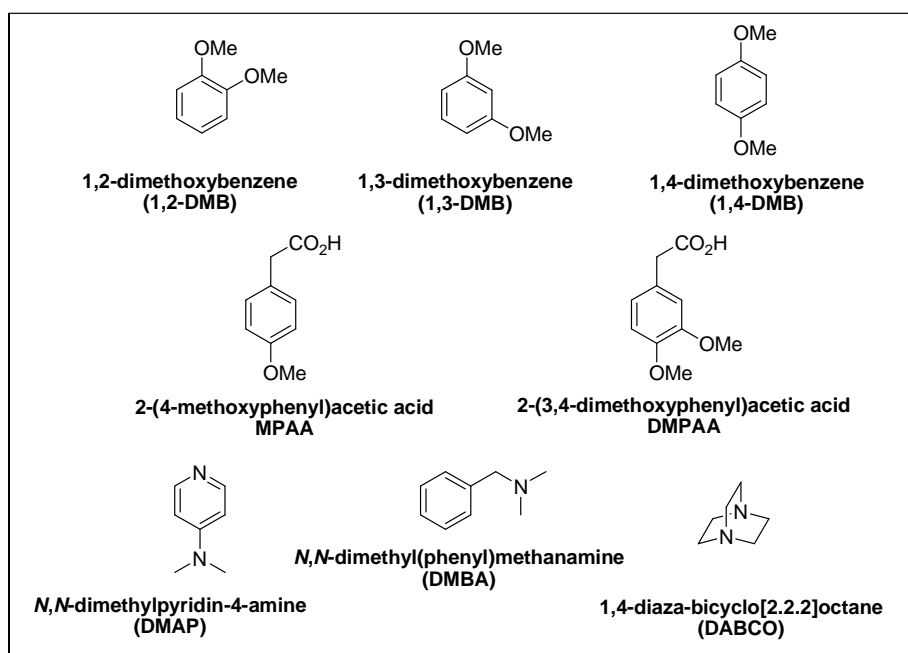
Figure 43: Various Molecular Quenchers

3.4.1 Quenching study of 4-amino-2-benzylisoindoline-1,3-dione

For these experiments the excitation and emission slits were adjusted at 2.5 nm. The fluorescence emission (λ_{em} = 454 nm) intensity of product **47** gradually decreased (λ_{ex} = 388 nm) with increasing concentration of the quencher. This result indicates that a quenching process occurred between product **47** and the different quenchers.

Figure 44 shows the fluorescence emission of fluorophore **47**, which decreases with increasing concentrations of DABCO in CH_3CN. The same tendency was observed for the other quenchers only that the quenching effect was weaker than with DABCO.
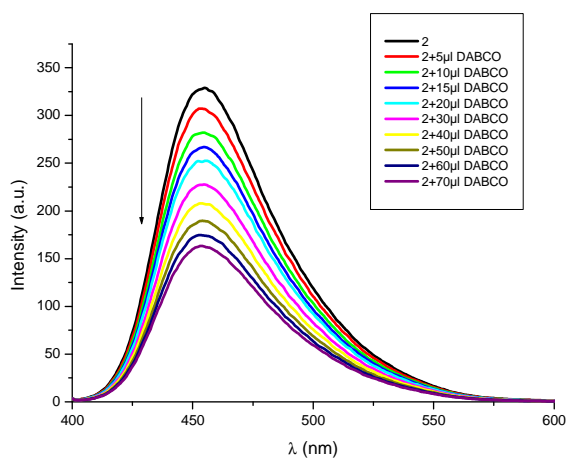

Figure 44: Fluorescence spectra of 47 with increasing equivalents of DABCO. λ_{exc} = 388nm

The Stern-Volmer constants for the different quenchers with product **47** were calculated *via* a Stern-Volmer plot. [6]

The Stern-Volmer equation can also be obtained by considering the fraction of excited fluorophores, relative to the total, which decay by emission. This factor (F/F$_0$) gives the ratio of the decay rate in the absence of a quencher (γ) to the total decay rate in the presence of quencher ($\gamma + k_q$[Q]):

$$F / F_0 = \gamma / \gamma + k_q[Q] = 1 / 1 + k_q[Q] \tag{9}$$

This is again one from of the Stern-Volmer equation. Since collisional quenching is a rate process that depopulates the excited state, the lifetimes in the absence (τ_0) and presence (τ) of a quencher are given by:

$$\tau_0 = \gamma^{-1} \tag{10}$$

$$\tau = (\gamma + k_q[Q])^{-1} \tag{11}$$

and therefore,

$$\tau_0 / \tau = 1 + k_q \tau_0 [Q] \tag{12}$$

This equation illustrates an important characteristic of collisional (dynamic) quenching, which is an equivalent decrease in fluorescence intensity and lifetime. For dynamic quenching the following equation applies:

$$F_0 / F = \tau_0 / \tau \tag{13}$$

The decrease in lifetime occurs because quenching is an additional rate process that depopulating the excited sate.

The Stern-Volmer plots for our system resulted in a linear correlation, that is shown in figure 45. The slope represents the Stern-Volmer quenching constant that is given by

$$K_D = k_q \tau_0 \tag{14}$$

The linear correlation showes a possible dynamic process. It is clear that with only one experiment it can not be proved that the involved mechanism is dynamic. Experiments such as lifetime measurement and variation of the temperature can distinguish between dynamic and static quenching mechanism and will be carried out in future work.
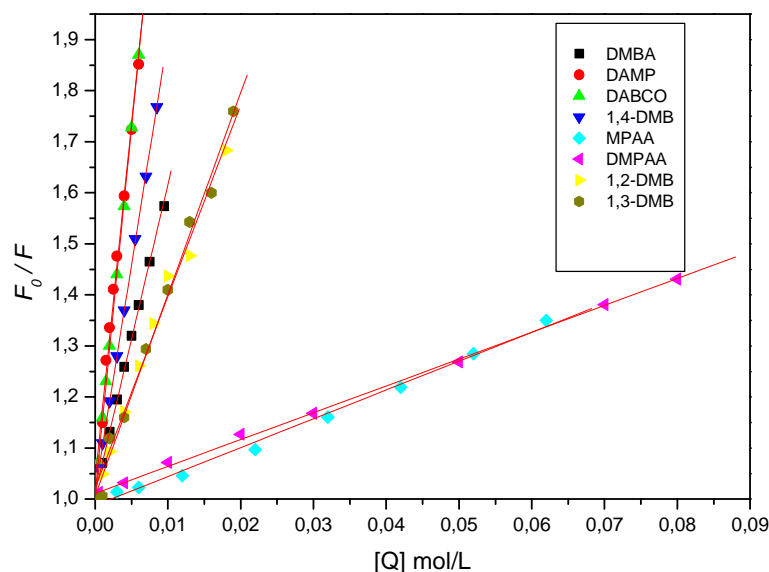
Figure 45: Stern-Volmer plots of the product 47 with the different molecular quenchers

The next table shows the Stern-Volmer constants that were obtained from the Stern-Volmer plots as well as the bimolecular quenching constants (k_q) that were calculated with equation 6. For the bimolecular quenching constants the lifetime of the 3-amino phthalimide (3-AP) were used (12.5 ns). [58]

Table 13: Stern-Volmer constant (K_D) and bimolecular quenching constant (k_q) of fluorophore 47.

Quencher[a,b]	K_D (M)$^{-1 c}$	k_q (M s)$^{-1}$ x 10^9
DABCO	143.75 ± 1.17	11.50
DMAP	139.61 ± 4.76	11.17
1,4-DMB	89.10 ± 0.80	7.13
DMBA	61.12 ± 0.46	4.89
1,2-DMB	38.48 ± 1.37	3.08
1,3-DMB	37.56 ± 1.43	3.00
DMPAA	5.65 ± 0.17	0.45
MPAA	5.26 ± 0.08	0.42

[a] The concentration of product **47** was 1 mM. [b] The concentration of the quencher stock solutions was 0.3 M, all solutions were prepared in CH_3CN. [c] The plot was carried out with Origin 6.0 and all correlation coefficient were obtained between 0.995 and 0.999.

3.4.2 Quenching study of *N*-(2-Benzyl-1,3-dioxoisoindolin-4-yl)acet-amide

The excitation and emission slits were adjusted at 2.5 nm for the quenching experiments. Fluorophore emission **48** was excited at 342 nm. The fluorescence emission intensity with a

maximum at 412 nm was monitored after the titration of fluorophore **48** with increasing concentration of quencher. The monitoring of the fluorescence emission showed a gradual decrease after addition of the quencher which indicates that quenching process occurred between fluorophore **48** and the different quenchers.

The quenching experiments of fluorophore **48** were carried out in the same way as for fluorophore **47**. Figure 46 shows the emission fluorescence spectra which were received upon titration of fluorophore **48** with DABCO. The decreasing effect is also presented for all other quenchers. This effect is less pronounced for compound **48.**

The Stern-Volmer plot was conducted to obtain the respective constant for each quenching processes. This constant distinguishes for the better quenching efficiency and can be used to calculate the bimolecular quenching constant (k_q), which reflects the efficiency of quenching or the accessibility of the fluorophores to the quencher. As shown below, diffusion-controlled quenching typically results in values of k_q near 1×10^{10} $M^{-1}s^{-1}$. Values of k_q smaller than the diffion-controled value can result from steric shielding of the fluorophore or a low quenching efficiency. Apparent values of *kq* larger than the diffusion-controlled limit usually indicate some type of primary binding interaction.

The Stern-Volmer plots were linear depending on the concentration of the quencher. Linear Stern-Volmer plots are in general indicative for a dynamic process.
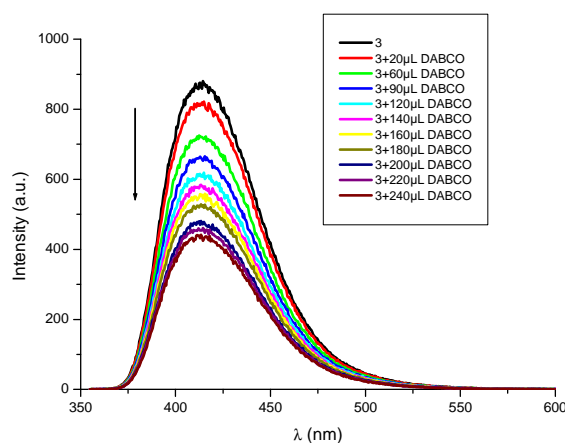

Figure 46: Fluorescence spectra of 48 with increasing equivalents of DABCO. λ_{exc} = 388nm

The next table shows the Stern-Volmer constants which were obtained from Stern-Volmer plots and bimolecular quenching constants (k_q).Those were calculated according to eq. **6**. For the bimolecular quenching constants the lifetime of the 3-amine phthalimide (3-AP) (12.5 ns) was used. [58]

Table 14: Stern-Volmer constant (K_D) and bimolecular quenching constant (k_q) of fluorophore 48.

Quencher[a,b]	K_D (M)$^{-1}$ [c]	k_q (M s)$^{-1}$ x 10^9
DABCO	40.75 ± 1.49	3..26
DAMP	40.14 ± 0.33	3.21
DMPAA	27.76 ± 0.59	2.22
DMBA	27.32 ± 0.24	2.18
1,2-DMB	26.02 ± 1.11	2.10
1,4-DMB	25.16 ± 0.30	2.01
1,3-DMB	21.36 ± 0.21	1.71
MPAA	14.57 ± 0.11	1.16

[a] The concentration of **48** was 1 mM. [b] The concentration of the quencher stock solutions was 0.3 M. All solutions were prepared in CH_3CN. [c] The plot was prepared with Origin 6.0 and all correlation coefficients were obtained between 0.998 and 0.999.

As illustrated in table 13 and table 14, DABCO shows the best quenching effect for both fluorophores. This indicates the high electron-transfer efficiency of DABCO as a quencher. Quenchers with methoxy groups as substituents on the aromatic ring such as 1,4-dimethoxybenzene and 1,2-dimethoxybenzene only show a moderate quenching effect.

The interaction between quenchers and fluorophore was stronger with fluorophor **47** for all quenchers than for fluorophore **48**. The only structural difference between these fluorophores is the protection of the amine group with an acetamide functionality. This substitution change from amine to acetamide can affect several properties involved in the quenching process; one of them is the ground state reduction potential.

The dynamic fluorescence quenching can occur though PET (photoinduced electron transfer) from the ground state quencher to the excited state fluorophore. It is also possible that the radical cation of the quencher and the radical anion of the fluorophore are combined as last step of the dynamic quenching process. If the PET is involved as possible mechanism, a change in the reduction potential favors the quenching process. Another factor is the stability of the generated radical cation of the quencher. Functional groups that stabilize the radical cation assist the efficiency of the quenching process.

After PET of the quencher to the fluorophore, a combination of fluorophore and quencher can occur. This combination produces a new adduct, which is not a ground state complex. For that reason a static fluorescence quenching process does not occur during the combination.

Quenchers such as 2-(4-methoxyphenyl)acetic acid (MPAA) and 2-(3,4-dimethoxyphenyl) acetic acid (DMPAA) showed a poor quenching effect in presence of the fluorophor **47**. One possible reason could be that the quenchers in the solvent exist as carboxylate anions and induce

acid-basic reaction between the amine group of the fluorophore and the carboxylate anion of the quenchers. Thus, the dynamic quenching process is thus not observed.

The same quenchers interact with fluorophore **48** according to another mechanism. The Stern-Volmer constant of 2-(3,4-dimethoxyphenyl) acetic acid (DMPAA) shows a higher value than for amino and dimethoxy quenchers, which indicates that a dynamic quenching process is involved between fluorophore **3** and the quencher. But for 2-(4-methoxyphenyl)acetic acid (MPAA) another process of interaction can be involved between the fluorophore **48** and the quencher such as radical stabilization or decarboxylation which makes the process slower.

The proposed general mechanism is presented in scheme 18.
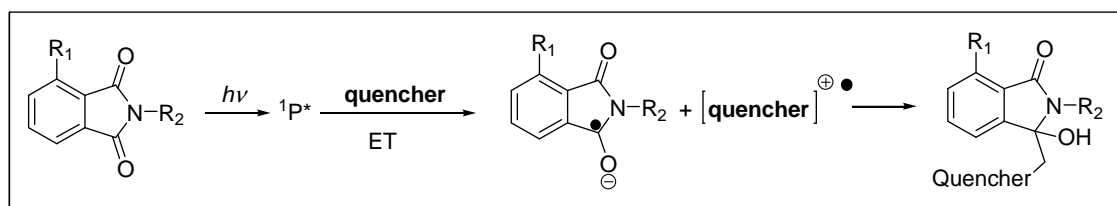
Scheme 18

3.4.3 Preliminary study: fluorescence activation of 2-(diphenyl-amino)-4-aminoisoindoline-1,3-dione through cation coordination

This experiment was based on the addition of more equivalents of the cation into a quartz cells containing fluorophor **53**. After each addition of the cation the emission fluorescence spectrum was measured. The concentration of **53** was adjusted to 1 mM and for the cations (Ba^{2+}, Cu^{2+}, Ni^{2+}, Mg^{2+}, Ag^+, Zn^+, Fe^{3+} as nitrate and Eu^{3+} as triflate salt) it was varied between 0.01-0.1 M. For excitation and emission experiments, slit widths were adjusted to 5.0 nm.

The activation of emission fluorescence of product **53** was measured after excitation at 388 nm with increasing concentration of the cations.

Considerable changes of the fluorescence emission were not observed. The fluorescence emission maximum was detected at 420 nm with an intensity between 0 and 13.85 a.u. for product **53** with the cations. The histogram shows that zinc ions contributed the most to an increase of the emission intensity with a factor of nearly 14. However, this is still a weak effect for the detection of a cation. Other fluorescence sensors reported in literature exhibit an increase of about 1200-fold [17] for the detection of copper and other metal ions.
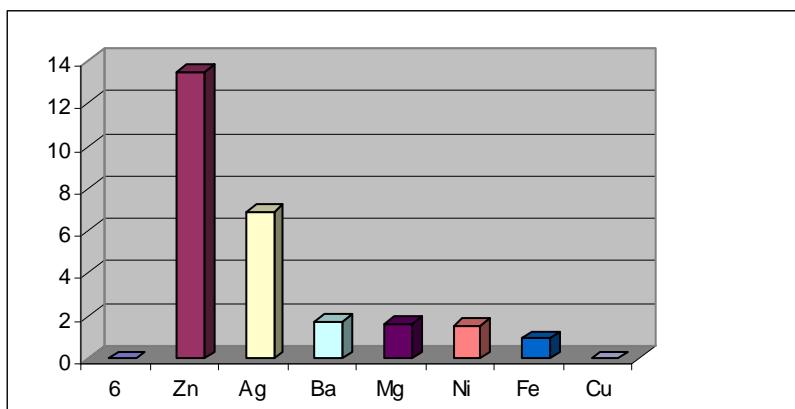
Figure 47: Histogram of the fluorescence quenching efficiency between 53 and metal ions

It is possible that the coordination site of product **53** is not suitable for these cations and thus PET between fluorophore and cations was not possible. Another reason can be a competition between the primary and the tertiary amine groups in the fluorophore. It would be possible to confirm this speculation by protecting the amine group with acetamide or another protecting group and to repeat the quenching experiment (figure 48).

In conclusion, the idea of synthesizing a simple fluorescence sensor for the detection of cations (product **53**) due to PET did not lead to the expected results.
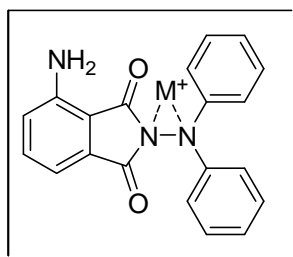

Figure 48: Possible complex between 53 and the metal ions

Many examples for cations fluorescence sensors exist, the great majority containing complexing groups such as chelators or calixarenes.[10] Possible phthalimide derivatives containing one of these complexing groups can be proposed as new cation sensors and are shown in figure 49. Increasing the capability to bind cations could possibly increase the efficiency of the cation detection by fluorescence emission.
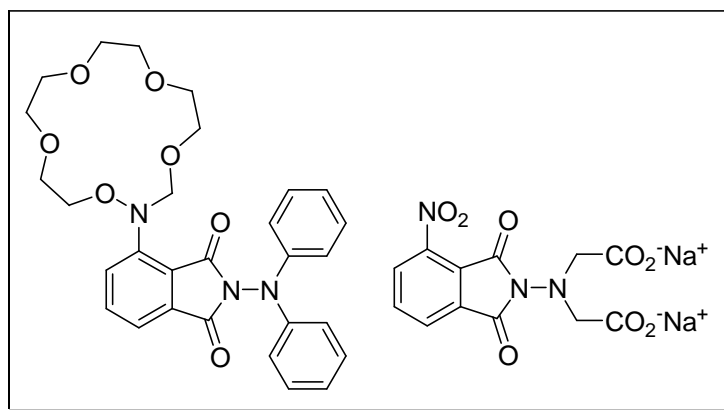
Figure 49: Proposed sensors

A fluorescence study of product **53** was carried out applying the same procedure and concentration conditions mentioned above with europium salts and the results were comparable with those of the previously described cations.

For excitation and emission experiments, slits were adjusted at 3.5 nm. Figure 50 shows the emission fluorescence spectra after increasing the concentration of Eu(III) in the solution of product **53.**
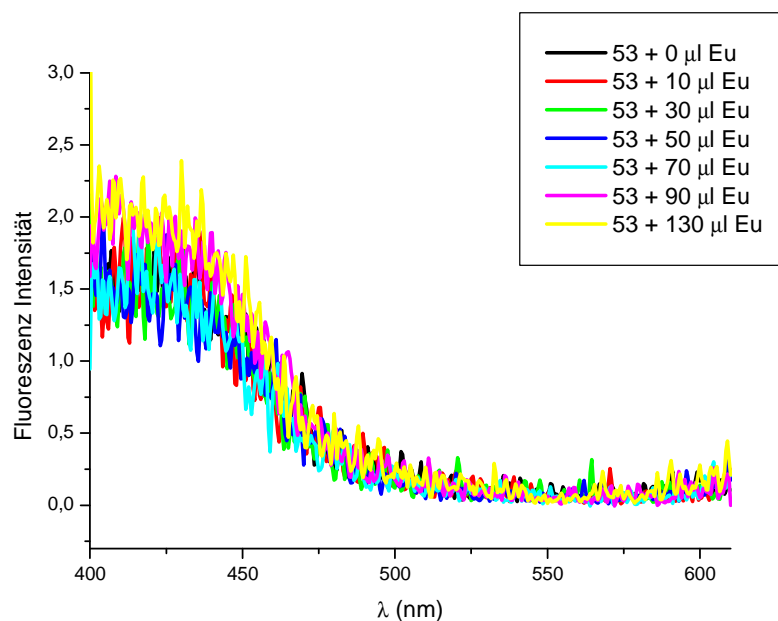

Figure 50: Emission spectra of 53 in the presence of increasing amounts of Eu(III)

The recorded emission spectra of this system can be considered noise level signals, which mean that product **53** does not emit any fluorescence signal. With increasing concentration of Eu ions no changes in fluorescence were observed, indicating that no interaction between Eu(III) and product **53** takes place.

To induce the detection of Eu (III) with product **53** the last probe of the titration process containing 100µl of Eu (III) solution was irradiated for about 180 min. The irradiation was performed in the photoreactor Luzchem LZC-4V (14 lamps, $\lambda = 350 \pm 20$ nm), and every 30 minutes a fluorescence spectrum was measured.

Two new bands appeared in the emission spectra with their maxima centered at 452 and 531 nm (figure 51). In the course of the irradiation, the intensity of these maxima increased reaching a maximum after 60 min and declined when the experiment was continued.
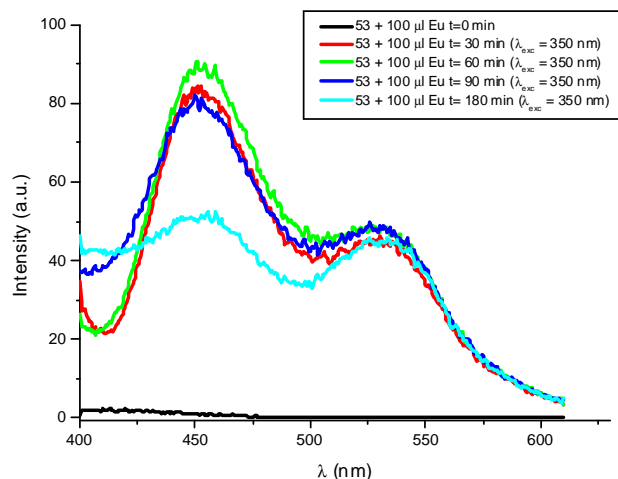

Figure 51: Emission spectra after irradiation of the solution 53 + 100µL Eu(III)

This increase can be interpreted as an interaction signal between compound **53** and Eu(III), because the blank sample (only fluorophore solution, same irradiation conditions) did not show changes in fluorescence emission after irradiation. However, this increase of the fluorescence emission intensity was not very remarkable considering that the slits were opened to at 3.5 nm. The deployed fluorospectrometer is able to measure a fluorescence intensity up to 1000 a.u. thus an increase of 100 a.u. does not represent a significant change.
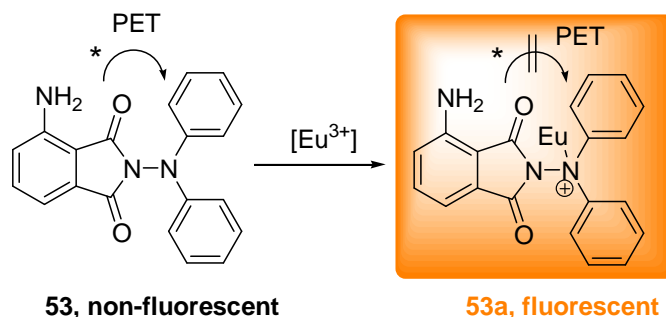
Scheme 19: Possible quenching mechanism between 53 and Eu(III)

However, a rationale for this fluorescence increase can be Eu(III) complexation promoted by irradiation which hinders the amine nitrogen lone pair to take part in the PET. This

complexation slightly inhibits the PET process and consequently only a slight fluorescence enhancement was observed (scheme 19).

In an effort to increase the fluorescence activation of compound **53** a pH experiment was performed. Figure 52 shows that with changing pH the emission fluorescence was not considerably enhanced. However, smaller changes were observed: at pH 12 the fluorescence intensity was lowered and raised at pH 3. But the effect was too small for this system to give a good pH dependent fluorescence sensor.
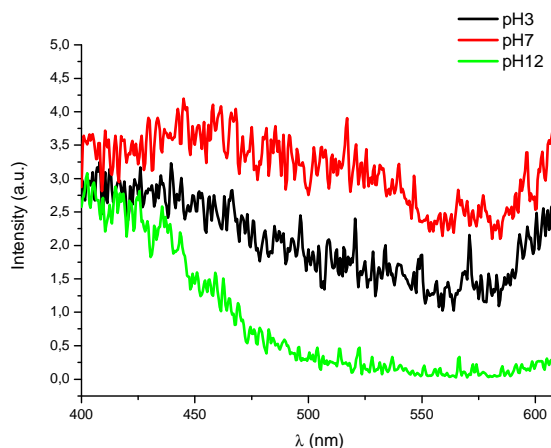

Figure 52: Emission spectra at different pH (3, 7, 12) of 53

3.5 From 1-(2-Aminonaphthalen-1-yl) naphthalene-2-amine to chiral phthalimides

1-(2-Aminonaphthalen-1-yl) naphthalene-2-amine (**54**) is a commercially available reagent in various enantioselective organocatalytic reactions[59], [60], [61], but some authors also reported the properties of this chiral amine as fluorescence sensor.[62]

54 exhibit a good capability to differentiate between enantiomeric substrates and phthalimide derivatives evidentially act as good chromophores. In order to obtain an enantioselective optical sensor, efforts were made to combine these two activities in one molecule and simply react **54** with phthalic anhydride.

Scheme 20 shows the different reaction routes that were followed to obtain products **55** and **57**. The reactions involving phthalic anhydride to generate the phthalimide product were not successful, presumably because of steric hindrance as a result of the molecular geometry being too unfavorable for this coupling. The acetylation reaction however, was carried out without any difficulty.
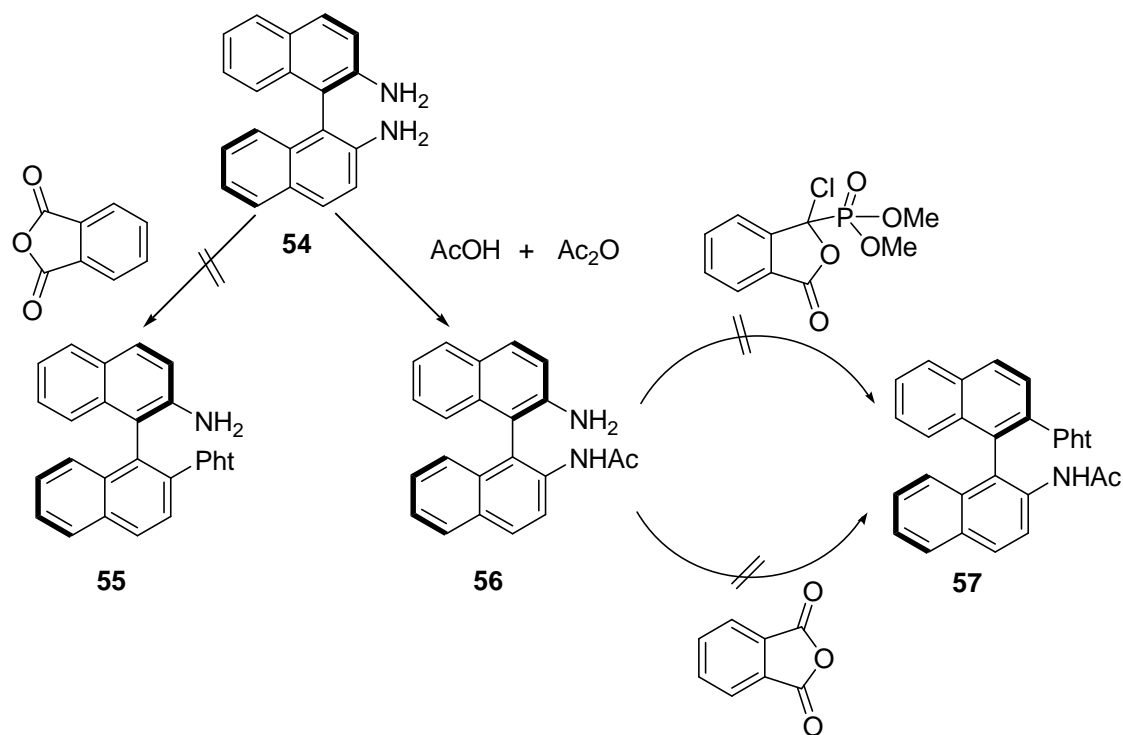
Scheme 20

These first trials were performed with racemic **54**. We then wanted to apply an optimized synthetic route in the synthesis of an enantiomerically pure compound.

Wang and coworkers [63] reported the reaction depicted in scheme 21. In the last step a reaction between the primary amine group of 1-(2-aminonaphthalen-1-yl) naphthalene-2-amine and 3,5-bis(trifluoromethyl)phenyl thioisocyante was carried out to produce the corresponding thiourea.
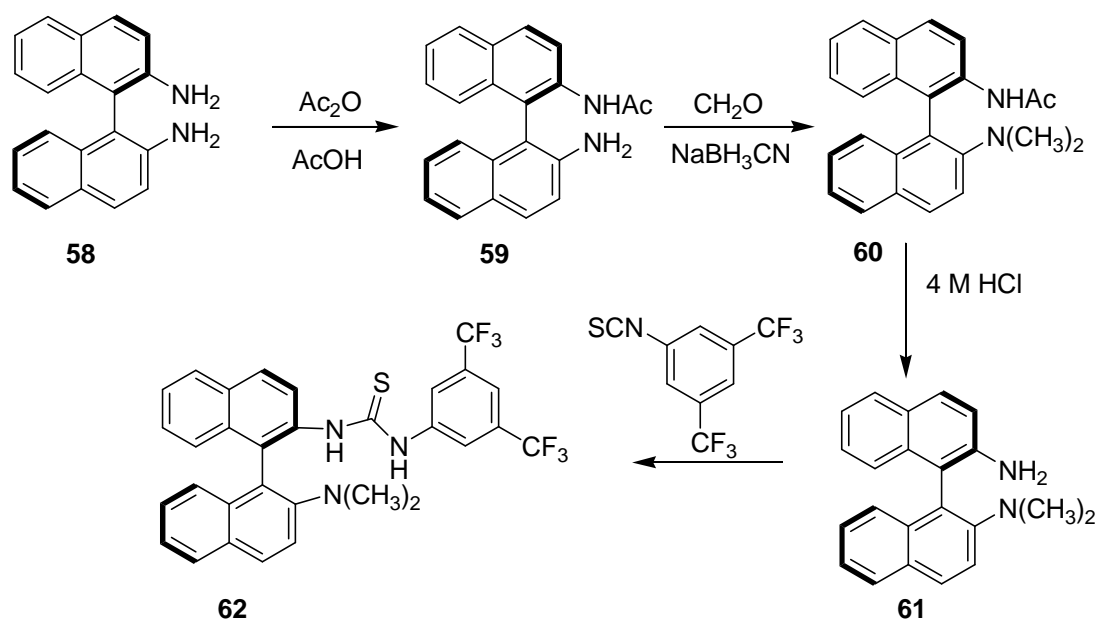
Scheme 21

Consequently, with this route it should be possible to synthesize an enantioselective fluorescence sensor containing the two key elements by reaction of **54** and a thioisocianate or isocyanate substituted phthalimide derivative.

Taking into account the synthetic problems that appeared in the attempt to directly couple the amine group and the phthalic anhydride, it was proposed to modify the route to get a similar phthalimide derivative. This modification consists of the application of a thioisocyanate or isocyanate phthalimide derivatives which in a second step will be coupled with **54**. The proposed synthetic route is depicted in scheme 22.
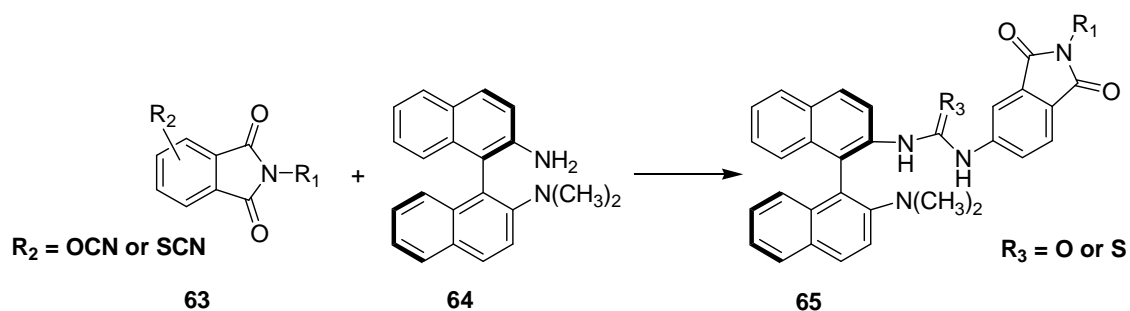
Scheme 22

3.6   Multicomponent Reaction

Looking for new higher substituted phthalimide derivatives, a new synthesis route was developed by applying multicomponent reactions based on Diels-Alder chemistry in the first step. The principle of this multicomponent reaction consists of the reaction between amines and aldehydes with dienophiles to give a large variety of 1-acylamino-2-cyclohexene derivatives (scheme 23).

In the second step a dehydrogenative oxidation of the conjugated cyclohexadiene product was carried out using MnO_2. At last different ways were examined to conduct a direct reaction between the ester group of the cyclohexadiene and amine derivatives to achieve a phthalimide.

3.6.1   One-pot reaction with dienophilic dimethyl acetylenedicarboxylate

### 3.6.1.1   Synthesis of dimethyl 3-acetamido-4,6-dimethylbenzene-1,2-dioate

As dimethyl acetylenedicarboxylate (68) represents a molecule with high electron-deficiency it was used as dienophile in the Diels-Alder reaction to obtain dimethyl 6-acetamido-3,5-dimethylcyclohexa-1,3-diene-1,2-dicarboxylate (69) in 66 % yield.

The oxidation of 69 was carried out with 89 % yield, demonstrating that MnO$_2$ acts as a good oxidation agent to achieve polysubstituted anilide derivativess via dehydrogenative oxidations. Polysubstituted anilides are important substructures in pharmaceuticals and herbicides. [64]
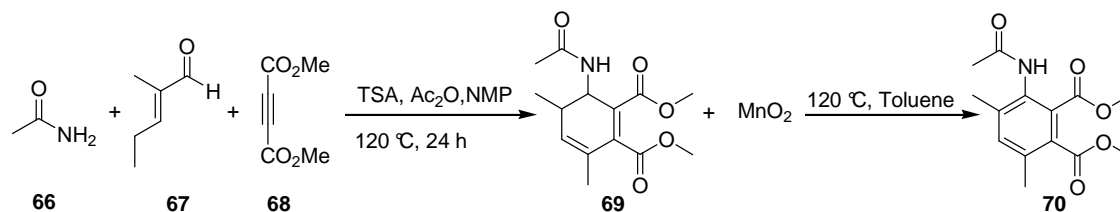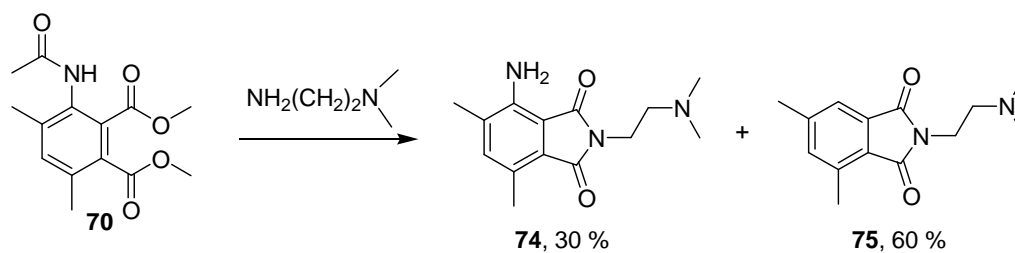

Scheme 23

Different reaction conditions were examined to synthesize the phthalimide derivatives (see experimental part). When aromatic amines were used, it was not possible to obtain the expected product and only reactants were found after workup.
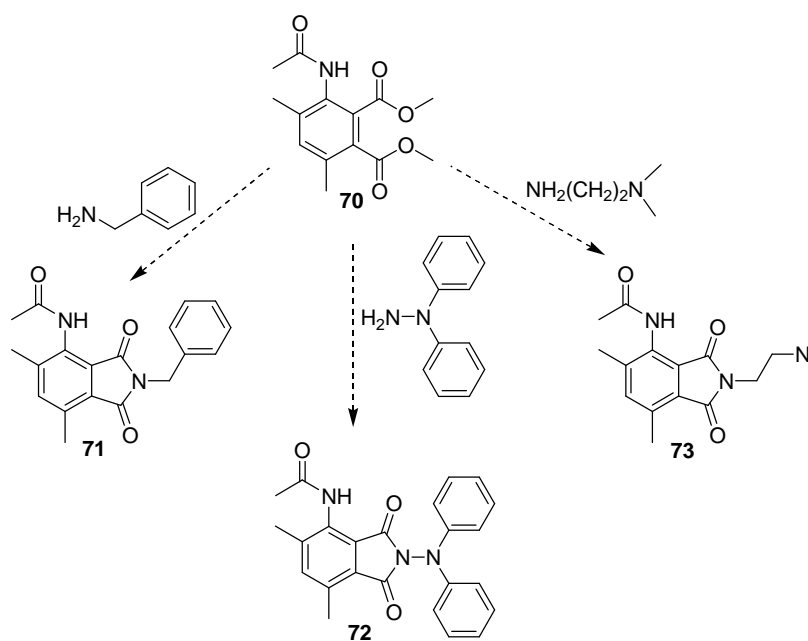
Scheme 24

The situation was different for the reaction with aliphatic amines. Here, the conditions described by Joseph and coworkers [65] were employed as the last step of this route. A solution of compound 70 in *N,N´*-dimethylethylenediamine was stirred at 100°C for 72 h. After evaporation of the solvent the residue was purified by column chromatography (see conditions in the experimental part) to give a mixture of the dehydroaminated phthalimide derivatives in 60% yield and the amino phthalimide derivatives in 30 % yield as shown in figure 53. The product structures were confirmed by X-ray structure analysis and ^{1}H NMR. A 2:1 ratio was observed in the crude mixture, three aromatic signals and the amine signal (scheme 25).

Also the variation of reaction time did not lead to the preferred formation of expected product. A 1:1 reaction between **70** and *N,N´*-dimethylethylendiamine could possibly lead to the desired product dimethyl 3-acetamido-4,6-dimethylbenzene-1,2-dioate (**73**) (scheme 24).
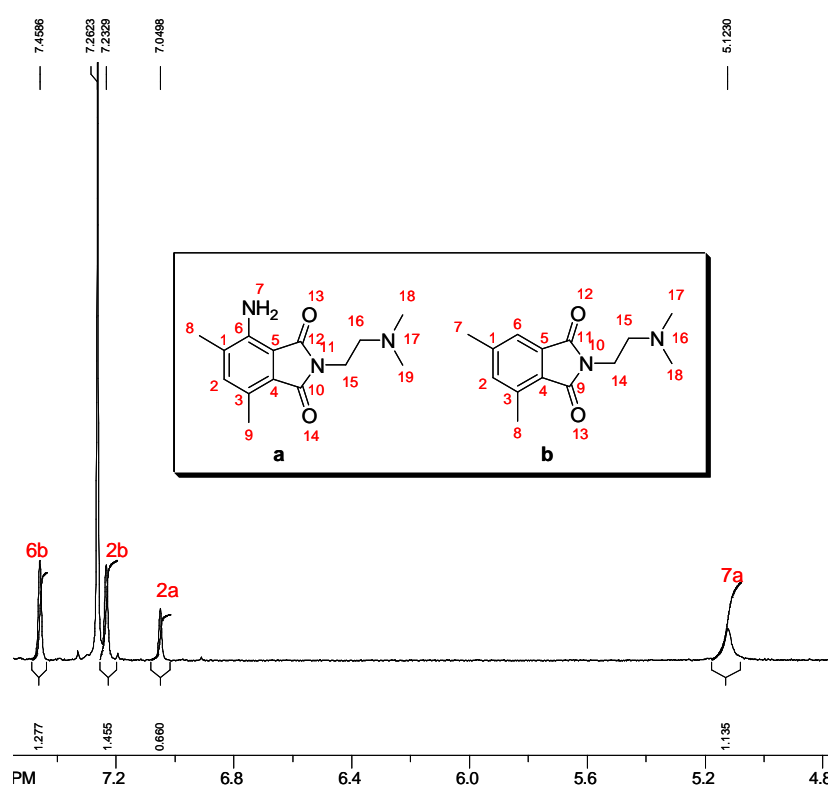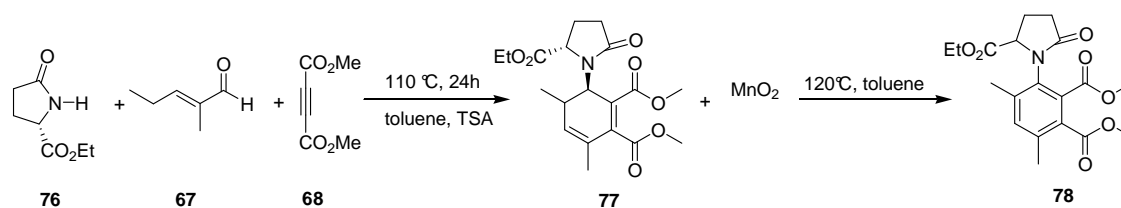

Scheme 25

Figure 53: ¹H NMR spectra of the mixture of 74 and 75

3.6.1.2 Synthesis of Ethyl 1-(2-(2-(dimethylamino)ethyl)-4,6-dimethyl-1,3-dioxoisoindolin-7-yl)-5-oxopyrrolidine-2-carboxylate

In this case, the amine moiety of the multicomponent reaction was changed from acetamide to (*S*)-ethyl 5-oxopyrrolidine-2-carboxylate (*S*-ethyl pyroglutamate) (**76**) along with the reaction conditions, in order to achieve better yields. Once again the Diels-Alder reaction was performed and the expected product ethyl 1-(2-(2-(dimethylamino)ethyl)-4,6-dimethyl-1,3-dioxoiso-indolin-7-yl)-5-oxopyrrolidine-2-carboxylate (**77**) was obtained in 80 % yield.

The following oxidation reaction was carried out using the same conditions like stated above. The product **78** was achieved in 85 % yield.
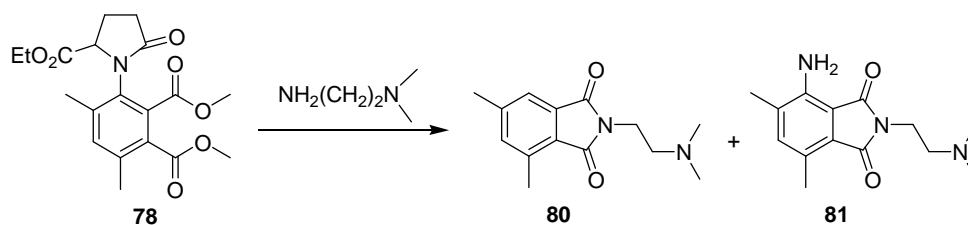

Scheme 26

In order to synthesize the final product the method of Joseph and coworkers [65] was used.
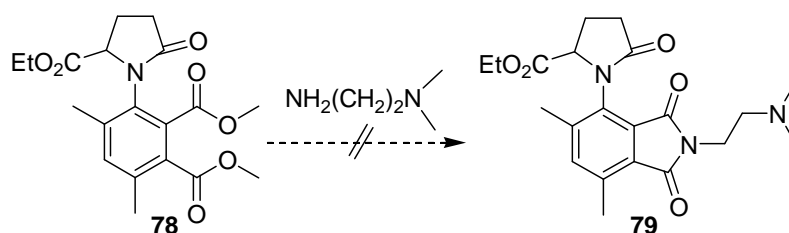
Scheme 27

After column chromatography one of the fractions consisted only of the dehydroaminated phthalimide derivatives (fraction a) and another fraction (fraction b) showed a mixture of the amine phthalimide derivative and the dehydroaminated phthalimide derivative in a 1:5 ratio (scheme 28). The ^{1}H NMR spectra of the two fractions is shown in figure 54.

Scheme 28

Obviously, the reaction conditions are too harsh and thus have to be modified by varying reaction time and temperature as the two easiest accessible variables.
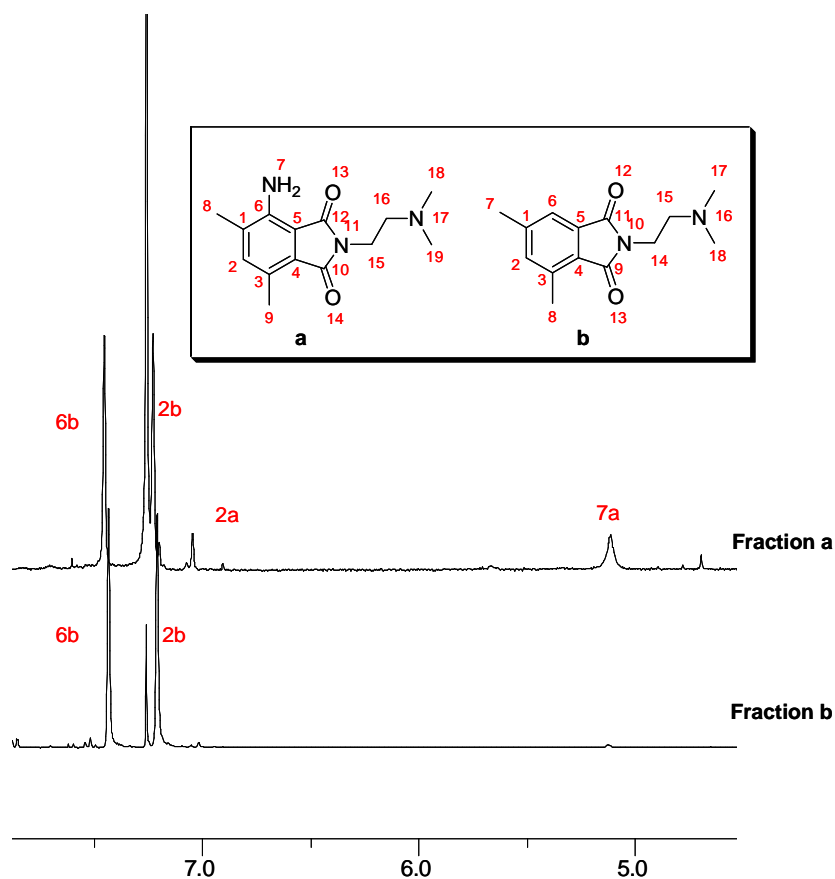
Figure 54: ^{1}H NMR spectra of fractions a and b *i.e.* the mixture of 80 and 81

3.6.1.3 Synthesis of Dimethyl 3-acetamido-4,6-diethylbenzene-1,2-dioate

The aim was to synthesize 3-amino-4,6-diethylbenzene-1,2-dioate (**84**) because of the studies of luminol derivatives which were carried out in this work. Again the multicomponent reaction and the following oxidation with MnO_2 were used to synthesize dimethyl 3-acetamido-4,6-diethylbenzene-1,2-dioate (**83**).

Acetamide (**66**), butyraldehyde (**82**) and dimethyl acetylenedicarboxylate (**68**) were used for the Diels-Alder reaction in the first step of this route. The product was isolated in 70 % yield and could be used without further purification in the next step. After dehydrogenative oxidation with MnO_2 dimethyl 3-acetamido-4,6-diethylbenzene-1,2-dioate (**83**) was obtained in 65 % yield. Scheme 29 shows the synthetic route.
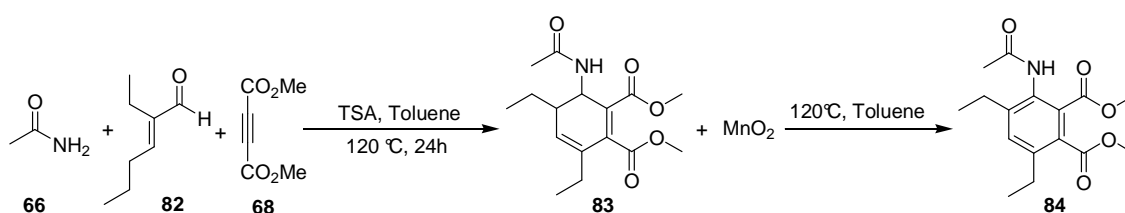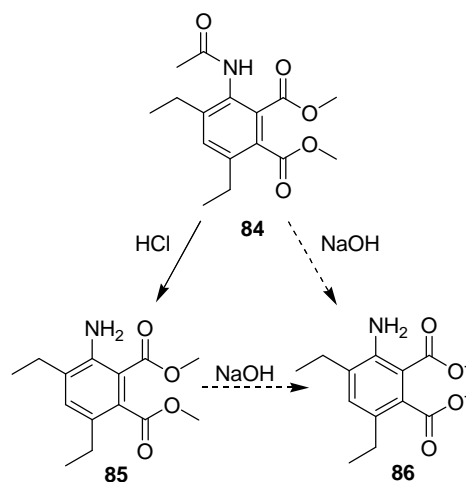

Scheme 29

Better yields in the last oxidation step were achieved for the described reaction routes by using toluene as a solvent instead of NMP and acetic anhydride.

To obtain the desired product **86,** two different methods were followed. The first method was the application of a mineralic acid (HCl), thus it was possible to obtain the dimethyl 3-amino-4,6-diethylbenzene-1,2-dioate (**85**). The product **85** was then subjected to a base (NaOH) but the expected molecule could not be isolated by normal workup conditions.

For the basic method, the same problem occurred extracting the product. Different methods of workup such as solvent extraction or continuous extraction were attempted. Finally it was tried to crystallize the product through solvent diffusion.
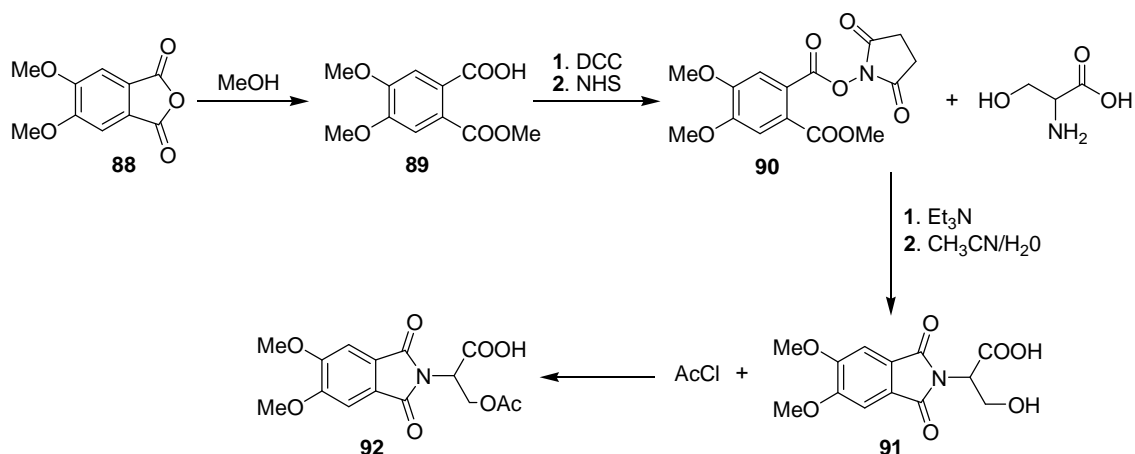

Scheme 30

3.7 Synthesis of Phthalimide-Serine Couples

Recently, the use of chiral phthalimide-serine/theonine couples for the photorelease of acetate was described to take place with high diastereoselectivity in the liberation process. [66] These so called photocages, however, absorb light in the UV-C region, which is not advantageous for the potential application environments, and furthermore no fluorescence process is involved, neither from the substrate nor from the separated chromophore.

Another study reports that the 4,5-dimethoxyphthalimide (**88**) is a chromophore that exhibits a strong fluorescence and acts as an excellent electron acceptor in the excited state based on PET. [67] A combination of both systems could lead to new photocages.

The synthetic route consists of four steps and starts with methanolysis that induces a phthalate ring opening to give **89**. Consecutive DCC-coupling in the presence of *N*-hydroxysuccinimide (NHS) led to the activated phthalates **90**. These were subsequently reacted with serine in the third step to produce 3-hydroxy-2-(5,6-dimethoxy-1,3-dioxoisoindo-lin-2-yl)propanoic acid (**91**) which was finally acyleted to give the photocage **92** (scheme 31).

Scheme 31

The synthesis of 3-acetoxy-2-(5-methoxycarbonylamino-1,3-dioxoisoindolin-2-yl)propionic acid (**100**) was performed following a synthetic route of eight steps. In order to generate the isocyanate derivative (**95**) the carboxylate group of **93** was converted to the acid chloride and then reacted with sodium azide to obtain the isocyanate **95** (scheme 32).

Product **95** was converted by methanolysis to the carbamate (**96**). The following methanolysis process with an excess of methanol produced the ring-opened phthalates to give product **97**. The following DCC-coupling with *N*-hydroxysuccinimide (NHS) led to the activated phthalate **98**, which was reacted with serine to give **99**.
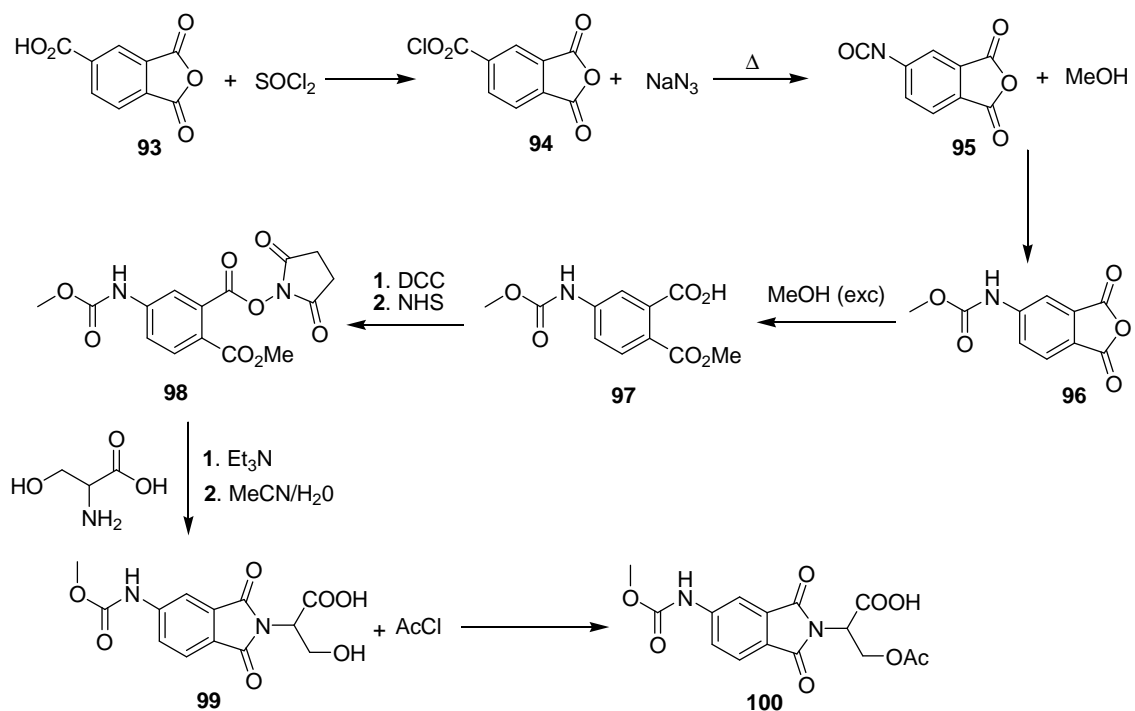
Scheme 32

The synthesis route was completed by acyletion, which was conducted under the same conditions presented in the previous synthesis. The product **100** represents an improved photocage.

3.7.1 Irradiation of caged acetates 3-acetoxy-2-(5,6-dimethoxy-1,3-dioxoisoindolin-2-yl)propionic acid and 3-acetoxy-2-(5-meth-oxycarbonylamino-1,3-dioxoisoindolin-2-yl) propanoic acid

The absorption spectra of compounds **92** and **100** showed two absorption maxima at 300 and 360 nm for **92** and one maximum at 340 nm for **100.** Both compounds showed a red-shift of the absorption band in comparison to the unsubstituted equivalent serine derivative figure 55.

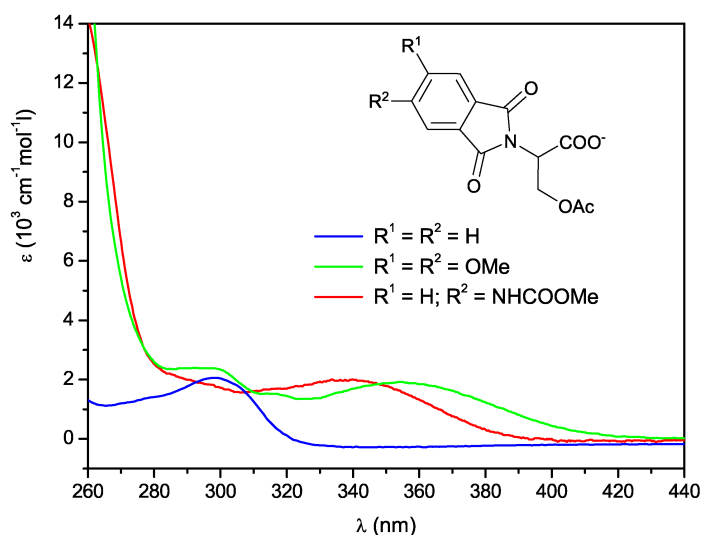**Figure 55: Absorption spectra of substituted phthalimide-photocages 92 and 100**

Photocage **92** showed a fluorescence maximum at 511 nm. After irradiation in the Rayonet Reactor at 350 nm, acetate release and thus the formation of the vinyl phthalimide derivative was observed by NMR studies. The resulting photoproduct **101** was isolated and characterized. Figure 56 shows the ^{1}H NMR of the isolated photoproduct.
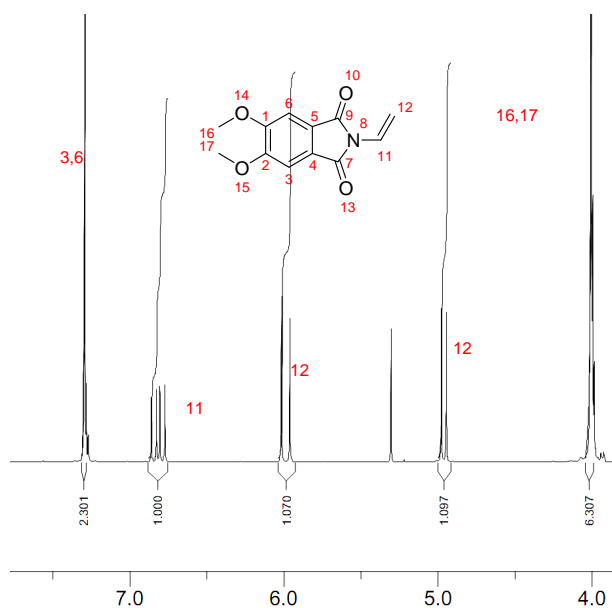
Figure 56: ¹H NMR spectrum of photoproduct 101

Carbamate photocage **100** displays a combination process of decarboxylation and release. The formation of product **102** was accompanied by an increase of the fluorescence emission. This was observed by taking a sample of the irradiated solution every minute over a period of 8 minutes and examining it by fluorescence measurement. In order to detect the weak fluorescence signal of compound **100** at the beginning of the experiment the excitation and emission slit had to be adjusted to 3.5 nm. The fluorescence maximum was located at 458 nm with a comparably small intensity.

Photoproduct **102** was isolated and characterized. Figure 57 shows the ¹H NMR of the isolated photoproduct.

Figure 57: ¹H NMR spectrum of photoproduct 102
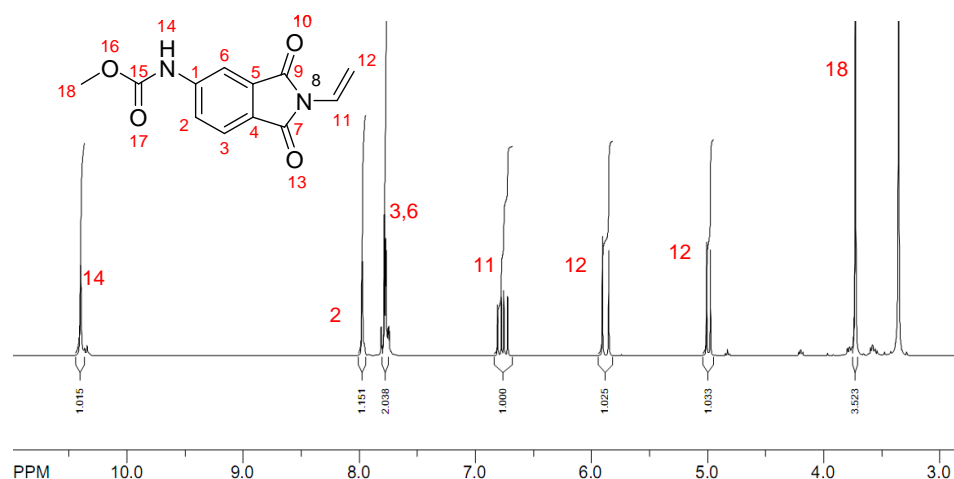
Figure 58 shows the emission spectra of **92** and **100** after different irradiation times where it can be seen that the *increasing* fluorescence effect of the photocages **92** is lower than the *decreasing* fluorescence effect of photocages **100**.
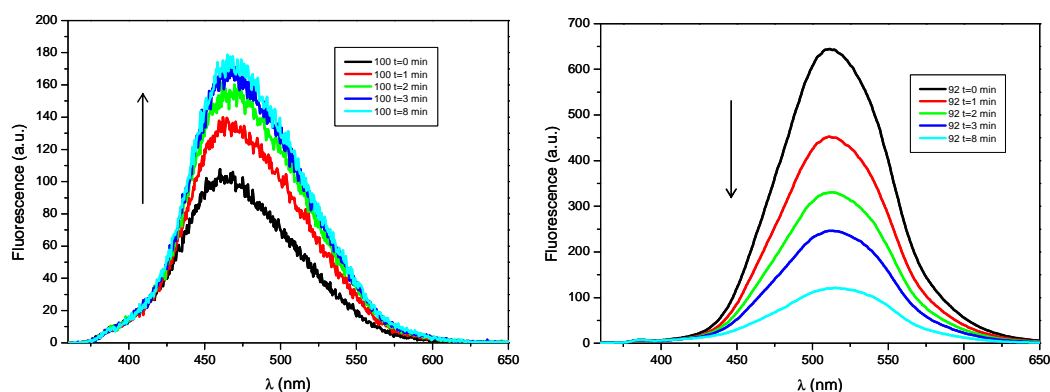

Figure 58: Emission spectra at different irradiations times, showing a fluorescence increase for 100 (left spectrum) and a fluorescence decrease for 92 (right spectrum)

In order to compare the process that is involved in the decarboxylation, the fluorescence intensities were normalized. Thus, the carbamate photocage **100** shows a fluorescence *increase* with a red shift of the maximum of about 10 nm and the dimethoxy photocage **92** presents a *decrease* of fluorescence emission after 8 min irradiation without any changes of the maximum position. A similar fluorescence increase has been observed in xanthone acetic acids, also involving a decarboxylation process but without liberation of caged molecular fragments.[68]
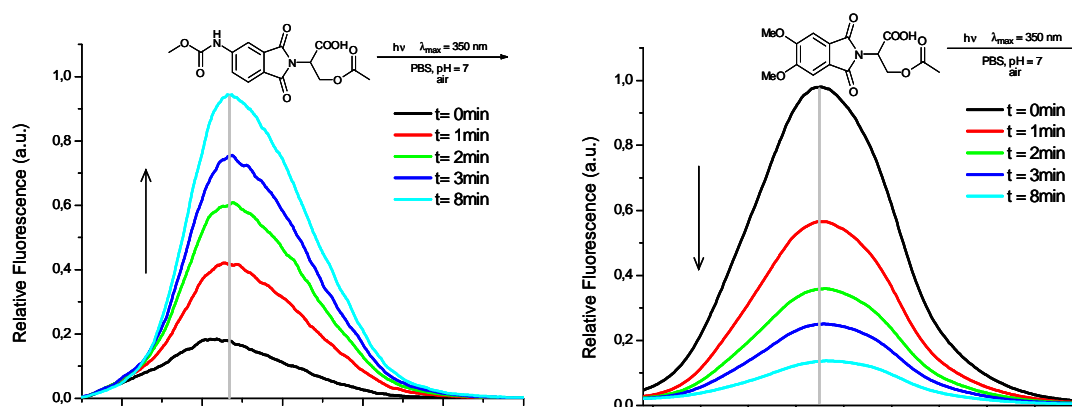
Figure 59: Relative emission spectra at different irradiations times, showing a fluorescence increase for 100 (left spectrum) and a fluorescence decrease for 92 (right spectrum)

In figure 60, the maxima of the normalized fluorescence intensities are plotted against time for both processes. It can be seen that both photocages underwent the photodecarboxylation process but in one case fluorescence intensity *increases* and in the other case the opposite happens.
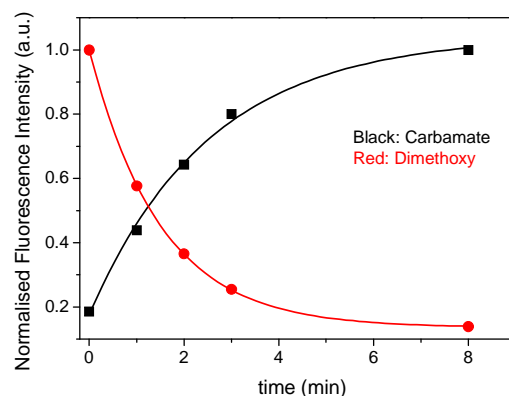
Figure 60: Normalized fluorescence intensities for the fluorescence increase and decrease process of 92 and 100

The fluorescence decrease indicates a stronger electron transfer donor capability of the enamide group in **101** in comparison with the carboxylate in the starting material **92**. The additional conjugation of the vinyl group in enamide **101** is represented by the bathochromic shift in absorption and emission. It is striking that the fluorescence of **92** is more than 50 times stronger than that of the glycine derivative under the same pH conditions. This indicates that the intramolecular fluorescence quenching is strongly inhibited by the presence of the acetate group in **92**.
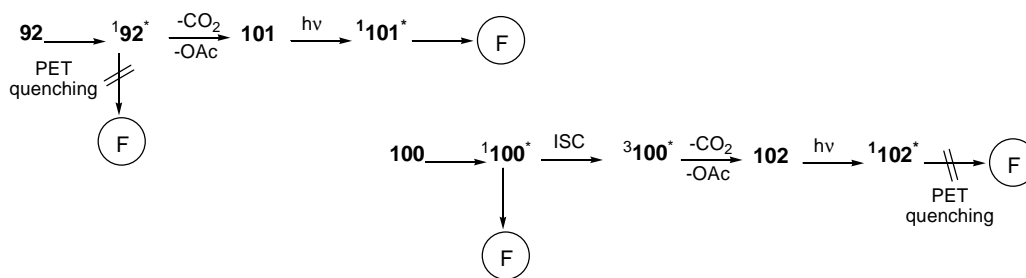
The photodecarboxylation mechanism of **100** supposably involves a competition between the singlet state decay and the intersystem crossing because most likely, the photodecarboxylation process occurs from the corresponding triplet state (scheme 33).

Scheme 33

In summary, an efficient and fast photoremovable protecting group has been described in two substituent-modified chromophores, which also includes a simple but effective fluorescent reporting function associated with a photorelease process. Depending on the substitution pattern at the aromatic ring, fluorescence up/down reporter function was observed. If the photocages would include a stereogenic element in proximity of a receptor group, these could be used for recognition of other chiral species and for enantiodifferentiation in combination with photo-decarboxylation. One possible approach is described in the following chapter.

$R_1 = R_2 = OMe$ **92**

$R_1 = NHCOOMe$ $R_2 = H$ **100**

$R_1 = R_2 = OMe$ **101**

$R_1 = NHCOOMe$ $R_2 = H$ **102**
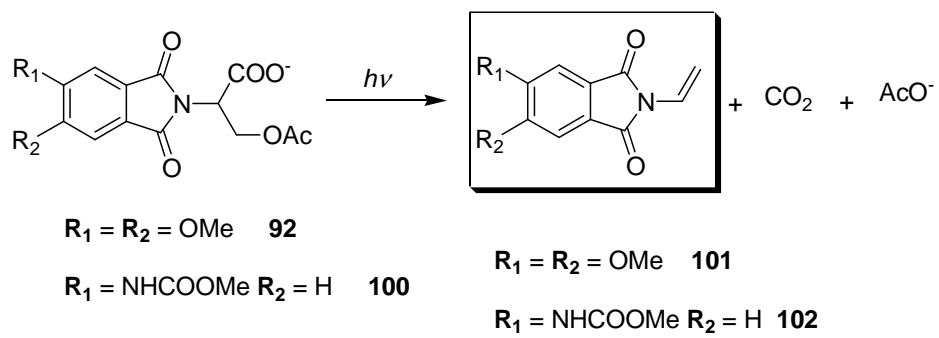
Scheme 34

3.8 Synthesis of Chiral Phthalimide-Urea-Conjugates

In a first attempt the synthesis of chiral phthalimide-urea conjugates was performed by a reaction of 3-aminophthalimide derivates with 1-((S)-1-isocyanatoethyl)benzene (**104**). Unfortunately, the expected product was not obtained by the applied methods (see experimental part), as the amino group in position 3 of the phthalimide derivate shows little reactivity towards electrophiles; in this case an isocyanate derivate. Scheme 35 shows the syntheses that were carried out for the two amino phthalimide derivates with phenylmethylisocyanate.
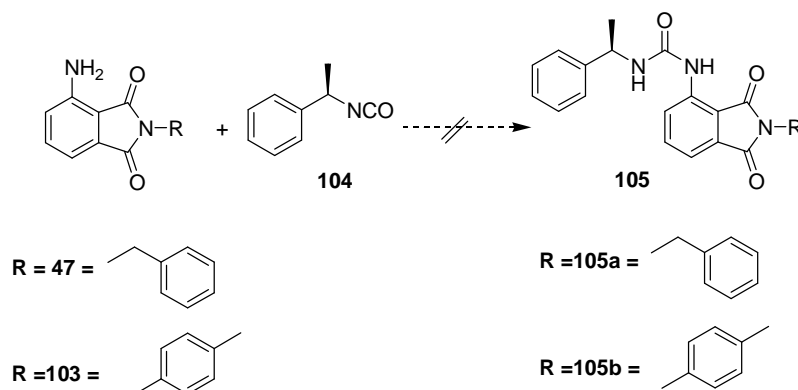
Scheme 35

Bearing in mind the results obtained in the previous reactions with 3-aminophthalimide derivates, a new synthetic route was proposed allowing the amino group to appear in another position of the aromatic ring. Thus, the synthesis of the urea-phthalimide derivates was achieved following a recently reported procedure of Lebel and coworkers [69] involving a very efficient employment of the Curtius rearrangment that allows the direct conversion of aromatic carboxylic acids into ureas.

A mixture of phenyl chloroformate (1.1 equiv.) and a less nucleophilic alcohol, *N*-benzyl-1,3-dioxoisoindoline-5-carboxylic acid (**106**, 1 equiv., received from the commercially available 1,2,4-benzenetricarboxylic anhydride) and sodium azide (1.7 equiv.) was prepared and heated to 75°C, leading to the formation of the acyl azide. The reaction mixture was then cooled to 25 °C and an amine derivate (1.5 equiv.) was added, which is able to trap the developing isocyanate intermediate and thus forms the corresponding urea.
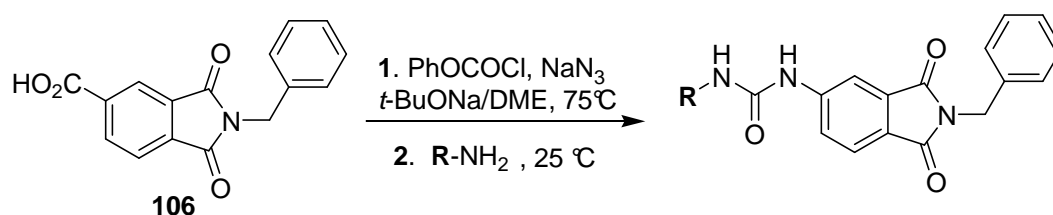
Scheme 36

The general synthesis is shown in scheme 36 and in table 15 the different urea phthalimide derivates synthesized by this route are given.

Table 15: Synthesis of urea phthalimide derivates from aromatic carboxylic acids *via* Curtius rearrangement.[a]

Entry	Urea	Yield (%) [b]
107		63
108		0 [c]
109		65
110		60
111		68
112		62

[a] Conditions: PhOCOCl (1.1 equiv.), NaN_3 (1.5 equiv.), *t*-BuONa (15 mol %), RNH_2 (1.5 equiv.). [b] Isolated yield. [c] Isolation of **108** was not possible.

Using several aromatic and aliphatic amines and amino alcoholes as nucleophiles, this method opened access to many urea phthalimide derivates, employing phenyl chloroformate and sodium azide as reagents.

Good yields were obtained for the formation of aromatic urea phthalimide derivates. The only exception (1*S*,2*R*)-cyclohexane-1,2-diamine did not led to the expected product **107**. No

characteristic signals of the coupling to generate the corresponding urea could be observed in the experiments.

In order to characterize sensor **111** it was necessary to carry out NMR experiments with variable temperature to clearly identify the OH signal, as this signal overlapped with the CH_2 signal of the benzyl group. The spectrum shows the low field shift of the OH signal upon temperature variation of 1 K (figure 61).
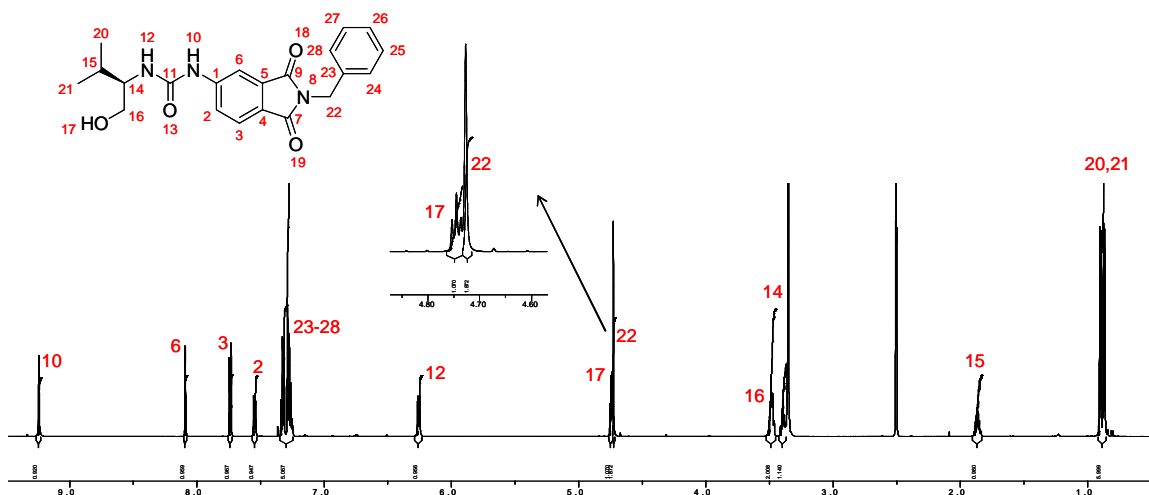
Figure 61: ¹H NMR spectrum of the sensor 111 in DMSO at 297 K

3.9 *Photophysical properties, anion sensing and chiral recognition by chiral phthalimide-urea-conjugate*

3.9.1 Photophysical properties

The photophysical properties of the sensors were determined in different solvents and are summarized in the tables corresponding to each sensor.

With increasing solvent polarity, no significant changes were observed for sensor **107**. However, the substantial red-shift in emission in the protic solvent methanol and the strongly increased Stokes shift account for the formation of an internal charge transfer state after excitation to the first excited singlet state. Singlet state deactivation by non-radiative pathways is also increased in the protic solvent methanol; in comparison with acetonitrile, the fluorescence quantum yield drops to one-third and the fluorescence lifetime increases to 17 ns.

Table 16: Photophysical data of sensor 107.

	$\lambda_{abs}{}^{a}$	$\lambda_{em}{}^{a}$	Stokes ^{b}	$E_s{}^{c}$	$\tau_f{}^{d}$	$\Phi_f{}^{e}$	$k_f \times 10^{7f}$
DMSO	353	443	5755	72	11.8	0.31	2.6
MeCN	339	430	6242	75	13.0	0.37	2.8
MeOH	337	465	8168	72	16.9	0.11	0.6
DCM	337	428	6309	75	14.8	0.22	1.4

^{a} In nm. ^{b} In cm^{-1}. ^{c} Singlet energy in Kcal / mol. ^{d} In ns. ^{e} From comparation with quinine sulfate reference. ^{f} Fluorescence rate constant ($k_f = (\Phi_f / \tau_f)$) in s^{-1}.

Sensor **109** did not show significant changes in the photophysical properties in dependence of the solvent polarity. In the presence of protic solvents such as methanol, however, a strongly increased Stokes shift accounts for the formation of an internal charge transfer state after excitation to the first excited singlet state. In contrast to **107**, the quantum yield of sensor **109** decreased in the presence of methanol to one-ninth of the value in acetonitrile, and a diminished fluorescence lifetime of 8.0 ns was detected, approximately half of the corresponding time of sensor **107**.

This difference in the fluorescence lifetimes is due to the hydroxy group that accounts for a fast deactivation from the first excited singlet state to the ground state. The non-radiative pathway that deactivates the singlet state is increased in methanol.

Table 17: Photophysical data of sensor 109.

	$\lambda_{abs}{}^{a}$	$\lambda_{em}{}^{a}$	Stokes ^{b}	$E_s{}^{c}$	$\tau_f{}^{d}$	$\Phi_f{}^{e}$	$k_f \times 10^{7f}$
DMSO	354	443	5675	72	7.8	0.16	2.0
MeCN	340	430	6155	74	14.8	0.36	2.4
MeOH	338	464	8034	71	8.3	0.04	0.5
DCM	337	425	6144	75	17.6	0.23	1.3

^{a} In nm. ^{b} In cm^{-1}. ^{c} Singlet energy in Kcal / mol. ^{d} In ns. ^{e} From comparison with quinine sulfate reference. ^{f} Fluorescence rate constant ($k_f = (\Phi_f / \tau_f)$) in s^{-1}.

For sensor **110**, **111** and **112** the photopysical properties are similar to those of sensor **107.** A substantial red-shift of the emission in the presence of MeOH was observed, in consequence the Stokes shift increases and the formation of an internal charge transfer state after excitation to the first excited singlet state is available.

The hydroxyl group of these three sensors does not contribute to a particular change of the fluorescence lifetime compared to sensor **107**. Sensor **109** is the only one where hydrogen bonding between the hydroxy group and the NH of the urea can take place so this structural reason results in a significantly different change of the lifetime.

The following tables show the photophysical data of the sensors **110, 111** and **112**.

Table 18: Photophysical data of sensor 110.

	$\lambda_{abs}{}^{a}$	$\lambda_{em}{}^{a}$	Stokes^{b}	$E_s{}^{c}$	$\tau_f{}^{d}$	$\Phi_f{}^{e}$	$k_f \times 10^{7f}$
DMSO	353	442	5704	71	13,2	0.32	2.4
MeCN	340	435	6423	73	15.1	0.34	2.3
MeOH	340	466	7952	71	18.4	0.11	0.6
DCM	341	435	6337	73	15.6	0.25	1.6

^{a} In nm. ^{b} In cm^{-1}. ^{c} Singlet energy in Kcal / mol. ^{d} In ns. ^{e} From comparison with quinine sulfate reference. ^{f} Fluorescence rate constant ($k_f = (\Phi_f / \tau_f)$) in s^{-1}.

Table 19: Photophysical data of sensor 111.

	$\lambda_{abs}{}^{a}$	$\lambda_{em}{}^{a}$	Stokes^{b}	$E_s{}^{c}$	$\tau_f{}^{d}$	$\Phi_f{}^{e}$	$k_f \times 10^{7f}$
DMSO	353	443	5755	72	13.8	0.34	2.5
MeCN	339	434	6457	73	16.0	0.36	2.3
MeOH	341	467	7912	71	19.0	0.12	0.6
DCM	341	434	6284	73	15.8	0.26	1.6

^{a} In nm. ^{b} In cm^{-1}. ^{c} Singlet energy in Kcal / mol. ^{d} In ns. ^{e} From comparison with quinine sulfate reference. ^{f} Fluorescence rate constant ($k_f = (\Phi_f / \tau_f)$) in s^{-1}.

Table 20: Photophysical data of sensor 112.

	$\lambda_{abs}{}^{a}$	$\lambda_{em}{}^{a}$	Stokes^{b}	$E_s{}^{c}$	$\tau_f{}^{d}$	$\Phi_f{}^{e}$	$k_f \times 10^{7f}$
DMSO	352	443	5835	72	13.8	0.39	2.8
MeCN	341	435	6337	73	15.3	0.38	2.5
MeOH	341	463	7727	71	18.3	0.13	0.7
DCM	344	435	6081	73	14.5	0.30	2.1

^{a} In nm. ^{b} In cm^{-1}. ^{c} Singlet energy in Kcal / mol. ^{d} In ns. ^{e} From comparison with quinine sulfate reference. ^{f} Fluorescence rate constant ($k_f = (\Phi_f / \tau_f)$) in s^{-1}.

3.9.2 Anion Sensing

In order to examine the capability of sensor **107** to sense anions like halides, absorption and fluorescence measurements were carried out in acetonitrile solution using the anions of the corresponding tetrabutylammonium salts (TBA^{+}). The absorption spectrum of **107** in the absence of anion showed three bands centered at 241, 253 and 340 (log ε = 2.95) nm. Upon titration with F^{-}, the ground state was affected and the absorption was weakly shifted to the red because of anion-recognition. Three distinctive isosbestic points were observed at 258, 317 and 372 nm respectively, which can be seen in the absorption spectrum in figure 62.
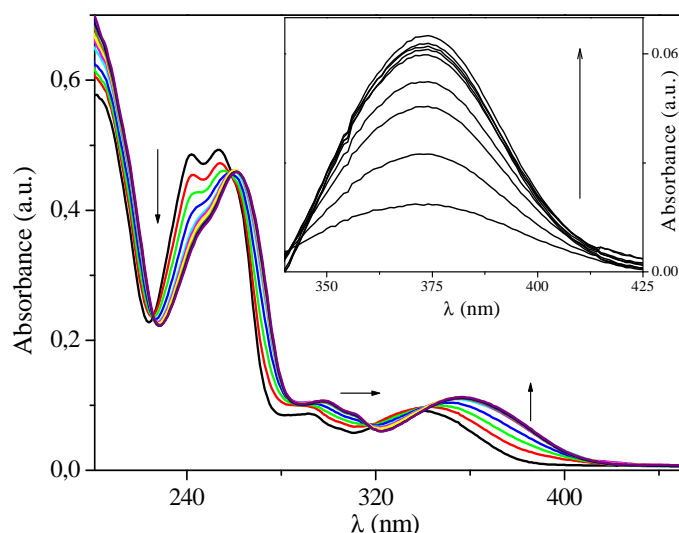
Figure 62: Absorption spectra of 107 (10^{-4} M) in the presence of increasing amounts of F⁻ (0, 0.033 →0.3 mM) in acetonitrile. Inset: difference UV-spectra of [107 + F⁻] – 107 in the long wavelength region

In order to examine the formation of a charge transfer (CT) complex, difference spectra ([1 + F⁻] – 1) were recorded (figure 62, insert). A new band was clearly observed at *ca*. 380 nm which was attributed to the CT complex absorption maximum. The formation constant of the CT complex (K_{CT}) was estimated spectrophotometrically by the Benesi-Hildebrand [70] procedure (eq. 15). A concentration plot is shown in figure 63.

$$[1] / Abs_{CT} = [1 / K_{CT}\, \varepsilon_{CT}\, [F^-])] + (1 / \varepsilon_{CT}) \tag{15}$$
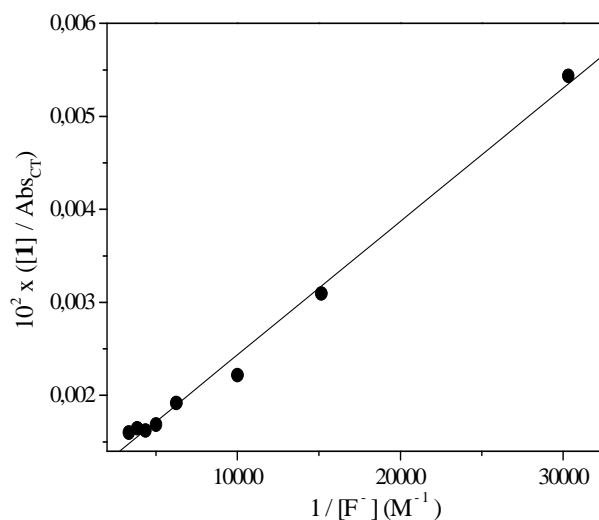

Figure 63: Benesi-Hildebrand plot to obtain the formation constant from the absorbance of the CT complex (λ_{max} = 380 nm) at different concentrations of F⁻

Abs_{CT} describes the absorbance due to the CT band at 380 nm at different concentrations of F⁻ and ε_{CT} represents the molar absorption coefficient. The ε_{CT} value in acetonitrile was

calculated from the intercept and found to be 1000 M^{-1} (log ε_{CT} = 3). The corresponding K_{CT} value determined from the slope was 6966 M^{-1}. The high value of K_{CT} indicates a strong intermolecular interaction between **107** and F^- in the ground state. This behavior was not observed in the presence of Cl^-, Br^- or I^-.
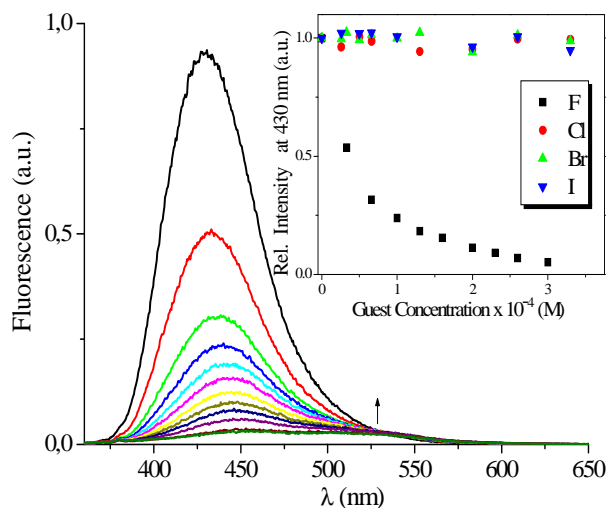

Figure 64: Emission spectra of 107 (λ_{exc} = 340 nm) in the presence of increasing amounts of F^- (0, 0.033 →0.3 mM) in acetonitrile. Insert: Changes in the emission at 430 nm upon titration with F^-, Cl^-, Br^- and I^- with 107

In order to detect changes in the excited state, the fluorescence behavior of **107** was studied in the presence of increasing amounts of anions. In contrast to the small variation observed in the ground state, the emission of **107** was strongly affected in the presence of F^- (figure 64) where it was fully quenched. A weak band at *ca*. 520-550 nm was detected with the formation of an isoemissive point at 515 nm. Concerning Cl^-, Br^- and I^- no changes in the maximum fluorescence intensity of **107** were observed (figure 64, insert) clearly supporting the assumption that the sensor **107** was suitable for F^- recognition in the family of halides. Besides, color changes in the emission of **107** upon addition of F^- were perceptible to the naked eye whereas no variation in the fluorescence was observed for the rest of the halides colorimetric sensors.
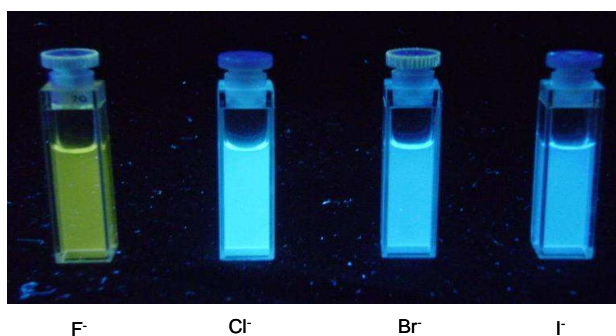

Figure 65: Photo of the cells containing sensor 107 and different halides in acetonitrile

The Stern-Volmer plot shows a non-linear behavior at high concentration of F$^-$ supporting the idea that a static quenching process of the fluorescence is taking place (figure 67). To corroborate the static fluorescence quenching, the singlet lifetime τ_F of **107** (3.3 x 10^{-6} M) was determined in the absence and in the presence of F$^-$ (3 x 10^{-3} M) under similar conditions. The τ_F values were 13 ns and 12.5 ns, respectively (figure 66).
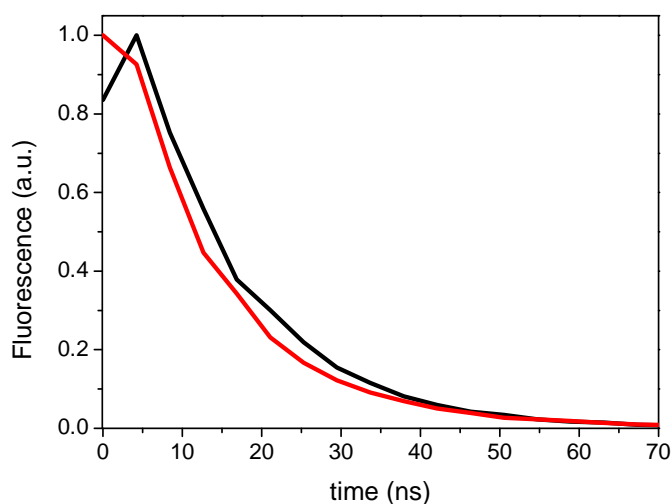

Figure 66: Normalized fluorescence decay traces of 1 (3.3 x 10^{-6} M) in the absence (—) and in the presence of fluoride anion (3 x 10^{-4} M) (—) in acetonitrile

For comparison, the emission of **107** was recorded in the presence of increasing amounts of a strong non-nucleophilic base such as 1,8-diazabyclico[5,4,0]undec-7-ene (DBU) (figure 67). In this case, fluorescence quenching is clearly linear in contrast to that found for F$^-$. Additionally, new fluorescence bands at larger wavelengths were not observed. Therefore, the different effects obtained for the emission of **107** in the presence of DBU and fluoride appear to support CT complex formation between sensor **107** and F$^-$. Figure 67 shows the Stern-Volmer plots of both quenchers.
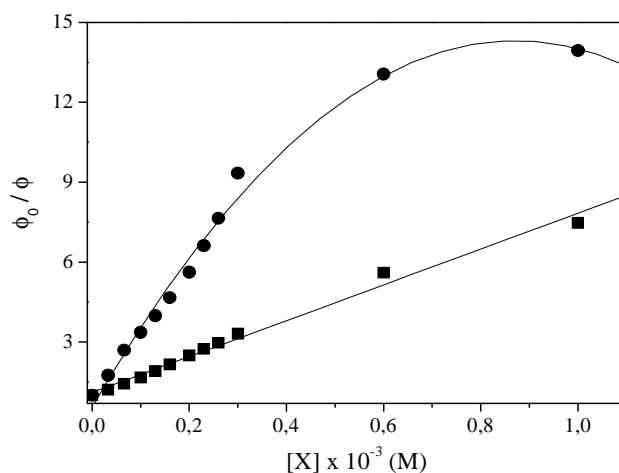

Figure 67: Stern-Volmer plots for the fluorescence quenching of 107 upon F$^-$ (●) and DBU (■) titration (0, 0.0033 → 0.3 nM)

Taking the formation of a [**107**-F⁻] complex as a basis, a steady state fluorescence measurement was carried out with a solution of **107** (10⁻⁴) and F⁻ (3.4 x 10⁻³ M) in acetonitrile. A fluorescence maximum at 520 nm was observed under selective CT complex excitation at 380 nm. The excitation maximum appears at 380 nm in good agreement with the UV-absorption measurement. Figure 68 shows the normalized absorption spectra.
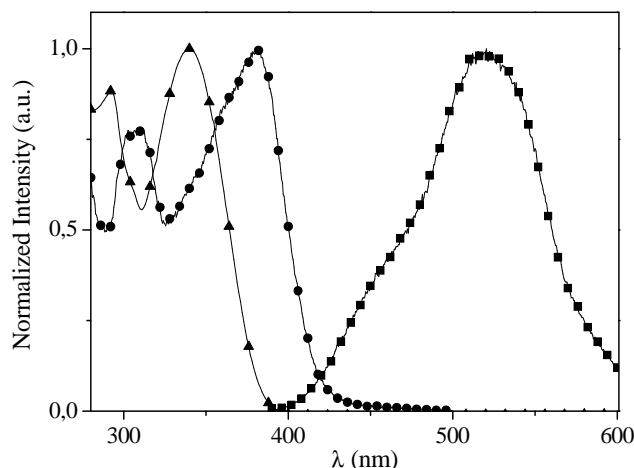

Figure 68: Normalized absorption bands of 107 (▲), excitation (●, λ_{em} = 520 nm) and emission (■, λ_{exc} = 380 nm) spectra of the complex [107-F⁻] in acetonitrile. All measurements were made under aerated conditions

To further confirm the formation of the [**107**-F⁻] complex though H-bonding interaction between F⁻ and the urea moiety, we also performed ¹H NMR titration experiments in CD₃CN. As stated above, the urea protons appeared at 5.89 ppm (H¹) and 7.81 ppm (H²) (figure 69, top spectrum). In the presence of increasing equivalents of F⁻, the urea resonances were gradually shifted downfield by 2 ppm and 4.5-5 ppm, respectively, reflecting an H-bond between the receptor and the anion. The NMR titration experiment is shown in figure 69.

More information about the nature of [**107**-F⁻] complex could be achieved from the aryl-protons H_a and H_b. It is worth to consider that H-bonding interaction between urea subunit and anion could induce also effects on the aryl group. As an example a polarization induced shift of the C-H bonds *via* a through-space effect, producing downfield shifts due to a deshielding effect by a partial positive charge formed on the proton. [71] In fact, this electrostatic effect was observed for the aromatic protons H_a and H_b as indicated by the weak downfield shift upon addition of F⁻ equivalents (figure 69), being in agreement with previous studies. [32] Besides, proton H_c was too far away from the N-H protons to undergo any electrostatic effect. On the other hand, the H¹ proton signal did not vanish even at a high concentration of anion concluding that **complete deprotonation was not taking place**, although the bond-length of N-H amide may increase considerably.
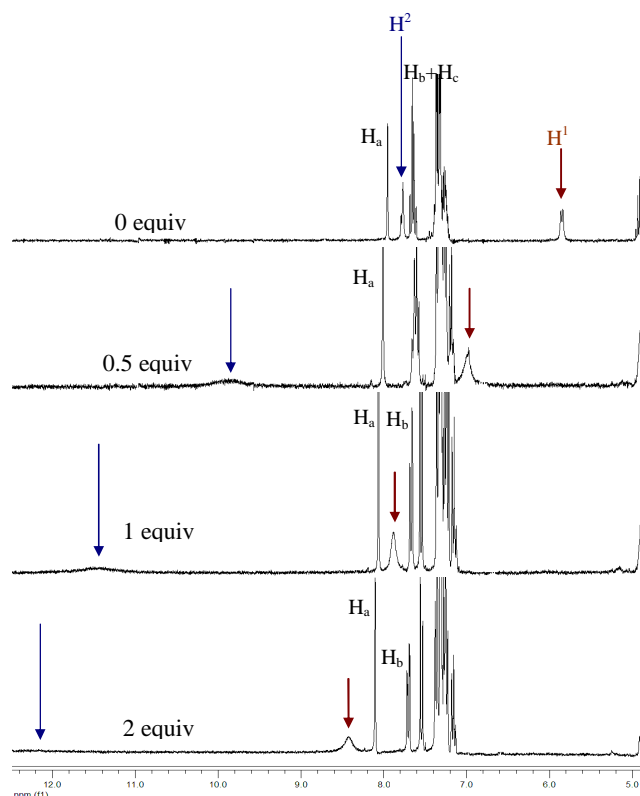
Figure 69: Changes in the ^{1}H NMR (300MHz) spectra of 107 in CD$_3$CN upon addition of F$^-$

The explanation by H-bonding interaction was supported by the effect of protic solvents on the emission of the [**107**-F$^-$] complex. Addition of methanol to a mixture of **107** and F$^-$ led to the recovery of the blue emission, *i.e.* the [**107**-F]$^-$ interaction was cancelled (figure 70).
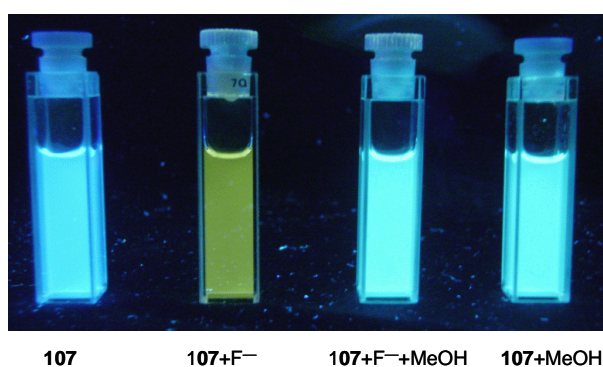

Figure 70: Colour changes observed in the emission on addition of F$^-$ in the absence/presence of methanol (10%) to an acetonitrile solution of 107

The fluorescence spectrum in methanol was red-shifted in comparison to acetonitrile, which is shown in table 16. Subsequently, addition of F$^-$ to a **107** acetonitrile solution containing 10% of methanol led to no change in the emission, thus clearly supporting the interaction between the urea moiety and the protic solvent.

Sensor **107** was found to selectively detect F⁻ since the absorption as well as the fluorescence changes were only observed in the presence of this halide anion. In this context, a fluorescence static quenching was proposed for the signalling mechanism, like depicted in scheme 37.
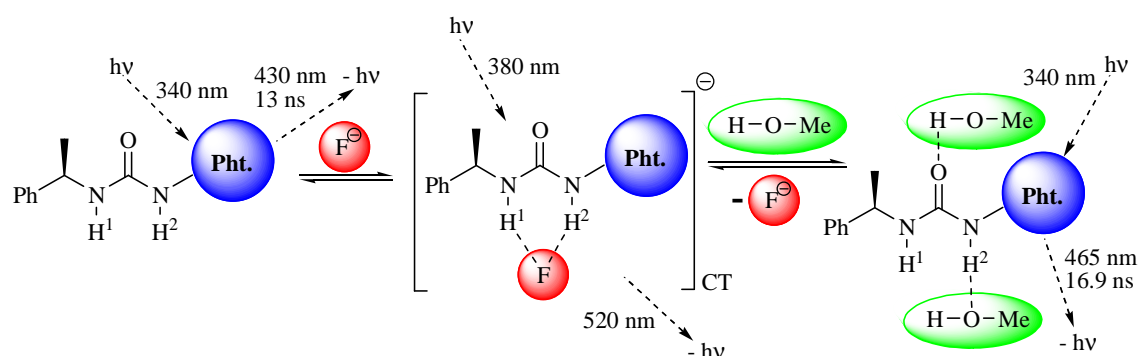
Scheme 37: The proposed mechanism for the interaction between 107 and F⁻

To ensure whether the recognition process involves a CT complex formation through H-bonding interaction between **107** and F⁻, computational calculations based on B3LYP/6-31G* [72] level of theory using the CPCM method (acetonitrile as solvent) [73] were carried out. Model system geometries were optimized in the absence and presence of the fluoride ion (figure 71) and corresponding N-H bond distances were calculated. [74] Hence, N-H_1 and N-H_2 bond lengths in the absence of anion were found to be 1.022 Å and 1.024 Å, respectively, whereas values of these bond distances after fluoride binding complex optimization were 1.035 Å for N-H_1 bond and 1.051 Å for N-H_2 bond. Although bond-elongation was observed in both cases (+0.013 Å for N---H_1 and +0.025 Å for N---H_2), it appeared no sufficient for hydrogen abstraction by F⁻, in contrast of previous observations.[75] The H---F distances were also estimated and found to be 1.710 Å (H_1---F) and 1.602 Å (H_2---F) which were close to that experimentally found in the literature for complexation of isophthalimide-like compounds with fluoride ions.[76]
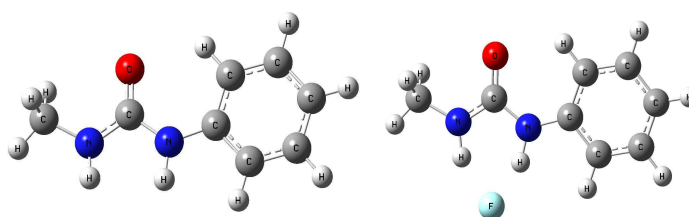

Figure 71: Geometries of the free (left) and fluoride bonded (right) model system

Moreover, both N-H_1 and N-H_2 GIAO-NMR shifts (δ) were also theoretically calculated in the absence/presence of fluoride ion. These data were in line with that obtained experimentally where δN-H values for H_1 and H_2 in the absence of F⁻ were 4.0 ppm and 5.7 ppm, respectively whereas they shifted to downfield at 7.7 ppm (Δ δN-H = 3.7 ppm) and 10.7 ppm

(Δ δN-H = 5 ppm), respectively, after complexation with F$^-$. Overall, these computational results are in agreement with experimental observations where formation of a complex between sensor **107** and F$^-$ in the ground state prevails over a possible deprotonation of the urea moiety.

Upon recognition of the anion, absorption studies revealed the typical band of a CT complex at longer wavelengths with a large formation constant. Moreover, in the presence of F$^-$ neither changes in the singlet lifetime of **107**, nor a non-linear dependence of the Stern-Volmer plot was observed, ruling out the possibility of a dynamic fluorescence quenching. The formation of the [**107**-F]$^-$ complex through H-bonding interaction was proved by ^{1}H NMR studies.

Furthermore, the capability of the other sensors (**109-112**) to detect anions such as halides, acetate and dihydrogen phosphate was tested in acetonitrile solution using the corresponding tetrabutylammonium salts (TBA$^+$) of the anions. The absorption spectra of the sensors **109-112** in absence of anions presented bands centered between 239-241, 250-253 and 339-345 nm.

With the addition of F$^-$, AcO$^-$ and H$_2$PO$_4^-$ anions to the solution containing sensors **109-112**, the characteristic absorption peak of the host at *ca.* 340 nm increased gradually with a red-shift (about 15 nm) and the formation of three isosbestic points around 258, 320 and 420 nm was observed.

Gradually increasing the concentration of F$^-$ induced a color change of the sensor solution from colorless to yellow, which could be observed by the naked eye. The most drastic color change appeared with sensor **111** in presence of F$^-$. The absorption spectrum for this recognition shows a new band at 430 nm that is an evidence for the formation of a complex.

Figure 72 and figure 73 clearly show the difference in intensity of the new band of the complex. With sensor **109** (figure 72) it is possible to detect this new band at *ca.* 430 nm by the difference spectra ([**109**- F] - **109**) (**a**-inset) with low intensity. With sensor **111** (figure 73) the new band at *ca.* 430 nm can be detected directly in the titration spectra.

These results show, that after addition of F$^-$, the ground state is affected and the absorption is weakly shifted to the red through recognition of the anion, which can be assigned to an intramolecular charge transfer (CT).
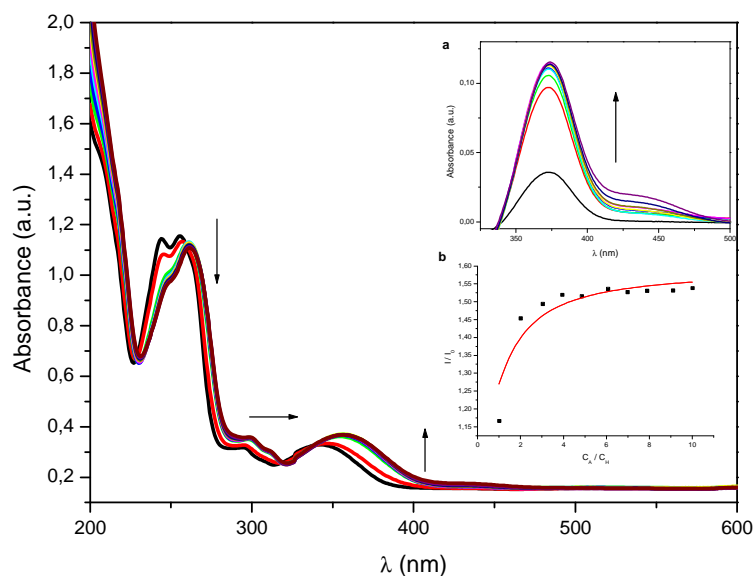
Figure 72: Absorption spectra of 109 (3.3 x 10⁻⁵) in the presence of increasing amounts of F- (0, 0.033 →0.3 mM) in acetonitrile. Inset: a) difference UV-spectra of [109 + F⁻] – 109 in the long wavelength region, b) non-linear fitting curve of change in absorbance at 343 nm

The non-linear fitting curve of the [**109** – F]⁻ complex signal intensities at 345 and 430 nm did not show an adequate adjustment. Therefore, it was not possible to calculate the association constant of this complex. However, the non-linear fitting curve confirms that **109** and F⁻ do not form a 1:1 complex. These observations make another strong equilibrium or a deprotonation process very likely to be present in the recognition mechanism.
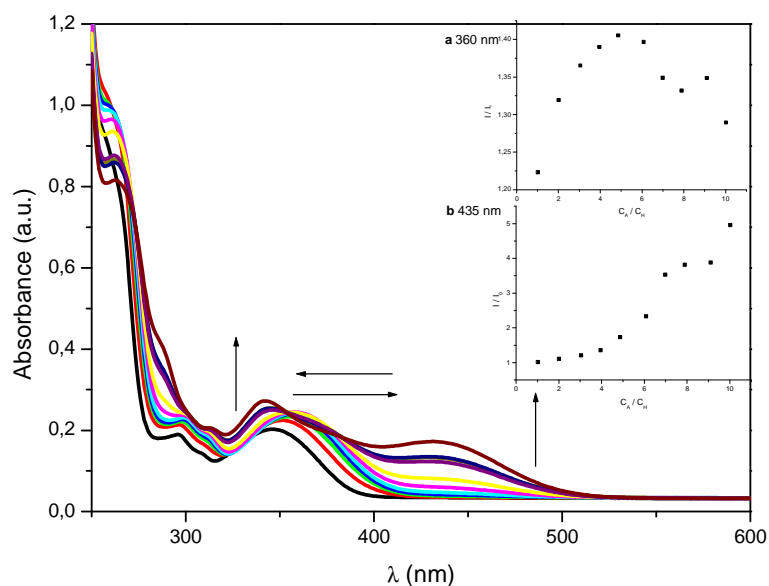

Figure 73: Absorption spectra of 111 (3.3 x 10⁻⁵) in the presence of increasing amounts of F- (0, 0.033 →0.3 mM) in acetonitrile. Inset: a- non-linear fitting curve of change in absorbance at 345 nm, b- non-linear fitting curve of change in absorbance at 430 nm

As shown in figure 74 and figure 75, a phenomenon similar to the [**109** + F⁻] complex was observed when AcO⁻ and $H_2PO_4^-$ were added into the solution of receptor **109** in acetonitrile. The new band at 430 nm was not observed with both anions but AcO⁻ and $H_2PO_4^-$ also induced an increase of the band at *ca*. 360 nm. The prepared non-linear fitting curve confirms that **109** and the anions form a 1:1 complex.
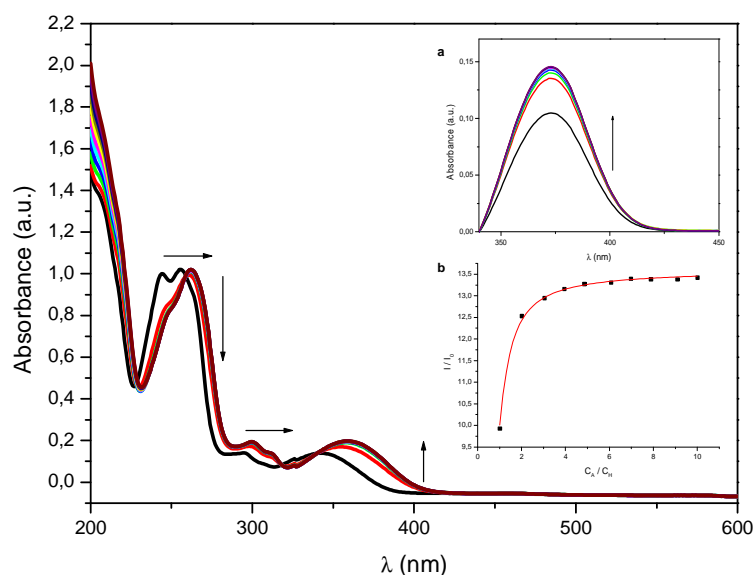

Figure 74: Absorption spectra of 109 (3.3 x 10⁻⁵) in the presence of increasing amounts of AcO⁻ (0, 0.033 →0.3 mM) in acetonitrile. Inset: a) difference UV-spectra of [109 + AcO⁻] – 109 in the long wavelength region, b) non-linear fitting curve of change in absorbance at 343 nm

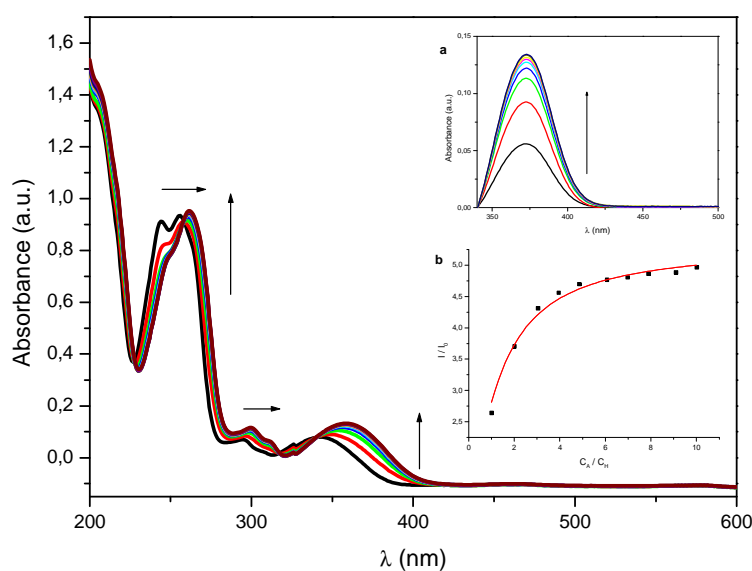**Figure 75: Absorption spectra of 109 (3.3 x 10⁻⁵ M) in the presence of increasing amounts of $H_2PO_4^-$ (0, 0.033 →0.3 mM) in acetonitrile. Inset: a) difference UV-spectra of [109 + $H_2PO_4^-$] – 109 in the long wavelength region, b) non-linear fitting curve of change in absorbance at 343 nm**

For the complexes, the association constant K_{ass} was calculated by using the following equation and optimizing the coefficients (Origin 6.0): [36]

$$A/A_0 = 1 + \frac{A_{lim}/A_0 - 1}{2}\left[1 + \frac{C_A}{C_H} + \frac{1}{K_a C_H} - \sqrt{\left(1 + \frac{C_A}{C_H} + \frac{1}{K_a C_H}\right)^2 - 4\frac{C_A}{C_H}}\right] \quad (16)$$

A_0 is the absorption intensity of the host without anions, A_{lim} is the absorption intensity reaching a limit by adding excessive anions, C_A is the concentration of anions added. C_H is the concentration of the host molecule and A is the absorption intensity of the complex. By allowing $1/K_a C_H$ to be varied, the K_a values can be obtained by non-linear least-squares analysis of A/A_0 $vs.C_A / C_H$.

The association constants of all sensors with F⁻, AcO⁻ and H₂PO₄⁻ obtained by non-linear least-squares analysis and the Benesi-Hildebrand approach are listed in table 21. The other halide anions such as Cl⁻, Br⁻ and I⁻ show a very small change in the absorption spectra that did not allow an accurate evaluation of the binding constants.

Table 21: Association constants (K_{ass}) of all sensors (107, 109-112) with F⁻, AcO⁻ and H₂PO₄⁻ in acetonitrile.

Sensor	K_{ass} (F⁻) [a]	K_{ass} (AcO⁻) [a]	K_{ass} (H₂PO₄⁻) [a]
107 [d]	6966 [b]	[c]	[c]
109 [d]	45.97 (± 18.99) x 10³	265.51 (± 13.71) x 10³	36.79 (± 4.37) x 10³
110 [d]	53.14 (± 25.16) x 10³ [e]	59.81 (± 3.36) x 10³	48.00 (± 5.13) x 10³
111 [d]	[f]	20.75 (±4.19) x 10³	2.61 (±1.02) x 10³
112 [d]	24.73 (± 2.38) x 10³	13.15 (± 3.21) x 10³	13.62 (±2.2) x 10³

[a] In M⁻¹. [b] Calculated by Benesi-Hildebrand. [C] Not measured [d]. The host concentration was 3.3 x 10⁻⁵ M. [e] R² was 0.81. [f] The constant of **111** with fluoride could be not calculated with a tolerable error by non-linear least –squares.

These high values of the constants indicate a strong intermolecular interaction between the sensor and the three anions, where F⁻ and AcO⁻ are recognized better than H₂PO₄⁻. Recognition takes place through a CT complex and in the case of [**111** – F]⁻ very likely deprotonation of the sensor is also involved.

In order to detect changes in the excited state, the fluorescence behavior of the sensors was studied in the presence of increasing amounts of anions.

In these fluorescence studies, the emission of the sensor was dramatically affected by the presence of F⁻, AcO⁻ and $H_2PO_4^-$, where AcO⁻ presents the strongest quenching effect of all sensors.

The emission at the 430 nm band was substantially quenched to nearly 100 % upon anion recognition *i.e.* formation of the anion-receptor complex. It is possible that CT complex formation is involved in these emission changes because also a small increasing band at *ca.* 520 nm appeared.
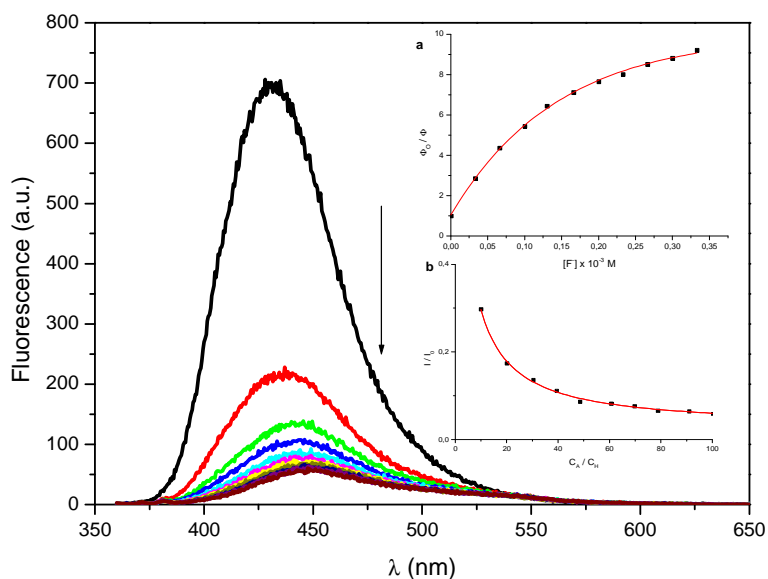

Figure 76: Emission spectra of 109 (λ_{exc} = 340 nm) in the presence of increasing amounts of F⁻ (0, 0.033 →0.3 mM) in acetonitrile

The quenching effect was stronger with AcO⁻ compared to F⁻ which can be observed directly in the emission spectra. However, only the addition of F⁻ produces a color change in the solution that is perceptible to the naked eye.
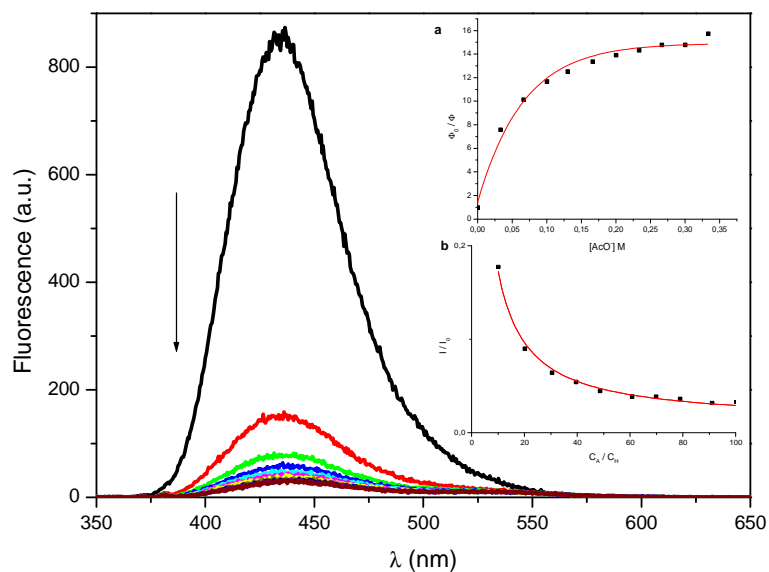
Figure 77: Emission spectra of 109 (λ_{exc} = 340 nm) in the presence of increasing amounts of AcO⁻ (0, 0.033 →0.3 mM) in acetonitrile

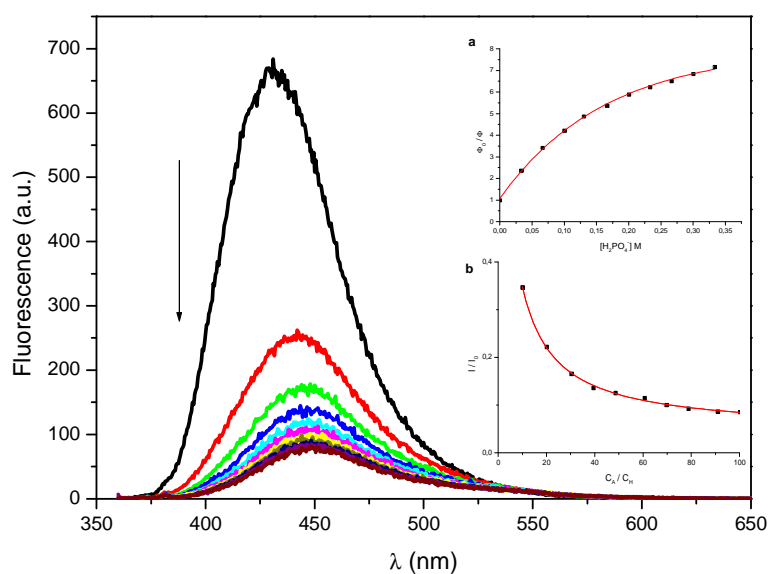**Figure 78: Emission spectra of 107 (λ_{exc} = 340 nm) in the presence of increasing amounts of H₂PO₄- (0, 0.033 →0.3 mM) in acetonitrile**

The anion recognition process due to CT is reversible and can be suppressed by addition of a protic solvent like methanol by competitive hydrogen bonding. The fluorescence emission was restored with 210 µL of methanol by a 380-fold. This indicates that the anion-receptor complexes are broken and the methanolic solvated sensor presents a red-shift of about 10 nm (445 nm).
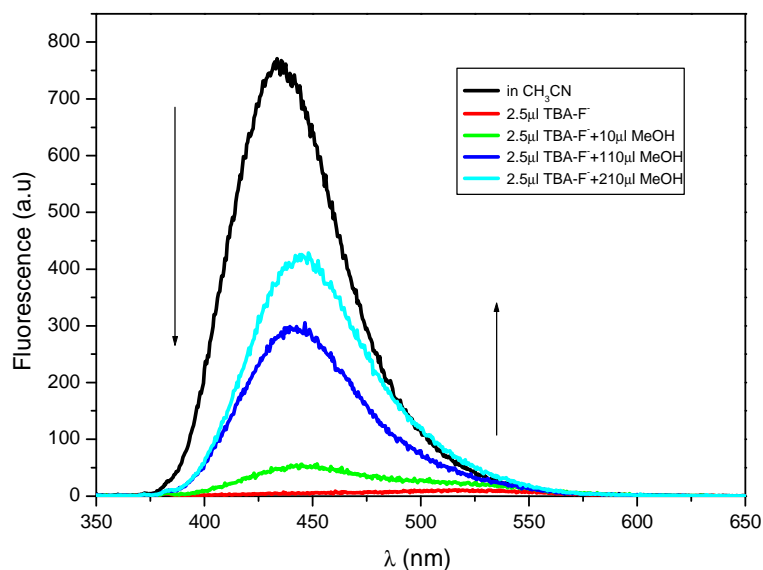
Figure 79: Emission spectra of 109 (λ_{exc} = 340 nm) in the presence of F$^-$ (0.83 mM) and increasing amounts of methanol

The Stern-Volmer plots showed a non-linear behavior at high concentration levels of anions supporting the theory that a static quenching process of the fluorescence was taking place. For comparison, the emission of the sensors **109-112** was recorded in the presence of increasing amounts of a strong non-nucleophilic base (1,8-diazabyclico[5,4,0]undec-7-ene, DBU) which is depicted in figure 80. In this case, fluorescence quenching followed a clearly fitted-linearity in contrast to that found for F$^-$, AcO$^-$ and H$_2$PO$_4^-$. Figure 80 shows the Stern-Volmer plots of the sensor **109** with different anions in presence of DBU.
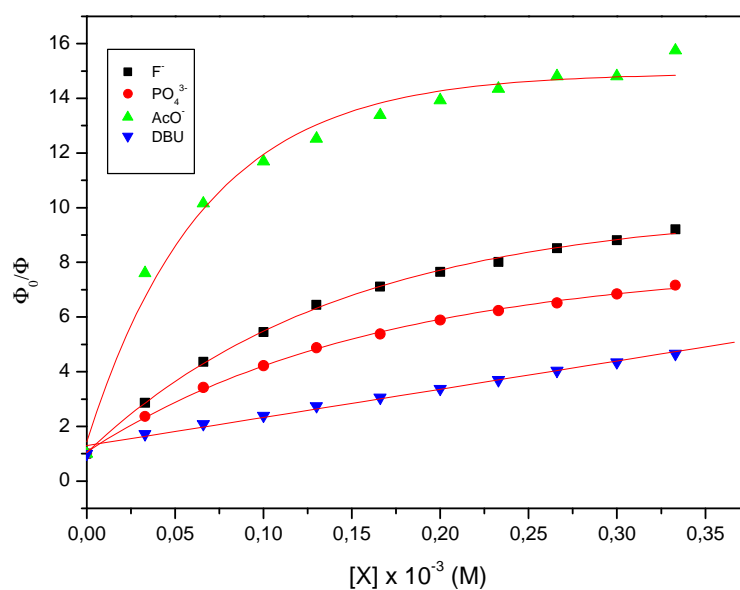

Figure 80: Stern-Volmer plots for the fluorescence quenching of 109 upon AcO$^-$ (▲), F$^-$ (■), H$_2$PO$_4^-$ (●) and DBU (▼) titration (0, 0.033 → 0.3 mM)

Conducting the experiment with Cl⁻, Br⁻ and I⁻, no changes in the maximum fluorescence intensity of the sensors were observed. A plot of the relative intensity *vs.* guest concentration shows that no interaction of these halides with the sensor occurs, clearly supporting the notion that the sensors **109-112** were suitable for F⁻, AcO⁻, and $H_2PO_4^-$. A possible reason can be a heavy atom effect for the halides Cl⁻, Br⁻ and I⁻ with the sensors. The recognition effect is depicted in figure 81.
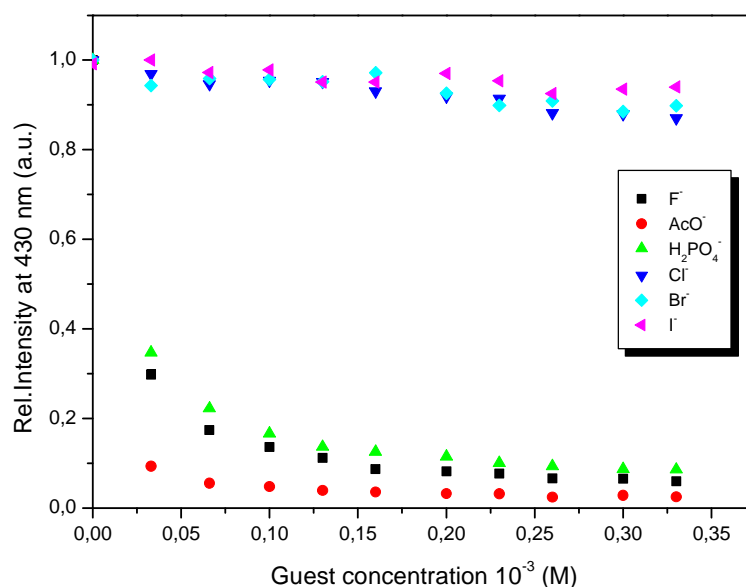

Figure 81: Changes in the emission at 430 nm upon titration with F⁻, Cl⁻, Br⁻, I⁻, AcO⁻ and $H_2PO_4^-$ with 109

The photophysical properties did not show significant changes upon changing the solvent polarity. However, the hydrogen bonding competition is always present in the process. With increasing amounts of methanol the fluorescence signal returns (figure 79). Figure 82 illustrates the Stern-Volmer plot indicating that the quenching process in DMSO is significantly slower than in CH_3CN.

Sensors **109-112** (containing hydroxy groups) can interact with the solvent through hydrogen bonds thus inhibiting the formation of the complex between anion and sensor; DMSO is a solvent that can act as a hydrogen bond acceptor. Therefore, the quenching process can not take place rapidly.
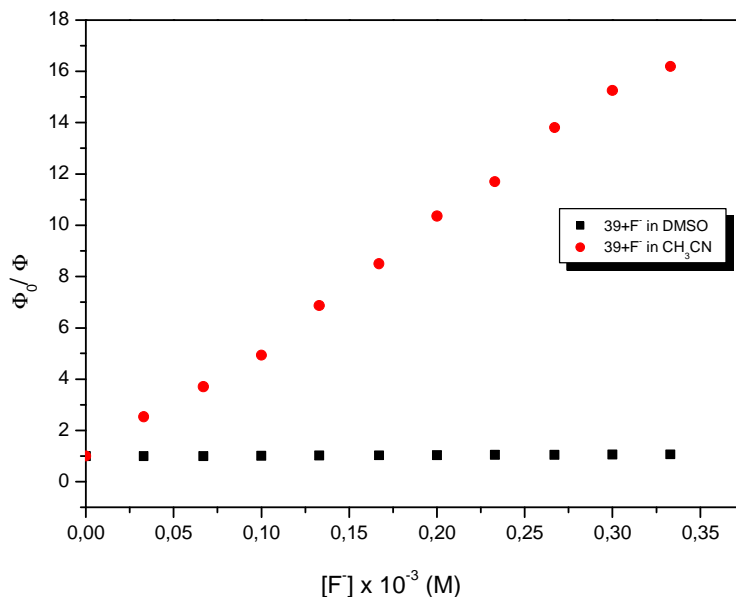
Figure 82: Changes in the emission at 430 nm upon titration with F⁻ in DMSO and CH₃CN with 111

For the complexes, the association constant K_{ass} was calculated by using the following equation and optimizing the coefficients (Origin 6.0): [36]

$$I/I_0 = 1 + \frac{I_{lim}/I_0 - 1}{2}\left[1 + \frac{C_A}{C_H} + \frac{1}{K_a C_H} - \sqrt{\left(1 + \frac{C_A}{C_H} + \frac{1}{K_a C_H}\right)^2 - 4\frac{C_A}{C_H}}\right] \quad (8)$$

I_0 is the fluorescence intensity of the host without anions, I_{lim} is fluorescence intensity reaching a limit by addition of an excess of anions, C_A is the concentration of anions added, C_H is the concentration of host molecule and I is the fluorescence intensity of the complex.

Table 22: Association constants (K_{ass}) of all sensors (109-112) with F⁻, AcO⁻ and H₂PO₄⁻ in acetonitrile

Sensor	K_{ass} (F⁻) [a]	K_{ass} (AcO⁻) [a]	K_{ass} (H₂PO₄⁻) [a]
109 [b]	86.32 (± 3.14) x 10³	169.70 (± 5.64) x 10³	70.15 (± 2.04) x 10³
110 [b]	26.74 (± 1.92) x 10³	195.31 (± 7.71) x 10³	57.24 (± 3.93) x 10³
111 [b]	46.89 (± 2.02) x 10³	90.42 (± 3.25) x 10³	41.84 (± 1.40) x 10³
112 [b]	25.37 (± 1.35) x 10³	169.71 (± 7.80) x 10³	49.61 (±2.01) x 10³

[a] In M⁻¹. [b] The host concentration was 3.3 x 10⁻⁶ M. [e] R² was between 0.990-0997. [f] The constant of all sensors with the anions could be calculated with a tolerable error by non-linear least–squares method.

By allowing $1/K_aC_H$ to be varied freely one can obtain the K_a values by non-linear least-squares analysis of I/I_0 *vs.*C_A / C_H. The association constants of all sensors with F⁻, AcO⁻ and H₂PO₄⁻ obtained by non-linear least-squares analysis and Benesis-Hildebrand are listed in table 22. The other halides anions Cl⁻, Br⁻ and I⁻ induce a very small change in the fluorescence emission spectra that did not allow an accurate evaluation of the binding constant.

The high values of the association constants represent a good recognition of the anions by the receptors through formation of the respective complex.

Sensor **109** shows high association constants with F⁻ compared to the other sensors. Possibly the complex with F⁻ involves the protons of both the amine and the hydroxyl group. In the ¹H NMR titration experiments it can be observed that the urea protons appear at 6.42 (H_1) and 9.32 (H_2) ppm, and the proton of the hydroxy group in absence of F⁻ at 5.58 ppm. In the presence of increasing equivalents of this anion, the proton signal of OH and H_2 disappear. The H_1 proton of the urea was gradually shifted downfield by *ca.* 0.5 ppm.
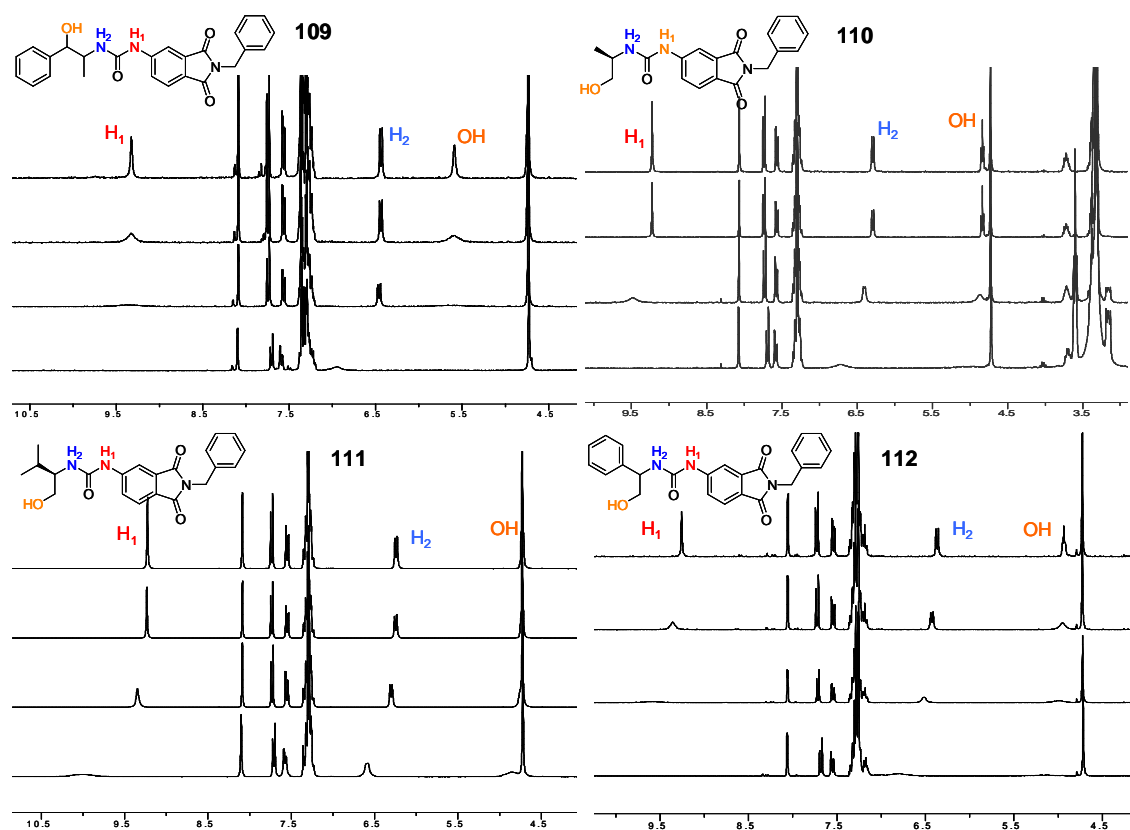

Figure 83: Changes in the ¹H NMR (300 MHz) spectra of 109-112 in DMSO upon addition of F⁻

Sensors **110-112** present smaller association constants with the examined anions. The simultaneous interaction between the proton of the hydroxyl group and the protons of the urea

with the anions is not possible here because the hydroxyl group may generate hydrogen bonding with the carbonyl group of the urea. Therefore, the association constants have smaller values than for sensor **109**. ^{1}H NMR titration experiments show a similar behavior like sensor **109** but the proton signal of the hydroxy group disappears slower. This is due to the fact that the hydrogen bonding between the carbonyl group of the urea and the hydroxyl group has to be broken before interaction with the anions can take place which delays the process.

To ensure whether the recognition process involves a CT complex formation through H-bonding interactions between **109-112** and F[-], computational calculations based on B3LYP/6-31G(d) [72] (gas phase) were carried out. Model system geometries were optimized in the absence and presence of the fluoride ion (figure 84). To compare the stable geometry of the complexes the conformation of the sensor owing the lowest energy was set to zero (kcal/mol).
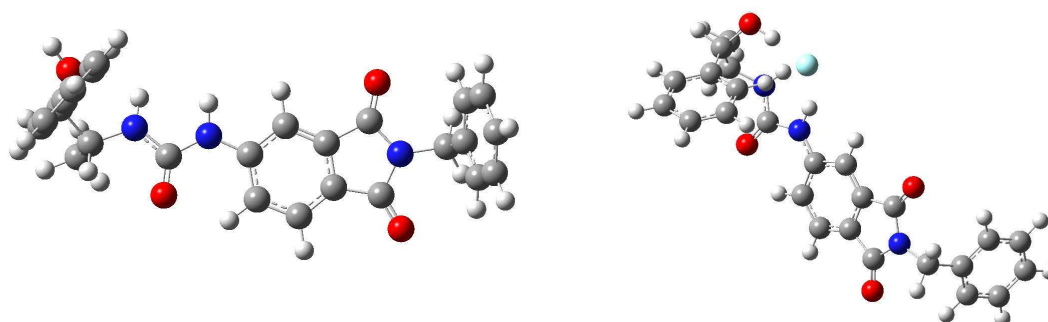

Figure 84: Geometries of the free (left) and fluoride bonded (right) model system for 109

For sensor **109,** the optimum geometry is given by a conformation where the fluoride is centered between the OH and the two NH of the urea. This conformation makes multiple hydrogen bonding possible.

Sensors **110-112** showed a similar geometry for complex formation. Again the fluoride is centered between OH and the two NH of the urea moiety, which makes hydrogen bonging possible (figure 85).
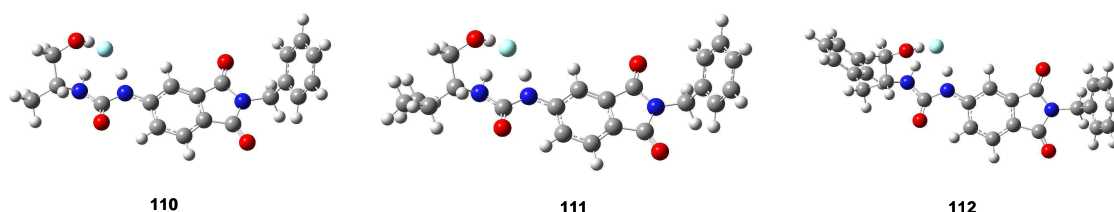

Figure 85: Calculated geometries of fluoride bound to sensors 110-112

Alternative complex conformations were also observed for all sensors with hydrogen bonding between the hydroxy group and the carbonyl group of the urea moiety. As a

consequence the fluoride interacts with the NH group of the urea in a first step to generate the hydrogen bonding. These complexes showed the second lowest energy (figure 86). The energy difference between the complexes of figure 85 and the complexes of figure 86 corresponds to the energy of the hydrogen bonding between the hydroxy group and the carbonyl group of the urea moiety. The energy for sensors **109**-**112** is 3.89, 2.25, 1.11, 0.21 kcal/mol respectively. For **109**, F$^-$ showed the largest association constant and energy, which means that F$^-$ interacts stronger with the proton of the NH group before the hydrogen bond between the hydroxy group and the carbonyl group is lost. On the other hand, the opposite situation occurrs for **112**. For compounds **110** and **111** this association constant differs from the expected, which means that another effect is involved in complex formation. This could be the neighboring effect of the *iso*-propyl group in comparison with the methyl group.
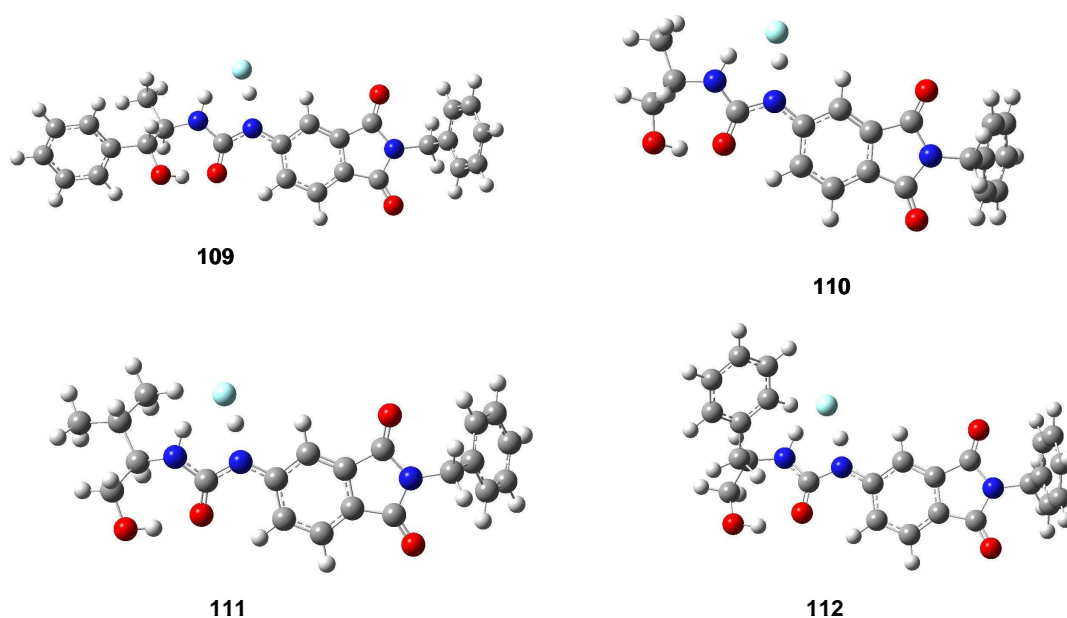

109

110

111

112

Figure 86: Calculated geometries of complexes between sensors 109-112 and fluoride

In the ^{1}H NMR experiments fluoride interaction is only marginal affected by the substituent of the receptor as can be seen in figure 83. To confirm this observation further theoretical calculations are necessary considering NH bond distance and solvent influence.

Acetate (AcO$^-$) interacts stronger with the sensor than F$^-$ and H$_2$P$_4$O$^-$ showing the highest value of the association constants with **110**. Hydrogen bonding between the receptor and AcO$^-$ can be depicted as shown in figure 87. The delocalization of the charge between both acetate oxygen atoms results in two independent hydrogen bonds with the NH-groups of the urea receptor.
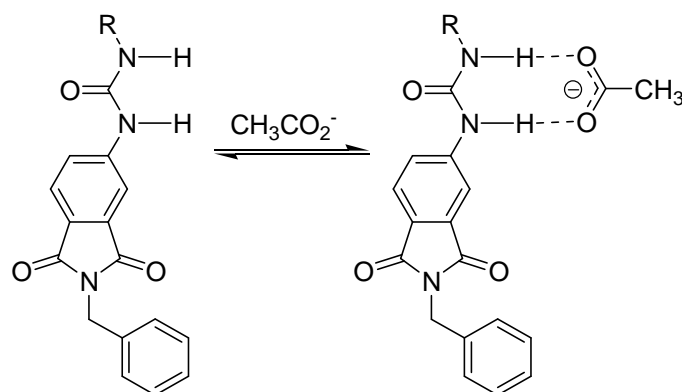
Figure 87: Hydrogen bonding of the urea receptor with acetate

The hydroxyl group of the R-substituent at the urea moiety can be responsible for an increase or decrease of the association constant depending on possible groups that can interact through a competing hydrogen bonding.

In summary the new sensors also showed a good binding selectivity towards the anions AcO⁻, F⁻, $H_2PO_4^-$ that in most cases followed the order K_{ass} AcO⁻ > K_{ass} F⁻ > K_{ass} $H_2PO_4^-$ or K_{ass} AcO⁻ > K_{ass} $H_2PO_4^-$ > K_{ass} F⁻. Evidence for the hydrogen bonding nature of the urea-anion and hydroxyl group-anion was further obtained by ^{1}H NMR titration of the sensors with the anion in DMSO-d_6. The fluoride complexes established through hydrogen bonding were proved by theoretical calculations. For the other anions this still has to be calculated in future investigations.

3.9.3 Chiral recognition

Molecular recognition, especially chiral recognition, is one of the most fundamental and crucial properties of various natural systems. [77]

Erwing and coworkers [78] found that *meningococci* (bacterium that causes cerebrospinal meningitis) are able to grow on either enantiomer of lactate. The enzymes for the lactate-oxidizing activity in the bacteria are specific for one of the two isomers which is *D*-lactate.

Chan and coworkers [79] explored the neurological toxicity of the isomeric form of lactate in experimental animals to determine the serum levels of *D*- and *L*-lactate achieved in stable patients during routine peritoneal dialysis (a treatment for patients with severe chronic kidney failure). In patients undergoing peritoneal dialysis who develop abnormal neurological changes they observed serum levels of *D*-lactate. *L*-lactate is produced in the anaerobic metabolism of glucose and its determination is of interest in clinical analysis, sports medicine and food analysis.[80] The important role of the lactate in a wide variety of biological processes motivates the development of other methods for detection and chiral discrimination of the lactate isomers.

Taking into account the stereogenic centre of the sensors **107, 109-112**, enantiodifferentiation studies were performed by fluorescence quenching in the presence of enantiomerically pure amines (*D*- and *L*-methylbenzylamine, *D*- and *L*-phenylethanol) as well as *D*- and *L*-lactate as sodium salts.

Fluorescence investigation showed that amines efficiently quench the emission of these sensors whereas no important changes were detected in the presence of alcohols. No enantio-differentiation was however observed in the quenching process with chiral amines. Figure 88 and figure 89 show the fluorescence emission change upon addition of the four quenchers and (only for the *D*- and *L*-methylbenzylamine) the Stern-Volmer plot.
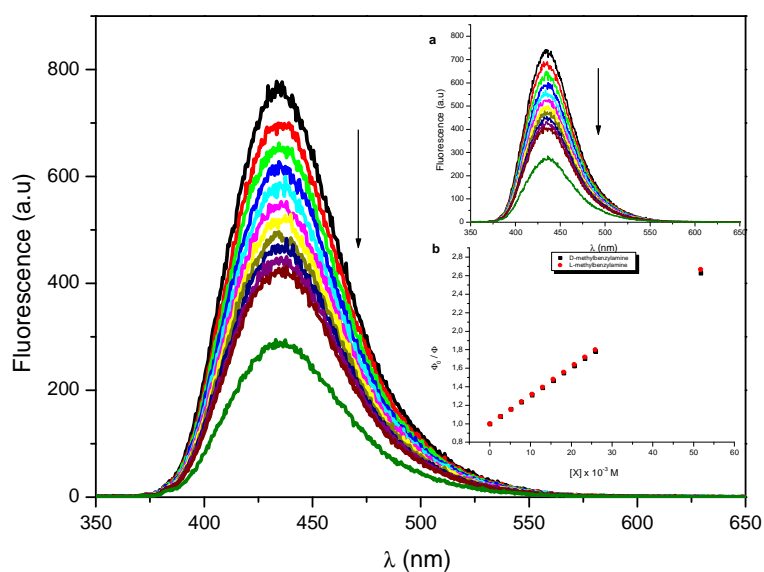

Figure 88: Emission spectra of 110 (λ_{exc} = 340 nm) in the presence of *D*-methylbenzylamine (0, 2→50 mM) in acetonitrile. Insert: a) Emission spectra of 110 (λ_{exc} = 340 nm) in presence of *L*-methylbenzylamine (0, 2→50 mM) in acetonitrile. b) Stern-Volmer plots for fluorescence quenching of 38 by *D*-methylbenzylamine (■) and *L*-methylbenzylamine (♦)
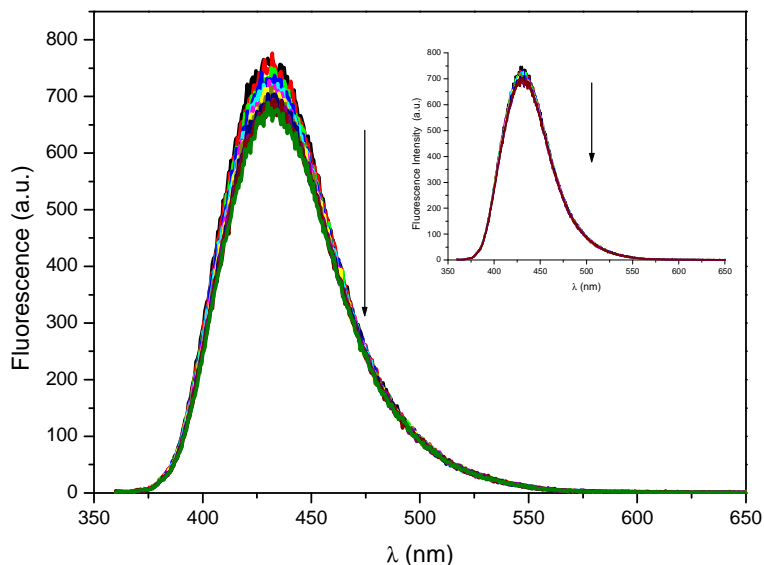
Figure 89: Emission spectra of 110 (λ_{exc} = 340 nm) in the presence of *D*-phenylethanol (0, 2→220 mM) in acetonitrile. Insert: Emission spectra of 38 (λ_{exc} = 340 nm) in the presence of *L*-phenylethanol (0, 2→220 mM) in acetonitrile

Chiral recognition of *D*- and *L*-lactate was carried out through UV-vis absorption and fluorescence quenching.

Upon addition of *D*- and *L*-lactate no drastic changes were observed in the absorption spectra of the sensors, but a new band at 340 nm with weak intensity was detected together with an isosbestic point at 317 nm. To examine the formation of a new complex between the sensors and the *D*- and *L*-lactate, the difference spectra [**Sensor** + *D*- or *L*-lactate]-**Sensor** were calculated and are shown for sensor **107** in figure 90 and figure 91.
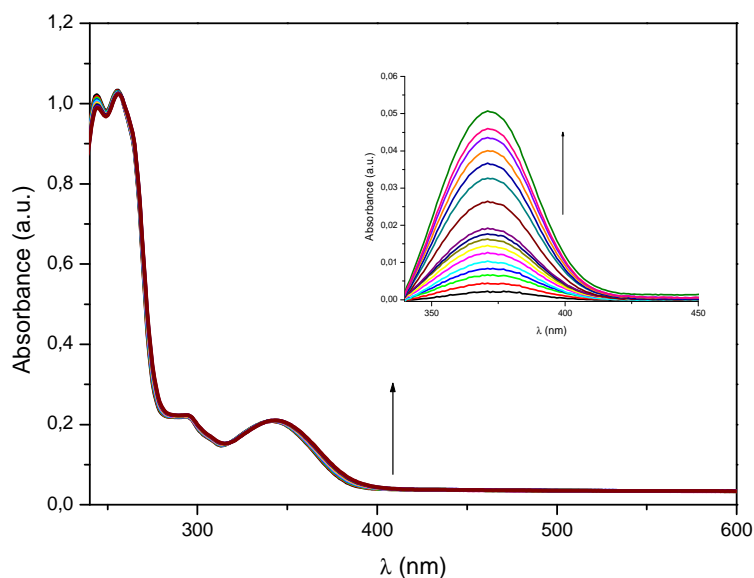

Figure 90: Absorption spectra of 107 (3.3 x 10^{-5} M) in the presence of increasing amounts of *D*-lactate (0, 0.033 →0.3 mM) in acetonitrile. Inset: a) difference UV-spectra of [107 + *D*-lacate] – 107 in the long wavelength region

Figure 91: Absorption spectra of 107 (3.3 x 10^{-5} M) in the presence of increasing amounts of *L*-lactate (0, 0.033 →0.3 mM) in acetonitrile. Inset: a) difference UV-spectra of [107 + *L*-lacate] – 107 in the long wavelength region
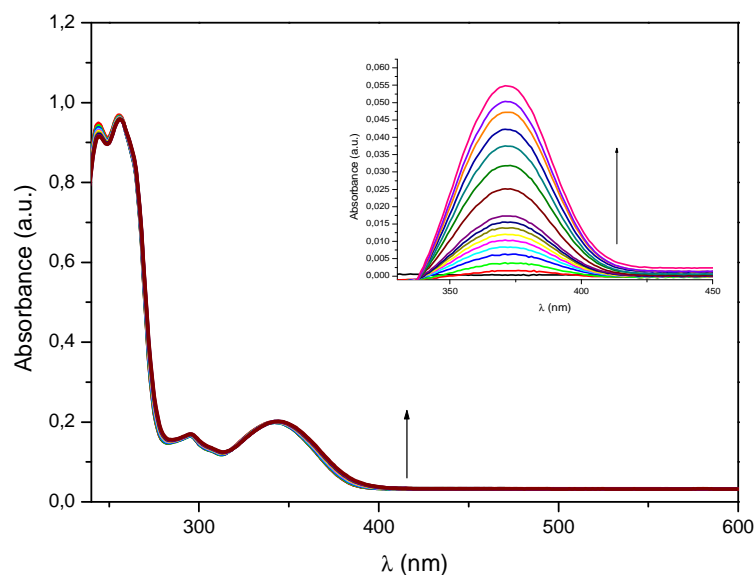
The results of the difference spectra confirm the formation of new species. The association constant could not be calculated from these absorption spectra because the changes were not strong enough. However, this effect was found for all interactions between sensors and the lactate isomers.

Chiral recognition requires multiple-point interaction. [40] In this work the interaction was based on hydrogen bonding between the receptor and *D*- and *L*-lactate. Enantioselective detection of *D*- and *L*-lactate due to fluorescence quenching promises a higher sensitivity than detection by absorption, so fluorescence experiments were conducted. The fluorescence emission of the sensors was decreased upon addition of *D*- and *L*-lactate (0.033 → 0.3 mM) and was observed for all sensors with stronger or weaker effect. The next figures show the emission spectra (λ_{em} = 430 nm) of sensor **107** and its changes upon addition of *D*- and *L*-lactate (figure 92 and figure 93).
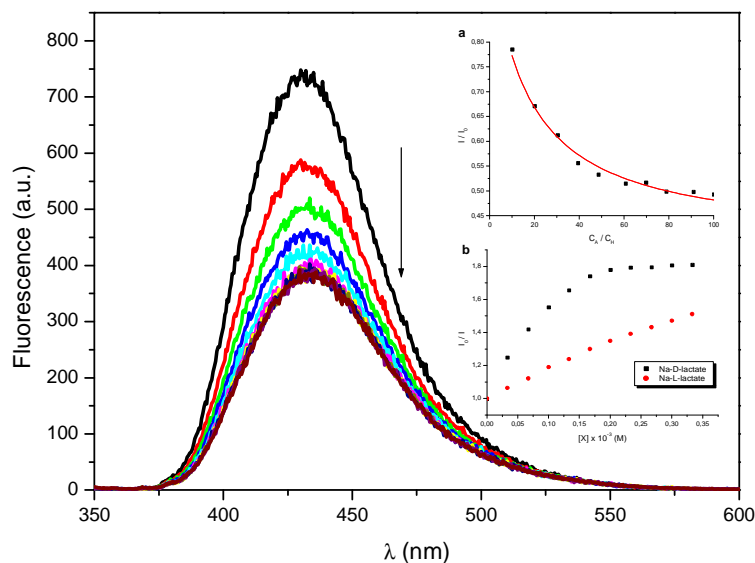
Figure 92: Emission spectra of 107 (λ_{exc} = 340 nm) in the presence of increasing amounts of D-lactate (0, 0.033 →0.3 mM) in acetonitrile. Insert: a) changes in the fluorescence intensity of 107 upon addition of D-lactate. The red line is a line-fitted curve. b) Stern-Volmer plots for the fluorescence quenching of 107 upon addition of D-lacatate (■) and L-lactate (♦)

The quenching efficiency of D-lactate was much higher than that of L-lactate for all sensors which can be seen in the difference of the emission spectra in figure 92 and figure 93. Figure 92 insert (b) shows the Stern-Volmer plot that indicates two different processes being involved in the recognition of D- and L-lactate. D-lactate presents a non-linear curve that can be associated with a static quenching process, and the quenching with L-lactate presents a linear slope that can be associated with a dynamic process.
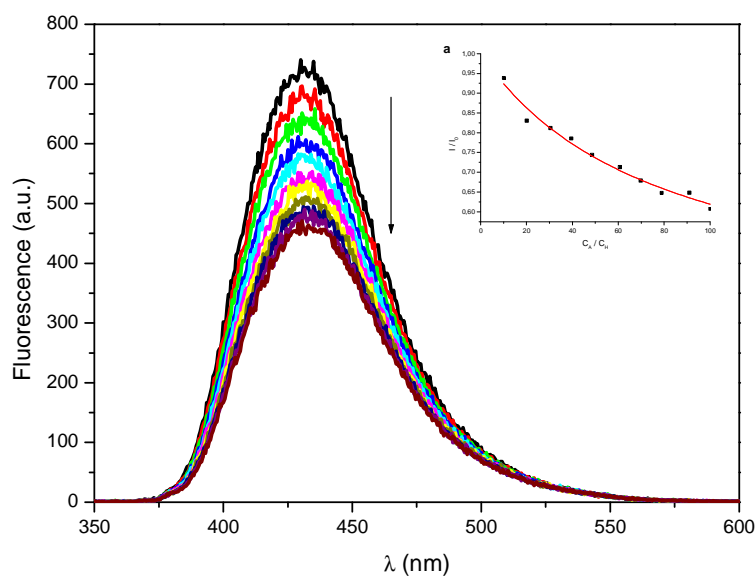

Figure 93: Emission spectra of 107 (λ_{exc} = 340 nm) in the presence of increasing amounts of L-lactate (0, 0.033 →0.3 mM) in acetonitrile Insert: a) changes in the fluorescence intensity of 107 upon addition of L-lactate. The red line is a line-fitted curve.

Measurements of the fluorescence lifetimes is the most definite method to distinguish between static and dynamic quenching: for static quenching $\tau_0 / \tau = 1$, in contrast to dynamic quenching where $F_0 / F = \tau_0 / \tau$. [6]

To confirm the nature of the quenching process lifetime measurements of sensor **109** were performed upon addition of *D*- and *L*-lactate. For *D*-lactate it could be confirmed that the interaction between the sensor and anion occurs by a static process. The lifetimes of the complex [*D*-lactate-**109**] remain almost constant and satisfy the equation $\tau_0 / \tau = 1$.

Lifetime measurement of complex [*L*-lactate-**109**] presents results that can not confirm a pure static quenching because equation $F_0 / F = \tau_0 / \tau$ is not satisfied. The Stern-Volmer plots for both lactates are shown in figure 94.
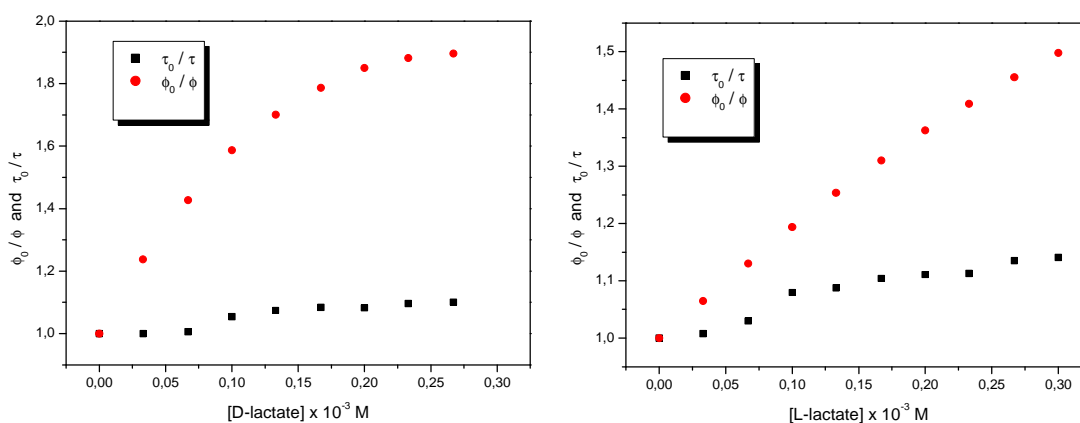

Figure 94: Stern-Volmer plot for the fluorescence quenching of 109 in function of the intensity (ϕ, ◆) and lifetimes (τ, ■) upon addition of *D*-lacatate (right) and *L*-lactate (left)

In most instances the fluorophore can be quenched both collisional and by complex formation with the same quencher. [6] This combination of quenching processes can be represented by the following mechanism:
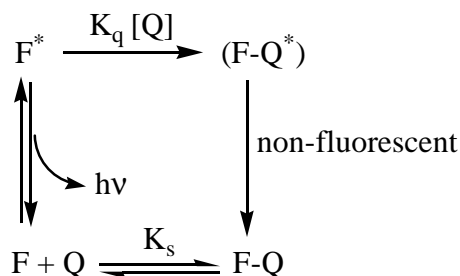

Figure 95: Mechanism of combined dynamic and static quenching

Satisfactory non-linear curve fitting (the correlation coefficient is over 0.99) confirmed that *D*-lactate forms a complex with all sensors whereas *L*-lactate shows the formation of a weaker complex compared to *D*-lactate.

Sensor **109** shows a high value for the association constant, indicating that the interaction of lactate with the sensor may occur in a similar way like it happens with acetate (due to charge delocalization between two oxygen atoms).

With the results of these absorption and fluorescence quenching studies the formation of a complex between *D*- and *L*-lactate with the urea receptors is obvious, which can be observed at longer wavelengths.

The enantioselectivity was satisfactory because recognition of the enatiomers takes place by different mechanisms. The *D*-lactate recognition occurs under static quenching and *L*-lactate is very likely recognized by a combination of static and dynamic quenching. For these complexes, the association constant K_{ass} was calculated by using the following equation and optimizing the coefficients (Origin 6.0): [36]

$$I/I_0 = 1 + \frac{I_{\lim}/I_0 - 1}{2}\left[1 + \frac{C_A}{C_H} + \frac{1}{K_a C_H} - \sqrt{\left(1 + \frac{C_A}{C_H} + \frac{1}{K_a C_H}\right)^2 - 4\frac{C_A}{C_H}}\right] \tag{8}$$

where I_0 is the fluorescence intensity of the host without anions, $I_{\lim}$ is the fluorescence intensity reaching a limit by addition of an excess anions, C_A is the concentration of anions added, C_H is the concentration of host molecule and I is the fluorescence intensity of the complex.

By allowing $1/K_a C_H$ to be varied free, the K_a values can be obtained by non-linear least-squares analysis of I/I_0 *vs.* C_A / C_H.

Table 23: Association constants (K_{ass}) for all sensors (107, 109-112) with *D*- and *L*-lactate in acetonitrile

Sensor	K_{ass} (Na-*D*-Lactate)[a]	K_{ass} (Na-*L*-Lactate)[a]	$K_{ass}D/K_{ass}L$
107[b]	19.16 ($\pm$ 1.80) x 10^3	3.84 ($\pm$ 0.74) x 10^3	4.99
109[b]	25.89 ($\pm$ 2.08) x 10^3	5.54 ($\pm$ 0.47) x 10^3	4.67
110[b]	17.75 ($\pm$ 2.08) x 10^3	4.15 ($\pm$ 0.40) x 10^3	4.27
111[b]	15.80 ($\pm$ 3.62) x 10^3	3.37 ($\pm$0.57) x 10^3	4.70
112[b]	20.40 ($\pm$ 1.49) x 10^3	2.93 ($\pm$0.40) x 10^3	6.96

[a] In M^{-1}. [b] The host concentration was 3.3 x 10^{-6} M. [e] R^2 was between 0.987-0998. [c] The constant of all sensors with *D*- and *L*-lactate could be calculated with a tolerable error by non-linear least – squares method.

To ensure whether the chiral recognition process involves a CT complex formation *via* H-bonding interaction between **107, 109-112** and *D*- and *L*-lactate, computational calculations

based on B3LYP/6-31G(d) (gas phase) were carried out. Model system geometries were optimized in the absence and presence of *D*- and *L*-lactate (figure 96). To compare the geometry of the complexes the most advantageous energy conformations (zero point energies, Kcal/mol) were used.
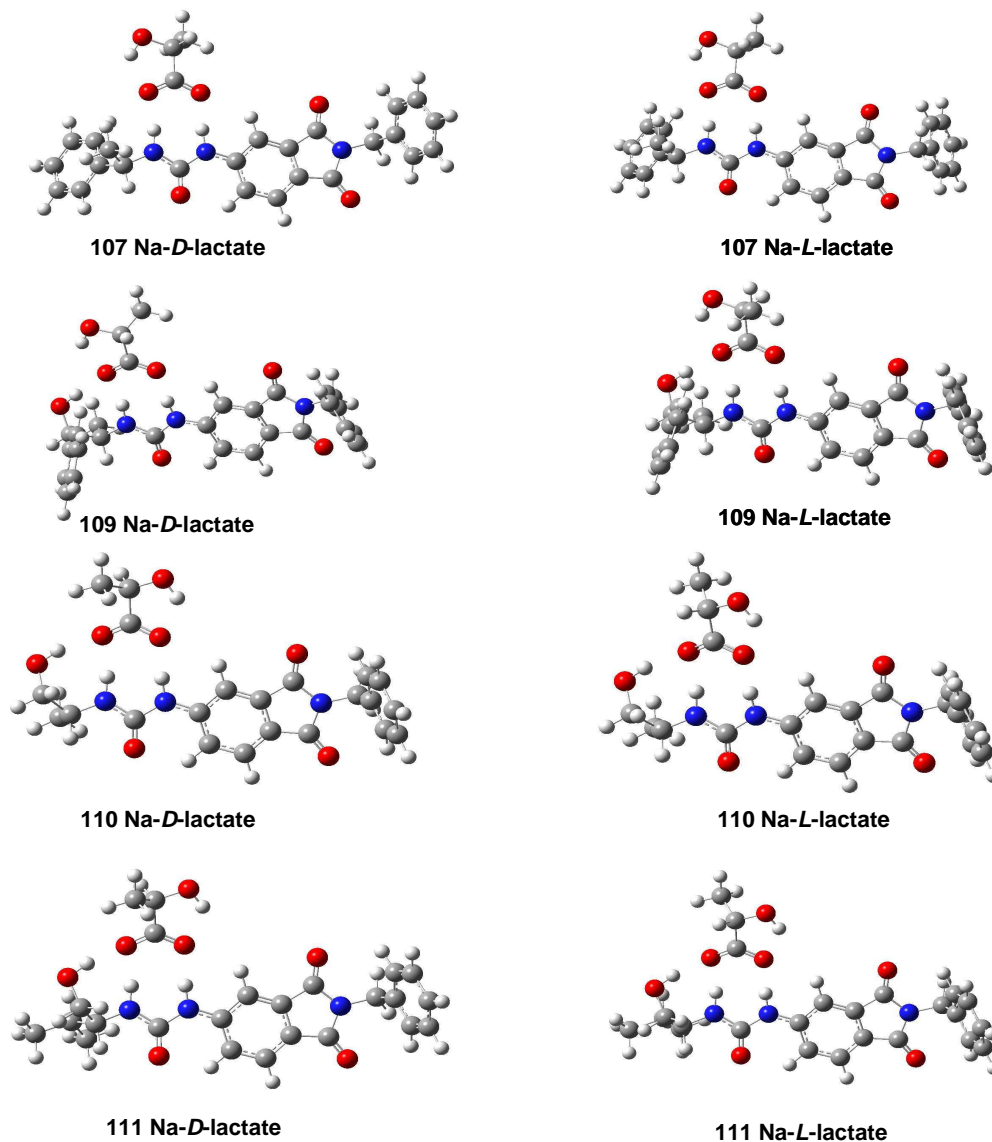

107 Na-*D*-lactate   **107 Na-*L*-lactate**

109 Na-*D*-lactate   **109 Na-*L*-lactate**

110 Na-*D*-lactate   **110 Na-*L*-lactate**

111 Na-*D*-lactate   **111 Na-*L*-lactate**

Figure 96: Calculated geometries of complexes between sensors 107, 109-111 and *D*- and *L*-lactate

The zero point energies of the calculated complex did not show significant changes when *D*- or *L*-lactate interacted with the same sensor, in contrast to the absorption and fluorescence experiments reported in this chapter.

In conclusion, the phthalimide based chiral receptors **107, 109-112** containing a urea group showed enantioselective recognition towards chiral lactate ions. The recognition was evaluated by absorption, fluorescence, but not by theoretical calculations. Receptor **112** exhibits an

excellent chiral recognition ability towards the enantiomers of lactate, the other sensors can distinguish between both enantiomers with less efficiency. Fluorescence recognition of the anions involves two different processes for all sensors, *D*-lactate due to a static quenching process and *L*-lactate by a combination of a static and dynamic process. Theoretical calculations are ongoing to rationalize the enantioselectivity of the sensors towards *D*- and *L*-lactate.

3.10 Fluorescence study of the sensors 107 and 109-112 with different peroxides

Previous fluorescence experiments showed that sensors **107** as well as **109-112** interact directly with protic solvents such as methanol and thus exhibit changes in the fluorescence emission. The following experiments were executed in order to examine if this effect can be used for the recognition of hydrogen peroxide and other peroxides.

As it is well known, hydrogen peroxide is one of the most important analytes because of its involvement in explosives. Figure 97 shows that no fluorescence changes can be observed in the fluorescence emission of sensor **107** in dry acetonitrile solution as well as in the presence of water after two hours of irradiation. However, when hydrogen peroxide was present, the fluorescence of the probe in the UV-reactor (355 nm) which was perceptible to the naked eye completely disappeared. In a first assumption, sensor **107** seemed to be a suitable sensor for hydrogen peroxide recognition.

Subsequently time dependent fluorescence quenching studies were performed for this system. The samples were placed into quartz cells of 1 cm path length. Compound concentration was adjusted to 3.3 µM (10 µL of a 1 mM solution in 3 ml MeCN) for the phthalimide, hydrogen peroxide (H_2O_2) was used as a 25 % aqueous solution. Excitation and emission slit widths were adjusted to 2.5 nm and the experiment was carried out in two steps:

a. In the first step the fluorophor was treated with the corresponding peroxide (1µL up to 20 µL).

b. Then the mixture (3.3 µM fluorophor + 20 µM of peroxide) was irradiated in the photoreactor Luzchem LZC-4V (14 lamps, $\lambda = 350 \pm 20$ nm) for about 180 min, while every 30 min a fluorescence spectrum was measured.
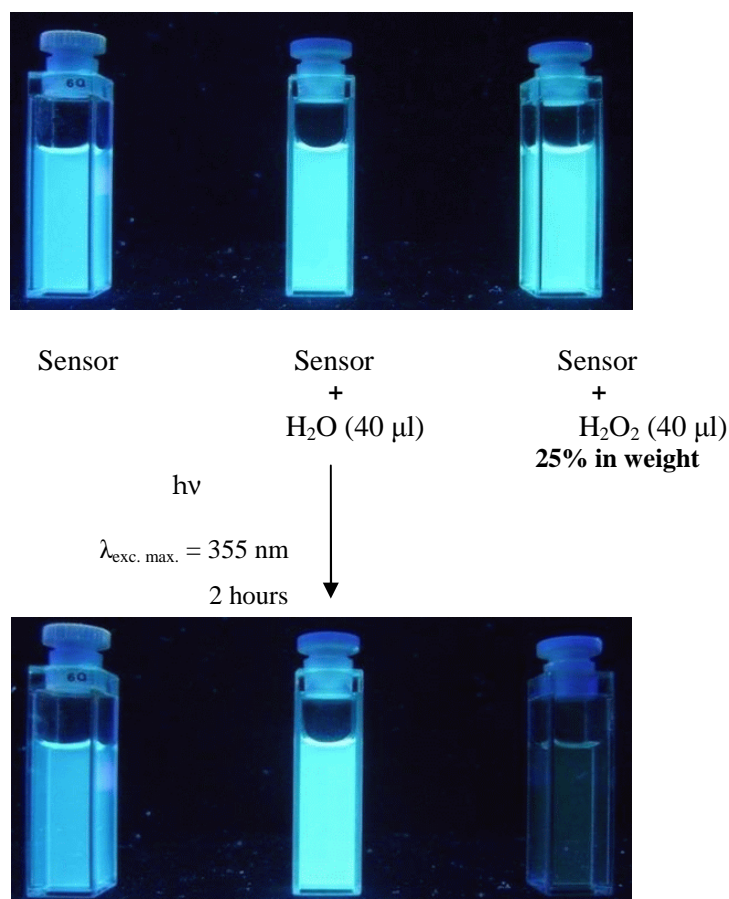
Figure 97: Pictures of the quenching of the sensors with H₂O₂

The fluorescence emission upon addition of H_2O_2 showed a slight shift to the red of about 10 nm and no significant decrease of emission intensity. The changes can be seen in figure 98 where the titration of sensor **107** with H_2O_2 is depicted.
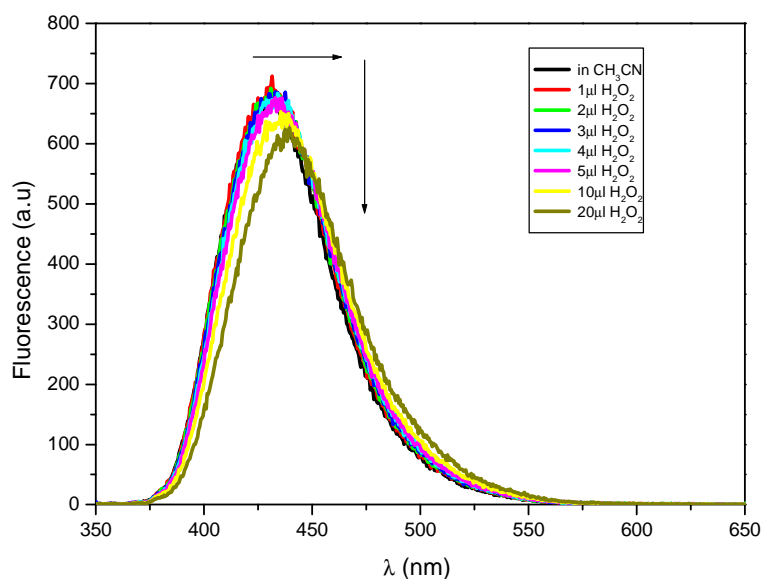

Figure 98: Emission spectra of 107 (λ_{exc} = 340 nm) in the presence of increasing amounts of H₂O₂ (0, 1→20 μL) in acetonitrile

The irradiation of the last titration probe (3.3 µM of fluorophor + 20 µM of H_2O_2) showed stronger changes in the spectra. Fluorescence emission diminished *ca.* 96 % after 180 min of irradiation (λ_{exc} = 350 ± 20 nm) in respect to the starting emission. The difference becomes obvious by comparison with the not irradiated probe (figure 99 insert a and b). The irradiation mixture of the sensor with H_2O_2 induces a considerable emission decrease.
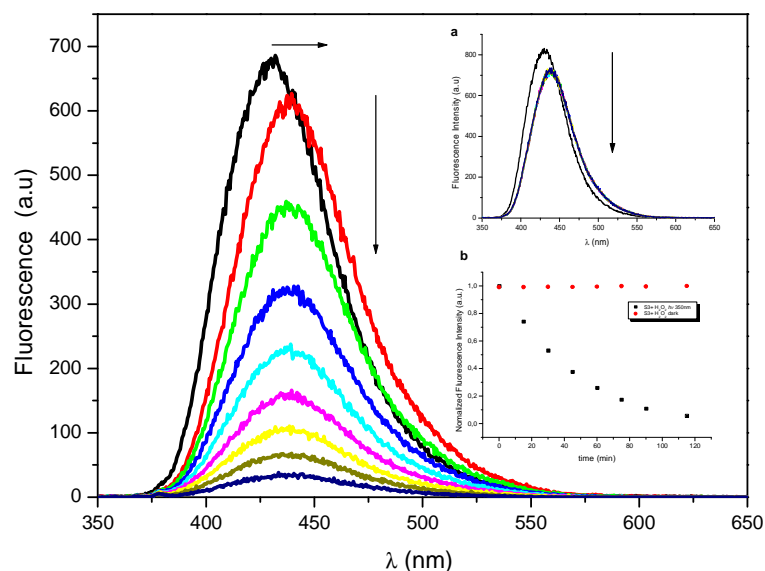

Figure 99: Emission spectra of the irradiation experiments of 107 (λ_{exc} = 340 nm) in the presence of H_2O_2, 20 µL in acetonitrile. Insert: a-Control experiment in dark. b-Normalization of the fluorescence emission *vs.* time

The same experiments were carried out for sensors **109-112**, revealing that emission changes were the strongest for sensors **107** and **109.** Obviously, the presence of some substituents on the fluorophore produces a small effect (about 20% in the final emission record at 120 min, figure 100) in the interaction between H_2O_2 and the sensor. However, all sensors present a good H_2O_2 recognition induced by irradiation at 350 nm during 180 min. The emission changes can be detected by the naked eye.

To examine the selectivity of the sensors in presence of H_2O_2 a comparative experiment with different peroxides was performed. The samples were placed into quartz cells of 1 cm path length. Concentrations were adjusted to 3.3 µM (10 µL of a 1 mM solution in MeCN) for the phthalimide and for the peroxide at 6.6 µM (20 µL of a 1mM solution in MeCN) and the excitation and emission slit widths were set to 2.5 nm. The experiment was carried out in two parts:

a. The first part was the treatment of the fluorophor with the corresponding peroxide (1μL up to 20μL).

b. The mixture (3.3 µM of fluorophor + 6.6 µM of peroxide) was irradiated in the Luzchem LZC-4V photoreactor (14 lamps, $\lambda = 350 \pm 20$ nm) for about 180 min, and every 30 min a fluorescence spectrum was measured.
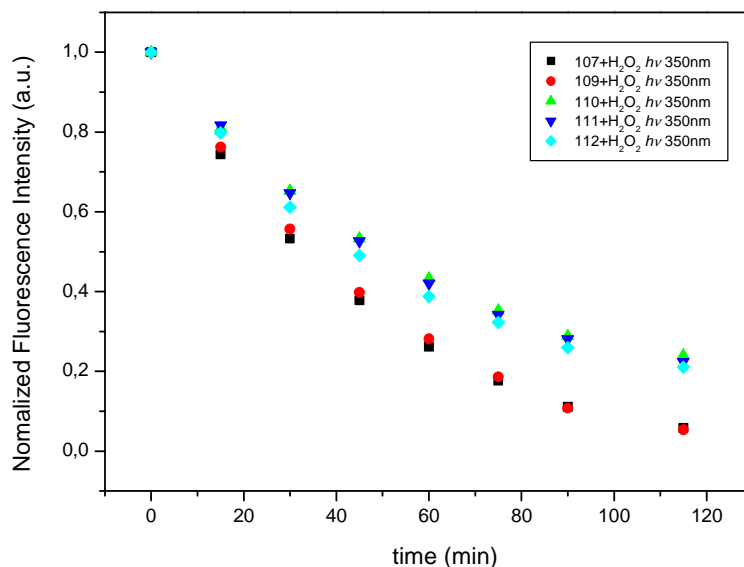

Figure 100: Normalized emission intensity after the irradiation process of the sensors 107 (■), 109 (●), 110 (▲), 111 (▼) and 112 (♦) in the presence of H_2O_2, 20 µL

The different peroxides used for this experiment are given in figure 101. The peroxide targets were hydrogen peroxide (H_2O_2), hydroperoxides (R-OOH) and dialkylperoxydes (R-OO-R).
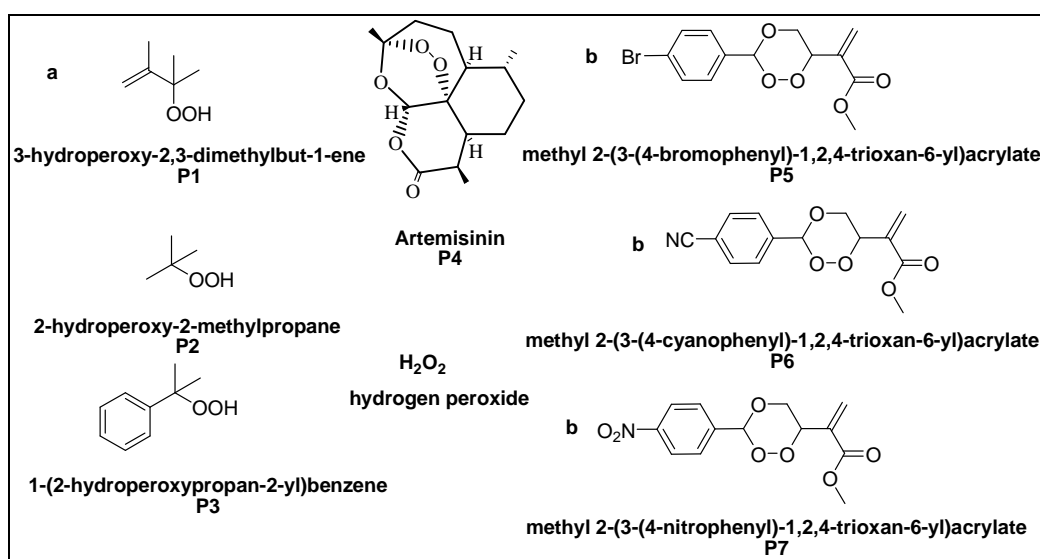

Figure 101: Peroxide molecules used in the fluorescence emission experiments

These quenching experiments showed results similar to those conducted with H_2O_2: a slight red shift of the emission intensity and a weak decrease of the intensity. The most striking difference is shown in Figure 102, where the efficiency of sensor **107** to recognize H_2O_2 compared to other peroxides can be observed. However, comparing the selectivity to peroxides other than H_2O_2 the sensor shows better recognition for peroxides (R-OO-R) than to hydroperoxides (R-OOH).

Irradiation of sensor **107** under nitrogen atmosphere resulted in small changes in the fluorescence emission compared to the experiments carried out under normal atmosphere / aerobic conditions, which indicates that air oxygen is interacting weakly with the sensor.

In presence of water, changes in the fluorescence emission appear but in a minor proportion than with the peroxides. This change can not be observed with the naked eye as can be seen in figure 97.
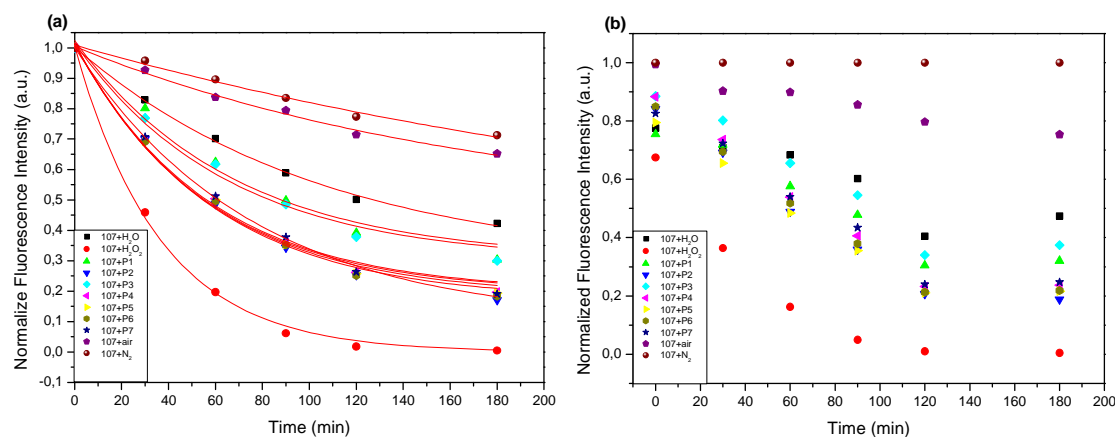

Figure 102: Normalized emission intensity after the irradiation process of sensor 107 with the different peroxides.

The new fluorescence sensors **107** and **109** exhibit a excellent recognition of H_2O_2: nearly 100 % of the fluorescence emission disappears in the presence of H_2O_2. Other hydroperoxides can also be detected but only with moderate efficiency.

After 180 min the detection of H_2O_2 is perceptible to the naked eye which can be very advantageous for possible applications.

Until now the mechanism involved in the recognition of H_2O_2 and other hydroperoxides is unclear. One possibility is a nucleophilic attack of H_2O_2 to the phthalimide. H_2O_2 thus induces ring-opening of the imide group. Route **a** in scheme 38 shows the product **113** that could be obtained by a nucleophilic attack of the NH group to the hydroperoxide. Another possibility would be route **b**, where the hydroperoxide attacks the carbonyl group to form a cycle and the benzylamine leaves the molecule by a rearrangement. Finally as possible products phthalate **115** or a benzodioxinedione **114** could be obtained.
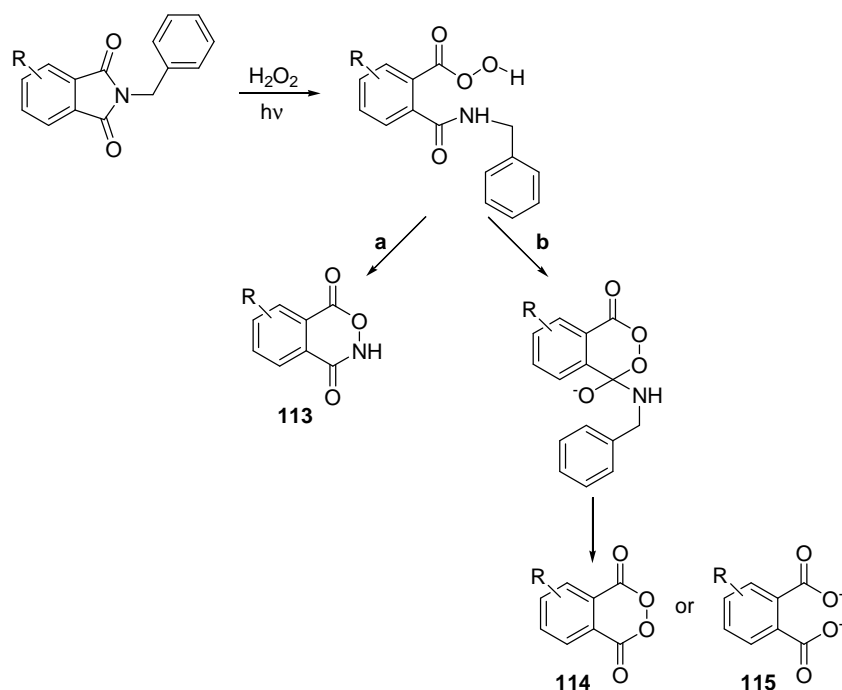
Scheme 38

In order to clarify which reaction is taking place between the sensor and H_2O_2, 2-benzyliso-indoline-1,3-dione (**117**) was synthesized according to **GP1**. The product was isolated with 83 % yield (scheme 39).

Scheme 39
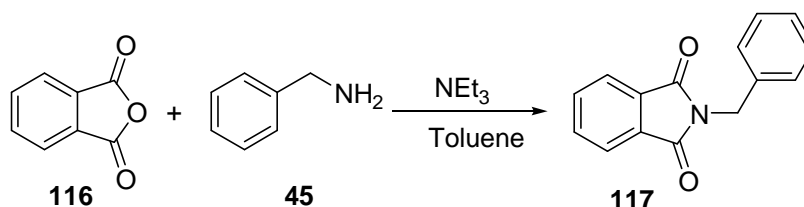
^{1}H NMR experiments were performed to elucidate which mechanism is involved in the interaction between **117** and H_2O_2. A 1:1 solution of **117** and H_2O_2 in DMSO-d_6 was prepared. The solution was irradiated at 300 nm in the Luzchem LZC-4V photoreactor (14 lamps, $\lambda = 300 \pm 20$ nm) for 180 min and every 30 min a ^{1}H NMR spectrum was recorded. The resulting ^{1}H NMR spectra after 30, 60 and 180 min of irradiation are shown in figure 103.
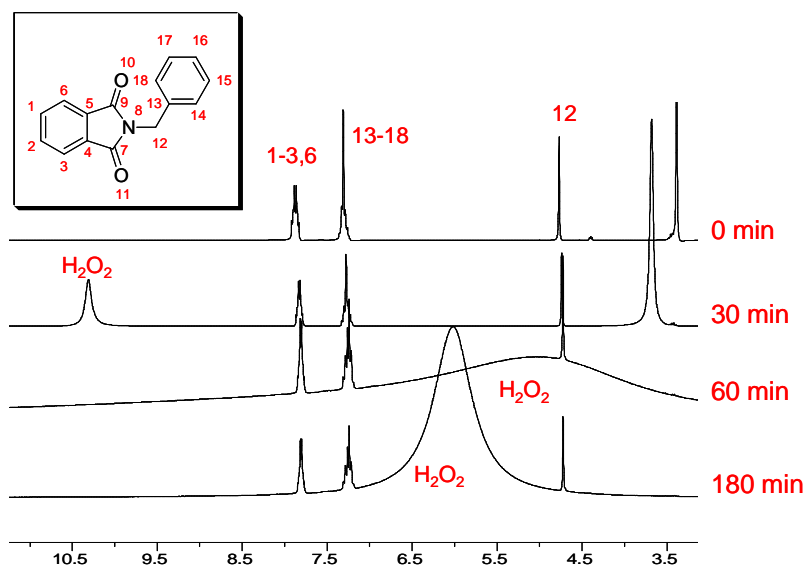
Figure 103: ^1H **NMR spectra of the solution** $(107 + H_2O_2)$ **after different intervals of irradiation time**

The experiment shows no changes of the proton signals after irradiation of the solution. With both mechanisms, the CH_2 signal as well as the phenyl signals of the benzylamine would disappear when the reaction is complete. The spectra show only the position changes of the H_2O_2 signal but no changes on the aromatic signals.

Considering the previous results another experiment was carried out, this time in a preparative scale experiment. A 1:1.1 equiv. solution of sensor **107** and H_2O_2 in acetronitrile was irradiated in a Rayonet chamber photoreactor PRR-100 (16 x 3500 Å lamps, *ca.* 400 W; $\lambda = 350 \pm 20$ nm) for 90 min, the reaction mixture being cooled with tap water (15 °C). After evaporating the organic solvent *in vacuo* the reaction mixture was dissolved in CH_2Cl_2 and washed with water. The organic layer was dried over $MgSO_4$ and concentrated *in vacuo*. After extraction of the crude product, the recorded NMR spectra showed only the starting material **107**. Unfortunately, a possible photoproduct could not be isolated in this case. Therefore, no information is yet available about the mechanism in the reaction between sensors **107, 109-112** and H_2O_2.

The fluorescence experiments indicate that the interaction is only possible when the solution containing a sensor and H_2O_2 is irradiated. This leads to the assumption that the reaction takes place from the excited state. Taking into account that phthalimides are versatile electron acceptors in PET reactions [81] and H_2O_2 is a strong oxidant (electron donor) the possibility that a PET process occurs in the excited state is high. However, further experiments are necessary to understand this process and to propose a valid mechanism.

3.11 Synthesis of Chiral Phthalimide-Thiourea-Conjugate

The synthesis of thiourea-phthalimide couples was achieved following the synthetic route shown in scheme 40. The synthetic route involves five steps. The first is an electrophilic aromatic substitution on C-4 of the phthalimide ring system through nitration with H_2SO_4 and HNO_3, which yielded 58 % isolated product. [82]

2-Benzyl-5-nitroisoindoline-1,3-dione (**120**) was obtained in the second step of this route by nucleophilic substitution in 47 % yield. [83] In the following reaction, **120** was reduced with catalytic amounts of Pd/C under H_2-atmosphere in EtOH, giving the product 5-amino-2-benzyl-isoindoline-1,3-dione (**121**) in 78% yield. [57]

2-Benzyl-5-isothiocyanatoisoindoline-1,3-dione **122** was obtained through a reaction of the aminophthalimide derivate (**121**) and thiosphosgene. [84] The thioisocyanate derivate **122** was isolated in 57% yield. In the last step, a coupling between ((*S*)-1-phenylethanamine) and **122** and 1-(2-benzyl-1,3-dioxoisoindolin-5-yl)-3-((*R*)-1-phenylethyl)thiourea (**123**) in 81% yield is performed.[32]
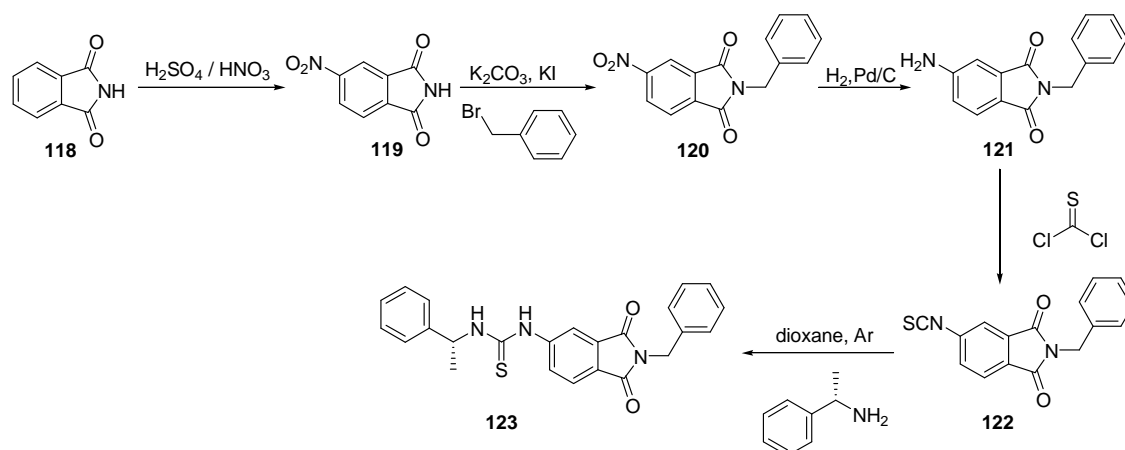
Scheme 40

3.12 Photophysical Properties, Anion Sensing and Chiral Recognition by Chiral Phthalimide-Thiourea-Conjugates

Absorption spectra were recorded using a Perkin-Elmer Lambda 35 UV/vis spectrometer. The samples were placed into quartz cells of 1 cm path length and compound concentrations were adjusted to 3.3 x 10^{-5} M in DMSO while the quencher concentrations were adjusted between 0 and 333.33 x 10^{-6} M.

First, the absorption spectrum of sensor **123** was measured in absence of anions in acetonitrile and shows bands centered at 272 and 350 nm.

Then absorption spectra of sensor **123** were determined in different solvents which are shown in figure 104. The observed bands refer to two electronic transitions, the π, π^* transition at higher energy and the n, π^* transition at lower energy.
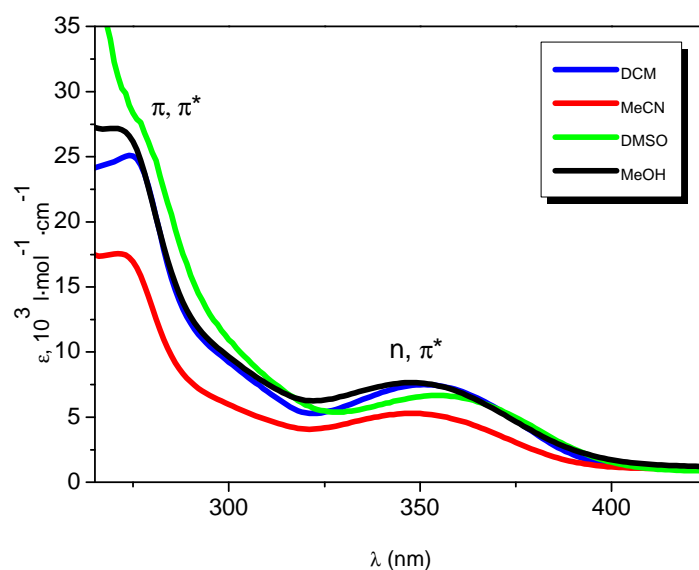

Figure 104: Absorption spectra of 123 (3.3 x 10^{-5} M) in different solvents

Table 24 shows the absorption bands of sensor **123** in different solvents, the π, π^* transition band appears between 270 and 276 nm and the n, π^* transition band between 347 and 356 nm. The calculated absorption coefficient (log ε) corresponds to the n, π^* transition. No significant changes were observed with increasing solvent polarity and a protic solvent like methanol did not produce changes in the absorption of the sensor.

Table 24: Absorption bands of sensor 123 and log ε for the transition n, π^* in different solvents

Solvent	π, π^* (nm)	n, π^* (nm)	Log ε of n, π^* (nm)[a]
DCM	274	351	3.87
MeCN	271	347	3.73
DMSO	276	356	3.82
MeOH	270	348	3.88

[a] A = ε x c x l where A = absorption, ε = absorption coefficient (M^{-1} cm^{-1}), c = concentration of the sensor (3.3 x 10^{-5} M) and l = length of the cell 1cm.

In the next step, anion recognition was studied by absorption spectra. The sensor solution was titrated with different anions such as F$^-$, Cl$^-$, Br$^-$, I$^-$, AcO$^-$ and H$_2$PO$_4^-$, each applied as the corresponding tetrabutylammonium salt (TBA$^+$) in acetronitrile.

Upon titration with F⁻, the ground state was affected and the absorption at 347 nm was weakly shifted to the blue due to recognition of the anion. Furthermore, two isosbestic points were observed at 286 and 367 nm and a new band at 434 nm also appeared upon addition of the F⁻. These absorption changes confirm the formation of a new species after recognition of F⁻ by the sensor **123**. Figure 105 shows the titration spectra with F⁻ in an acetonitrile solution of the sensor. Unfortunately the observed changes in the absorption spectra of sensor **123** did not permit to calculate the association constant of this new species because the different plots that were produced do not presented a good adjustment. The least-squares plot (A/A$_0$ *vs*. C$_A$/C$_H$) of sensor **123** upon addition of F⁻ is shown in figure 105 insert as an example of the poor correlation for this system.
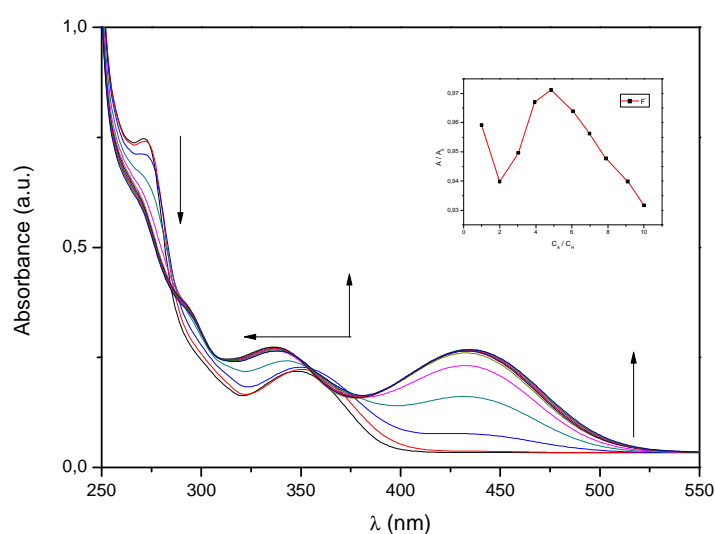

Figure 105: Absorption spectra of 123 (3.3 x 10^{-5} M) in the presence of increasing amounts of F⁻ (0, 0.033 → 0.3 mM) in acetronitrile. Insert: changes in the absorption intensity of 123 upon addition of F⁻. The line does not show a line-fitted curve

These results suggest that complex formation can be ruled out as possible recognition mechanism for F⁻. Fabbrizzi and coworkers [32] compared the H-bond donor tendencies of urea and thiourea and verified the occurrence of deprotonation processes in the presence of certain basic anions such as halides and carboxylates in DMSO solution. Taking into consideration the results of the previous authors, the possible mechanism for this system could be related to a deprotonation reaction of the NH group of the thiourea (receptor part) to F⁻. The potential deprotonated species are shown in figure 106.
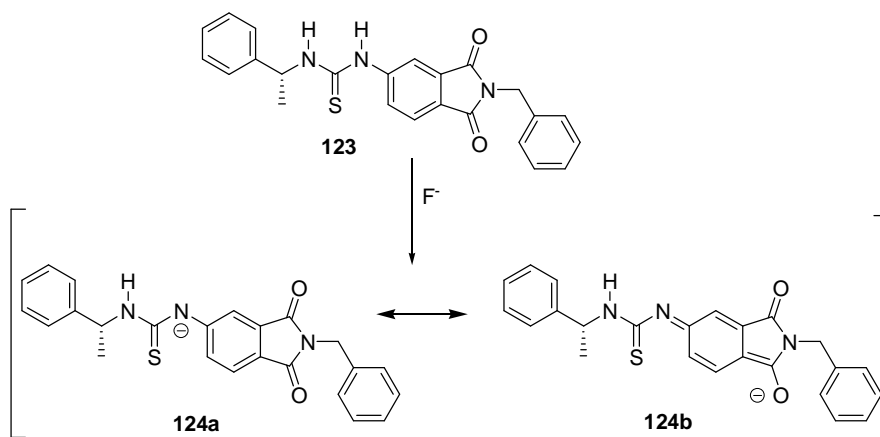
Figure 106

To confirm the deprotonation process of **123** ^{1}H NMR titration experiments were performed in DMSO-d_6 as described above. The thiourea protons appeared at 8.36 (H_2) and 9.35(H_1) ppm (figure 107). In presence of increasing equivalents of F$^-$, the H_1 signal disappeared and the H_2 signal was gradually shifted highfield and progressively disappeared.

The deprotonation of H_1 produced changes on the three proton signals H_a, H_b and H_c. The formation of a negative charge generated an electrostatic effect, which led to a highfield shift of the three aromatic proton signals. After addition of 3 equiv. of F$^-$ a strong deprotonation tendency of $H_1$was produced, although deprotonation of the H_2 could not be observed. A rationale could be bond-lengthening of the N-H_2-bond that is responsible for this upfield shift.
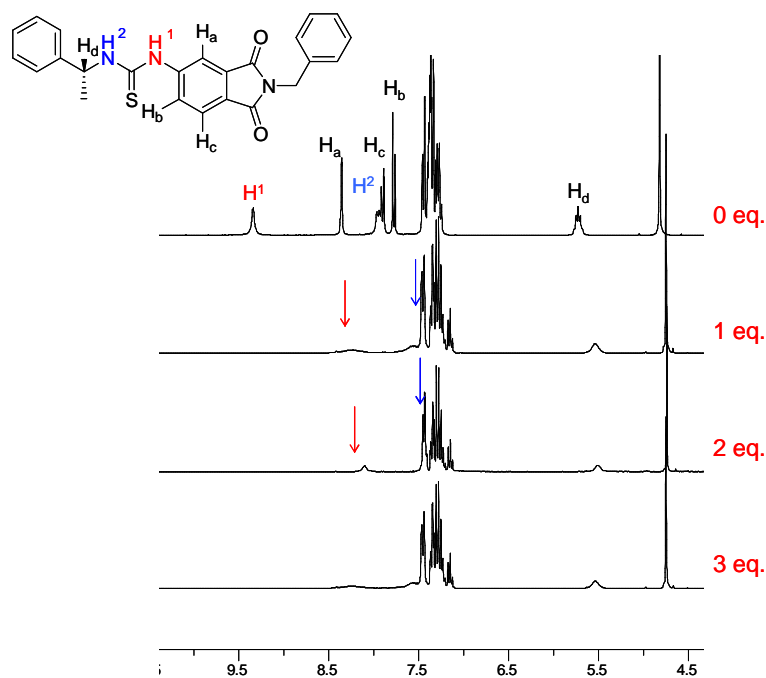

Figure 107: Changes in ^{1}H NMR (300MHz) spectra of 123 in DMSO-d_6 upon addition of F$^-$

Other anions such as AcO⁻ and $H_2PO_4^-$ were also recognized. The absorption spectra of sensor **123** show an isosbestic point at 353 nm on increasing concentration of AcO⁻ and the band at 347 nm is weakly shifted to the red for about 19 nm. Figure 108 shows the absorption spectra of this titration.

The absorption shift indicates that the ground state of sensor **123** is affected *i.e.* these changes in the absorption spectra can be the consequence of a complex formation or deprotonation process of the thiourea protons.

In this case it was possible to calculate the association constant by a non-linear least-squares method (eq. 8), the insert in figure 108 shows the corresponding plot.
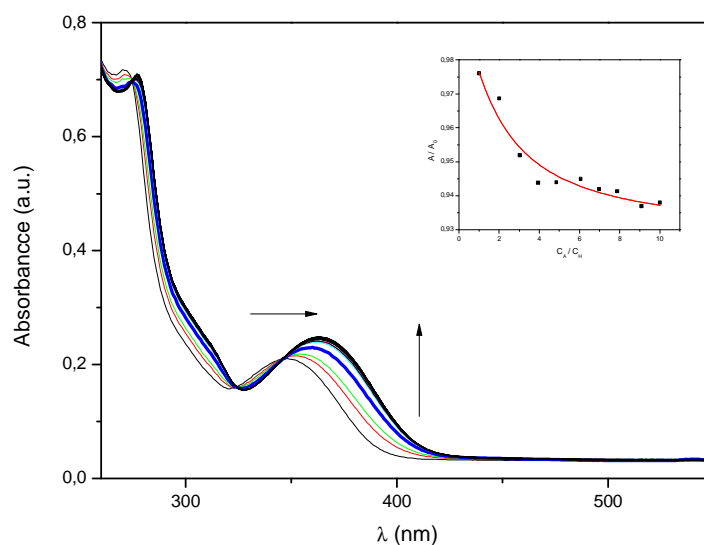

Figure 108: Absorption spectra of 123 (3.3 x 10⁻⁵ M) in the presence of increasing amounts of AcO⁻ (0, 0.033 → 0.3 mM) in acetronitrile. Insert: changes in the absorption intensity of 123 upon addition of AcO⁻. The line shows a fitted curve
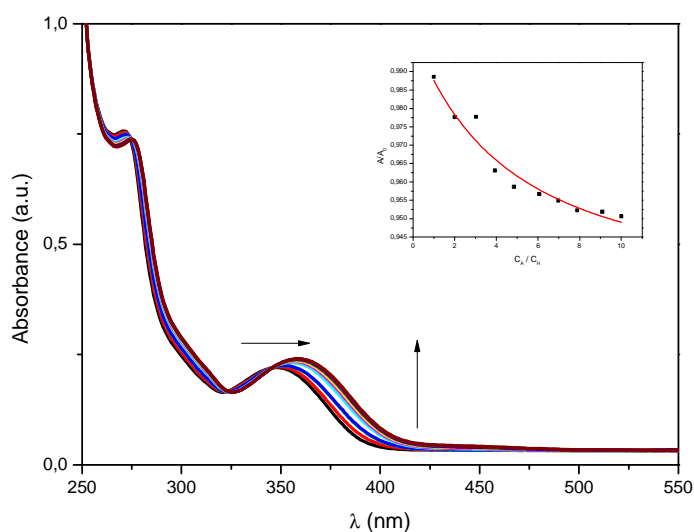

Figure 109: Absorption spectra of 123 (3.3 x 10⁻⁵ M) in the presence of increasing amounts of $H_2PO_4^-$ (0, 0.033 → 0.3 mM) in acetronitrile. Insert: changes in the absorption intensity of 123 upon addition of $H_2PO_4^-$. The line show a line-fitted curve

With increasing amounts of $H_2PO_4^-$ the absorption spectra of **123** present an isosbestic point at 323 nm and the band at 347 nm is weakly shifted to the red for about 13 nm. The recognition of $H_2PO_4^-$ by sensor **123** seems similar to the AcO$^-$ recognition.

The results of the titration with the anions AcO$^-$ and $H_2PO_4^-$ are shown in figure 110. The obtained absorption spectra allow the assumption that a charge transfer complex (CT) is formed with each anion. To confirm these CT complexes it was necessary to perform NMR experiments, comparison with a non-nucleophilic base and confirmation of the reversibility of the process in presence of a protic solvent like methanol, ethanol or water.
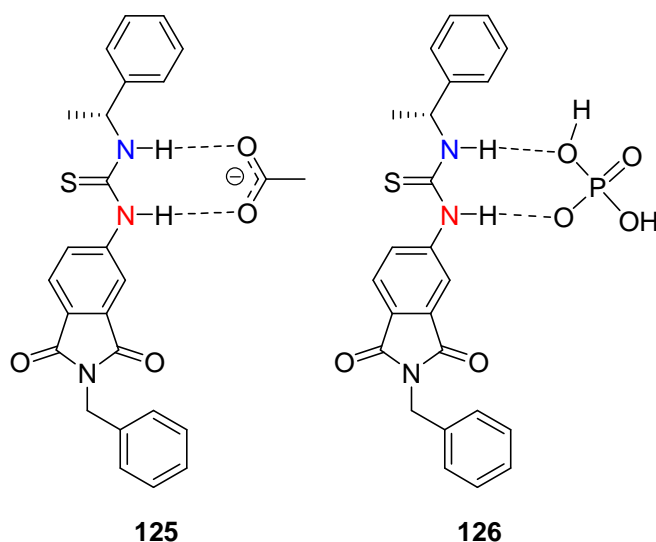

125   **126**

Figure 110: Possible CT complexes between sensor 123 and the anions AcO$^-$ and $H_2PO_4^-$.

Concerning Cl$^-$, Br$^-$ and I$^-$ no changes in the maximum absorption intensity of **123** were observed. In the family of halides **123** recognized F$^-$ and Cl$^-$. Figure 111 shows the changes of the absorption upon addition of the anions. The slopes corresponding to Br$^-$ and I$^-$ addition are nearly identical, no significant changes were observed. The slope for the recognition of AcO$^-$ and $H_2PO_4^-$ respectively increases gradually with rising concentration.

F$^-$ presents a special behavior, as the absorption spectra shows a maximal at 1.0×10^{-4} M and a minimum at 1.5×10^{-4} M. These changes can be associated with the deprotonation of H_1 and the hydrogen bonding with H_2.

Comparison of the behavior of AcO$^-$ and F$^-$ shows that the complex formed with AcO$^-$ is more stable than the F$^-$ complex. The small fluoride ion interacts with H_1 to release HF that in presence of F$^-$ seems to preferably form HF_2^-. The reason for this is the relatively low stability of the intermediate complex [**123H**$\cdots$F]$^-$ in comparison to the stability of HF_2^-. The sensors studied by Fabbrizi *et al.* [32] presented the same behavior as sensor **123** in the presence of F$^-$ and AcO$^-$.
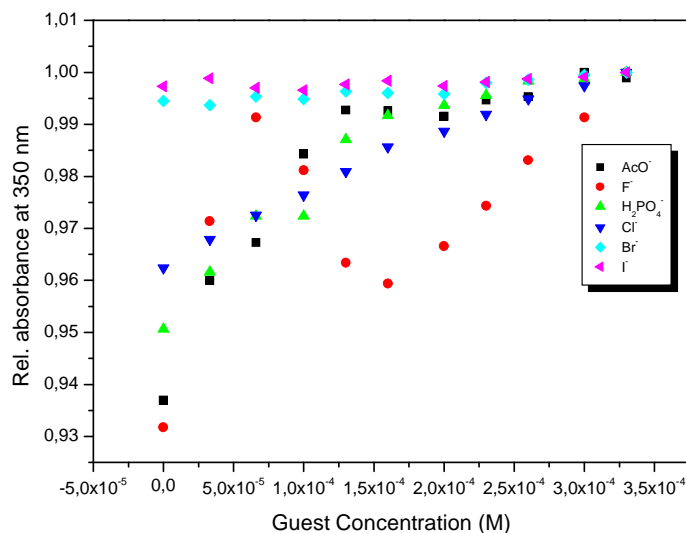
Figure 111: Changes in the absorption of 123 at 350 nm upon titration of F⁻, Cl⁻, Br⁻, I⁻, AcO⁻ and H₂PO₄⁻

Motivated by the formerly described successful experiments with sensor **107-112** chiral recognition experiments were also carried out. The absorption spectra of sensor **123** in the presence of *D*- and *L*-lactate did not show significant changes. Figure 112 shows the absorption spectra of **123** in the presence of *L*-lactate. Only a weak increase of the absorption band at 373 nm was observed. This can be interpreted again as complex formation in the ground state. A similar behavior was observed for *D*-lactate.
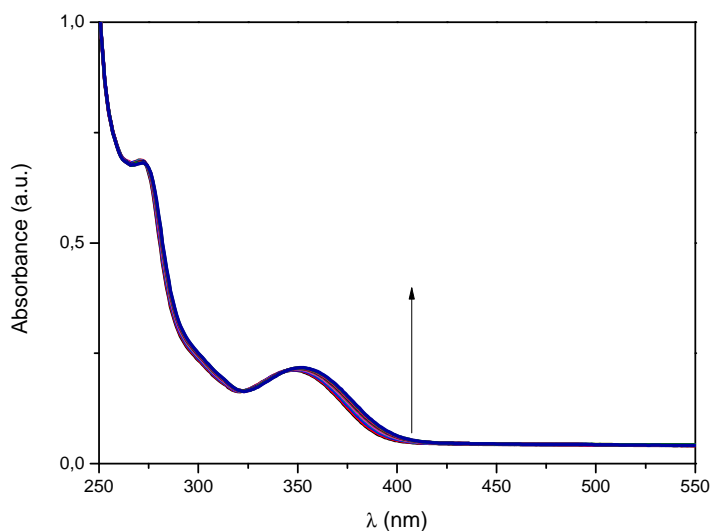

Figure 112: Absorption spectra of 123 (3.3 x 10⁻⁵ M) in the presence of increasing amounts of *L*-lactate (0, 0.033 → 0.3 mM) in acetonitrile

Figure 113 shows the plot of the absorption changes of **123** in the presence of *D*- and *L*-lactate. The difference between both anions can be observed in the plot towards lower

concentrations of the anion. The association constants were calculated according to equation 8 and the resulting plot is depicted in figure 113.
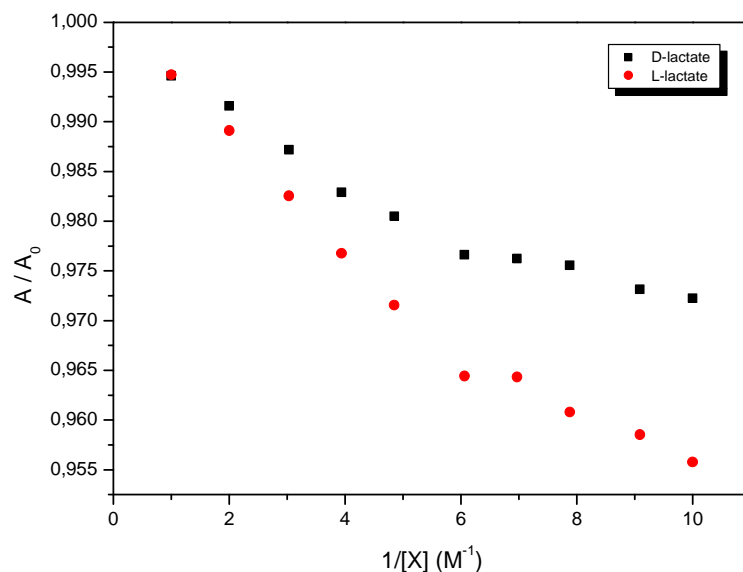

Figure 113: Changes in the absorption of 123 upon addition of *D*- and *L*-lactate

Association constants for all anions are summarized in Table 25. The calculated enantioselectivity coefficient is 1.93 which shows only a marginal enantiodifferentiation between *D*- and *L*-lactate.

AcO$^-$ shows the strongest association constant compared to the other anions recognized by sensor **123**. F$^-$ did not form a CT complex with sensor **123**.

In summary, a new sensor for F$^-$, AcO$^-$ and H$_2$PO$_4^-$ was discovered. F$^-$ recognition involves a deprotonation process and the recognition of AcO$^-$ and H$_2$PO$_4^-$ shows formation of CT complexes. Sensor **123** shows a low enantioselectivity between *D*- and *L*-lactate, however it is possible to detect a slight difference between the enantiomers.

Table 25: Association constants (K_{ass}) of sensor 123 with F$^-$, AcO$^-$, H$_2$PO$_4^-$ *D*- and *L*-lactate in acetonitrile and the enantioselectivity of the *D*- and *L*-lactate.

Sens.	K_{ass} (F$^-$)^a	K_{ass}(AcO$^-$)x $10^{3\,a}$	K_{ass} (H$_2$PO$_4^-$)x $10^{3\,a}$	K_{ass} (*D*-lact.)x $10^{3\,a}$	K_{ass} (*L*-lact)x $10^{3\,a}$	K_{ass} (*D/L*)
123	^{b}	21.79 ± 5.26^c	$7.48 \pm 2.11^{\,c}$	$4.03 \pm 0.76^{\,c}$	$2.07 \pm 0.58^{\,c}$	1.93

^{a} In M^{-1}.^{b} Not calculated. ^{c} R^2 was between 0.989-0998.

Fluorescence experiments were not carried out because sensor **123** is non-fluorescent. The reason for this unusual effect is not clear until now.

In literature other examples of thioureas are reported that do present fluorescence. [16] However, these compounds posses a different fluorophor and constitution. Gunnlaugson

presents sensors that are constructed with a *fluorophore-spacer-receptor* structure, whereas sensor **123** is constructed in the form *fluorophore-receptor*. Due to the acidity of the NH protons very likely a non-fluorescent anion is generated (figure 114). To confirm this assumption pH experiments were performed but no increase in fluorescence was observed.
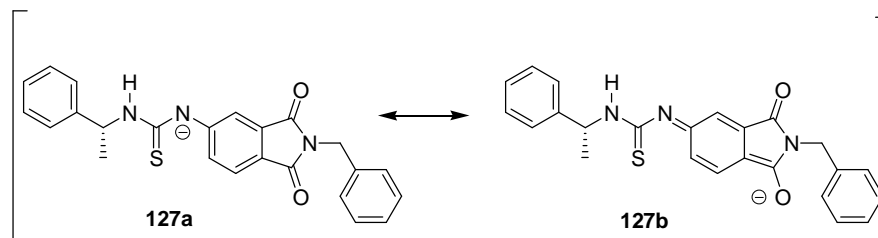

Figure 114: Possible non-fluorescent structure of sensor 123

The NH protons play an important role in the operating mode of the sensor, but as pH experiments elucidated anion formation is not the only reason why the sensor does not show fluorescence. Thus another internal process has to be involved in the deactivation of the fluorescence which has to remain under investigation.

In summary, the thiourea showed a different behavior than the urea concerning recognition of the examined anions. The acidity of the NH protons gives rise to of the different interactions between sensor and anions. The recognition of these anions through hydrogen bonding and deprotonation was observed by absorption spectra and ^{1}H NMR. The sensor showed efficient recognition of AcO$^-$ though hydrogen bonding and for F$^-$ the recognition occurs due to deprotonation of the receptor. In comparison with the urea receptor of the previous sensors the enantioselectivity of this thiourea receptor was moderate. The enantioselectivity of the urea receptors is *ca.* 50% higher compared with the thiourea moiety.

3.13 Synthesis and Photophysical Properties of Luminol Derivates
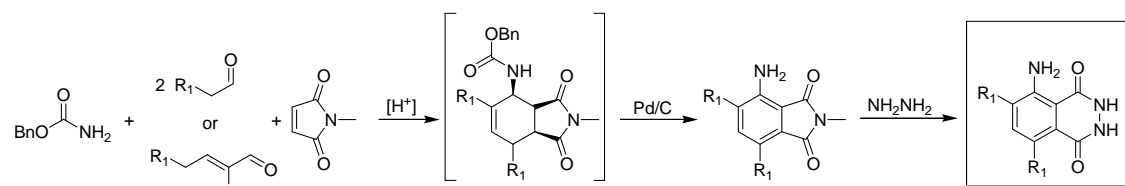
Scheme 41

This synthesis was conducted by Robert Fitchler (AK. Jacobi).The overall yields over the three synthetic steps were in the range of 31-62%.The next table shows the intermediates of the reaction and the luminol derivates.
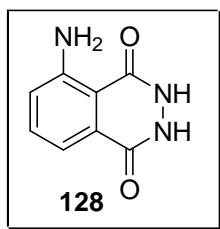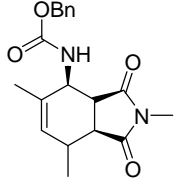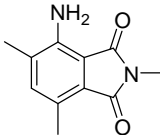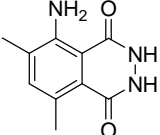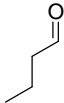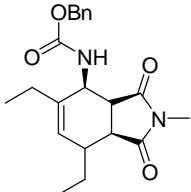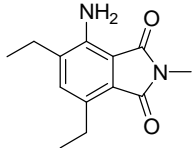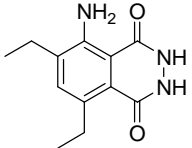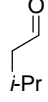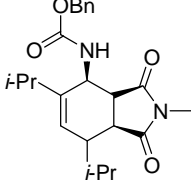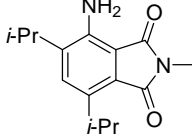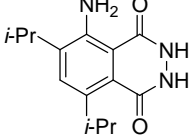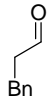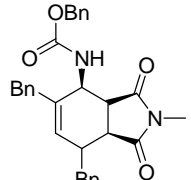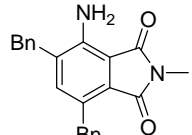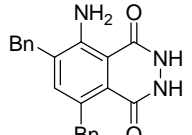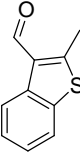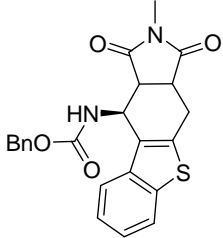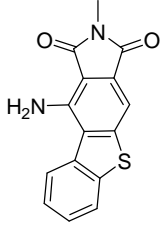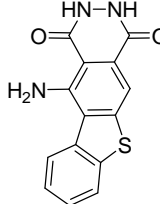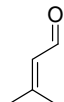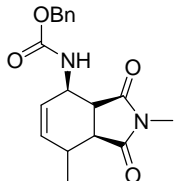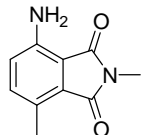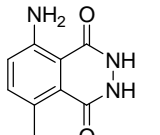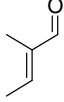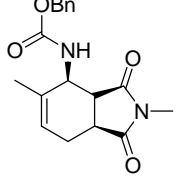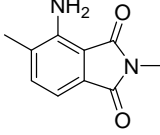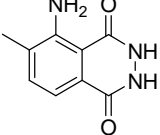

Figure 115: Luminol 128, reference product

Table 26 : Aldehydes were used by the MCRs, MCR-Adducts, oxidation products (Anilines) and the luminol derivates.

Entry	Aldehyde	*MCR-Adducts* *Gruppe a*	*Anilines* *Gruppe b*	*Luminol* *Gruppe c*
129				
130				
131				
132				
133				
134				
135				

3.13.1   Photophysical data and spectroscopic properties

Photophysical data of luminol were determined in DMSO in literature studies. [85],[86] The parent luminol was used as reference system for all studies of photophysical properties of luminol derivates. The photophysical measurements of luminol derivates were performed in DMSO to compare the spectroscopic data with luminol. The absorption spectra of derivates **129-132**, **134** and **135** in DMSO exhibited two distinct bands which were comparable to the reference compound **128**, whereas three red-shifted maximum were found for compound **133**.

The excitation and absorption spectra of the luminol derivates showed the same position of the maximum. The band in the 355-380 nm region was in all cases stronger than the 295-320 nm band. The presence of these two bands in the absorption as well as excitation spectra indicate the presence of two distinct electronically excited states S_1 and S_2. The excited luminol derivates relax from the S_2 (π, π^*)-state to the S_1 (π, π^*)-state. The NH_2 group in luminol and the derivates may be a possible site of interaction with an electron donating polar aprotic solvent such as DMSO.[85] This interaction between the NH_2 group and DMSO could be generate a complex through hydrogen bonding in the excited state S_1 (π, π^*) and its emission is associated with the minor energy absorption band.
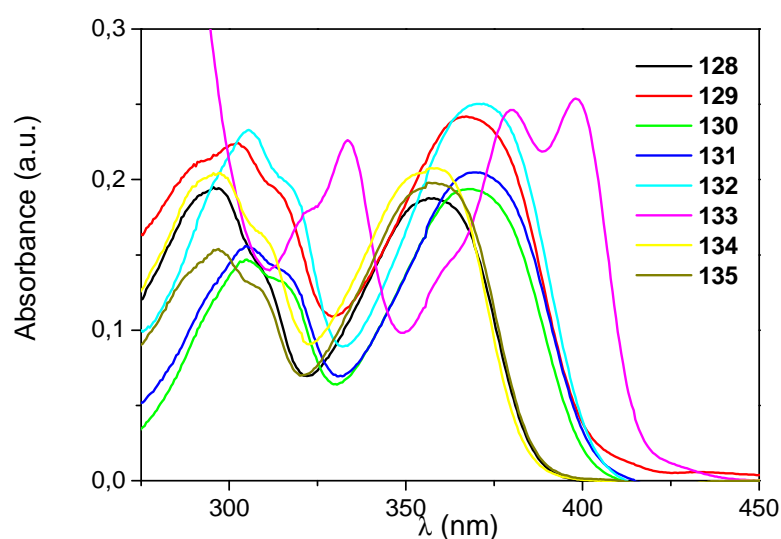
Figure 116: Absorption spectra of 128-135 in DMSO (c = 2.5 x 10^{-6} M)

133 compound showed three absorption and excitation bands, all slightly red-shifted in comparision to **128**. Benzothiophene is an excellent additional electron-donating group and might stabilize an internal charge transfer state additionally to the two local excited singlet states. Table 27 summarizes the relevant spectral data that were collected for the luminol derivates **129-135**.

Table 27: Spectroscopic properties and photophysical properties of luminol derivates (125-131).

Luminol	$\lambda_{max}^{Abs\,a}$	ε^{b}	$\lambda_{max}^{Em\,a}$	Stokes^{c}	E_s^{d}	Φ_F^{e}	τ_S^{f}	$10^8\,K_s^{g}$
128	297	7768		3241	75	0.15	1.8	0.8
	358	7508	405					
129	302	8972		3718	72	0.23	2.0	1.1
	367	9676	425					
130	305	5872		3863	72	0.21	2.0	1.0
	368	7752	429					
131	304	6232		3771	72	0.31	2.0	1.5
	370	8196	430					
132	305	9320		3625	72	0.48	2.2	2.1
	372	10016	430					
133	333	9048		2392	70	0.21	0.9	2.3
	380	9852	418					
	398	10152	435					
134	297	8176		2995	75	0.40	2.8	1.4
	358	8304	401					
135	297	6156		3501	75	0.34	1.8	1.8
	357	7916	408					

[a] In nm, concentration of 2.5×10^{-5} M. [b] Concentration of 2.5×10^{-5} M. [c] In nm, concentration of 2.5×10^{-6} M. [d] in cm^{-1}. [e] Fluorescence quantum yield (ref to luminol $\Phi_F = 0.15$). [f] In ns. [g] Fluorescence rate constant ($K_F = \Phi_F / \tau_S$) [h] All measurement was performed in DMSO.

The emission spectra of the luminol derivates **128-132, 134-135** showed broad bands in the region between 405-430 nm (table 27). For compound **133** two fluorescent separated bands at 418 and 435 nm were observed.

Addition of one methyl group in the donor-acceptor system of the parent luminol **128** did not significantly alter the fluorescence properties (**134-135**). Although the *para* orientation of methyl substituents and one carbonyl moiety is likely to exert electronic communication across the arene, steric effects appear to be more dominant. The introduction of 6,8-disubstitution in **129, 130, 131** and **132** as well as anellation with benzothiophene (**133**) prompoted moderated red-shift of the emission band ($\Delta\lambda_{em} = 20$-25 nm) in comparison with **128**. This red-shift can be a direct consequence of the electron-donor abilities of the substituents and may be include the formation of an ICT state after local excitation to S_1.

Steric effect placing two substituents in relative *ortho* positions to the amino and carbonyl groups of the parent luminol derivates could produced directly a effect the stability of the excited state geometries and thus influence the energy and lifetime of the corresponding excited state. Moderate Stokes shifts (≥ 3000 cm^{-1}) were determined for all compounds except the **133** (table 27).

The excited singlet state energies were calculated from the intersection of excitation and emissions bands and exhibited no significant dependence on the substitution pattern (table 27). In contrast to the excited state energies, the fluorescence quantum yields showed significant changes in comparison to luminol **128**. The derivate **132** showed a threefold increased

fluorescence quantum yield (0.48 *vs.* 0.15 for **128**). The singlet lifetimes of compounds **128-135** are summarized in table 27, in all cases their decay traces predominantly exhibit exponential behavior (R^2 = 0.9997, figure 117). As expected from the significantly lower Stokes shifts of compound **133**, also the singlet state lifetime was decreased. This is in accord with the largest fluorescence rate constant for **133** in the investigated series.
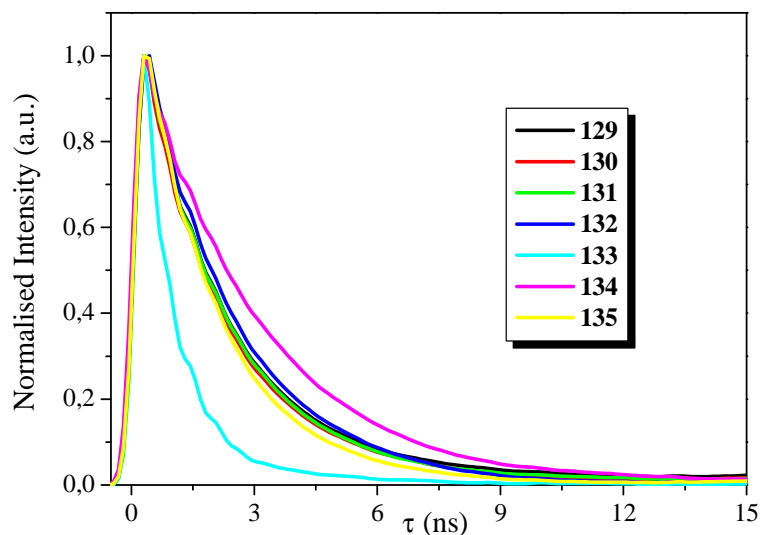
Figure 117: Normalized fluorescence decays (λ_{exc} = 355 nm) of luminol derivates 129-135 in DMSO under aerobic conditions. All concentrations 1.3 x 10^{-3} M

3.13.2 pH-Dependence on absorption and steady-state fluorescence of 129-135

A recent spectrophotometric study of luminol **128** under different solvent conditions such as DMSO, DMSO-water showed pH dependence of its absorption and fluorescence properties. [86] In order to investigate the photophysical properties of the new luminol derivates under these conditions, their behavior was investigated at different pH buffer-solution conditions.

The absorption as well as the steady-state fluorescence measurements of compounds **128-135** were performed in water at different pH (commercial buffer solutions at pH 3, 7 and 12), the data are summarized in table 28.

Two absorption maxima were found in all cases except for derivate **132** at pH 3 and 7 and for **133** at pH 3 due to partial insolubility. As depicted in figure 118 for the diethyl-substituted compound **130**, the low energy transition is slightly bathochromic when going from low to high pH-values with a moderate increase in extinction coefficients. More pronounced effects appeared for high energy transition that is subsequently shifted hypso-and hyperchromic.

Table 28: Spestroscopic data in aqueous buffer solutions at different pH.

	pH = 3			pH = 7			pH = 12
	$^a\lambda_{max}^{Abs}$	$^b\lambda_{max}^{Em}$	$^c\Delta$	$^a\lambda_{max}^{Abs}$	$^b\lambda_{max}^{Em}$	$^c\Delta$	$^a\lambda_{max}^{Abs}$
128	294, 351	430	5234	301, 351	-	-	301, 351
129	301, 360	443	5240	309, 356	443	5516	312, 354
130	303, 360	446	5356	311, 357	446	5589	316, 357
131	304, 362	450	5402	313, 359	450	5632	317, 357
132	-	-	-	-	-	-	317, 362
133	-	-	-	322, 337, 381	437, 492	3294 5852	322, 337, 381
134	296, 350	428	5206	303, 347	427	5399	303, 347
135	294, 351	431	5288	304, 349	429	5343	305, 349

[a]. In nm, concentration 1.5×10^{-4}. [b] In nm, concentration 2.5×10^{-6} M, λ_{exc} = 350 nm, for **133** λ_{exc} = 380 nm. [c] Stokes shift in cm^{-1}.
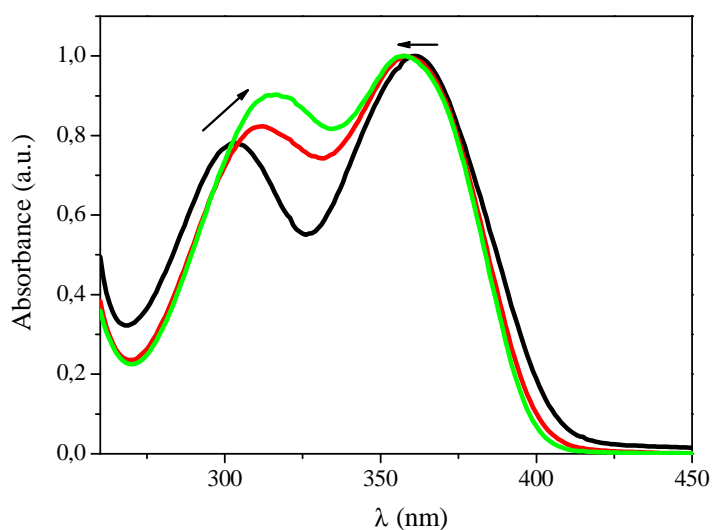
Figure 118: Normalized absorption spectra of 130 in H$_2$O/DMSO 9:1 at pH 3 (−), pH 7(−) and pH 12 (−); c = 1.3 x 10^{-3} M

Taking into account the high acidity of the phthalhydrazine group (pK$_a$ 12.7 in DMSO [87], compared with the pK$_a$ of acetic acid in DMSO 12), it can be safely assumed that at high pH the phthalhydrazine group is doubly deprotonated and fully protonated at pH 3, which is not the case for the aniline-type group at C5. The more pronounced changes in absorption behavior at shorter wavelength can thus be correlated with the phthalhydrazide part of the molecule and its S$_2$ electronic excitation. These effects were also detected (with different magnitudes but

identical tendencies) for the luminol derivates **128, 129, 131** and **132** as well as for the monoalkylated compounds **134** and **135**, respectively. As expected, strong fluorescence was observed at pH 3 for all derivatives whereas their intensities decreased to 50% at pH 7 under the same conditions. In line with the literature results, [86] no emission was detected for any luminol derivative at pH 12 and this observation is in agreement with the formation of the phthalhydrazide dianion species which could delocalize the negative charges and consequently quench the fluorescence by ICT (scheme 42). Finally, the increase in Stokes shift at higher pH can be interpreted as an increased charge shift stabilization of the excited state relative to the ground state.
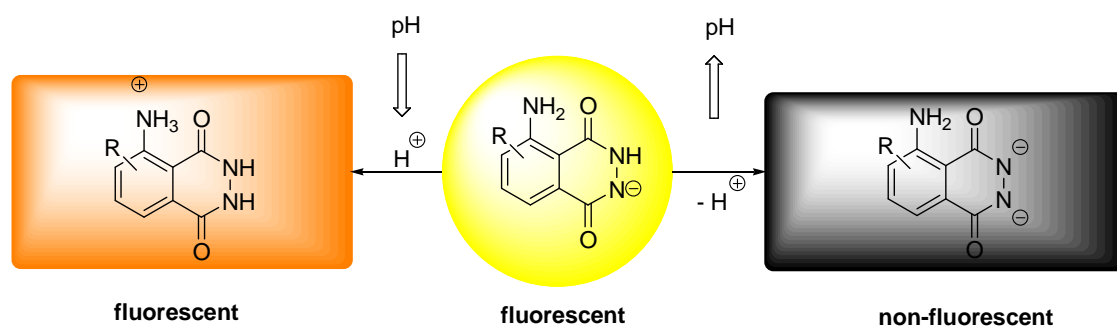
Scheme 42: pH-dependent fluorescence of luminol derivates

3.13.3 Chemoluminescence (CL)

The CL resulting from the reaction of **128** with an oxidant (H_2O_2 in particular) in strong alkaline medium has been extensively studied and applied to determination of several inorganic and organic species. Luminol **128** CL promotion has been used as a superior tool of metal ion determination where at least 20 metal ions increase the rate of CL for this reaction. In this context, many previous studies of **128** CL have usually employed different conditions concerning the oxidant and the catalyst. [88]

The CL effect dependence on the ring substitution of the luminol derivatives **129-135** was investigated under the same conditions (*i.e.*, same catalyst/oxidant system such as Fe^{+3}/H_2O_2) [89]. Aside from that, luminescence intensities were recorded with a fluorescence plate reader which allowed to obtain fast information *in situ* about: i) the suitable amount of catalyst/oxidant system equivalents which might be added; ii) rapid comparison study of the CL process between compounds belonging to the same family under the same conditions, iii) to estimate relative CL quantum yields.

Hence, solutions of luminol derivatives **128-135** (7.5 μM) in alkaline medium (pH 12) were placed in a plate reader in combination with increasing amounts of Fe^{+3}/H_2O_2 (5%). Figure 119 shows an illustration of the plate reader where 2 mL solution of combined luminol derivatives

and catalyst/oxidant was used. After a fast luminescence measurement, detailed values were obtained which represented the emitted photons due to the CL process. According to these data, luminescence enhancement reached a maximum when 40 equivalents of catalyst/oxidant system were added in all cases.

	Fe^{+3} / H$_2$O$_2$ (5%) (eq)					
	0	10	20	30	40	50
128	2116	69947	1.2E5	2.2E5	2.8E5	1E5
129	3317	1.2E6	2.7E6	4E6	4.3E6	4.4E5
130	3171	1.7E6	3E6	4.2E6	5.7E6	3E5
131	1988	2E6	3.4E6	3.7E6	3E6	2.1E5
132	2889	6.2E5	2.1E6	2.6E6	2.9E6	4.8E5
133	1350	27996	77640	1E5	1.6E5	64409
134	622	12271	34126	53489	52315	40754
135	490	14368	49638	80376	1E5	59117

Figure 119: Picture of the fluorescence plate reader combining the luminol derivatives together with increasing equivalents of Fe^{+3} (25 mg/ml)/H$_2$O$_2$ (5%). Numbers represent the emitted luminescence photons by corresponding solutions (2 ml per well)

Once the methodology including suitable conditions concerning the addition of catalyst/oxidant equivalents was available, the next step was to make comparison studies of the CL process with the parent **128**. Thus, data treatment by plotting the luminescence enhancement *vs.* the corresponding derivative was carried out (figure 120). Interestingly, derivatives **129-135** presented an immense increase in the emission of the CL whereas **133-135** showed even less intensity in the process than **128**.
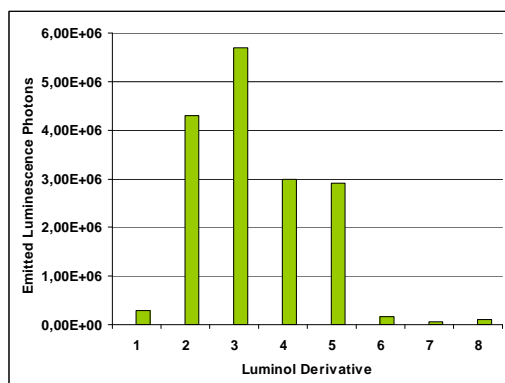
Figure 120: Luminescence enhancement of luminol derivatives (7.5 μM) in addition of 40 equivalents of Fe^{+3}(25 mg/ml)/H_2O_2 (5%)
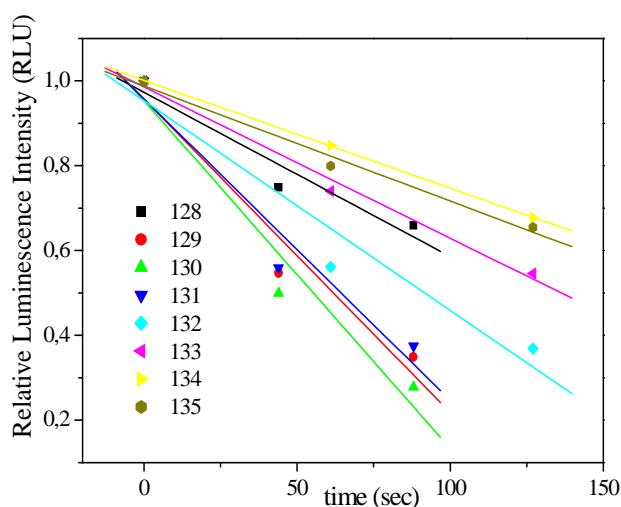
Figure 121: Variation of the relative luminescence intensities with time of derivatives 128-135

It is well-assumed that oxidation of **128-135** led to the formation of the corresponding carboxylates excited singlet state that was the responsible of the light emission.[90]

The absolute CL efficiency depends on three important factors: i) fraction of molecules that follow the correct chemical path to give the critical intermediates; ii) fraction of molecules that cross over to the excited state of the product and iii) fluorescence quantum yield of the emitters. With this method the absolute CL efficiencies could not be obtained because of technical restrictions as well as missing relative data. Relative CL quantum yields (Φ_{CL}^{Rel}) could be estimated by eq **9** since **128-135** luminescence intensities were found to be dependent on the time (figure 121).

$$\Phi_{CL}^{Rel} = (d_0/d_{sample}) \, (I_{sample}/I_0) \, \Phi_{CL}^{0} \qquad (17)$$

where Φ_{CL}^0 is the CL quantum yield as reference that, in this case, assumed to unity, d is the decay rate of luminescence disappearance which is directly related with the slopes obtained in figure 121 and I is the number of photons obtained in the luminescence plate reader (figure 121) after addition of 40 equiv. of Fe^{+3} (25 mg/ml)/H_2O_2 (5%).

Φ_{CL}^{Rel} values for the luminol derivatives are given in table 29. Assuming the parent reference **128** 1.0, compound **130** appeared to obtain the highest Φ_{CL}^{Re} with an increase of 10% of the CL efficiency. Taking into account these values, the CL efficiency followed the order **130** > **129** ≈ **132** > **133** > **128** > **133** > **135** > **134**.

Table 29: Relative CL efficiencies of luminol derivates.

Lum.[a]	Slopes	Φ_{CL}^{Rel}
128	-0.00387	1.0
129	-0.0074	7.3
130	-0.0082	10.0
131	-0.0071	5.3
132	-0.0049	7.3
133	-0.00357	0.6
134	-0.00254	0.3
135	-0.00271	0.5

[a] Luminol as reference.

Some conclusions could be drawn from these data: i) tri-substituted ring luminol derivatives increased ≈5-10 times the luminescence intensity in comparison with the parent **128**; this would be directly related with the Φ_{CL}^{Rel} where their CL efficiency were found to be 10-5% higher; ii) di-substituted ring derivatives decreased the CL effect; indeed, no significant changes were found when the methyl group was in *ortho* or *meta* position related to the amine group; iii) introduction of a heterocyclic compound as substituent appeared not to be suitable for the increase of the CL efficiency.

Luminol **128** CL promotion has been used as a perfect tool for metal ion determination where at least 20 metal ions increase the rate of CL for this reaction. [88] In view of these results for **128,** the capability to increase the CL rate of luminol derivatives **125-131** in presence of different metal ions (Ba^{2+}, $Fe3^+$, Cu^{2+}, Ni^{2+} and Mg^{2+} as nitrate salts) was investigated.

Chemoluminescence measurements were performed using a luminometer "Lumat LB 9507". H_2O_2 (25 µL, 5%) was dispensed to luminol **124** or the luminol derivates **129-135** (10 µL, 1.5

mM solution in DMSO), cation solutions (Ba^{2+}, $Fe2^+$, Cu^{2+}, Ni^{2+} and Mg^{2+}, 6 µL, 6.18 mM solution in PBS, pH ≈ 12) and 0.98 mL of PBS (pH ≈ 12). The generated chemiluminescence at 25 °C was measured continuously for about 250 s.

With this method the corresponding kinetic curve associated to the CL process can be obtained directly, an example is shown in figure 122. When the concentration of peroxide/metal ion diminishes to react with the luminol a decrease of CL intensity is observed. The generally accepted mechanism for this system is shown in scheme 43.
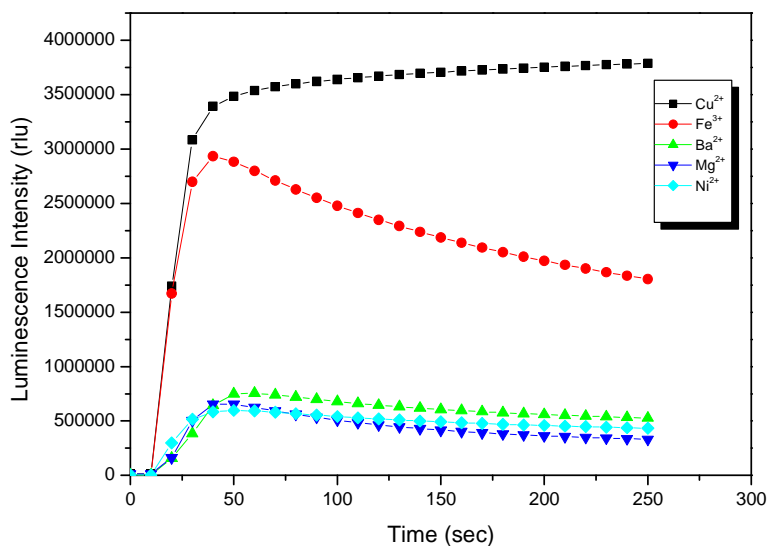
Figure 122: Plots of the CL kinetic process of 129 with the different metal ions

Copper presents a different behavior in comparison with the other metal ions. The maximum CL can not be determined exactly for this metal because the high signal saturated the detector. It is possible that the copper reacted much stronger with hydrogen peroxide than the other metals, and consequently the production of the oxygen species that reacts with the luminol is higher.
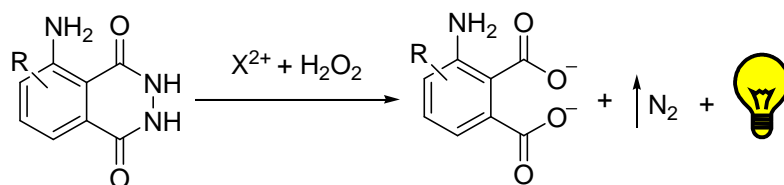
Scheme 43: General mechanism to produce CL due to hydrogen peroxide and metal ion

The histogram (figure 123) shows that some luminol derivates present a better detection for the examined metal ions than luminol **128**. For quantitative results the relative CL quantum yields (Φ_{CL}^{Rel}) were calculated using eq. 17. The results are summarized in table 30.
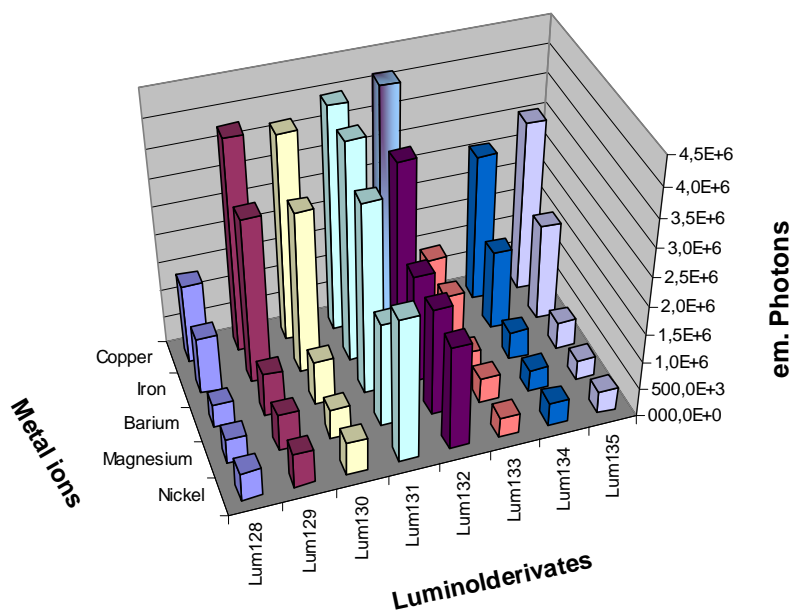
Figure 123: Luminescence enhancement of luminol derivatives 128-135 upon addition of 2.5 equivalents of X^{2+}/H_2O_2 (5%). Copper exceeds the range

Defining the parent reference **128** as unity, compound **132** appeared to obtain the highest Φ_{CL}^{Re} in presence of all metal ions within an increment between 7 and 43% of the CL efficiency.Luminol **133** showed the lowest CL efficiency in the reaction with iron, and for the other metal ions the reaction with luminol **134** was the least efficient. The experiment covering Ni^{2+} showed a threefold better efficiency of CL in comparison with Fe^{+2}. CL efficiency of Ba^{2+} was similar to that of Fe^{2+} and Mg^{2+} showed the lowest CL efficiency of this metal ions group because Mg^{2+} did not undergo the redox reaction with H_2O_2.

The type of metal ion plays an important role on the examined CL reaction. The CL intensity generally increases with increasing H_2O_2 concentration and the decomposition rate of H_2O_2. The catalytic decomposition of H_2O_2 is directly affected in presence of metal ions as can be seen in table 30.

Table 30: Relative CL efficiencies of luminol derivates with different metal ions.

Lum. [a]	Cu(NO$_3$)^{2} [a]	Fe(NO$_3$)^2	Ba(NO$_3$)^2	Mg(NO$_3$)^2	Ni(NO$_3$)^2
128	-	1.00	1.00	1.00	1.00
129	-	10.33	5.70	4.07	6.58
130	-	7.74	8.06	3.16	8.18
131	-	12.56	14.58	3.50	24.15
132	-	19.45	31.79	7.09	43.18
133	-	0.96	1.14	0.94	2.52
134	-	1.34	1.06	0.67	1.21
135	-	2.10	1.95	0.69	3.11

[a] Luminol as reference. [b] Not calculated.

In summary the photophysical properties of a series of luminol derivates were investigated and compared with the parent luminol. Spectroscopic properties of the compounds **128-135** were determined with focus on absorption as well as fluorescence behaviour. Additionally, singlet lifetimes and quantum yields of the fluorescent excited singlet states were determined in DMSO. Significant differences were found depending on the substituents attached to the luminol core in particular for the heterocyclic ring annulation. Additionally, the photophysical behavior of derivates **128-135** was studied under difference pH conditions in buffer solutions. The absorption spectra revealed several species which were present at different pH conditions with a major presence of the dianion luminol derivates at pH 12. Chemiluminescence studies of **128-135** were performed using a luminescence plate reader and a luminometer injector system. The luminescence plate reader allowed obtaining fast and detailed information about the intensity as well as efficiency of the process depending on the substituents under the same conditions. It was experimentally observed that tri-substituted luminol derivatives enhanced the luminescence in comparison with that of **128** together with a better CL efficiency a factor of 10. Employing the luminometer was possible to obtain the kinetics of the process with a high efficiency of light collection. The substituents of the luminol derivates showed a significant influence on the CL efficiency of the processes under the same experimental conditions, concurrently the type metal ions in the process is important to the CL efficiency process where iron and nickel presented the better efficiency values. The new luminol derivates can be applied for detection of trace metals with a good CL efficiency and can thus be applied as analytical tool for practical applications.

4 Conclusion

The fluorescent and non-fluorescent sensors (**47, 48** and **53**) presented in the first part of this work were synthesized by a straightforward synthetic route that consisted of straight-forward reactions such as aromatic substitution and reduction reactions and in one case acetylation with good reaction yields.
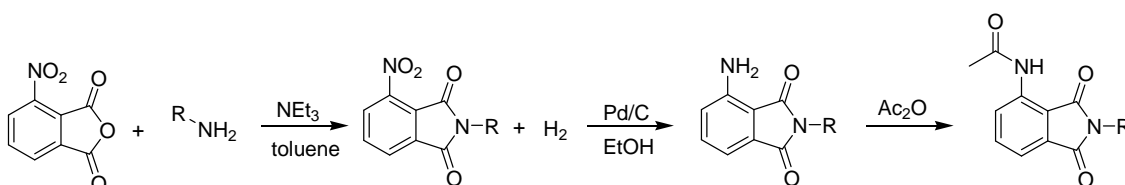
Scheme 44

Fluorescence quenching studies of compounds **47** and **48** were conducted with different molecular quenchers. By menas of Stern-Volmer plots the quenching constants (K_D) and the bimolecular quenching constants (k_q) were calculated. From all quenchers DABCO showed the best quenching effect for both fluorophores in comparison with the other molecular quenchers as can be seen from the high quenching constant.

Linear Stern-Volmer plots were obtained for all quenching processes which is indicative for dynamic processes taking place. This dynamic fluorescence quenching can occur through PET from the ground-state quencher to the excited fluorophore. It is also possible that the radical cation of the quencher and the radical anion of the fluorophore combine as last step of the dynamic quenching process (scheme 45).
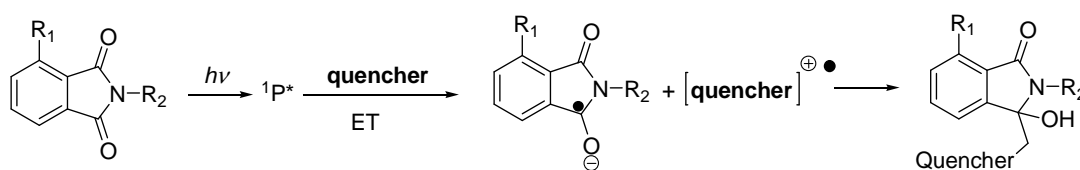
Scheme 45

The activation of fluorescence emission *via* metal ion recognition of product **53** was investigated. Considerable changes in the fluorescence emission were not observed. It is possible that the coordination site of product **53** is not suitable for the cations used and thus PET between the fluorophore and cations is not possible (figure 124). Another reason can be a competition in the complex formation between the primary and the tertiary amine groups in the fluorophore. It would be possible to confirm this speculation by protecting one amine group with acetamide or another protecting group and to repeat the quenching experiment.
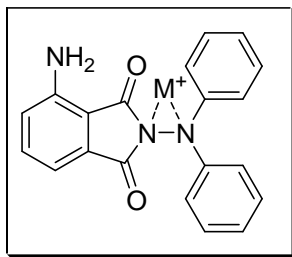
Figure 124: Possible complex between 53 and the metal ions

The results of the fluorescence experiments with **53** and Eu(III) were comparable with the other metal ions. Emission fluorescence changes were not observed. The mechanism shown in scheme 46 could thus not be realized.
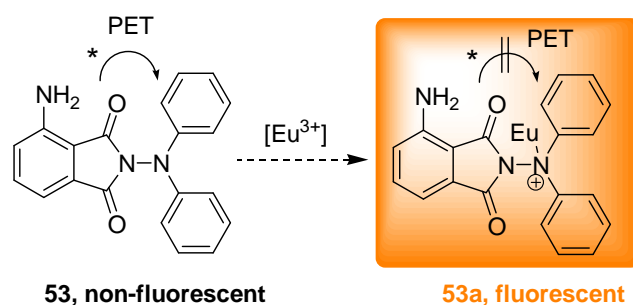
Scheme 46

Unfortunately, attempts to synthesize 1-(2-aminonaphthalen-1-yl) naphthalene-2-amine (**54**) were not successful (scheme 47) and taking into account the synthetic problems, it is proposed to modify target structure and synthesis route.
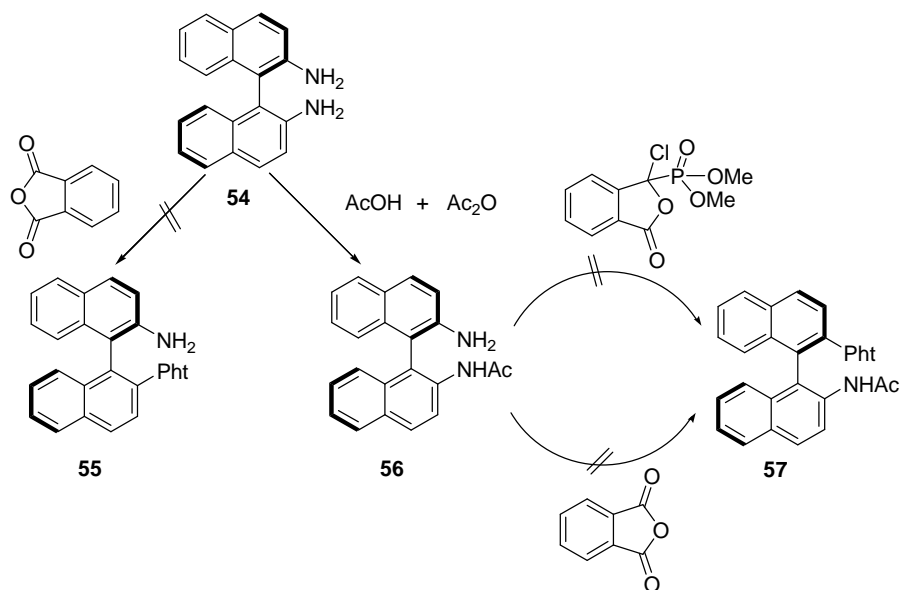
Scheme 47

The modification would consist in changing the coupling position of binaphthyldiamine (with one amine group methylated as described in literature [3]) and couple it with the a thioisocyanate or isocyanate group of the corresponding phthalimide derivate. The consequential route is depicted in scheme 48 and should be followed in future examinations.
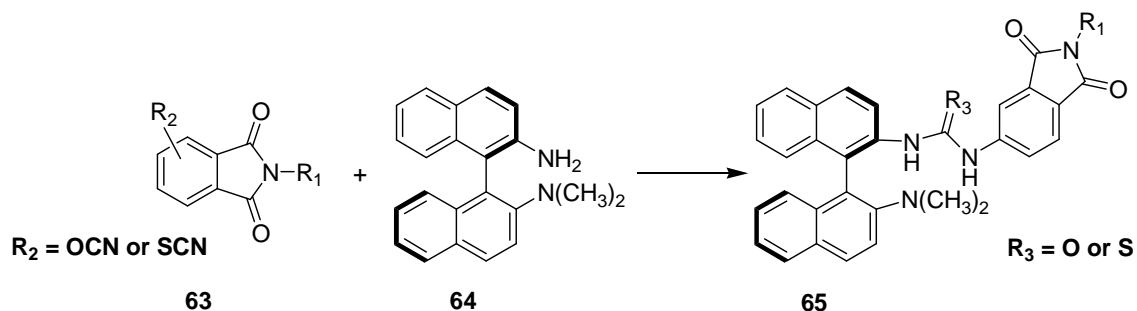
Scheme 48

Looking for new higher substituted phthalimide derivatives a new synthesis route was developed by applying multicomponent reactions based on Diels-Alder chemistry in the first step. In the second step a dehydrogenative oxidation of the conjugated cyclohexadiene product was carried out using MnO_2. At last, different ways were examined to conduct a direct reaction between the ester group of the cyclohexadiene and amine derivatives to achieve a phthalimide.

The last step of the synthetic route could not be conducted because the aromatic amine compounds showed no tendency the react with the phthalic diester to give the phthalimide. However with aliphatic amines the formation of the phthalimide was possible but nevertheless a mixture of the dehydraminated phthalimide and amino phthalimide derivates as final products was obtained and not the desired product (scheme 49).
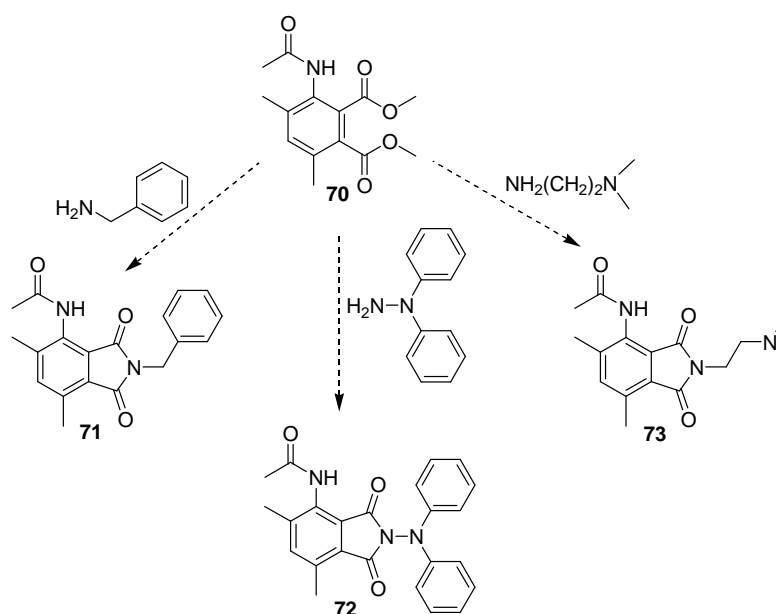
Scheme 49

The synthesis of new photocages based on an aminophthalimide-serine system was carried out and the fluorescence quenching behavior of these photocages was investigated (scheme 50).
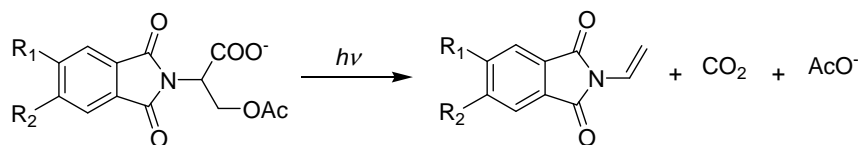
Scheme 50

Both photocages **92** and **100** exhibit fluorescence changes associated with acetate photorelease. The photodecarboxylation mechanism of **92** involves a competition between decarboxylation releases in the singlet excited state and the PET quenching to come back to the ground state. The photodecarboxylation mechanism of **100** involves a competition between the singlet state decay and the intersystem crossing because most likely, the photodecarboxylation process occurs from the corresponding triplet state (scheme 51).
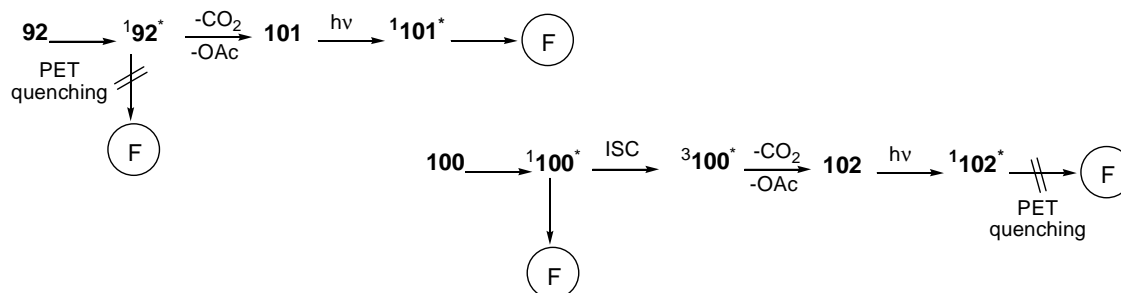
Scheme 51

Syntheses of chiral phthalimide-urea conjugates were carried out employing a Curtius rearrangement that allows the direct conversion of aromatic carboxylic acids into ureas (scheme 52).
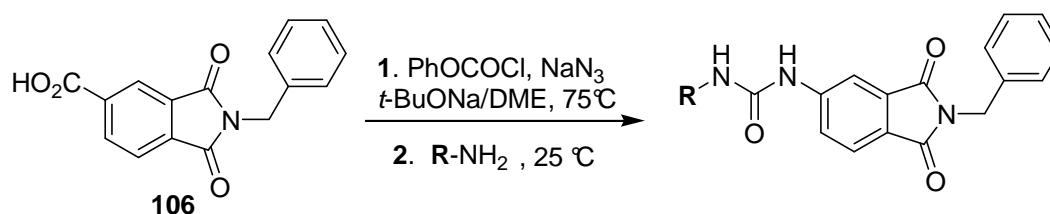
Scheme 52

For the sensors **107**, **109-112** photophysical properties were determined in different solvents. Sensors **107**, **110-112** did not show changes in the photophysical properties depending on solvent polarity. In the presence of protic solvents such as methanol however, a strongly increased Stokes shift accounts for the formation of an internal charge transfer state after excitation to the first excited singlet state. Unlike the others, in the presence of methanol sensor

109 showed a decrease of the quantum yield in the ratio of one-ninth compared to acetonitrile, and a diminished fluorescence lifetime of 8.0 ns was detected, approximately half of the corresponding time of sensor **107**.

This difference in the fluorescence lifetimes is probably due to the hydroxy group that accounts for a fast deactivation from the first excited singlet state to the ground state. The non-radiative pathway that deactivates the singlet state is not favored in methanol.

Sensor **107** was found to selectively detect F$^-$ since the absorption as well as fluorescence changes were only observed in presence of this halide anion. In this context, a fluorescence static quenching was proposed for the signalling mechanism, like depicted in scheme 53.
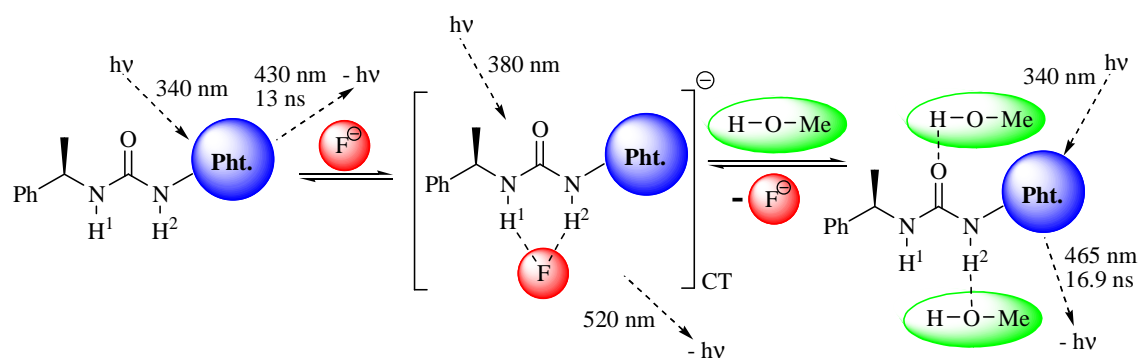
Scheme 53: Proposed mechanism for the interaction between 107 and F$^-$

Hydrogen bonding interactions between sensors and fluoride are evidenced by ^{1}H-NMR studies, and the reversibility of these interactions is observed upon addition of a protic solvent like methanol.

The new sensors **109**-**112** also showed a good binding selectivity towards the anions AcO$^-$, F$^-$, H$_2$PO$_4^-$ that in most cases followed the order K$_{ass}$ AcO$^-$ > K$_{ass}$ F$^-$ > K$_{ass}$ H$_2$PO$_4^-$ or K$_{ass}$ AcO$^-$ > K$_{ass}$ H$_2$PO$_4^-$ > K$_{ass}$ F$^-$. Evidence for the hydrogen bonding nature of the urea-anion and hydroxy group-anion interaction was further obtained by ^{1}H NMR titration of the sensors with the anions.

The high values for the association constants represent a good recognition ability of the anions F$^-$, AcO$^-$ and H$_2$PO$_4^-$ by the receptors of the sensors **107**, **109**-**112** through formation of the respective complexes.

Taking into account the stereogenic center of the sensors **107, 109-112**, enantiodifferentiation studies were performed by fluorescence quenching in the presence of enantiomerically pure amines (*D*- and *L*-methylbenzylamine, *D*- and *L*-phenylethanol) as well as *D*- and *L*-lactate as sodium salts.

This recognition was investigated by absorption and fluorescence spectroscopy and by theoretical calculations. Receptor **112** exhibits an excellent chiral recognition ability towards the enantiomers of lactate, the other sensors can also distinguish between both enantiomers but with less efficiency. Fluorescence recognition of the anions involves two different processes for all sensors, for *D*-lactate due to a static quenching process and for *L*-lactate by a combination of a static and a dynamic process. Theoretical calculations are on the way to evaluate the enantioselectivity of the sensors towards *D*- and *L*-lactate.

Experiments to recognize peroxides through the receptors of the sensors **107**, **109**-**112** were also carried out. The fluorescence experiments indicate that interaction is only possible when the solution, containing a sensor and H_2O_2 is irradiated. This leads to the assumption that the reaction takes place from the excited state. Taking into account that phthalimides are versatile electron acceptors in PET reactions [81] and H_2O_2 is a strong oxidant (electron donor) the possibility that a PET process occurs in the excited state is high. The interaction with hydroperoxides was not stronger than with hydrogen peroxide. However, further experiments are necessary to understand this process and to propose a valid mechanism.

The non-fluorescent sensor **123** based on a thiourea-activated phthalimide with a stereogenic center was synthesized following a five-step synthetic route. The thiourea showed a different behavior than the urea concerning recognition of the examined anions. The acidity of the NH protons gives reason to different interactions between sensor and anions. Recognition of these anions through hydrogen bonding and deprotonation were observed by absorption spectra and ^{1}H NMR. The sensor showed efficient recognition of AcO^- through hydrogen bonding, and for F^- the recognition occurs due to deprotonation of the receptor. In comparison with the urea receptor of the previous sensors **107**, **109**-**112** the enantioselectivity of the thiourea receptor was moderate. In comparison with the thiourea the enantioselectivity of the urea receptors is *ca.* 50% higher.

The last chapter of this thesis elucidated photophysical data, spectroscopic properties and chemioluminescence of luminol derivatives. Differences in the photophysical properties and spectroscopic properties were found depending on the substituents at the luminol core in particular in the case of heterocyclic ring annulation. The photophysical behavior of the derivatives **128**-**135** was studied under different pH conditions in buffer solutions. The absorption spectra revealed several species, which were present at different pH with a major presence of the dianion at pH 12.

Chemoluminescence studies of **128**-**135** were performed using a luminescence plate reader and a luminometer injector system. It was experimentally observed that trisubstituted luminol derivatives enhanced the luminescence in comparison with that of **128** combined with a better

CL efficiency a factor of 10. Employing the luminometer it was possible to obtain the kinetics of the process with a high efficiency of light collection. The substituents of the luminol derivates showed a significant influence on the CL efficiency under identical experimental conditions. The type of metal ions in the process is important to the CL efficiency where iron and nickel presented the better efficiency values. The new luminol derivates can be applied for detection of metal traces with a good CL efficiency and can thus be applied as a convenient analytical tool for practical applications.

5   Experimental Part

5.1   General Remarks

5.1.1 Spectroscopic methods

^{1}H NMR: The ^{1}H spectra were recorded on Bruker DPX300 spectrometers operating at 300 MHz, a Brucker DRX 500 spectrometer operating at 500 MHz or a on Bruker AV 600 spectrometer operating at 600 MHz. Chemical shifts are reported as δ in ppm and the coupling constant is J in Hz units. In all spectra solvent peaks were used as internal standard. Solvents used were $CDCl_3$ (δ = 7.24 ppm), d_3-acetonitrile (δ = 1.96 ppm), d_4-Methanol (δ = 3.35, 4.78 ppm), and d_6-DMSO (δ = 2.49 ppm). Splitting patterns are designated as follows: s, singlet; d, doublet; t, triplet; q, quartet; m, multliplet; br, broad.

^{13}C NMR: The ^{13}C NMR spectra were recorded either on a Bruker AC 300 spectrometer operating at 75 MHz, a Bruker DPX 300 spektrometer operating at 75 MHz or on a Bruker AV 600 spectrometer instrument operating at 126 MHz. In all spectra solvent peaks were used as internal standard. Solvents used were $CDCl_3$ (δ = 77.0 ppm), d_3-acetonitrile (δ = 118.0 ppm), d_4-Methanol (δ = 49.3 ppm) and d_6-DMSO (δ = 39.7 ppm). Carbon multiplicities were determined either by DEPT experiments (distortional enhancement by polarization transfer) or by APT experiments (attached proton test).

IR-spectroscopy: Infrared spectra were recorded using a Perkin-Elmer 1600 series FTIR spectrometer and are given in cm^{-1} units. Splitting patterns are designated as follows: s (strong), m (medium) and w (weak).

UV-vis: Absorption spectra were recorded using a Beckman Coulter UV-DU800 spectrometer or a Perkin-Elmer Lambda 35 UV/vis spectrometer. The samples were placed into quartz cells of 1 cm path length. Compound concentrations were fixed as indicated.

Fluorescence spectroscopy: Fluorescence and excitation spectra were carried out using a Perkin-Elmer LS-50B luminescence spectrometer. The samples were placed into quartz cells of 1 cm path length. Compound concentrations were fixed as indicated.

Time-resolved fluorescence spectroscopy: Fluorescence lifetimes were measured using a gated intensified CCD equipped monochromator. The spectral resolution had been set to 2 nm. The samples were excited with the third harmonic (355 nm) of a Nd:YAG laser. The overall

instrument response function is 1.5 ns. The samples were placed into quartz cells of 1 cm path length.

Singlet lifetime experiments were determined after excitation with laser pulses about 120 fs length. The pump laser was an "Integra-C" from Quantronix providing pulse of 2 mJ with 120 fs duration at 796 nm and 500 MHz repetition rate The Optical Parametric Amplifier "TOPAS" was from Light Conversion and an oscilloscope WavePro 960XL was from LeCroy (2 GHz bandwhidth). Compound concentrations were fixed as indicated.

Luminescence: Luminescence measurements were performed using a computer-controlled fluorimeter Tecan SPECTRAFluor Plus for microplate, and Lumat LB 9507 from Berthold Technologie for measuring individual samples.

Ms: Mass spectra were recorded on a MAT Incos 50 Galaxy System Mass spectrometer and on a Finnigan MAT H-SQ 30 Mass spectrometer and ESI experiments were measured using a Bruker Daltonics Esquire 3000

5.1.2 Analytical methods

CHN-Elementary analysis: CHN-combustion analyses were measured using a Elementar Vario EL Instrument.

M.p: M.ps were measurements using a Büchi melting point apparatus type B-535 and are uncorrected.

X-ray analysis: All X-ray measurements were recorded using a Nonius KappaCCD diffractometer ($2\Theta_{max} = 54°$, $Mo_{K\alpha}$ radiation, $\lambda = 0.71073$ Å), graphite monochromator, φ / ω scans. The structures were solved using the direct methods SHELXS-97 and SHELXL-97.

5.1.3 Chromatographic methods:

Column Chromatography: Silica gel 60, 0.0063-0.200 nm (70-230 mesh ASTM) purchased from Merck Company, silica gel 60, 0.040-0.063 nm (230-240 mesh ASTM) purchased from Macherey-Nagel Company or basic aluminium oxide from ICN Biomedicals was used as stationary phase.

TLC: Thin layer chromatography was performed on plastic sheets precoated with silica gel 60 F_{254} (Merck) or aluminium sheets precoated polygram SIL G/UV_{254} (Macherey-Nagel). Spots were visualized under a UV lamp (254 or 366 nm) or with a $KMnO_4$ solution.

PLC: Preparative thin layer chromatography was carried out on 20 x 20 cm glass plates coated with silica gel (Merck silica gel G F_{254}) and eluted with the solvent system indicated. The

separated compounds were located under 254 or 366 nm UV light and extracted using ethyl acetate.

5.1.4 Photolyses

Glass apparatus: Quartz and Pyrex ® vessels were used for irradiation.

Reactors: Rayonet chamber photoreactors PRR-100 (16 x 3500 Å lamps, ca. 400 W; $\lambda = 350 \pm 20$ nm) were used for irradiation as well as the photoreactor Luzchem LZC-4V (14 lamps, $\lambda = 350 \pm 20$ nm).

Solvents and reagents: Solvents (acetonitrile (MeCN), dimethylsulfoxide (DMSO), methanol (MeOH) and dichloromethane (DCM)) used for irradiations and spectroscopy study were purchased from Fisher Scientific Company. All reagents were purchased from standad chemical suppliers and purified to match the reported physical and spectra data.

Gas: Nitrogen (Linde) was used for irradiation.

5.1.5 Computational Calculations

The structures were optimized with GAUSSIAN03, [91] using B3LYP/6-31 *[72] and the CPCM-SCRF method, solvent = acetonitrile. [73] NMR shifts were computed of the optimized structures using the GIAO method. [74]

5.2 General Procedures

GP1:   General procedure for the synthesis of 3-nitro-phthalimides

A mixture of benzylamine (10.0 mmol), 3-nitrophthalic anhydride (1.93 g, 10.0 mmol) and triethylamine (0.5 mL) in toluene (70 mL) is refluxed with a Dean-Stark apparaturs for 3 hours. The reaction mixture is cooled and concentrated *in vacuo*. The residue is dissolved in dichloromethane, washed with 10% hydrochloric acid solution and then with hydrogen carbonate solution. The organic layer is separated and dried over magnesium sulfate, and concentrated *in vacuo*. Recrystalization of the residue from ethanol gives the product. [56]

GP2:   General procedure for reduction of 3-nitro-phthalimides to 3-amine-phthalimides

A mixture of the substrate (10.0 mmol), 5% Pd/C in EtOH (100 mL) is vigorously stirred at room temperature (appr. 22°C) under hydrogen atmosphere with the pressure of a hydrogen balloon for 4 hours. The reaction mixture is then filtered over Celite® and concentrated *in*

vacuo. The residue is purified by column chromatography or recrystallization; see the paragraph pertinent to the respective product. [57]

GP3: General procedure for multicomponent coupling with a simple aldehyde and dimethyl acetylenedicarboxylates.

a. Amide ($\geq$ 15 mmol), aldehyde (15 mmol), dienophile (15 mmol), acetic anhydride (1.53 g, 15 mmol) and *p*-toluensulfonic acid monohydrate (43 mg, 1.5 mol%) are combined in a round bottomed flask and NMP (10 mL) is added. Then the reaction is stirred at elevated temperature (120°C). After 24 h, the solvent and other volatile compounds is removed by oil pump vacuum. For work up procedures (silica gel chromatography) see the paragraph pertinent to the respective product. [50]

b. The amine (1 equiv) is placed in a threaded pressure tube, then toluene (0.25 mL/mmol), aldehyde (1.5 equiv), dienophile (1.5 equiv), and *p*-toluenesulfonic acid monohydrate (2 mol%) are added. The reaction mixture is stirred at elevated temperature (120°C) for 24 h. After cooling, all volatile compounds are removed under reduced pressure. For work up procedures (silica gel chromatography) see the paragraph pertinent to the respective product. [49]

GP4: General procedure for alanines via MnO$_2$-mediated oxidation

A 100 mL flask is charged with an N-acylaminocyclohexene or diene derivate (5 mmol), then 85% activated MnO$_2$ (1.52 g, 15 mmol) and toluene (10 mL) are added, and the reaction is stirred at 120°C. After 5 h, the solvent is removed by oil pump vacuum. The residue is subjected to silica gel chromatography. [50]

GP5: General procedure for the synthesis of the urea-phthalimide derivaivtes.

To a solution of sodium azide (110 mg, 1.70 mmol), potassium *tert*-butoxide (14.4 mg, 0.150 mmol), and 2-benzyl-1,3-dioxoisoindoline-5-carboxylic acid (281 mg, 1.00 mmol) in DME (10.0 mL) at 75 °C, the phenylchloroformate (140 µL, 1.10 mmol) is added. The resulting mixture is stirred at 25 °C overnight. Then, the mixture is slowly cooled down to room temperature, the amine (1.50 mmol) was added and the reaction mixture was stirred for 16 hours. Afterwards, the mixture is diluted with hexane (40 mL) and the resulting solution poured into ice-cold water with continuous stirring. 10 mL water are added and stirring was maintained during 20 minutes. The white solid is filtered off; for work up procedures (silica gel chromatography or precipitation) see the paragraph pertinent to the respective product. [69]

GP7:   General procedure for fluorescence spectroscopy measurements

The samples are placed into quartz cells of 1 cm path length. Compound concentrations were adjusted as indicated in the text. The excitation and emission slit widths are between 2.5 and 5.0 nm.

5.3 Synthesis of nitro; amino- and acetamide-substituted phthalimide derivatives

5.3.1 Synthesis of 2-Benzyl-4-nitroisoindoline-1,3-dione
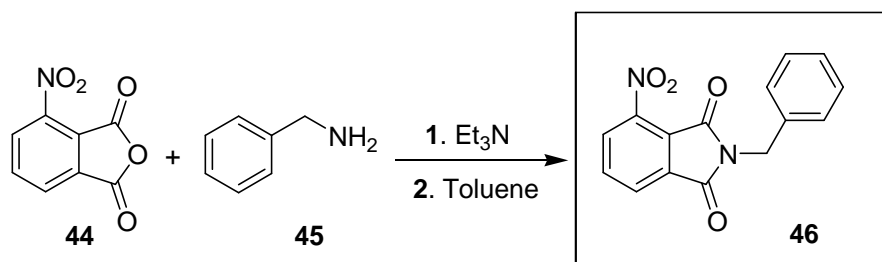
Preparation and workup was carried out according to **GP1**. The crude product was crystallized from EtOH. The product was a yellow solid.
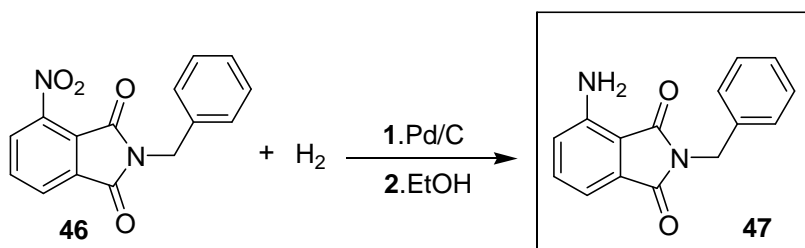
Yield: 2.4g, 8.5 mmol, 85%, Lit (87%) [56]

^{1}H NMR (CDCl$_3$, 300 MHz)

δ (ppm) = 4.82 (s; 2H; CH$_2$), 7.27 (m; 3H; CH$_{ar}$), 7.41 (m; 2H; CH$_{ar}$), 7.87 (m; 1H; CH$_{ar}$), 8.05 (m; 2H, CH$_{ar}$).

^{13}C NMR (CDCl$_3$, 75.46 MHz)

δ (ppm) = 42.3 (CH$_2$), 123.8 (CH$_{ar}$), 127.1 (CH$_{ar}$), 128.2 (CH$_{ar}$), 128.6 (CH$_{ar}$), 128.8 (CH$_{ar}$), 128.9 (CH$_{ar}$), 134.1 (CH$_{ar}$), 135.4 (CH$_{ar}$), 135.5 (C$_{ar}$), 145.1 (C$_{ar}$), 162.6 (C=O), 165.5 (C=O).

5.3.2 Synthesis of 4-amino-2-benzylisoindoline-1,3-dione

Preparation and workup was carried out according to **GP2**. The residue was purified by column chromatography Rf: 0.68 (SiO$_2$, CH$_2$Cl$_2$) to give a yellow fluorescent solid.

Yield: 3.1g, 12.29 mmol, 82%.

^{1}H NMR (CDCl$_3$, 300 MHz)

δ (ppm) = 4.80 (s; 2H; CH$_2$), 5.22 (s; 2H; NH$_2$), 6.82 (d; 1H; J = 8.32 Hz; CH$_{ar}$), 6.85 (d; 1H; J = 7.12 Hz; CH$_{ar}$), 7.14-7.40 (m; 3H; CH$_{ar}$), 7.41-7.45 (m; 3H; CH$_{ar}$).

^{13}C NMR (CDCl$_3$, 300 MHz)

δ (ppm) = 41.2 (CH$_2$), 112.3 (C$_{ar}$), 112.8 (CH$_{ar}$), 121.0 (CH$_{ar}$), 127.7-128.6 (CH$_{ar}$ x 5), 132.8 (C$_{ar}$), 135.2 (CH$_{ar}$), 136.7 (C$_{ar}$), 145.2 (C$_{ar}$), 162.3(C=O), 168.3 (C=O).

IR

ν (cm^{-1}) = 3472 (m), 3351 (m), 1743 (s), 1682 (s), 1633 (s), 1480 (s), 1454 (m), 1431 (s), 1403 (s), 1371 (s), 1328 (s), 1180 (m).
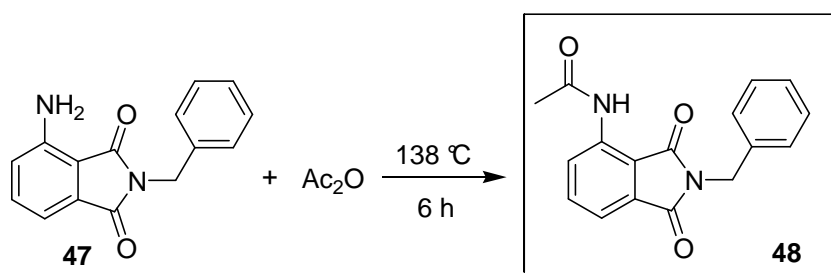
UV-Vis (CH$_3$CN, 33.33 x 10^{-6} M)

λ$_{max}$ (nm), Log(ε$_{max}$): 226 (4.48), 237 (4.42), 255 (3.90), 380 (3.81).

GC-Ms:

[M$^+$] = 252 (100%).

M.p.

145-146 °C.

5.3.3 Synthesis of *N*-(2-benzyl-1,3-dioxoisoindolin-4-yl)acetamide

Freshly distilled acetic anhydride (10 mL) was added into a flask with 200 mg (0.8 mmol) of 4-amino-2-benzylisoindoline-1,3-dione (**47**). The reaction mixture was stirred at 138°C for 6 h. After cooling, the mixture was poured into a beaker with ice, the resulting mixture was extracted with CH$_2$Cl$_2$ (2 x 30 mL) and the organic phase was washed with NaHCO$_3$ (3 x 20 mL). The organic phase was dried over MgSO$_4$. The solvent was evaporated under reduced pressure and the residue purified by column chromatography Rf: 0.65 (SiO$_2$, EtOAc / cyclohexane 1:1). The product was isolated as a colorless solid.

Yield: 211 mg, 0.71 mmol, 90%.

^{1}H NMR (CDCl$_3$, 300 MHz)

δ (ppm) = 2.25 (s; 3H; CH$_3$), 4.81 (s; 2H; CH$_2$), 7.29-7.39 (m; 5H; CH$_{ar}$), 7.41 (d; 1H; J = 6.39 Hz; CH$_{ar}$), 7.49-7.65 (m; 1H; CH$_{ar}$), 8.75 (d; 1H; J = 8.43 Hz; CH$_{ar}$), 9.52 (s; 1H; NH).

^{13}C NMR (CDCl$_3$, 75.46 MHz)

δ (ppm) = 21.8 (CH$_3$), 41.5 (CH$_2$), 117.5 (C$_{ar}$), 118.0 (CH$_{ar}$), 124.8 (CH$_{arc}$), 127.9 (CH$_{ar}$), 128.4 (CH$_{ar}$), 128.5 (CH$_{ar}$ x 2), 128.2 (CH$_{ar}$ x 2), 133.8 (C$_{ar}$) 135.8 (C$_{ar}$), 145.2 (C$_{ar}$) 168.4 (C=O), 168.4 (C=O), 168.9 (NH-C=O).

IR

ν (cm^{-1}) = 3346 (w), 1760 (m), 1693 (s), 1606 (m), 1530 (s), 1480 (s), 1433 (w), 1396 (s), 1340 (m), 1293 (m), 1226 (m), 1176 (w).

UV-Vis (CH$_3$CN, 33.33 x10^{-6} M)

λ$_{max}$ (nm), Log(ε$_{max}$): 226 (4.49), 237 (4.44), 258 (3.92), 380 (3.83).
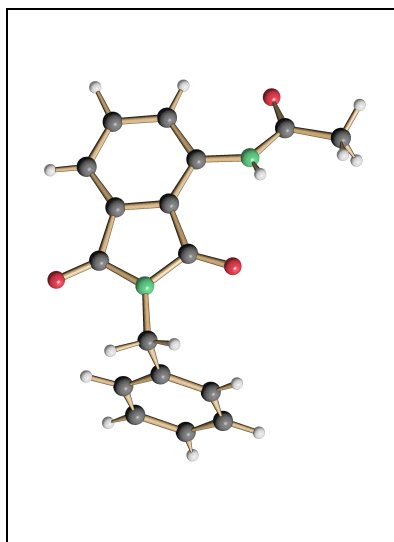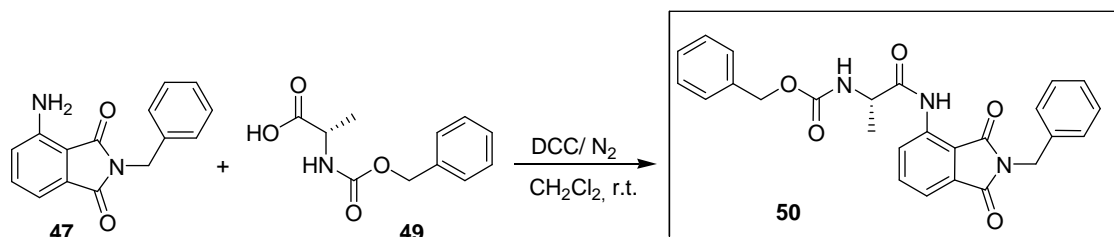
M.p.

137-138 °C.

X-ray

Figure 125: Crystal structure of *N*-(2-benzyl-1,3-dioxoisoindolin-4-yl)acetamide (48)

5.3.4 Synthesis of Benzyl (*S*)-1-(2-benzyl-1,3-dioxoisoindolin-4-ylcarbamoyl)ethylcarbamate


To a stirred solution of 100 mg of Z-L-alanine (**49**) (0.44 mmol) in 10 mL of dry CH_2Cl_2, 110 mg of **47** (0.44 mmol) and *N, N*-dicyclohexyl-carbodiimide (DCC 90,7 mg (0.44 mmol)) were added to the reaction mixture which was kept in an ice bath. The mixture was stirred in the ice bath for 10 min and then stirred at room temperature for two days. The solvent was evaporated and then EtOAc was added. The precipitate was filtered off by vacuum filtration. The product was purified by column chromatography R*f* : 0.46 (SiO$_2$, EtOAC / cyclohexane, 7:3).[105] In the discussion part are given the reasons why the characterization is not complete.

Yield: 70 mg, 0.15 mmol, 35%.

[1] H NMR (DMSO-d$_6$, 300 MHz)

δ (ppm) = 1.36 (d; 3H; *J* = 7.32 Hz; CH$_3$), 4.20 (m; 1H; CH), 4.76 (s; 2H; CH$_2$), 5.06 (m; 2H; CH$_2$), 7.27- 7.38 (m; 10H; CH$_{ar}$), 7.60 (d; 1H; *J* =7.24 Hz; CH), 7.81 (dd; 1H; *J$_1$* = 7.70 Hz; *J$_2$* = 8.10 Hz; CH$_{ar}$), 8.11 (d; 1H; *J* = 5.79 Hz; NH), 8.59 (d; 1H; *J* = 8.69Hz; CH$_{ar}$) 10.02 (s; 1H; NH).

5.3.5 Synthesis of 2-(Diphenylamino)-4-nitroisoindoline-1,3-dione
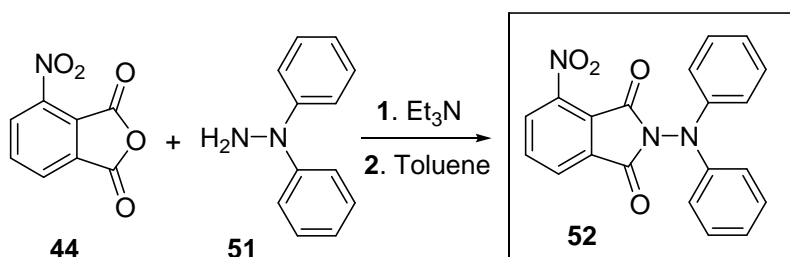
Preparation and workup was carried out according to **GP1**. The product was purified by column chromatography R*f* : 0.55 (SiO$_2$, EtOAc / cyclohexane,4:6). The product was a yellow solid. The product **52** was used directly for reaction 4.3.6, which after the important functional groups were identified. Therefore ^{13}C NMR spectra were not recorded for this compound.

Yield: 650 mg, 1.81 mmol, 70%.

¹H NMR (CDCl₃, 300 MHz)

δ (ppm) = 7.13 (m; 6H; CH$_{ar}$), 7.3 3 (m; 4H; CH$_{ar}$), 8.01 (m; 1H; CH$_{ar}$), 8.21 (m; 2H; CH$_{ar}$).

IR

γ(cm^{-1}) = 2958 (w), 2853 (w), 1732 (s), 1700 (m), 1683 (m), 1652 (m), 1158 (m), 1543 (m), 1495 (m), 1456 (m), 1289 (s).
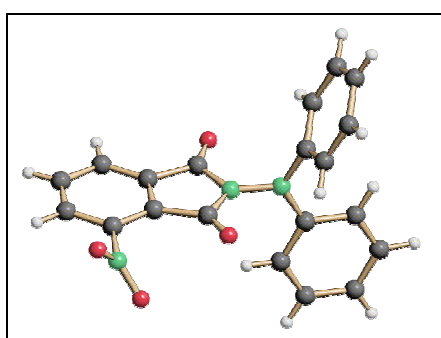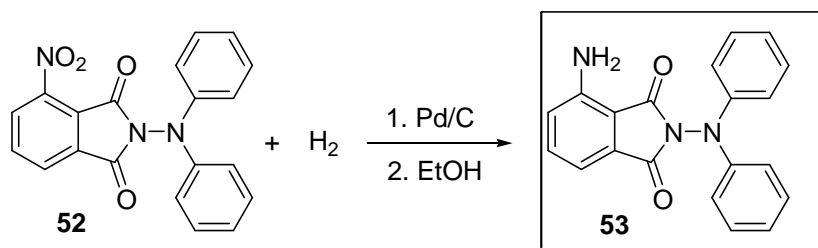
M.p.

> 250 °C.

X-ray:

Figure 126: Crystal structure of 2-(Diphenylamino)-4-nitroisoindoline-1,3-dione (52)

5.3.6 Synthesis of 2-(Diphenylamino)-4-aminoisoindoline-1,3-dione

Preparation and workup was carried out according to **GP2**. The residue was purified by column chromatography Rf : 0.68 (SiO₂, CH₂Cl₂).

Yield: 1.1 g, 3.34 mmol, 67%.

¹H NMR (CDCl₃, 300 MHz)

δ (ppm) = 5.30 (s; 2H; NH₂), 6.92 (d; 1H; J = 8.31 Hz; CH$_{ar}$), 7.08 (m; 2H; CH$_{ar}$), 7.21 (m; 4H; CH$_{ar}$), 7.31(m; 5H; CH$_{ar}$), 7.49 (m; 1H; CH$_{ar}$).

¹³C NMR (CDCl₃, 75.46 MHz)

δ (ppm) = 113.3 (CH$_{ar}$), 120.1 (CH$_{ar}$ x 4), 121.7 (CH$_{ar}$), 123.8 (CH$_{ar}$ x 3), 129.4 (CH$_{ar}$ x 4), 136.0 (CH$_{ar}$), 136.3 (CH$_{ar}$), 144.7 (C$_{ar}$ x 2), 148.5 (C$_{ar}$), 165.3 (C=O), 165.8 (C=O).

IR

ν (cm^{-1}) = 3368 (w), 3059 (w), 1769 (m), 1715 (s), 1632 (m), 1589 (s), 1493 (s), 1392 (m), 1219 (m), 1173 (w),1096 (m).

UV-Vis (CH₃CN, 33.33 x10^{-6} M)

λ$_{max}$ (nm)**,** Log(ε$_{max}$): 223 (4.40), 260 (4.21), 388 (3.80).

GC-Ms

[M$^+$] = 329 (100%).

M.p.

210 °C, decomposition.

5.4 Preliminary quenching study of 4-amino-2-benzylisoindoline-1,3-dione, N-(2-benzyl-1,3-dioxoisoindolin-4-yl)acetamide.

Fluorescence and excitation studies were carried out using a Perkin-Elmer LS-50B luminescence spectrometer. For **47** and **48** a fluorescence quenching study was conducted with different molecular quenchers, shown in figure 127. The concentrations of the quencher were adjusted to0.3 M and for the fluorophor at 1mM. The excitation and emission slit widths were set to 2.5 nm. The experiment was to add more equivalents of quencher into the quartz cells containing the fluorophor and the fluorescence spectrum was measured for each addition step.
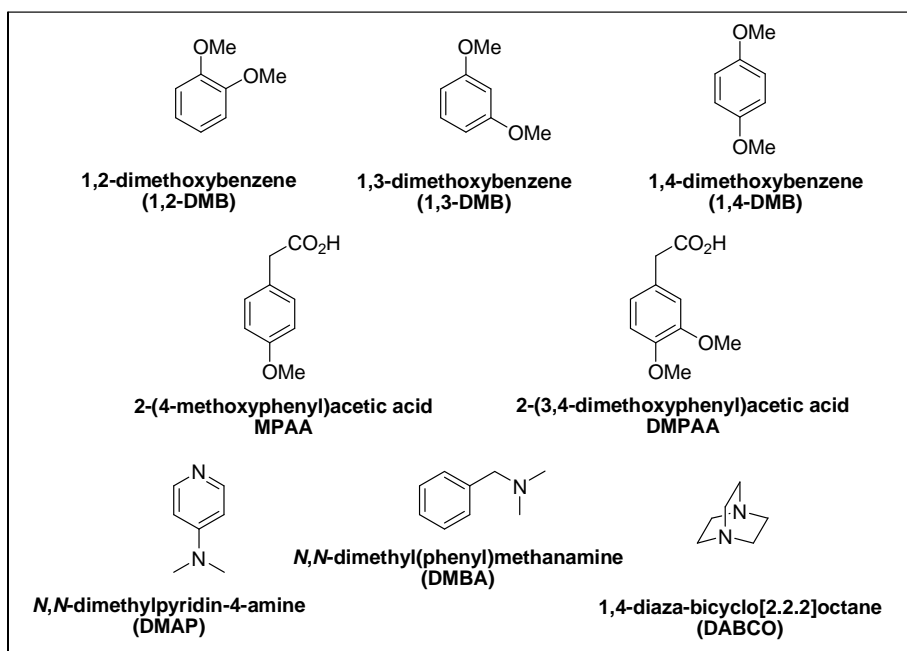

**Figure 127: Various Molecular Quenchers**

5.5 Preliminary study for fluorescence activation of 2-(diphenylamino)-4-aminoisoindoline-1,3-dione through cation coordination

Fluorescence and excitation studies were carried out using a Perkin-Elmer LS-50B luminescence spectrometer. The samples were placed into quartz cells of 1 cm path length. The concentration of **53** at 1 mM and for the cations (Ba^{2+}, Cu^{2+}, Ni^{2+}, Mg^{2+}, Ag+, Zn+, $Fe^{3+}$and Eu^{3+} as nitrate and triflate salts) between 0.01-0.1 M. For excitation and emission experiments, slit widths were 5.0 nm. The experiment was to add more equivalents of the cation into the

quartz cells containing the fluorophor and the fluorescence spectrum was measured after each addition step.

5.6 Reactions with 1-(2-Aminonaphthalen-1-yl) naphthalene-2-amine to get chiral phthalimides

5.6.1 Synthesis of 2-(1-(2-Aminonaphthalen-1-yl)naphthalen-2-yl)isoindoline-1,3-dione
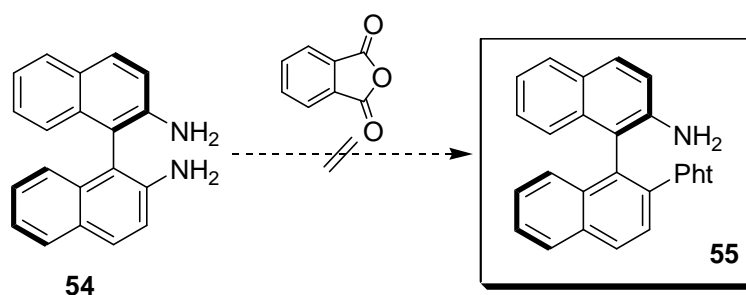

Different conditions were used for this reaction but none was successful to obtain the product **55**. The reactions conditions are given in table 31.

Table 31: Reaction conditions for the synthesis of 2-(1-(2-Aminonaphthalen-1-yl)-naphthalen-2-yl)isoindoline-1,3-dione (55).

	Equiv.	Solvent	Temp. °C	h (hours)	Work-up
a.	1:1	Toluene	120	4	According to GP1.
b.	1:1	DMF	120	6	The reaction mixture was cooled to r.t, water was added to precipitate and the product mixture was filtered. Purification by column chromatograpy (EtOAc / cyclohexane, 2:1).
c.	1:1	DMF	120	6	The reaction mixture was cooled to r.t, water was added to precipitate and the product mixture filtered. The crude product was crystallized from toluene. The desired product could not be isolated
d.	1:1	Toluene	110	7 min	This reaction was conducted in a MW. The crude product was from EtOH. The desired product could not be isolated

5.6.2 Synthesis of *N*-(1-(2-Aminonaphthalene-1-yl)naphthalen-2-yl)acetamide
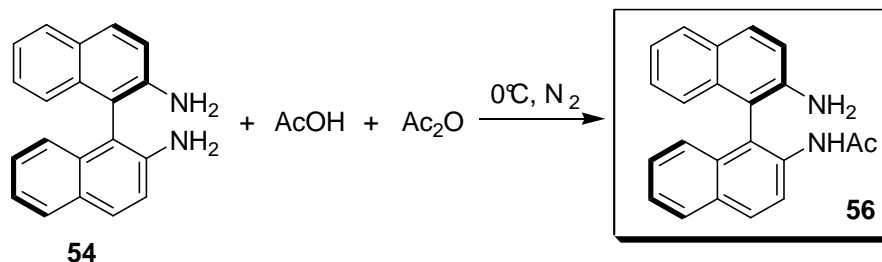
To a solution of (±)1-(2-aminonaphthalen-1-yl)naphthalen-2-amine (**54**) (1.14 g, 4mmol) and AcOH (2.4 mL 40 mmol) in 40 mL of dried CH_2Cl_2 was added Ac_2O (0.42 mL, 4 mmol) at 0 °C under N_2. The resulting solution was stirred overnight at room temperature, and then 2 N NaOH aqueous solution was added until a pH ≈ 7. The reaction mixture was extracted with CH_2Cl_2 (3 x 50 mL) and the combined organic phases were washed with saturated brine and dried over $MgSO_4$. The solvent was removed under reduced pressure and the crude product was purified by flash chromatography R*f* : 0.52 (SiO_2, EtOAc / hexane, 2:1) to afford a colorless solid [92] The product was used directly for reactions 5.6.3.

Yield: 913 mg, 2.8 mmol, 70%.

^{1}H NMR (CDCl$_3$, 300 MHz)

δ (ppm) = 1.89 (s; 3H; CH$_3$), 3.68 (s; 2H; NH$_2$), 6.93 (d; 1H; *J* = 7.63 Hz; CH$_{ar}$), 7.15-7.30 (m; 6H; CH$_{ar}$), 7.40-7.46 (m; 1H; CH$_{ar}$), 7.82-7.94 (m; 3H; CH$_{ar}$), 8.02 (d; 1H; *J* = 8.90 Hz; CH$_{ar}$), 8.6 (d; 1H; *J* = 8.90 Hz; CH$_{ar}$).

^{13}C NMR (CDCl$_3$, 75.46 MHz)

δ (ppm) = 24.7 (CH$_3$); 118.3 (CH$_{ar}$); 121.1 (CH$_{ar}$); 123.0 (CH$_{ar}$); 123.8 (CH$_{ar}$), 125.2 (CH$_{ar}$), 125.4 (CH$_{ar}$), 126.9 (CH$_{ar}$), 127.4 (CH$_{ar}$ x 2), 128.3 (CH$_{ar}$ x 2), 129.3 (C$_{ar}$ x 2), 130.4 (CH$_{ar}$), 131.3 (C$_{ar}$ x 2), 132.4 (C$_{ar}$ x 2), 133.6 (C$_{ar}$), 135.2 (C$_{ar}$), 168.9 (C=O).

5.6.3 Synthesis of *N*-(1-(2-(1,3-Dioxoisoindolin-2-yl)naphthalen-1-yl)naphthalen-2-yl)acetamide

a.
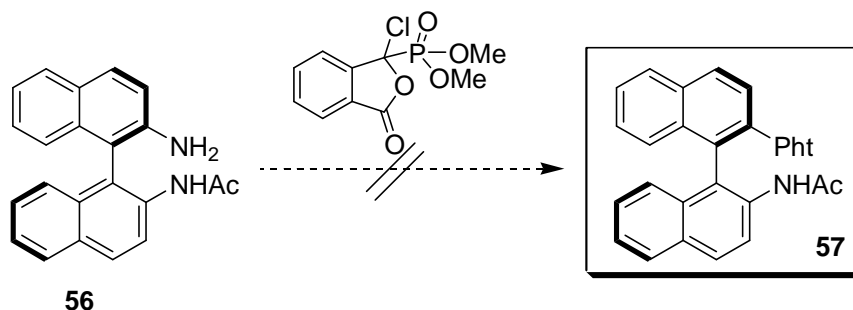
A solution of *N*-(1-(2-aminonaphthalen-1-yl)naphthalen-2-yl)acetamide (**56**) (222 mg, 0.65 mmol), and dimethyl 1-chloro-1,3-dihydro-3-oxoisobenzofuran-1-yl-1-phosphonate (140 mg, 0.5 mmol) in 10 mL CH₃CN was stirred at room temperature and 90 µL of Et₃N were added to the solution. The reaction mixture was stirred at room temperature for 15 min. The solvent was removed under reduced pressure and the residue was extracted with CH₂Cl₂. The organic phase was washed with NaHCO₃ and dried over MgSO₄. The product was purified by PLC (SiO₂, EtOAc / cyclohexane, 2:1 and 3:1). [93] This method was not succesessful.
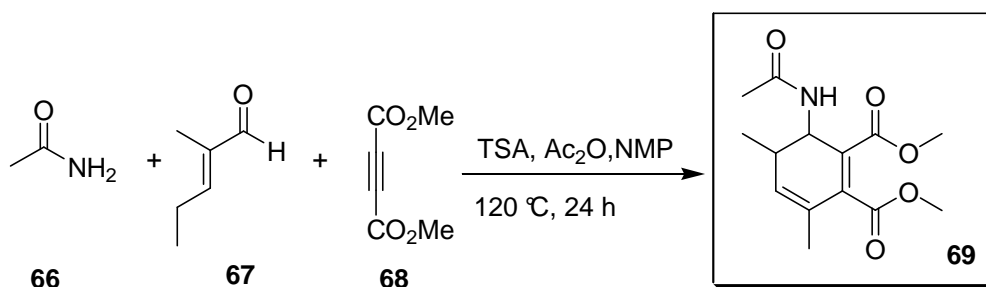
b.
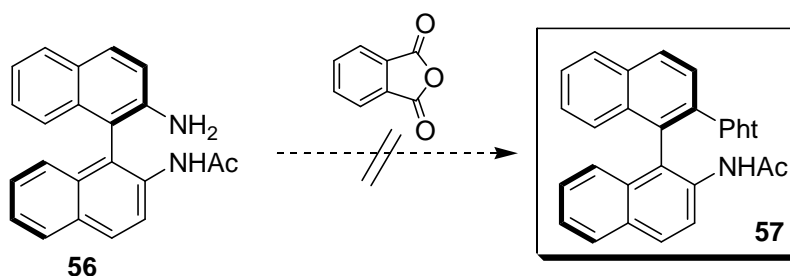
For this reaction the methods a, b and d of table 31 were used. However, the product could not be obtained under these conditions.

5.7 Multicomponent coupling with dienophilic dimethyl acetylenedicarboxylate

5.7.1 Synthesis of Dimethyl 6-acetamido-3,5-dimethylcyclohexa-1,3-diene-1,2-dicarboxylate

Acording to **GP3-a**, acetamide 891 mg (**66**) (15 mmol), propionaldehyde (**67**) (870 mg, 15 mmol), and diethyl acetylenedicarboxylate 2.13 g (**68**) (15 mmol) were reacted. The product **69** was purified by column chromatography Rf : 0.38 (SiO$_2$, EtOAc / cyclohexane 2:1). The product was isolated as white solid.

Yield: 3.71 g, 13.18 mmol, 66%.

^{1}H NMR (CDCl$_3$, 300 MHz)

δ (ppm) = 1.02 (d; 3H; J = 7.58 Hz; CH$_3$), 1.75 (s; 3H; CH$_3$), 2.01 (s; 3H; CH$_3$), 2.75 (m; 1H; CH), 3.61 (s; 3H; CH$_3$), 3.67 (s; 3H; CH$_3$), 5.21 (m; 1H; CH), 5.57 (s; 1H; NH).

^{13}C NMR (CDCl$_3$, 75.46 MHz)

δ (ppm) = 18.4 (CH$_3$), 19.8 (CH$_3$), 23.0 (CH$_3$), 30.0 (CH), 47.1 (CH), 52.4 (CH$_3$), 52.4 (CH$_3$), 130.5 (C x 1), 132.0 (CH), 141. 0 (C x 2), 167.2 (C=O), 167.9 (C=O), 170.0 (C=O).

5.7.2 Synthesis of (6*R*)-Dimethyl 6-((*S*)-2-(ethoxycarbonyl)-5-oxopyrrolidin-1-yl)-3,5-dimethylcyclohexa-1,3-diene-1,2-dicarboxylate
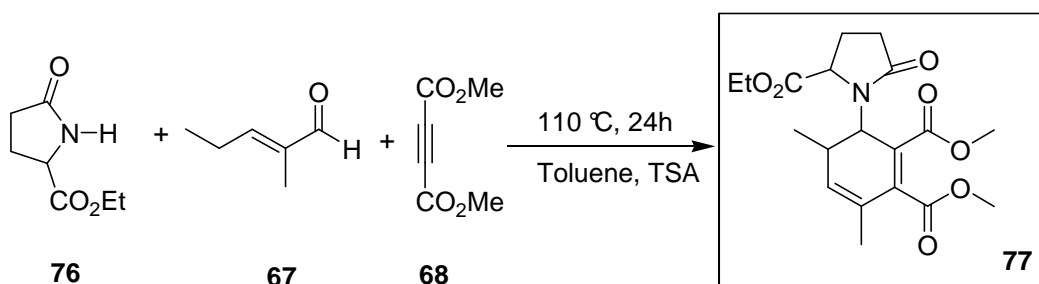
Acording to **GP3-b,** *N*-methylmaleimide 783 mg (**76**) (5 mmol), propionaldehyde (**67**) (1.10 g, 7.5 mmol), and diethyl acetylenedicarboxylate (**68**) (2.13 g, 15 mmol) were reacted. The product was purified by column chromatography R*f*: 0.30 (SiO$_2$, EtOAc / cyclohexane, 2:1). The isolated product (**77**) was a white solid.

Yield: 1.5 g**,** 4 mmol, 80%.

^{1}H NMR (CDCl$_3$, 300 MHz)

δ (ppm) = 1.14 (m; 6H; CH$_3$), 1.53 (s; 3H; CH$_3$), 2.33 (m; 4H; CH$_2$), 3.01(m; 1H; CH), 3.65 (s; 3H; CH$_3$), 3.70 (s; 3H; CH$_3$), 3.79 (m; 2H; CH$_2$), 3.82 (m; 1H; CH), 4.09 (m; 1H; CH), 5.56 (m; H; CH).

^{13}C NMR (CDCl$_3$, 75.46 MHz)

δ (ppm) = 13.7 (CH$_3$), 18.7 (CH$_3$), 19.4 (CH$_3$), 24.4 (CH$_2$), 29.8 (CH$_2$), 34.4 (CH), 48.5 (CH), 52.1 (CH$_3$), 52.1 (CH$_3$), 55.8 (CH), 61.6 (CH$_2$), 123.3 (C x 1), 127.7 (C x 1), 129.1 (CH), 148.9 (CH), 164.6 (C=O), 169.3(C=O), 172.4 (C=O), 174.9 (C=O).

5.7.3 Synthesis of (5*S*,6*R*)-Dimethyl-6-acetamido-3,5-diethylcyclo-hexa-1,3-diene-1,2-dicarboxylate
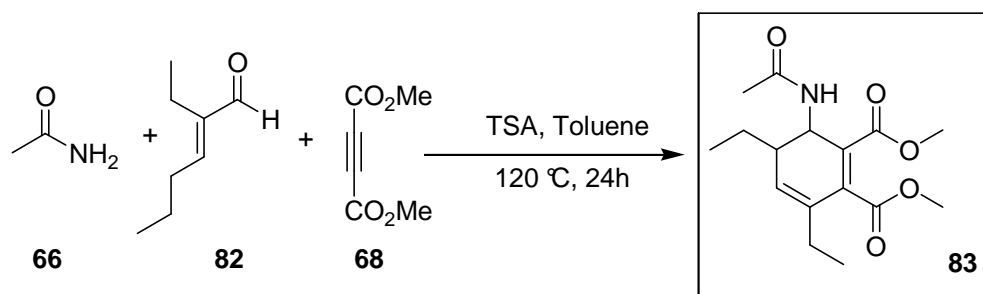
According to **GP3-b,** acetamide (**66**) 891 mg (15 mmol), butyraldehyde (**82**) (1.08 g, 15 mmol), and dimethyl acetylenedicarboxylate (**68**) 2.13 g (15 mmol) were reacted. The product **83** was purified by column chromatography R*f*: 0.38 (SiO$_2$, EtOAc / cyclohexane, 2:1). The product **83** (3.24 g**,** 10.5 mmol, 70%) was isolated as white solid and directly used for reaction 5.8.3without further characterization.

5.8 Anilines via MnO$_2$-mediated oxidation

### 5.8.1 Synthesis of Dimethyl 3-acetamido-4,6-dimethylbenzene-1,2-dioate
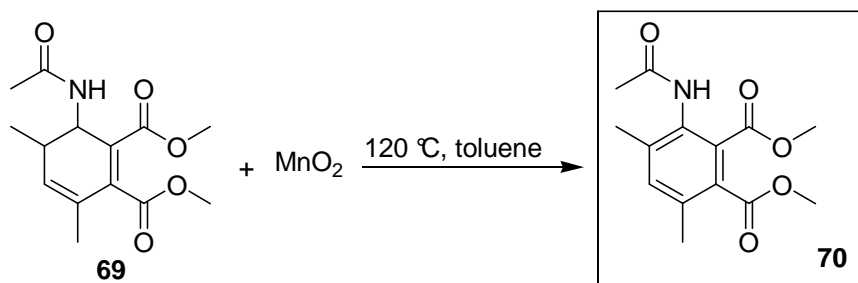
According to **GP4** dimethyl 6-acetamido-3,5-dimethylcyclohexa-1,3-diene-1,2-dicarboxylate (1.40 g, 5 mmol) was reacted. The product was purified by column chromatography R*f* : 0.52 (SiO$_2$, EtOAc). The product was isolated as white solid and was used for reaction 5.9.1, 5.9.2 and 5.9.3.

Yield: 1.24 g, 4.85 mmol, 89 %.

^{1}H NMR (CDCl$_3$, 300 MHz)

δ (ppm) = 2.15 (s; 3H; CH$_3$), 2.24 (s; 3H; CH$_3$), 2.35 (s; 3H; CH$_3$), 3.83 (s; 3H; CH$_3$), 3.84 (s; 3H; CH$_3$), 7.21 (s; 1H; CH$_{ar}$), 8.24 (s; 1H; NH).

5.8.2 Synthesis of dimethyl 3-(2-(ethoxycarbonyl)-5-oxopyrrolidin-1-yl)-4,6-dimethylbenzene-1,2-dioate
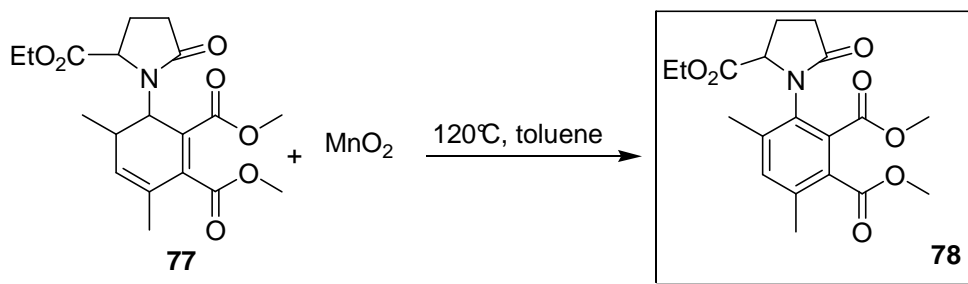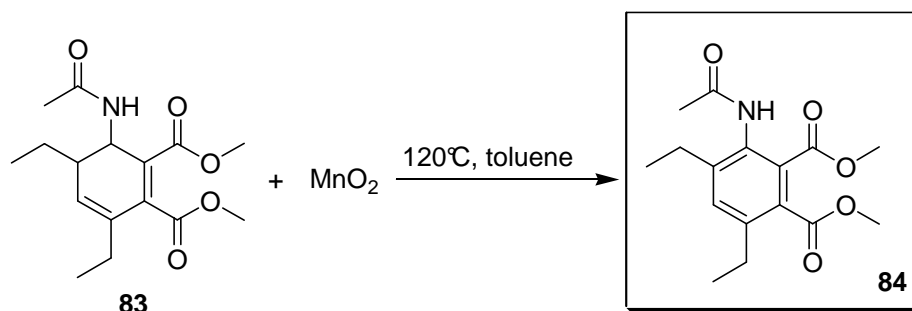

According to **GP4** (6*S*)-dimethyl 6-((*S*)-2-(ethoxycarbonyl)-5-oxopyrrolidin-1-yl)-3,5-dimethylcyclohexa-1,3-diene-1,2-dicarboxylate (**77**) (1.89 g, 5 mmol) was reacted. The product was purified by column chromatography R*f*: 0.52 (SiO$_2$, EtOAc). The product **78** was isolated as white solid and was used for reaction 4.9.4

Yield: 1.60 g, 4.25 mmol, 85 %.

δ (ppm) = 1.21 (m; 1H; CH$_3$), 2.36 (t; 6H; J_1 = 10.64 Hz; J_2 = 7.60 Hz; CH$_3$), 2.48 (m; 4H; CH$_2$), 2.71 (m; 2H; CH$_2$), 3.78 (m; 2H; CH$_2$), 3.84 (s; 3H; CH$_3$), 3.85 (s; 3H; CH$_3$), 4.14 (m; 1H; CH), 7.28 (s; 1H; CH$_{ar}$).

5.8.3 Synthesis of Dimethyl 3-acetamido-4,6-diethylbenzene-1,2-dioate

According to **GP4** (6*R*)-dimethyl 6-acetamido-3,5-diethylcyclohexa-1,3-diene-1,2-di-carboxylate (**83**) (1.54 g, 5 mmol) was reacted. The product was purified by column chromatography R*f* : 0.50 (SiO$_2$, EtOAc). The product **84** was isolated as white solid and was used for reactions 4.10.1 and 4.10.2.

Yield: 998 mg, 3.25 mmol, 65%.

^{1}H NMR (DMSO, 300 MHz)

δ (ppm) = 1.12 (m; 6H; CH$_3$), 1.97 (s; 3H; CH$_3$), 2.59 (m; 4H; CH$_2$), 3.69 (s; 3H; CH$_3$), 3.76 (s; 3H; CH$_3$), 7.36(s; 1H; CH$_{ar}$), 9.47 (s; 1H; NH).

^{13}C NMR (DMSO, 75.46 MHz)

δ (ppm) = 14.5 (CH$_3$), 16.2 (CH$_3$), 23.0 (CH$_3$), 24.5 (CH$_2$), 26.3 (CH$_2$), 52.7 (CH$_3$), 52.81(CH$_3$), 130.0 (C$_{ar}$), 130.7 (C$_{ar}$), 132.0 (CH$_{ar}$), 132.1 (C$_{ar}$), 140.6 (CH$_{ar}$), 144.2(CH$_{ar}$), 167.0 (C=O), 168.2 (C=O), 169.4 (C=O).
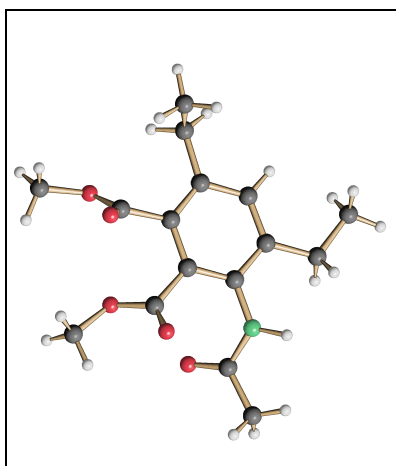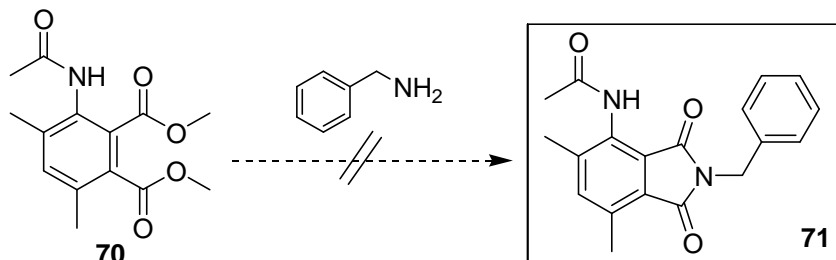
M.p.

120-121 °C.

X-Ray

Figure 128: Crystal structure of dimethyl 3-acetamido-4,6-diethylbenzene-1,2-diote (84)

5.9   Synthesis of Phthalimides from aniline derivatives

### 5.9.1 Synthesis of *N*-(2-Benzyl-4,6-dimethyl-1,3-dioxoisoindolin-7-yl)acetamide

This reaction was carried out using different conditions and could not be successfully performed. The reaction conditions are given in table 32.

Table 32: Reaction conditions for the synthesis of *N*-(2-benzyl-4,6-dimethyl-1,3-dioxoisoindolin-7-yl)acetamide (71).

	Equiv.	Solvent	Temp. °C	Cat.	h (hours)	Work-up
a.	1:1	No solvent	120	No cat.	24	Extraction with CH_2Cl_2
b.	1	Benzylamine	120	BF_3	24	Extraction with CH_2Cl_2
c.	1:6	Toluene	120	BF_3	24	Extraction with CH_2Cl_2 and washed with $NaHCO_3$
d.	1:6	Toluene	120	BF_3	56	Extraction with CH_2Cl_2, washed with $NaHCO_3$. PLC (2:1, EtOAc / cyclohexane)
e.	1:1	Toluene	120	10% *N*-MM	56	Extraction with CH_2Cl_2, washed with $NaHCO_3$. Column Chromatography (2:1, EtOAc / cyclohexane)

5.9.2 Synthesis of *N*-(2-(Diphenylamino)-4,6-dimethyl-1,3-dioxoiso-indolin-7-yl)acetamide
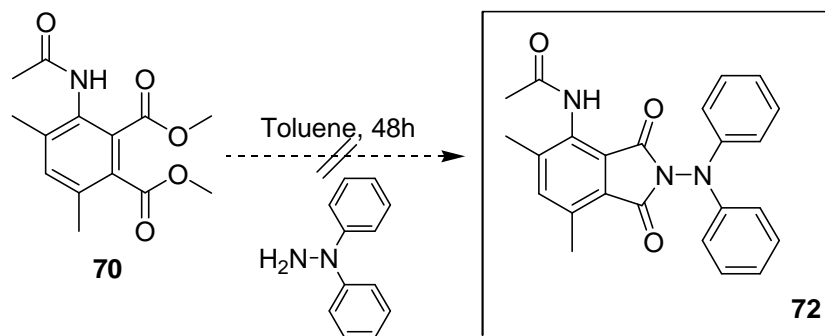
The preparation and work up were carried out according to **GP1.** Dimethyl 3-acetamido-4,6-dimethylbenzene-1,2-dioate (**70**) (152,3 mg, 0.54 mmol), 2,2-diphenylhydrazine (120.0 mg, 0.54 mmol) and Et$_3$N 0.05 mL were used. The reaction was not successful.

5.9.3 Synthesis of Dimethyl 3-acetamido-4,6-dimethylbenzene-1,2-dioate
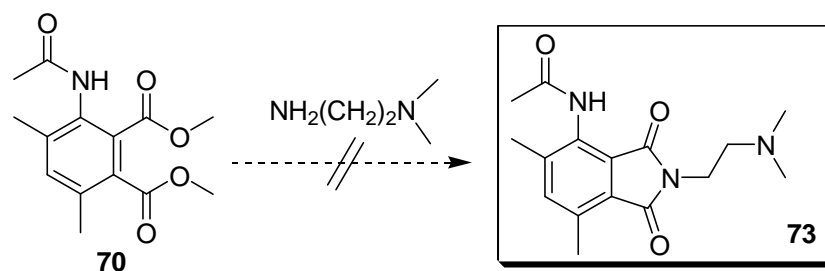
This reaction was carried out with different conditions and was not successful. [65] The conditions are given in table 33.

Table 33: Reaction conditions for the synthesis of dimethyl-3-acetamido-4,6-dimethyl-benzene-1,2-dioate (73).

	Equiv.	Solvent	Temp. °C	h (hours)	Work-up
a.	1:1	No solvent	100	72	Column Chromatography (EtOH / Cyclohexane, 9:1)
b.	1:1	No solvent	100	24	Column Chromatography (EtOH / Cyclohexane, 8:2)

5.9.4 Synthesis of Ethyl 1-(2-(2-(dimethylamino)ethyl)-4,6-dimethyl-1,3-dioxoisoindolin-7-yl)-5-oxopyrrolidine-2-carboxylate
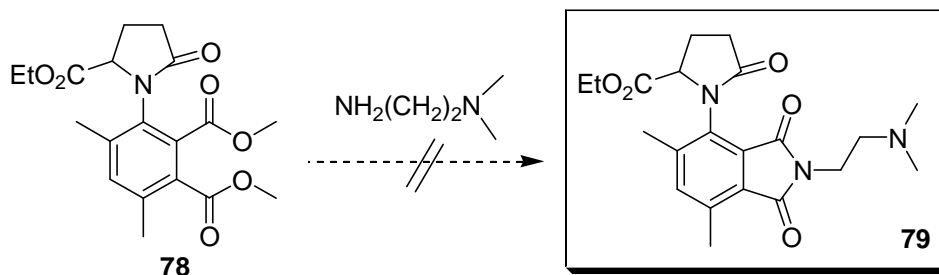

In a 25 mL flask 1.13 g (3.00 mmol) of dimethyl 3-(2-(ethoxycarbonyl)-5-oxopyrrolidin-1-yl)-4,6-dimethylbenzene-1,2-dioate (**78**) was dissolved in 10 mL of *N,N*-dimethylethane-1,2-diamine. The mixture was stirred at 100 °C for 24 h. After evaporation, the crude residue was purified by column chromatography (EtOAc / methanol 9:1).[65] The desired product (**79**) could not be isolated.

The conducted reaction led to the formation of the dehydroaminated phthalimide derivate (**80**) and the amine phthalimide derivate (**81**) in a 5:1 ratio.
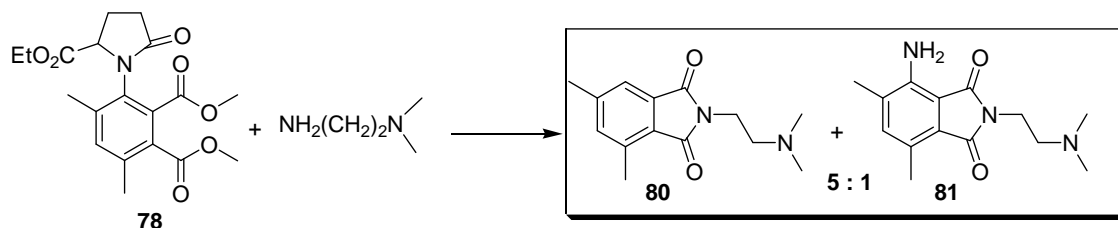
5.10 Reactions of Dimethyl 3-acetamido-4,6-diethylbenzene-1,2-dioate with acid and basic

5.10.1 Reaction with mineralic acid
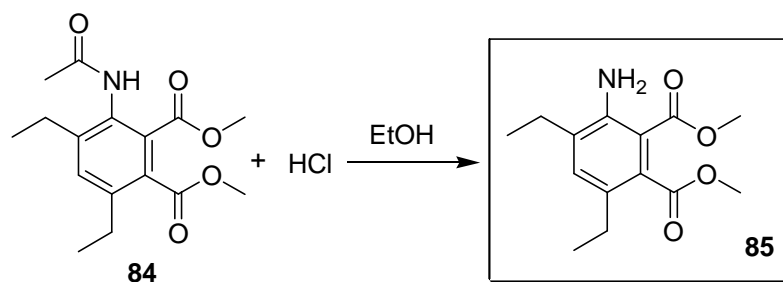
A mixture of dimethyl 3-acetamido-4,6-diethylbenzene-1,2-dioate (**84**) (100 mg, 0.32 mmol), 0.5 mL conc. HCl and 0.25 mL ethanol was heated to 85°C for 5 h. After cooling
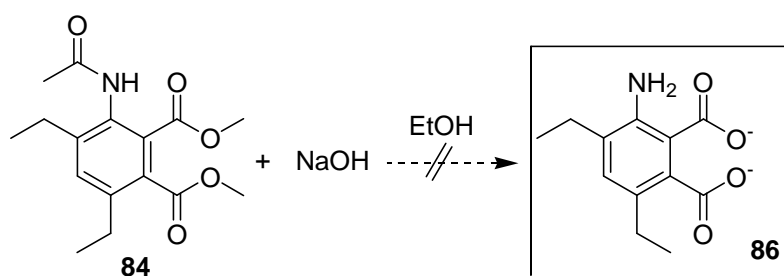
to room temperature, 2 mL of water were added. Then a 40% KOH solution was added until the solution became basic pH. The product **85** was extracted with EtOAc and purified by PLC (SiO$_2$, EtOAc / cyclohexane, 7:3).[94]

Yield: 56.8 mg, 0.21 mmol, 66%.

^{1}H NMR (CDCl$_3$, 300 MHz)

δ (ppm) = 1.20 (m; 3H; CH$_3$), 1.42 (m; 3H; CH$_3$), 2.52 (m; 4H; CH$_2$), 3.84 (s; 3H; CH$_3$), 3.87 (s; 3H; CH$_3$), 5.56 (s; 2H; NH$_2$), 7.07 (s; 1H; CH$_{ar}$).

5.10.2 Reaction with base

Dimethyl 3-acetamido-4,6-diethylbenzene-1,2-dioate (**84**) (100 mg, 0.32 mmol), and sodium hydroxide (65 mg, 1.62 mmol) were dissolved in EtOH (0.8 mL) and heated for 2 h at 90°C in a closed vessel. After heating was finished, water was added to the reaction mixture and the resulting solution was extracted. The extraction was tried with ether, EtOAc and CH$_2$Cl$_2$ but was not successful. [95]

5.11 Synthesis of Phthalimide-Serine Couples

5.11.1 Synthesis of 2-(methoxycarbonyl)-4,5-dimetoxy-benzoic acid
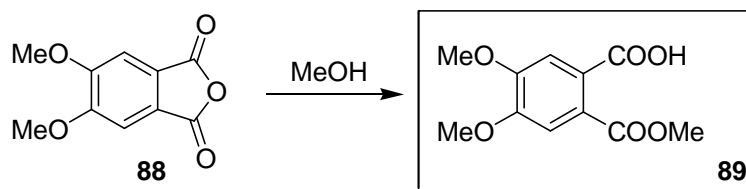
A 100 mL flask was charged with (1.04 g, 85 mmol) of 4,5-dimethoxyphthalic anhydride (**88**) [96] and 30 mL of dry methanol. The mixture was stirred and heated to reflux until the solid was completely dissolved. The heating and stirring was continued for 2h. Then, the excess of

methanol was evaporated *in vacuo*. The product **89** was a semicrystalline solid that could directly be used for the following transformation.
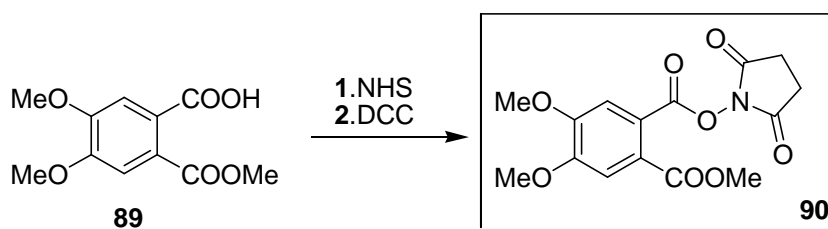
Yield: 1.14 g, 4.74 mmol, 95%.

^{1}H NMR (CD$_3$CN, 300 MHz)

δ (ppm) = 3.92 (s; 3H; CH$_3$), 3.96 (s; 3H; CH$_3$), 3.97 (s; 3H; CH$_3$), 7.19 (s; 1H; CH$_{ar}$), 7.47 (s; 1H; CH$_{ar}$).

^{13}C NMR (+APT, CD$_3$CN, 75.46 MHz)

δ (ppm) = 53.0 (CH$_3$), 56.3 (CH$_3$ x 2), 103.4 (CH$_{ar}$), 106.2 (CH$_{ar}$), 123.3 (C$_{ar}$), 126.3 (C$_{ar}$), 150.3 (C$_{ar}$), 151.6 (C$_{ar}$), 168.9 (C=O), 170.6 (C=O).

5.11.2   Synthesis of *N*-Hydroxysuccinimide ester of 2-(Methoxy-carbonyl)-4,5-dimethoxybenzoic acid

To a mixture of 1.20 g (5 mmol) of 2-(methoxycarbonyl)-4.5-dimethoxybenzoic acid (**89**) and (575 mg, 5 mmol) of *N*-hydroxysuccinimide 50 mL of dry CH$_2$Cl$_2$ was added and the reaction flask was cooled to 0-5 °C using an ice bath. Then (1.14 g, 5.5 mmol) of DDC were added and the mixture was vigorously stirred overnight. After completion of the reaction, determined by TLC, the mixture was diluted with 100 mL of EtOAc and the precipitated solid was filtered off. The remaining organic phase was evaporated. The product **90** was an amorphous solid.

Yield: 1.38 g, 4.09 mmol, 93%.

^{1}H NMR (CD$_3$CN, 300 MHz)

δ (ppm) = 2.6 (s; 4H; CH$_2$), 3.83 (s; 3H; CH$_3$), 3.89 (s; 3H; CH$_3$), 3.9 (s; 3H; CH$_3$), 7.31 (s; 1H; CH$_{ar}$), 7.35 (s; 1H; CH$_{ar}$).

^{13}C NMR (+APT, CD$_3$CN, 75.46 MHz)

δ (ppm) = 25.5 (CH$_2$ x 2), 52.5 (CH$_3$), 55.9 (CH$_3$), 56.0 (CH$_3$), 104.2 (CH$_{ar}$), 105.6 (CH$_{ar}$), 118.5 (C$_{ar}$), 126.6 (C$_{ar}$), 151.0 (C$_{ar}$), 152.6 (C$_{ar}$), 162.6 (C=O), 166.8 (C=O), 170.1 (C=O), 170.3 (C=O).

5.11.3 Synthesis of 3-Hydroxy-2-(5,6-dimethoxy-1,3-dioxoisoindo-lin-2-yl)propanoic acid
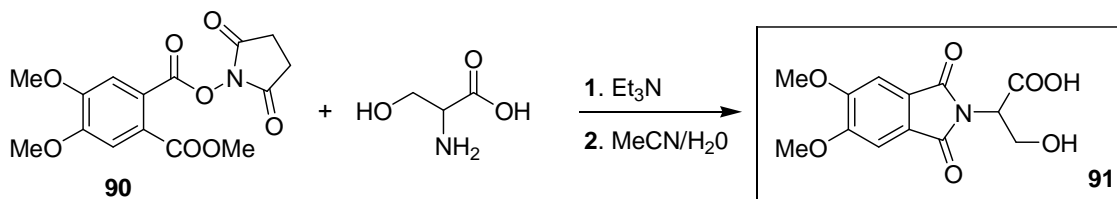
210 mg (2 mmol) of serine were dissolved in 2 mL of distilled water at room temperature. To this solution 0.7 mL (5 mmol) of triethylamine were added, followed by 10 mL of acetonitrile and 674 mg (2 mmol) of *N*-hydroxysuccinimide ester of 2-(methoxycarbonyl)-4,5-dimethoxybenzoic acid (**90**). The mixture was stirred for 6 h. After evaporating most of the acetonitrile *in vacuo*, the solution was treated with 15 mL of saturated NaHCO$_3$ solution and washed with EtOAc (2 x 15 mL). The aqueous phase was acidified with HCl 6 N until pH ≈ 2 and extracted with dichloromethane (3 x 15 mL). The organic phase was dried over MgSO$_4$, filtered and evaporated. The product **91** was isolated a viscous oil.
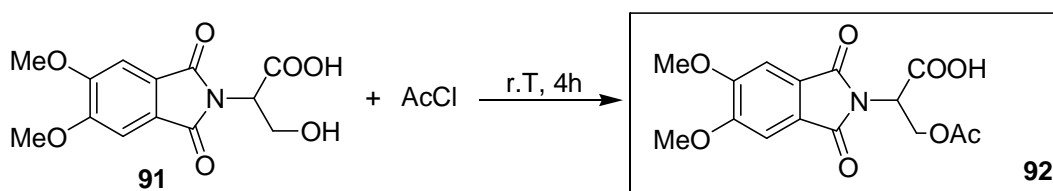
Yield: 440 mg, 1.49 mmol, 74%.

^{1}H NMR (CD$_3$CN, 300 MHz)

δ (ppm) = 3.97 (s; 6H; CH$_3$), 4.10 (m; 2H; CH$_2$), 4.90 (m; 1H; CH), 7.38 (s; 2H; CH$_{ar}$).

^{13}C NMR (+APT, CD$_3$CN, 75.46 MHz)

δ (ppm) = 53.8 (CH), 56.2 (OCH$_3$ x 2), 59.2 (CH$_2$), 105.6 (CH$_{ar}$), 125.0 (C$_{ar}$ x 2), 154.4 (C$_{ar}$ x 2), 167.9 (C=O), 168.7 (C=O).

5.11.4 Synthesis of 3-Acetoxy-2-(5,6-dimethoxy-1,3-dioxoisoin-dolin-2-yl)propanoic acid

In a 50 mL flask 295 mg (1 mmol) of 3-hydroxy-2-(5,6-dimethoxy-1,3-dioxoisoindolin-2-yl)propanoic acid (**91**) was dissolved in 4 mL of acetyl chloride at room temperature. The mixture was stirred for 4 h, then the excess of acetyl chloride was distilled off *in vacuo*. A 1:1 mixture of acetone and water (10 mL) was added and the acetone evaporated under reduced pressure. The solution was treated with 15 mL of NaHCO$_3$ solution and washed with ethyl

acetate (2 x 15 mL). The aqueous phase was acidified with HCl 6 N until pH ≈ 2 and extracted with dichloromethane (3 x 15 mL). The organic phase was dried over $MgSO_4$, filtered and evaporated under reduced pressure [97]. The product **92** was isolated as a viscous oil.

Yield: 350 mg, 0.95 mmol, 95%.

^{1}H NMR (CD$_3$CN, 300 MHz)

δ (ppm) = 1.92 (s; 3H; CH$_3$), 3.94 (s; 6H; CH$_3$), 4.59 (m; 1H; CH), 4.68 (m; 1H; CH), 5.09 (m; 1H; CH), 7.35 (s; 2H; CH$_{ar}$), 9.31 (s; 1H; OH).
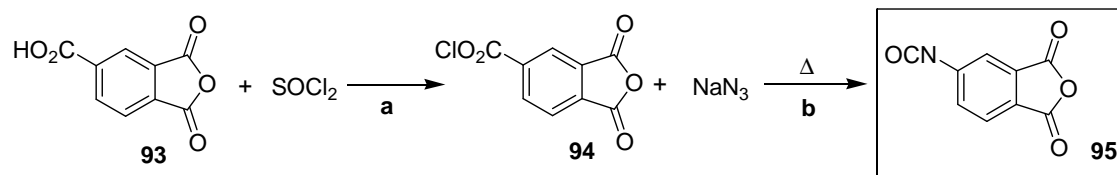
^{13}C NMR (+APT, CD$_3$CN, 75.46 MHz)

δ (ppm) = 19.7 (CH$_3$), 50.2 (CH), 56.2 (OCH$_3$ x 2), 60.7 (CH$_2$), 105.7 (CH$_{ar}$ x 2), 124.8 (C$_{ar}$ x 2), 154.4 (C$_{ar}$ x 2), 167.5 (C=O), 168.2 (C=O), 170.6 (C=O).

HRMS: EI, 70 eV, $C_{15}H_{15}NO_8Na^+$ (M-Na$^+$).

  Calcd.: M = 360.069 g/mol.

  Found: M = 360.069 ± 0.005 g/mol.

5.11.5 Synthesis of 5-5-Isocyanatoisobenzofuran-1,3-dione

a.-To a suspension of 5.0 g (26.02 mmol) of trimellitic anhydride (**93**) in anhydrous CCl$_4$ (40 mL), 4.64 g (2.85 mL, 39.04 mmol) thionyl chloride and pyridine (0.04 mL) were added. The mixture was refluxed for 2 h under nitrogen atmosphere, then cooled to room temperature and concentrated *in vacuo*. [98]

b.-The reaction mixture was suspended in CCl$_4$ (50 mL), and sodium azide (1.86 g; 28 mmol) was added. The resulting mixture was refluxed for 4 h and then cooled to room temperature. The resulting suspension was diluted with EtOAc (125 mL), and then washed with water (2 x 50 mL), saturated aqueous NaHCO$_3$ (2 x 50 mL), and brine (2 x 50 mL). The organic phase was dried over MgSO$_4$, filtered and evaporated.[98] The product **95** is a colorless solid.

  Due to the toxicity of CCl$_4$, all reactions and evaporation processes were carried out in the fume hood.

Yield: b-3.0 g, 15.86 mmol, 61%.

^{1}H NMR (acetone-d$_6$, 300 MHz)

δ (ppm) = 8.27 (d; 1H; J = 8.01 Hz; CH$_{ar}$), 8.53 (s; 1H; CH$_{ar}$), 8.62 (d; 1H; J = 8.26 Hz; CH$_{ar}$).

^{13}C NMR (acetone-d$_6$, 75.46 MHz)

δ (ppm) = 125.3 (CH$_{ar}$), 125.9 (CH$_{ar}$), 130.0 (C=O), 132.2 (C$_{ar}$), 132.4 (C$_{ar}$), 136.3 (CH$_{ar}$), 137.4 (C$_{ar}$), 162.5 (2-C=O).
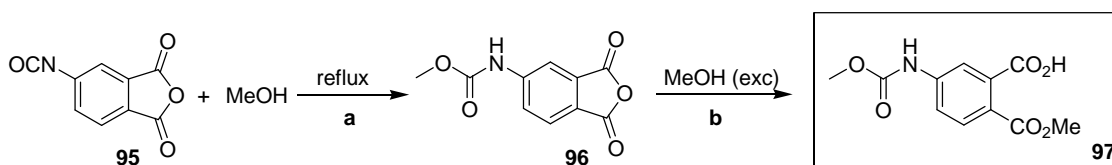
IR

ν (cm-1) = 3083 (w), 2935 (m),2931 (m), 2203 (m), 2151 (s), 1857 (ms), 1776 (s),1731 (ms), 1681 (s), 1430 (m), 1348 (m), 1271 (s), 1238 (s), 1178 (m).

GC-Ms

[M$^+$] = 189.00 (100%).

5.11.6   Synthesis of 2-(Methoxycarbonyl)-5-(methoxycarbonyl-amino)benzoic acid

A 100-mL flask was charged with 945 mg (5 mmol) of 5-isocyanatoisobenzofuran-1,3-dione (**95**) and 30 mL of dry methanol were added. The mixture was stirred and heated to reflux until the solid completely dissolved. The heating and stirring was continued for 2 h. Then the excess of methanol was evaporated *in vacuo*. The product **97** was a semycrystalline solid that could directly be used in the following step. A small amount of the regioisomeric hemiester could be detected, but was used as well since both lead to the same phthalimide. The reaction with the alcohol can be conducted stepwise, first treating with 1 equiv. of methanol in toluene [99] then with excess methanol.

Yield: 1.16 g, 4.58 mmol, 92%.

^{1}H NMR (DMSO-d$_6$, 300 MHz)

δ (ppm) = 3.70 (s; 3H; CH$_3$), 3.79 (s; 3H; CH$_3$), 7.60-7.80 (m; 3H; CH$_{ar}$), 10.10 (m; 1H; NH).

^{13}C NMR (+APT, DMSO-d$_6$, 75.46 MHz)

δ (ppm) = 52.3 (CH$_3$), 52.8 (CH$_3$), 116.9 (CH$_{ar}$), 119.3 (CH$_{ar}$), 124.4 (C$_{ar}$), 131.1 (CH$_{ar}$), 135.2 (C$_{ar}$), 142.8 (C$_{ar}$), 154.3 (OC=ONH), 167.5 (C=O), 169.0 (C=O).

5.11.7 Synthesis of *N*-Hydroxysuccinimide ester of 2-(Methoxy-carbonyl)-5-(methoxycarbonylamino)benzoic acid
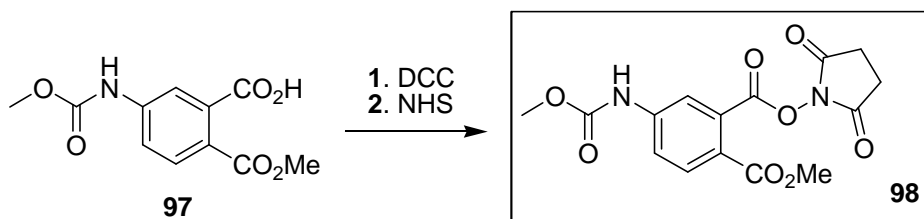
To a mixture of 1.27 g (5 mmol) 2-(methoxycarbonyl)-5-(methoxycarbonylamino) benzoic acid (**97**) and 575 mg of *N*-hydroxysuccinimide, 50 mL of dry CH_2Cl_2 were added and the reaction flask was cooled to 0-5 °C using an ice bath. Then, 1.14 g (5.5 mmol) of DCC were added and the mixture was vigorously stirred overnight. After completion of the reaction (determined by TLC) the mixture was diluted with 100 mL of EtOAc and the precipitated solid was filtered off. The remaining organic phase was evaporated *in vacuo*. The product was an amorphous solid. A small amount of the regioisomeric ester was present, but could used directly since both lead to the same phthalimide.

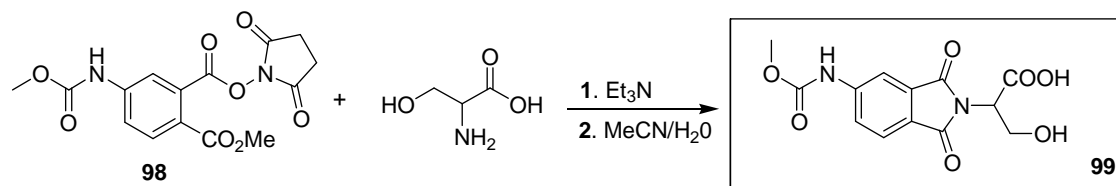**Yield:** 155 g, 4.42 mmol, 88%.

^{1}H NMR (DMSO-d$_6$, 300 MHz)

δ (ppm) = 2.88 (s; 4H; CH$_2$), 3.73 (s; 3H; CH$_3$), 3.81 (s; 3H; CH$_3$), 7.80-8.05 (m; 3H; CH$_{ar}$), 10.4 (m; 1H, NH).

^{13}C NMR (+APT, DMSO-d$_6$, 75.46 MHz)

δ (ppm) = 26.0 (CH$_2$ x 2), 52.6 (CH$_3$), 53.4 (CH$_3$), 117.4 (C$_{ar}$), 117.9 (CH$_{ar}$), 119.8 (CH$_{ar}$), 132.0 (CH$_{ar}$), 135.7 (C$_{ar}$), 145.1 (C$_{ar}$), 152.4 (OC=ONH), 161.8 (C=O), 167.5 (C=O), 170.6 (C=O x 2).

5.11.8 Synthesis of 3-Hydroxy-2-(5-methoxycarbonylamino-1,3-dioxoisoindolin-2-yl) propanoic acid

Serine 210 mg; 2 mmol was disolved in 2 mL of distillied water at room temparature. To this solution 0.7 mL (5 mmol) of triethylamine were added, followed by 10 mL of acetonitrile and 700 mg (2 mmol) of the *N*-hydroxysuccinimide ester of 2-(methoxy-carbonyl)-5-(methoxy-carbonylamino)benzoic acid (**98**). The mixture was stirred for 6 h. After evaporating most of the

acetonitrile *in vacuo*, the solution was treated with 15 mL of a saturated NaHCO$_3$ solution and washed with ethyl acetate (2 x 15 mL). The aqueous phase was acidified with 6 N HCl until pH $\approx$ 2 and extracted with dichloromethane (3 x 15 mL). The organic phase was dried over MgSO$_4$, filtered and evaporated. The product **99** was isolated as a viscous oil.
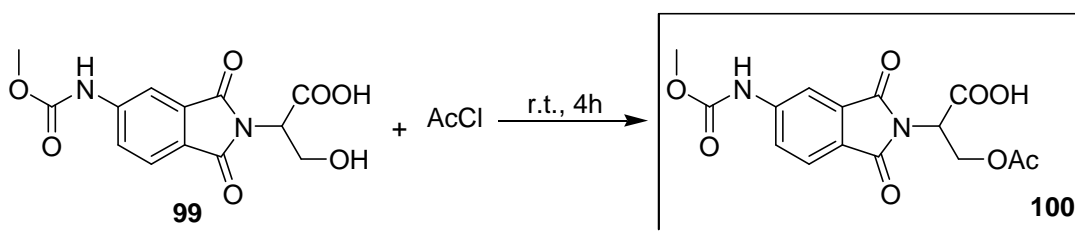
Yield: 155 g, 4.42 mmol, 88%.

^{1}H NMR (CD$_3$CN, 300 MHz)

δ (ppm) = 3.75 (s; 3H; CH$_3$), 4.10 (m; 2H; CH$_2$), 4.93 (m; 1H; CH), 7.74 (m; 2H; CH$_{ar}$), 7.98 (m; 1H; CH$_{ar}$), 8.37 (m; 1H; NH).

^{13}C NMR (+APT, CD$_3$CN, 75.46 MHz)

δ (ppm) = 52.3 (CH), 54.1 (CH$_3$), 59.0 (CH$_2$), 112.2 (CH$_{ar}$), 122.7 (CH$_{ar}$), 124.5 (CH$_{ar}$), 125.0 (C$_{ar}$), 133.4 (C$_{ar}$), 145.1 (C$_{ar}$), 153.9 (OC=ONH), 167.4 (C=O), 167.6 (C=O), 168.6 (C=O).

5.11.9 Synthesis of 3-acetoxy-2-(5-methoxycarbonylamino-1,3-dioxoisoindolin-2-yl)propanoic acid

In a 50 mL flask 308 mg (1 mmol) of 3-hydroxy-2-(5-methoxycarbonylamino-1,3-dioxoiso-indolin-2-yl)propanoic acid (**99**) was dissolved in 4 mL of acetyl chloride at room temperature. The mixture was stirred for 4 h, then the excess of acetyl chloride was distilled off *in vacuo*. A 1:1 mixture of acetone and water (10 mL) was added, and the acetone was evaporated. The solution was treated with 15 mL of a NaHCO$_3$ solution and washed with ethyl acetate (2 x 15 mL). The aqueous phase was acidified with 6 N HCl until pH $\approx$ 2 and extracted with dichloromethane (3 x 15 mL). The organic phase was dried over MgSO$_4$, filtered and evaporated. [97] The product **100** was isolated as a viscous oil.

Yield: 325 mg, 0.92 mmol, 93%.

^{1}H NMR (CD$_3$CN, 300 MHz)

δ (ppm) = 1.93 (s; 3H; CH$_3$), 3.77 (s; 3H; CH$_3$), 4.60 (m; 1H; CH$_2$), 4.70 (m; 1H; CH$_2$), 5.14 (m; 1H; CH), 7.77 (m; 2H; CH$_{ar}$), 8.03 (m; 1H; CH$_{ar}$), 8.39 (m; 1H; NH).

¹³C NMR (+APT, CD₃CN, 75.46 MHz)

δ (ppm) = 19.8 (CH₃), 50.5 (CH), 52.5 (CH₃), 60.6 (CH₂), 112.3 (CHₐᵣ), 122.8 (CHₐᵣ), 124.6 (CHₐᵣ), 124.8 (Cₐᵣ), 133.2 (Cₐᵣ), 145.2 (Cₐᵣ), 153.9 (OC=ONH), 166.9 (C=O), 167.1 (C=O), 167.7 (C=O), 170.5 (C=O).

HRMS: EI, 70 eV, $C_{15}H_{14}N_2O_8Na^+$ (M-Na$^+$).

  Calcd.: M = 373.064 g/mol.

  Found: M = 373.064 ± 0.005 g/mol.

5.11.10 Procedure for the irradiation of caged acetates, 3-acetoxy-2-(5,6-dimethoxy-1,3-dioxoisoindolin-2-yl)propanoic acid and 3-acetoxy-2-(5-methoxycarbonylamino-1,3-dioxoisoindolin-2-yl) propanoic acid

R₁ = R₂ = OMe 92

R₁ = NHCOOMe R₂ = H 100

R₁ = R₂ = OMe 101

R₁ = NHCOOMe R₂ = H 102
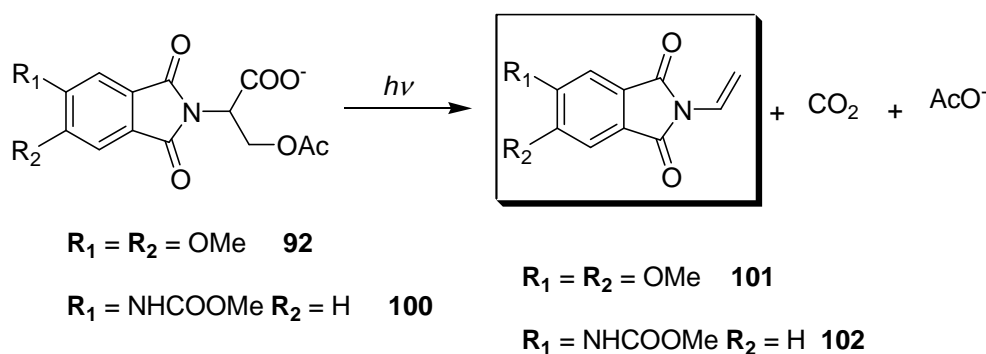
  Solutions of 0.2 mmol of 3-acetoxy-2-(5,6-dimethoxy-1,3-dioxoisoindolin-2-yl)propanoic acid (**92**) and 3-acetoxy-2-(5-methoxycarbonylamino-1,3-dioxoisoindolin-2-yl)propanoic acid(**100**) in 50 mL of phosphate buffer at pH = 7 were irradiated at 15-20°C for 2 h with phosphor-coated mercury low-pressure lamps (emission maximum at 350 ± 20 nm). The resulting alkenyl-phthalimide was extracted with CH₂Cl₂ (3 x 50 mL). The organic phase was dried over MgSO₄, filtered and the solvent evaporated *in vacuo*. The residue was dissolved in deuterated solvent and analyzed by NMR. In the aqueous phase, the liberated acetate was analyzed after irradiation using a modification of a published method. [100] By addition of benzyl bromide and warming at 50 °C for 4 h, acetate was derivatized as benzyl acetate. It was then extracted with CH₂Cl₂ and detected by GC, comparing with an authentic sample.

5.11.10.1 Irradiation of 3-Acetoxy-2-(5,6-dimethoxy-1,3-dioxo-isoindolin-2-yl)propanoic acid. Synthesis of 5,6-Dimethoxy-2-vinylisoindoline-1,3-dione
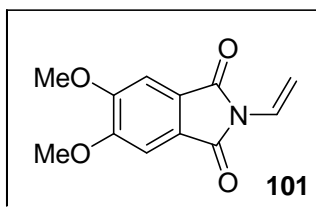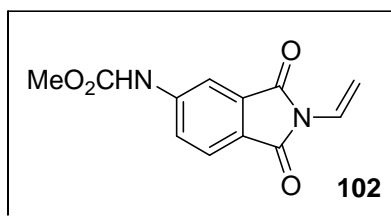

^{1}H NMR (CDCl$_3$, 300 MHz)

δ (ppm) = 4.00 (s; 6H; CH$_3$), 4.95 (d;1H; J = 10.0Hz, CH), 5.98 (d; 1H;J = 16.0 Hz; CH), 6.81 (dd; 1H; J_1 = 10.0 Hz; J_2 = 16.0 Hz; CH), 7.31 (s; 2H; CH$_{ar}$).

^{13}C NMR (+DEPT, CDCl$_3$, 75.46 MHz)

δ (ppm) = 53.6 (CH$_3$), 103.0 (CH$_2$), 105.3 (CH), 123.8 (CH$_{ar}$), 125.0 (C$_{ar}$), 154.2 (C$_{ar}$), 166.5 (C=O).

5.11.10.2 Irradiation of 3-Acetoxy-2-(5-methoxycarbonylamino-1,3-dioxoisoindolin-2-yl) propanoic acid. Synthesis of Methyl (1,3-dioxo-2vinylisoindolin-5-yl)carbamate


^{1}H NMR (DMSO-d$_6$ 300 MHz)

δ (ppm) = 3.73 (s; 3H; CH$_3$), 5.0 (d,1H; J = 10.0 Hz; CH), 5.87 (d; 1H; J = 16 Hz; CH), 6.76 (dd; 1H; J_1 = 10.0 Hz; J_2 = 16.0 Hz; CH), 7.77 (m; 2H; CH$_{ar}$), 8.01 (m; 1H; CH$_{ar}$), 10.40 (s; 1H; NH).

^{13}C NMR (+DEPT, DMSO-d$_6$, 75.46 MHz)

δ (ppm) = 52.6 (CH$_3$), 103.7 (CH$_2$), 112.1 (CH), 123.1 (CH$_{ar}$), 124.4 (C$_{ar}$), 124.7 (CH$_{ar}$), 125.2 (CH$_{ar}$), 133.3 (C$_{ar}$), 145.9 (C$_{ar}$), 154.2 (OC=ONH), 166.3 (C=O), 166.5 (C=O).

5.12 Synthesis of chiral phthalimide-Urea-Conjugates

5.12.1 Synthesis of 1-(2-Benzyl-1,3-dioxoisoindolin-4-yl)-3-((R)-1-phenylethyl)urea
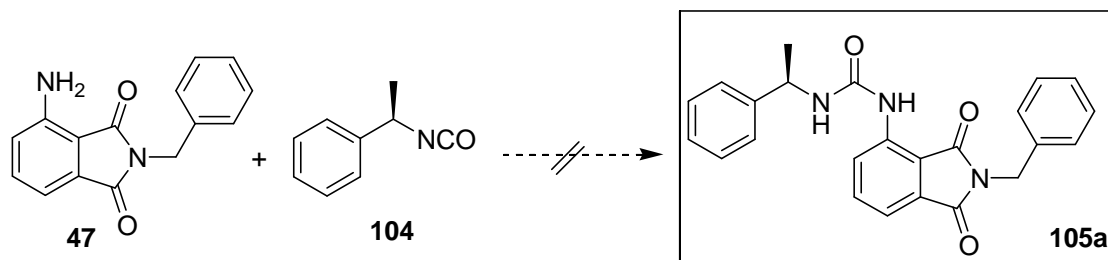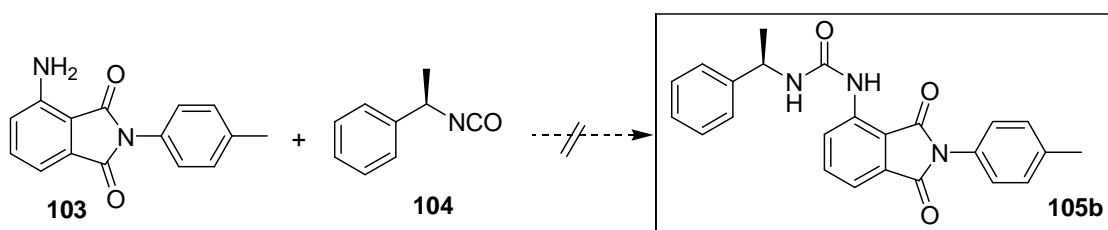

This product was not provided satisfactorily with the method presented in table 34.

Table 34: Reaction conditions for the synthesis of 1-(2-benzyl-1,3-dioxoisoindolin-4-yl)-3-((R)-1-phenylethyl)urea 105a.

	Equiv.	Solvent	Temp. °C	Cat.	time (min)	Work-up
a.	1:1.1	EtOAc	r.t	No cat.	10	After evaporation of the solvent, cyclohexane was added and the product was washed with ether.
b.	1:1	EtOAc	r.t	Et₃N	10	After evaporation of the solvent, cyclohexane was added and the product was washed with ether
c.	1:1.1	EtOAc	r.t	N-MM	30	After evaporation of the solvent, the residue was crystallized from benzene.

5.12.2 Synthesis of 1-(1,3-Dioxo-2-p-tolylisoindolin-4-yl)-3-((R)-1-phenylethyl)urea


This product was not provided satisfactorily with the methods presented in table 35.

Table 35: Reaction conditions for the synthesis of 1-(1,3-dioxo-2-p-tolylisoindolin-4-yl)-3-((R)-1-phenylethyl)urea 105b.

	Eq.	Solvent	Temp. °C	h (hours)	Work-up
a.	1:1	THF	50	1	The mixture was cooled to room temperature, and the solvent was removed in vacuo. [104]
b.	1:1	t-BuOH	80	4	The solvent was evaporated under reduced pressure. The residue was crystallized from benzene.

5.12.3   Synthesis of 1-(2-Benzyl-1,3-dioxoisoindolin-5-yl)-3-((S)-1-phenylethyl)urea
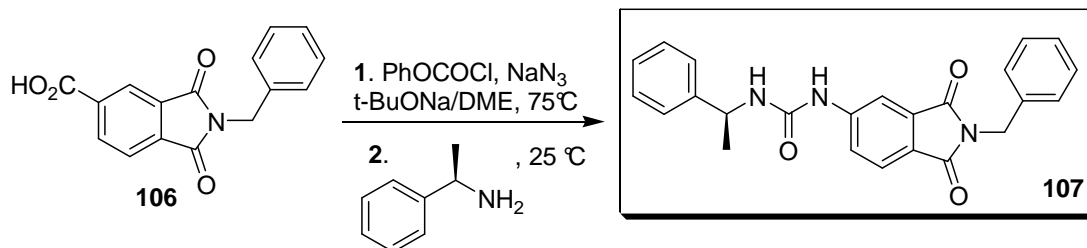
According to **GP5.** *R*-methylbenzylamine (200 μl, 1.50 mmol) was added. The white solid was filtered and washed several times with cold chloroform. The urea-phthalimide (**107**) was purified by column chromatography R*f* : 0.3 (Cyclohexane / EtOAc, 6:4). [71]

Yield: 253 mg, 0.63 mmol, 63%.

^{1}H NMR (600 MHz, DMSO-d_6)

δ (ppm) = 1.42 (d; 3H; J = 7.0 Hz,; CH$_3$), 4.72 (s, 2H, CH$_2$), 4.85 (d; 1H J = 7.0 Hz,; CH), 6.98 (d, 1H; J = 7.7, ,NH), 7.25-7.36 (m, 10H, CH$_{ar}$), 7.58 (dd, 1H; J_1 = 1.7 Hz and J_2 = 8.2 Hz, CH$_{ar}$), 7.73 (d, 1H; J = 8.2 Hz, CH$_{ar}$), 8.06 (s, 1H, CH$_{ar}$), 9.21 (s, 1H, NH).

^{13}C NMR (126 MHz, DMSO-d_6)

δ (ppm) = 22.7 (CH$_3$), 40.6 (CH$_2$), 48.7 (CH), 111.1 (CH$_{ar}$), 121.5 (CH$_{ar}$), 122.8 (C$_{ar}$), 124.4 (CH$_{ar}$), 125.8 (CH$_{ar}$ x 2), 126.7 (CH$_{ar}$), 127.3 (CH$_{ar}$ x 2), 127.3 (CH$_{ar}$), 128.3 (CH$_{ar}$ x 2), 128.5 (CH$_{ar}$ x 2), 133.2 (C$_{ar}$), 136.8 (C$_{ar}$), 144.6 (C$_{ar}$), 146.3 (C$_{ar}$), 153.8 ((NH)$_2$C=O), 167.4 (C=O), 167.6 (C=O).

MS (m/z (%)): 399 (12), 278 (25), 260 (11), 252 (100), 234 (19), 120 (23), 105 (79), 91 (32), 77 (39).
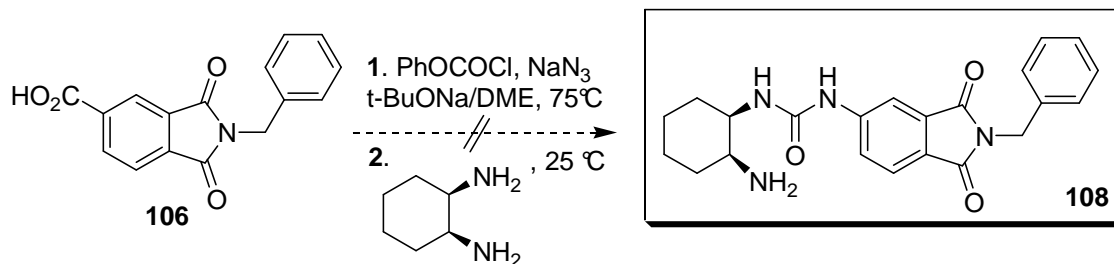
Exact mass (EI):

Calcd. C$_{24}$H$_{21}$N$_3$O$_3$: 399.1583 (M$^+$) g/ mol.
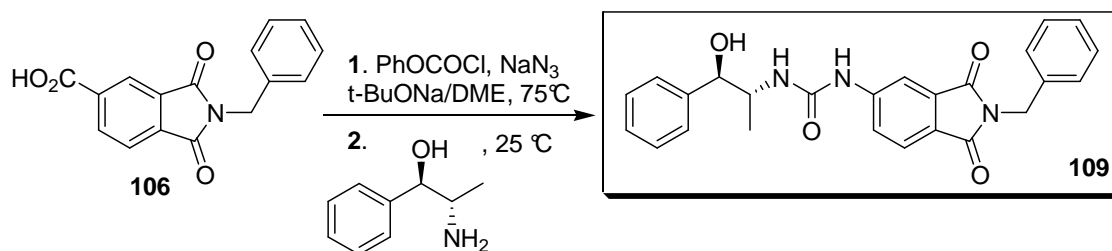
Found 399.159 g/mol.

M.p: 212-213 °C.

5.12.4 Synthesis of 1-((1R,2S)-2-Aminocyclohexyl)-3-(2-benzyl-1,3-dioxoisoindolin-5-yl)urea

This reaction was carried out according to **GP5** but the method did not provide the desired product **108**.

5.12.5 Synthesis of 1-(2-Benzyl-1,3-dioxoisoindolin-5-yl)-3-((1R,2R)-1-hydroxy-1-phenylpropan-2-yl)urea

Acoording to **GP5** (1R,2S)-2-amino-1-phenylpropan-1-ol (226 mg, 1.5 mmol) was added. The product **109** was purified by column chromatography Rf: 0.41 (SiO$_2$, EtOAc / hexane, 7:3) and crystallized from benzene / EtOH, 9:1.

Yield: 278 mg, 0.65 mmol, 65%.

^{1}H NMR (DMSO, 300 MHz)

δ (ppm) = 0.88 (d; 3H; J =6.78 Hz; CH$_3$), 3.89 (m; 1H; CH), 4.73 (s; 3H; CH$_2$ and OH), 5.59 (d; 1H; J = 4.90 Hz; CH), 6.42 (d; 1H; J = 9.42 Hz; NH), 7.21-7.38 (m; 10H; CH$_{ar}$), 7.56 (dd; 1H; J_1 = 1.88 Hz; J_2 = 8.67 Hz; CH$_{ar}$), 7.74 (d; 1H; J = 8.67 Hz; CH$_{ar}$), 8.08 (d; 1H; J =1.50 Hz; CH$_{ar}$), 9.33 (s; 1H; NH).

^{13}C NMR (75 MHz, DMSO-d_6)

δ (ppm) = 14.3 (CH$_3$), 41.2 (CH$_2$), 51,1 (CH), 74.5 (CH), 111.55 (CH$_{ar}$), 121.9 (CH$_{ar}$), 124.9 (C$_{ar}$), 126.4 (CH$_{ar}$), 127.2 (CH$_{ar}$ x 2), 127.8 (CH$_{ar}$ x 3), 128.4 (CH$_{ar}$ x 2), 129.1 (CH$_{ar}$ x 3), 133.8 (C$_{ar}$), 137.34 (C$_{ar}$), 143.6 (C$_{ar}$), 147.0 (C$_{ar}$), 154.4 ((NH)C=O), 167.4 (C=O), 168.2 (C=O).

IR

ν (cm^{-1}) = 3390-3340 (w); 2970 (w) 1700 (s); 1690 (s); 1560 (m).

Exact mass (EI):

Calcd. C$_{25}$H$_{23}$N$_3$O$_4$: 429.16 (M$^+$) g/mol.

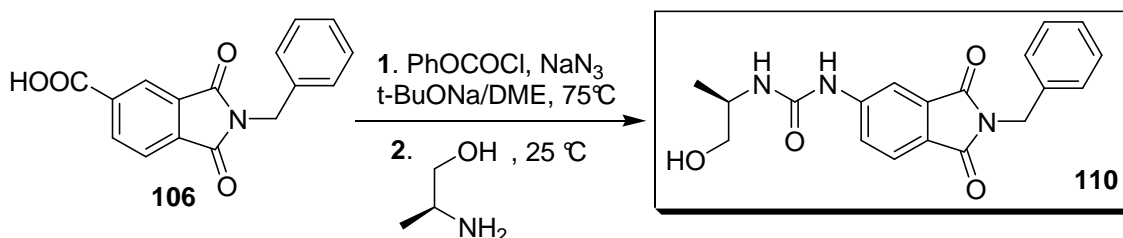**Found** 430,2 g/mol.

Anal:

Calcd: C 69.92   H 5.40   N 9.78.

Found: C 69.72   H 5.38   N 9.80.

M.p: 210-211 °C.

5.12.6 Synthesis of 1-(2-Benzyl-1,3-dioxoisoindolin-5-yl)-3-((*R*)-1-hydroxypropan-2-yl)urea

According to **GP5** (*S*)-2-aminopropan-1-ol (112 mg, 117 µL, 1.5 mmol) was added. The product **110** was crystallized from benzene / EtOH, 9:1. The product **110** was isolated as white powder.

Yield: 212 mg, 0.60 mmol, 60%.

^{1}H NMR (DMSO, 300 MHz)

δ (ppm) = 1.08 (d; 3H; J = 6.99 Hz; CH$_3$), 3.39 (m; 2H; CH$_2$), 3.72 (m; 1H; CH), 4.74 (s; 2H; CH$_2$), 4.84 (m; 1H; OH), 6.28 (d; 1H; J = 8.10 Hz; NH), 7.31 (m; 5H; CH$_{ar}$), 7.56 (dd; 1H; J_1 = 1.27 Hz; J_2 = 8.10 Hz; CH$_{ar}$), 7.73 (d; 1H; J = 8.27 Hz; CH$_{ar}$), 8.07 (s; 1H; CH$_{ar}$), 9.23 (s; 1H; NH).

^{13}C NMR (75 MHz, DMSO-d_6)

δ (ppm) = 18.1 (CH$_3$); 41.2 (CH$_2$); 47.3 (CH); 64.8 (CH$_2$); 111.6 (CH$_{ar}$), 121.8 (CH$_{ar}$); 123.2 (C$_{ar}$); 124.9 (CH$_{ar}$); 127.8 (CH$_{ar}$ x 3); 129.0 (CH$_{ar}$ x 2); 133.8 (C$_{ar}$); 137.3 (C$_{ar}$); 147.0 (C$_{ar}$); 154.6 ((N-H)C=O); 163.7 (2-C=O).

IR

ν (cm^{-1}) = 3390-3340 (w); 2970 (w); 1700 (s); 1690 (s); 1560 (m).

Exact mass (EI):

Calcd. $C_{19}H_{19}N_3O_4$: 353.14 (100%) g/mol.

Found 351.90 [M-H$^+$] g/mol.
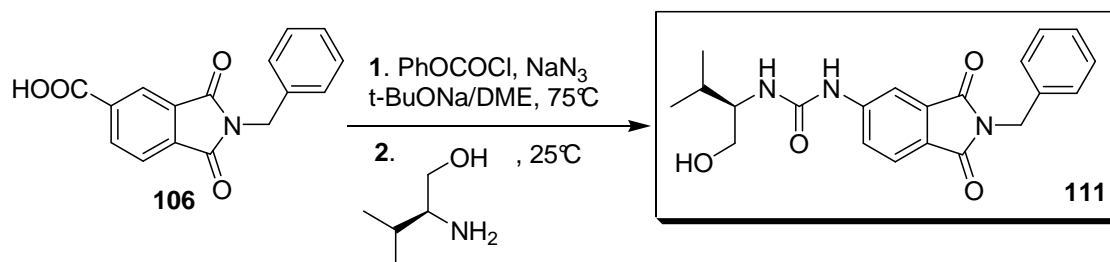
Anal:

Calcd: C 64.58   H 5.42   N 11.89

Found: C 64.47   H 5.59   N 11.78

M.p: 204-205 °C.

5.12.7   Synthesis of 1-(2-Benzyl-1,3-dioxoisoindolin-5-yl)-3-((R)-1-hydroxy-3-methylbutan-2-yl)urea

According to **GP5** (*S*)-2-amino-3-methylbutan-1-ol (154 mg, 166 µl, 1.5 mmol) was added. The product **111** was purified by column chromatography R*f*: 0.28 (SiO$_2$, EtOAc / cyclohexane, 9:1) and crystallized from benzene / EtOH, 9:1. The product **111** was isolated as white powder.

Yield: 259 mg, 0.68 mmol, 68%.

^{1}H NMR (DMSO-d_6, 600 MHz)

δ (ppm) = 0.88 (t; 6H; J_1 =15.60 Hz; J_2 = 7.80 Hz; CH$_3$), 1.86 (m; 1H; CH), 3.39 (m; 1H; CH), 3.50 (m; 2H; CH$_2$), 4.71(s; 3H; CH$_2$ and OH), 6.23 (d; 1H; J = 8.73 Hz; NH), 7.26-7.35 (m; 5H; CH$_{ar}$), 7.56 (dd; 1H; J_1 = 1.87 Hz; J_2 =8.42 Hz; CH$_{ar}$), 7.74 (d; 1H; J = 8.11 Hz; CH$_{ar}$), 8.08 (d; 1H; J =1.50 Hz; CH$_{ar}$), 9.23 (s; 1H; NH).

^{13}C NMR (150 MHz, DMSO-d_6)

δ (ppm) = 18.4 (CH$_3$); 20.2 (CH$_3$); 28.9 (CH); 41.2 (CH$_2$); 56.3 (CH); 61.8 (CH$_2$); 111.5 (CH$_{ar}$); 121.8 (CH$_{ar}$); 123.2 (C$_{ar}$); 124.9 (CH$_{ar}$); 127.8 (CH$_{ar}$ x 3); 129.0 (CH$_{ar}$ x 2); 133.8 (C$_{ar}$); 137.4 (C$_{ar}$); 147.01 (C$_{ar}$); 154.4 ((NH)C=O); 167.9 (C=O); 168.2 (C=O).

IR

ν (cm^{-1}) = 3330 (w); 2980 (w); 1700 (s); 1640 (s); 1560 (m).

Exact mass (EI):

Calcd. $C_{21}H_{23}N_3O_4$: 381.17 (100%) g/mol.

Found 379.90 [M-H] g/mol.
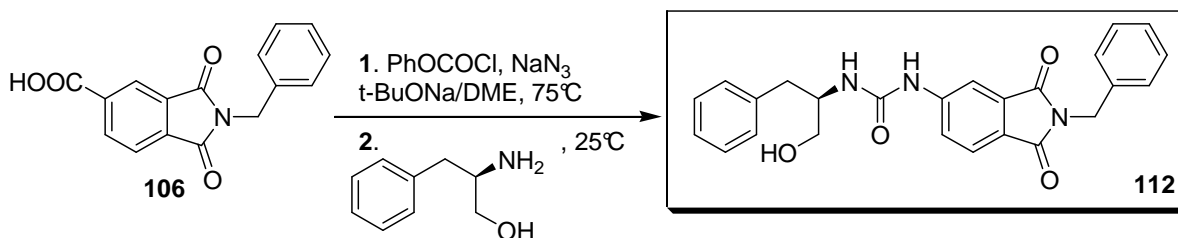
Anal:

Calcd: C 66.13   H 6.08   N 11.02.

Found: C 66.05   H 6.14   N 10.99.

M.p: 203-204 °C.

5.12.8   Synthesis of 1-(2-Benzyl-1,3-dioxoisoindolin-5-yl)-3-((R)-1-hydroxy-3-phenylpropan-2-yl)urea

According to **GP5** (*R*)-2-amino-3-phenylpropan-1-ol (226 mg, 1.5 mmol) was added. The product **112** was purified by column chromatography R*f*: 0.32 (SiO$_2$, EtOAc / cyclohexane, 9:1) and crystallized from benzene / EtOH, 9:1. The product **112** was isolated as white powder.

Yield: 266 mg, 0.62 mmol, 62%.

^{1}H NMR (DMSO-*d$_6$*, 300 MHz)

δ (ppm) = 2.57-2.77 (m; 2H; CH$_2$), 3.39 (m; 2H; CH$_2$), 3.85 (m; 1H; CH), 4.72 (s; 2H; CH$_2$), 4.92 (t; 1H; J_1 = 5.18 Hz; J_2 = 10.20 Hz; OH), 6.35 (d; 1H; J = 8.42 Hz; NH), 7.18-7.36 (m; 10H; CH$_{ar}$), 7.54 (dd; 1H; J_1 = 7.94 Hz; J_2 = 1.62 Hz; J_3 = 1.42 Hz; CH), 7.73 (d; 1H; J = 7.94 Hz; CH), 8.05 (d; 1H; J = 1.78 Hz; CH), 9.25 (s; 1H; NH).

^{13}C NMR (75 MHz, DMSO-*d$_6$*)

δ (ppm) = 37.5 (CH$_2$), 41.2 (CH$_2$), 53.0 (CH), 62.4 (CH$_2$), 111.6 (CH$_{ar}$), 121.9 (CH$_{ar}$), 123.3 (C$_{ar}$) 124.9 (CH$_{ar}$), 127.8 (CH$_{ar}$ x 3), 128.7 (CH$_{ar}$ x 2), 129.0 (CH$_{ar}$ x 3), 129.6 (CH$_{ar}$ x 2), 133.7 (C$_{ar}$), 137.3 (C$_{ar}$), 139.4 (C$_{ar}$), 146.9 (C$_{ar}$), 154.6 ((NH)C=O), 167.9 (C=O), 168.2 (C=O).

IR

ν (cm^{-1}) = 3370-3320 (w); 3000 (w); 1700 (s); 1660 (m); 1560 (s).

Exact mass (EI):

Calcd. $C_{25}H_{23}N_3O_4$: 429.17 (100%) g/mol.

Found 427.90 [M-H$^+$] g/mol.

Anal:

Calcd: C 69.92   H 5.40   N 9.78.

Found: C 69.83   H 5.44   N 9.64.

M.p: 213-214 °C.

5.13 Photophysical properties, anion sensing and chiral recognition by chiral phthalimide-urea-conjugate

Absorption spectroscopy

Absorption spectra were recorded using a Beckman Coulter UV-DU800 spectrometer and a Perkin-Elmer Lambda 35 UV/vis spectrometer. The samples were placed into quartz cells of 1 cm path length. Compound concentrations were adjusted to 10^{-5} M in DMSO or MeCN.

Steady-state fluorescence spectroscopy

Fluorescence and excitation spectra were carried out using a Perkin-Elmer LS-50B luminescence spectrometer. The samples were placed into quartz cells of 1 cm path length. Compound concentrations were adjusted as indicated. The excitation and emission slit widths were 2.5 nm. The fluorescence quantum yields in different solvents were measured with reference to quinine sulfate ($\phi_F = 0.546$ in 0.5 M H_2SO_4) by comparing the area of fluorescence and absorbance at the excitation wavelength of 340 nm, using the formula [101]

$$\phi_{sample} = (a_{sample}/a_{std}) \, (A_{std}/A_{sample}) \, (n_{sample}/n_{std}) \, \phi_{std} \tag{16}$$

where ϕ_{sample} and ϕ_{std}, a_{sample} and a_{std}, n_{sample} and n_{std} and A_{sample} and A_{std} are the quantum yield, area under emission spectra, refractive index and the absorbance of the sample under study (sensor **107, 109-112**) and the standard (quinine sulfate), respectively.

Time-resolved fluorescence spectroscopy

Fluorescence lifetimes were measured using a gated intensified CCD equipped mono-chromator. The spectral resolution has been set to 2 nm. The samples were excited with the third harmonic (355 nm) of a Nd:YAG laser. The overall instrument response function was 1.5 ns. The samples were placed into quartz cells of 1 cm path length. Compound concentrations were adjusted as indicated.

NMR study to confirm the formation of a complex

^{1}H NMR titration experiments were performed in CD_3CN and or DMSO-d_6. In the presence of increasing equivalents of anions, the changing field shift of urea-protons was followed. The concentrations of the solutions of the urea were between 10-15 mM and the equivalents of the anion were between 0.025-2 equiv.

5.14 Fluorescence study of chiral phthalimide-urea-conjugate with different peroxides

For 1-(2-benzyl-1,3-dioxoisoindolin-5-yl)-3-((S)-1-phenylethyl)urea

Fluorescence and excitation spectra were carried out using a Perkin-Elmer LS-50B luminescence spectrometer. The samples were placed into quartz cells of 1 cm path length. Compound concentrations were adjusted to 3.3 µM (10 µL of a 1 mM solution in MeCN) for the phthalimide and for the peroxide at 6.6 µM (20 µL of a 1mM solution in MeCN). The excitation and emission slits were adjusted to 2.5 nm. The experiment was carried out in two parts:

a. The first part was the treatment of the fluorophor with the corresponding peroxide (1µL up to 20µL).

b. The mixture (3.3 µM of fluorophor + 6.6 µM of peroxide) was irradiated in the photoreactor Luzchem LZC-4V (14 lamps, $\lambda = 350 \pm 20$ nm) for about 180 min, and every 30 min a fluorescence spectrum was measured.

Different commercial and non-commercial peroxide compounds were used for these experiments, the peroxide compounds are shown in figure 129.

Miyeon Cho[a][102] and Lars-Oliver Höinck[b][103] synthesized the non-commercial peroxides.
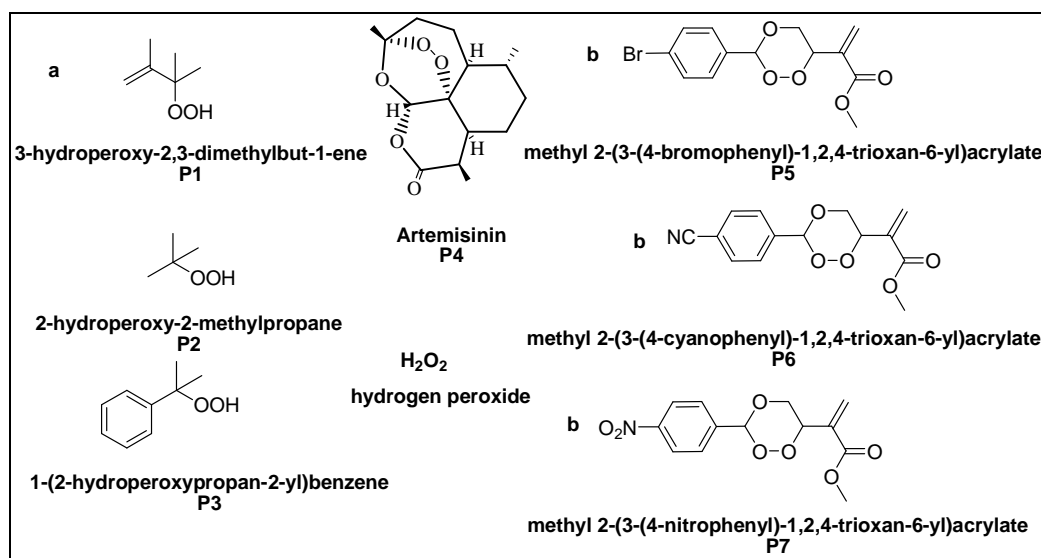

Figure 129: Peroxide molecule used in the fluorescence emission experiments

5.15 Fluorescence study of 107 and 109-112 with hydrogen peroxides

Fluorescence and excitation spectra were measured using a Perkin-Elmer LS-50B luminescence spectrometer. The samples were placed into quartz cells of 1 cm path length. Compound concentrations were adjusted to 3.3 µM (10 µL of a 1 mM solution in MeCN) for the phthalimide. Hydrogen peroxide was used as an 25% aqueous solution. The excitation and emission slit widths were 2.5 nm. The experiment was carried out in two parts:

a. The first part was the treatment of the fluorophor with the hydrogen peroxides (1µL up to 20 µL).

b. The mixture (3.3 µM of fluorophor + 20 µM of peroxide) was irradiated in the photoreactor Luzchem LZC-4V (14 lamps, λ = 350 ± 20 nm) for about 115 min, every 15 min a fluorescence spectrum was measured.

Preparative irradiation of S3 with hydrogen peroxide

In a pyrex ® vessel 199.58 mg (0.5 mmol) of 1-(2-benzyl-1,3-dioxoisoindolin-5-yl)-3-((S)-1-phenylethyl)urea, 5 mL hydrogen peroxide at 25%, and 30 mL MeCN were added. The reaction mixture was irradiated in a Rayonet chamber photoreactors PRR-100 (16 x 3500 Å lamps, ca. 400 W; λ = 350 ± 20 nm) for 90 min under nitrogen. The reaction system was cooled with tap water (15 °C). The organic solvent was evaporated *in vacuo*. The reaction mixture was dissolved in CH$_2$Cl$_2$ and washed with water. The organic layer was dried over MgSO$_4$ and concentrated *in vacuo*. The isolated product was the starting material.

5.16 Synthesis of Chiral Phthalimide-Thiourea-Conjugate

5.16.1 Synthesis of 5-Nitroisoindoline-1,3-dione
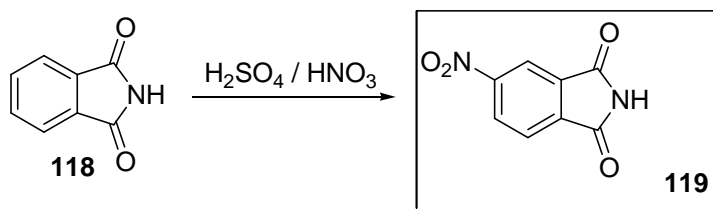
To 62.5 mL of a mixture of concentrated sulfuric acid and 100% nitric acid (4:1 v / v) at 15 °C was added 10 g (68.0 mmol) of phthalimide (**118**) in portions over a 15 min interval with stirring the reaction mixture. The temperature was raised slowly to 35 °C and held for 45 min. The solution turned yellow in color. The product **119** mixture was cooled to 0 °C, slowly stirred

into 250 g of ice at a rate such that the temperature was kept below 15 °C, collected by vacuum filtration and washed with cold water. The product **119** was recrystallized from ethanol to give colorless crystals. [82]

Yield: 7.59 g, 39.5 mmol, 58%

^{1}H NMR (DMSO-d_6, 300 MHz)

δ (ppm) = 8.07 (d; 1H; J = 8.2 Hz; CH $_{ar}$), 8.44 (d; 1H; J = 1.9 Hz; CH$_{ar}$), 8.61 (dd; 1H; J_1 = 8.2 Hz; J_2 = 2.0 Hz; CH$_{ar}$), 11.38 (s; 1H; NH).

5.16.2 Synthesis of 2-Benzyl-5-nitroisoindoline-1,3-dione
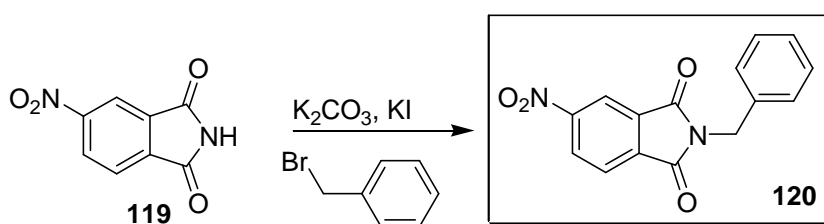
In a 100 mL round flask was placed 2.00 g (10.4 mmol) of 4-nitrophatlamide (**119**), 0.90 g (6.51 mmol) of anhydridus potassium carbonate and 0.20 g potassium iodide. Then 12.4 mL benzylbromide and 20 mL of dried DMF were added. The mixture was heated at 140°C for 1.5 h. The cooled reaction mixture was poured into 150 mL of cold water. After collecting the solid, it was washed successively with 40 mL portions of water, 2% sodium hydroxide solution, and water again. The dried crude product **120** was recrystallized from EtOH and filtered while hot. The solution was concentrated somewhat, and water was added dropwise until the turbidity just disappeared. [83]

Yield: 1.38 g, 4.89 mmol, 47%

^{1}H NMR (CDCl$_3$, 300 MHz)

δ (ppm) = 4.89 (s; 2H; CH$_2$), 7.32 (m; 3H; CH$_{ar}$), 7.44 (m; 2H; CH$_{ar}$), 8.04 (d; 1H; J = 8.1 Hz; CH$_{ar}$), 8.59 (dd; 1H; J_1 = 8.1 Hz; J_2 = 1.8 Hz; CH$_{ar}$), 8.66 (d; 1H; J = 1.7 Hz; CH$_{ar}$).

5.16.3   Synthesis of 5-amino-2-benzylisoindoline-1,3-dione
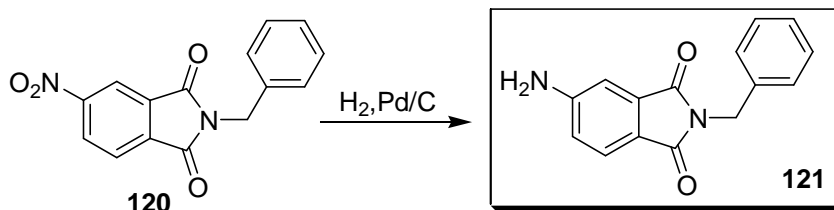
According to **GP2.** 2-Benzyl-5-nitroisoindoline-1,3-dione (**120**) (590 mg, 2.09 mmol) was used for this reaction. [57]
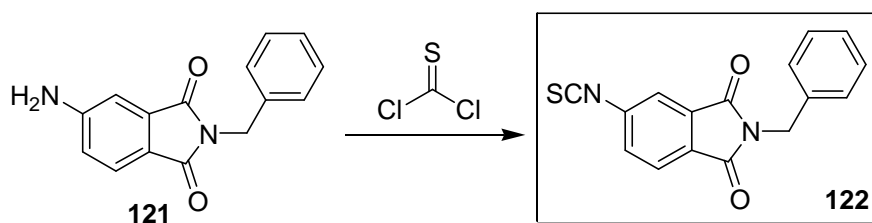
Yield: 1.04 g, 4.12 mmol, 78%

^{1}H NMR (CDCl$_3$, 300 MHz)

δ (ppm) = 4.33 (s; 2H; NH$_2$), 4.81 (s; 2H; CH$_2$), 6.82 (dd; 1H; J_1 = 8.1 Hz; J_2 = 2.1 Hz; CH$_{ar}$), 7.03 (d; 1H; J = 2.0 Hz; CH$_{ar}$), 7.34 (m; 5H; CH$_{ar}$), 7.61 (d; 1H; J = 8.1 Hz; CH$_{ar}$).

^{13}C NMR (CDCl$_3$, 75 MHz)

δ (ppm) = 41.3 (CH$_2$), 108.5 (CH$_{ar}$), 117.8 (CH$_{ar}$), 120.5 (C$_{ar}$), 125.1 (CH$_{ar}$), 127.6 (CH$_{ar}$ x 2), 128.4 (CH$_{ar}$), 128.5 (CH$_{ar}$ x 2), 134.9 (C$_{ar}$), 136.7 (C$_{ar}$), 152.2 (C$_{ar}$), 168.1 (C=O), 168.3 (C=O).

5.16.4   Synthesis of 2-benzyl-5-isothiocyanatoisoindoline-1,3-dione

To a stirred solution of 126 mg (0.50 mmol) 5-amino-2-benzylisoindoline-1,3-dione (**121**) in 2 mL CH$_2$Cl$_2$, 46.0 µL of thiophosgene (69.0 mg, 0.60 mmol) was added in one portion *via* syringe. After 10 min of stirring Et$_3$N (0.15 mL) was added in one portion. The whole mixture was stirred at room temperature for additional 4 h. Next, CH$_2$Cl$_2$ (2 mL) and water (5 mL) were added to the mixture. The layers were separated, the organic layer was washed with 1 N HCl (2 X 5 mL), dried over MgSO$_4$ and evaporated to drynes. The crude product was purified by column cromatography R*f:* 0.90 (SiO$_2$, CH$_2$Cl$_2$). [84]

Yield: 84.0 mg, 0.29 mmol, 57%.

¹H NMR (CDCl₃, 300 MHz)

δ (ppm) = 4.83 (s; 2H; CH₂), 7.34 (m; 5H; CH$_{ar}$), 7.47 (dd; 1H; J_1 = 7.9 Hz; J_2 = 1.8 Hz; CH$_{ar}$), 7.63 (d; 1H; J = 1.7 Hz; CH$_{ar}$), 7.82 (d; 1H; J = 7.9 Hz; CH$_{ar}$).

¹³C NMR (CDCl₃, 75 MHz)

δ (ppm) = 41.9 (CH₂), 120.5 (CH$_{ar}$), 124.7 (CH$_{ar}$), 127.9 (CH$_{ar}$ x 2), 128.6(C$_{ar}$), 128.7 (CH$_{ar}$ x 2), 129.6 (CH$_{ar}$), 130.8 (CH$_{ar}$), 133.9 (C$_{ar}$), 135.9 (C$_{ar}$), 137.4 (C$_{ar}$), 140.2 (S=C=N), 166.5 (C=O), 166.7 (C=O).

5.16.5 Synthesis of 1-(2-benzyl-1,3-dioxoisoindolin-5-yl)-3-((*R*)-1-phenylethyl)thiourea
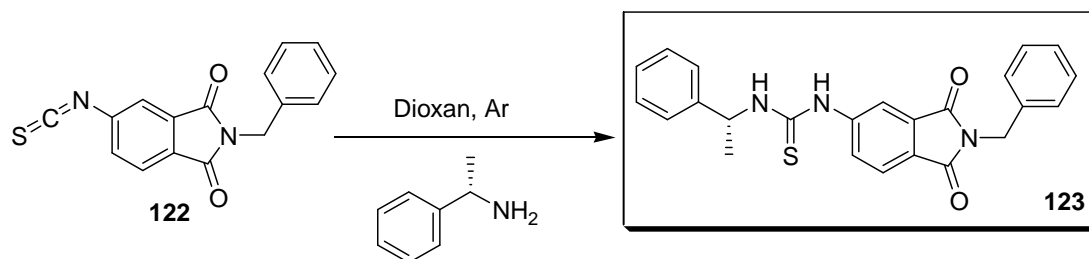
(*S*)-1-phenylethanamine 18.3 µL (17.3 mg, 0.143 mmol) was added into an argon filled reactor containing 42.2 mg of 2-benzyl-5-isothiocyanatoisoindoline-1,3-dione (**122**) (0.143 mmol) in dry dioxane (10 mL). The mixture was heated at 100 °C under stirring for 24 h. The solvent was evaporated. The crude product **123** was purified by column cromatography R*f*: 0.42 (SiO₂, EtOAc / cyclohexane, 2:3). [32]

Yield: 48.1 mg, 0.116 mmol, 81%.

¹H NMR (Aceton-*d₆*, 300 MHz)

δ (ppm) = 1.57 (d; 3H; J = 6.9 Hz, CH₃), 4.80 (s; 2H; CH₂), 5.71 (m; 1H; CH), 7.34 (m; 10H; CH$_{ar}$), 7.75 (d; 1H; J = 8.1 Hz; CH$_{ar}$), 7.89 (dd; 1H; J_1 = 8.1 Hz; J_2 = 1.8 Hz; CH$_{ar}$), 7.95 (d; 1H; J = 7.7, NH), 8.36 (m; 1H; CH$_{ar}$), 9.35 (s; 1H; NH).

¹³C NMR (Aceton-*d₆*, 75 MHz)

δ (ppm) = 22.9 (CH₃), 42.9 (CH₂), 55.0 (CH), 117.9 (CH$_{ar}$), 125.4 (CH$_{ar}$), 128.0 (CH$_{ar}$), 128.2 (CH$_{ar}$), 128.9 (CH$_{ar}$), 129.3 (CH$_{ar}$ x 2), 129.7 (CH$_{ar}$ x 2), 130.3 (CH$_{ar}$ x 2), 130.4 (CH$_{ar}$ x 2), 134.8 (C$_{ar}$ x 2), 139.0 (C$_{ar}$), 145.2 (C$_{ar}$), 147.5 (C$_{ar}$), 168.1 (C=O), 168.2 (C=O), 180.9 (C=S).

IR

ν (cm⁻¹) = 3306(w), 2920 (w), 1769 (m), 1697 (s), 1614 (m), 1530 (s).

Exact mass (EI).

    Calcd. $C_{24}H_{21}N_3O_2S$: 412.14 (100%) g/mol.

    Found 415.00 [M-H$^+$] g/mol.

Anal:

    Calcd: C 69.37   H 5.09   N 10.11

    Found: C 69.39   H 5.13   N 10.06

M.p: 175-176 °C.

5.17 Photophysical Properties, anion sensing and chiral recognition by Chiral Phthalimide-Thiourea-Conjugates

Absorption spectroscopy

Absorption spectra were recorded using a Perkin-Elmer Lambda 35 UV/vis spectrometer. The samples were placed into quartz cells of 1 cm path length. Compound concentrations were adjusted to 10^{-5} M in DMSO or MeCN.

NMR study to confirm the formation of complex

^{1}H NMR titrations experiments were performed in CD$_3$CN and or DMSO-d_6'. The changes of thiourea-protons were followed in the presence of increasing equivalents of anions. The concentrations of the solutions of thiourea were between 10-15 mM and the equivalents for the anion were between 0.025-2.

5.18 Synthesis and Photophysical Properties of Luminol Derivates

5.18.1 Synthesis of Luminol derivates
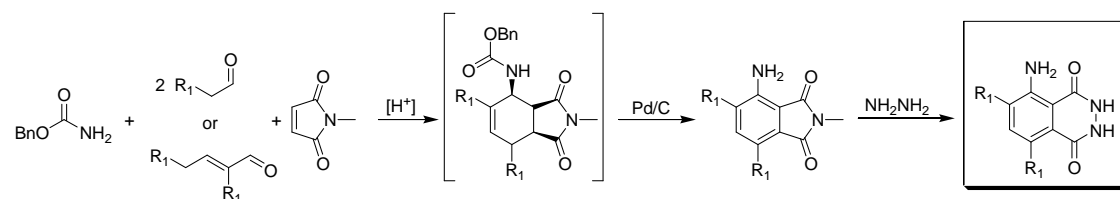
This synthesis was conducted by Robert Fitchler (AK. Jacobi).

Procedure for the synthesis of group a compounds [51]

A mixture of O-benzyl carbamate (9.06 g, 60 mmol), *p*-toluenesulfonic acid monohydrate (0.23 g, 1.2 mmol), aldehyde (60 mmol), acetic anhydride (5.53 mL, 60 mmol), *N*-methylmaleimide 5.55 g (50 mmol), and 50 mL of toluene was confined to a 100 mL flask and fitted with a 3 cm stirbar and a reflux condenser. The reaction mixture was refluxed at 120 °C for 16 h, after which the solvent and other volatic compounds were removed by destillation on a rotary evaporated at 60 °C / 25 mbar. The solid residue was subjected to flash column cromatography (SiO$_2$, EtOAc / heptane) to give the adducts that shown in table 36.

With α, β-unsaturated aldehydes, reactions were run in the presence of 30 mmol aldehyde and no added acetic anhydride.
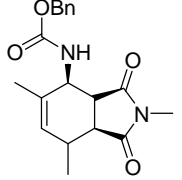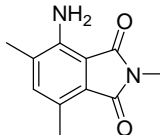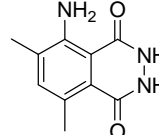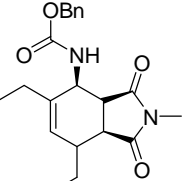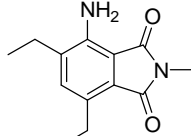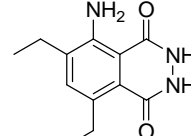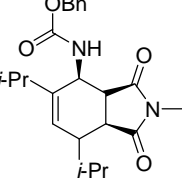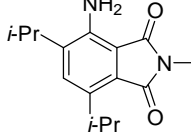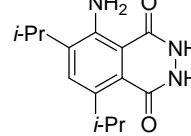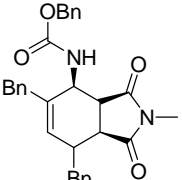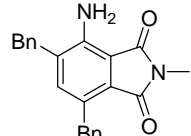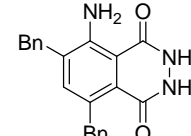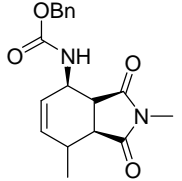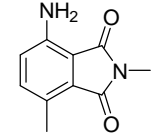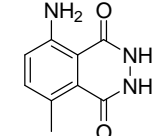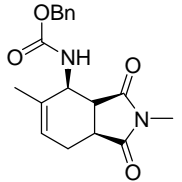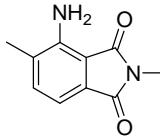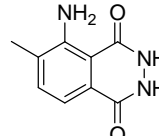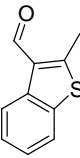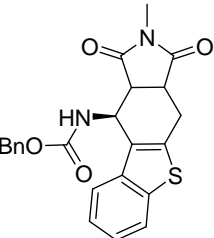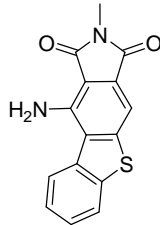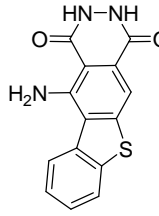
Procedure for the synthesis of group b compounds

A 250 mL flask was equipped with a reflux condenser and charged with the corresponding carbamate (20 mmol), Pd/C (10% Pd, 2.13 g, 2 mmol Pd) and trietyleneglycoldimethylether (80 mL). The reaction was stirred at 140 °C for 18 h. Then, the mixture was cooled, filtered trough a 2 cm celite pad and evaporated by high vacumm distillation (80 °C / 5 mbar). The residue was subjected to flash column cromatography (SiO$_2$, EtOAc / heptane).

Procedure for the synthesis of group c compounds

Phthalimide (10 mmol) and hydrazine hydrate 5 mL (100 mmol) were transferred to a pressure tube. The mixture was heated at 110 °C for 5 h. After cooling to ambient temperature, the volatic compounds were removed by high vacumm distillation and the residue suspended in MeOH (50 mL). The mixture was filtered and the solid product suspended in 1N HCl (50 mL), filtired and washed with water (3 x 10 mL). The resultant white to yellowish solid was dried in high vacuum at room temperature for 12 h.

Table 36 : Products of the one-pot reaction (group a), products of the Pd/C-catalyzed (group b) and luminol derivates (group c)

Entry	Aldehyde	MCR-Adducts Group a	Anilines Group b	Luminol Group c
129				
130				
131				
132				
133				
134				
135				

5.18.2   Photophysical Properties of Luminol Derivates

Absorption spectroscopy

Absorption spectra were recorded using a Beckman Coulter UV-DU800. The samples were placed into a quarts cells of 1 cm path length. Compound concentrations were adjusted to 10^{-4}M in DMSO.

Steady-state Fluorescence

Fluorescence and excitation spectra were carried out using a Perkin- Elmer LS-50B luminescence spectrometer. The samples were placed into a quartz cell of 1 cm path length. Compound concentrations were adjusted to 3.3 x10^{-6} M in DMSO under aerobic conditions. The excitation and emission slit were adjusted to 2.5-2.7 nm.

Absorption spectroscopy and steady-state at different pH (3,7 and 12)

Absorption as well as steady-state fluorescence measurements of luminol derivates were performed in water at different pH (commercial buffer solutions at pH 3,7 and 12).

Time-resolved fluorescence

These measurements were performed on the Department of Physics, University of Cologne with the collaboration of H. Neumann, and M. Beller.

Singlet lifetime experiments were performed after excitation with laser pulses of about 120fs length. The pump laser was an "Integra-C" from Quantronix providing pulses of 2 mJ with 120 fs duration at 796 nm and 500 Hz repetition rate was reduced to 50 Hz with the use of a chopper. The UV pulses were focused with a 10 cm focal lense onto the solution under investigation. The sample was placed slightly before the focous to avoid bubble formation, and the concentration of the probe was adjusted to exhibit complete absorption of the UV pulse and give light emission in a small region behind the quartz window. The emitted light was collected trough a lense and the focused light sent to ensure that not reflected or scattered light from the pump pulse impinged on the detector. The spectral traces of the ultra-fast diode were recorded on a WavePro 960XL oscilloscope from LeCroy (2 GHz bandwidth). Each trace was the average of 1000 single traces.

Luminescence

Luminescence measurements were performed using a computer-controlled fluorimeter Tecan SPECTRFluor Plus for measuring samples in a microplate. A mixture dynamic range was used for luminescence integration time with an optimal amplification value. Samples were

placed in a nunclon 24-well microplate with transparent flat-bottom. Sample concentrations were adjusted to 7.5 µM for the luminol derivates and 8 µM of Fe^{+3} (25mg/mL)/H_2O_2 (5%).

Luminescence measurements were performed using a luminometer "Lumat LB 9507". H_2O_2 (25 µL, 5%) was dispensed to the Luminol derivates (10 µL, 1.5 mM solution in DMSO), cation solutions (Ba^{2+}, Fe^{2+}, Cu^{2+}, Ni^{2+} and Mg^{2+}, 6 µL, 6.18 mM solution in PBS, pH ≈ 12) and 0.98 mL of PBS (pH ≈ 12). The generated chemiluminescence at 25 °C was measured continuously about 250 s.

6 Appendix
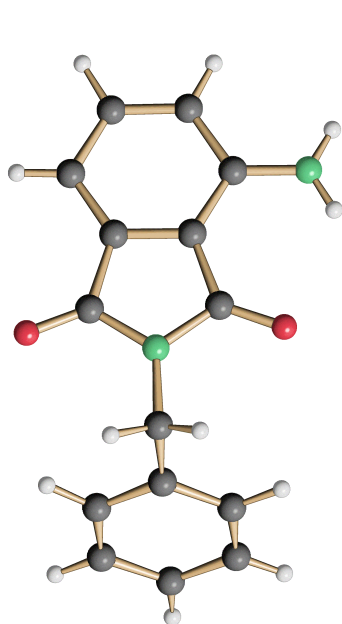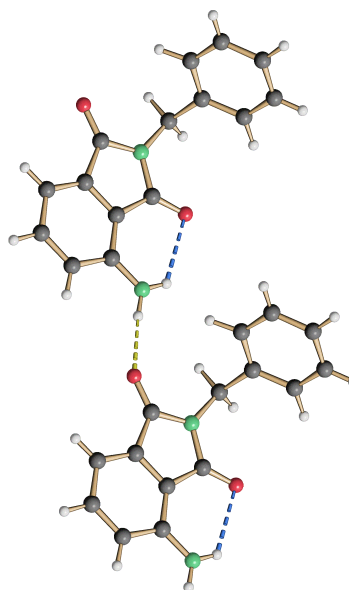
47 (Pydp092a)   **47 (Pydp092b)**

Crystal date	Pydp092
Empirical formula	$C_{15}H_{12}N_2 O_2$
Formula weight	252.27
Temperature (°K)	100(2)
Crystal system	triclinic
Space group	P-1
a [Å]	7.0740(5)
b [Å]	8.6459(8)
c [Å]	10.4195(11)
α [°]	96.067(4)
β [°]	100.715(5)
γ [°]	107.977(5)
Volume A^{-3}	586.45(9)
Z	2
Density [mg/m^3]	1.429
Crystal size [mm]	0.4 x 0.3 x 0.3
Refl. collected/unique	3916 / 2533
Refl. observed [I>2sigma(I)]	1705
R1[a]	0.0444
wR2[a]	0.1304
Largest diff. peak / hole[e/ Å^{-3}]	0.203 / -0.205
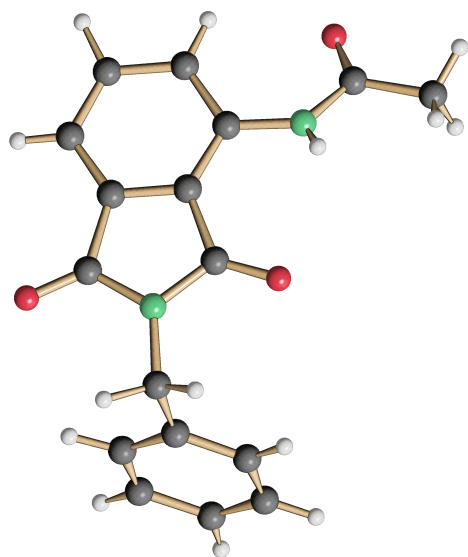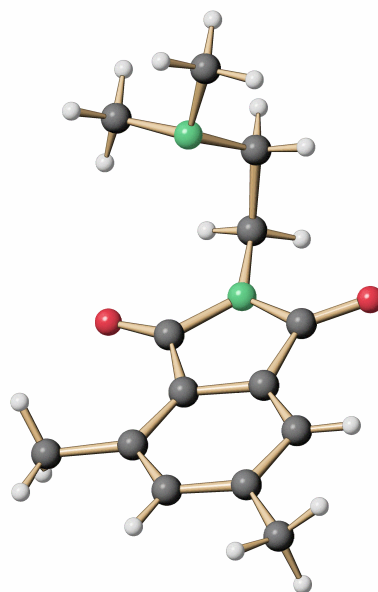
48 (pyd05a)   **75 (pydr160f)**

Crystal date	Pyd05a	Pydr160f
Empirical formula	$C_{17} H_{14} N_2 O_3$	$C_{14}H_{18} N_2 O_2$
Formula weight	294.30	246.30
Temperature (°K)	100(2)	100(2)
Crystal system	Monoclinic	Monoclinic
Space group	P21/n	P21/c
a [Å]	9.7004(15)	10.5840(16)
b[Å]	4.6954(9)	7.3141(8)
c [Å]	30.850(7)	17.059(3)
α [°]	90	90
β [°]	91.211(8)	95.487(5)
γ [°]	90	90
Volume A^{-3}	1404.8(5)	1314.5(3)
Z	4	4
Density [mg/m^3]	1.392	1.245
Crystal size [mm]	0.3 x 0.05 x 0.01	0.3 x 0.2 x 0.02
Refl. collected/unique	2426 / 1774	5781 / 276
Refl. observed [I>2sigma(I)]	854	1766
R1[a]	0.0472	0.0464
wR2[a]	0.0918	0.1154
Largest diff. peak / hole[e/ Å^{-3}]	0.212 / -0.199	0.588 / -0.216
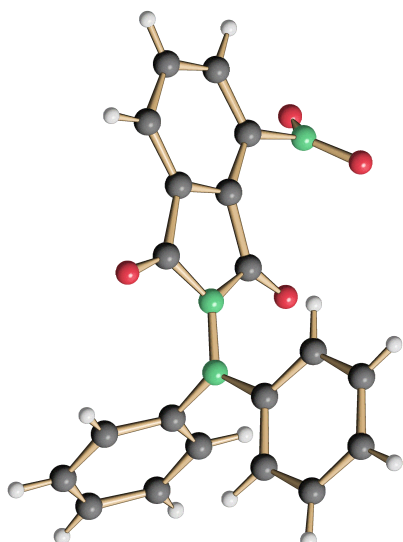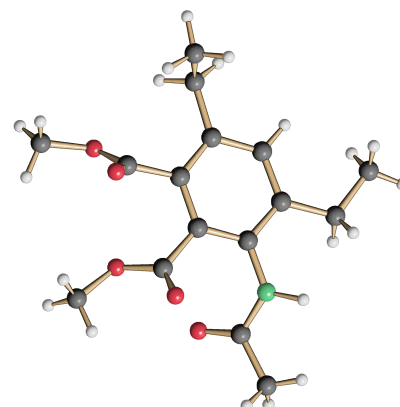
| **52 (Pydr215)** | **84 (Pydr 191)** |

Crystal date	Pydr215	Pydr191
Empirical formula	$C_{20}H_{13}N_3O_4$	$C_{16}H_{21}NO_5$
Formula weight	359.33	2458.70
Temperature (°K)	100(2)	100(2)
Crystal system	Orthorhombic	Monoclinic
Space group	P212121	C2/c
a [Å]	9.0793(5)	24.408(2)
b[Å]	11.2615(5)	0.2876(12)
c [Å]	16.5493(9)	5.4839(10)
α [°]	90	90
β [°]	90	126.543(5)
γ [°]	90	90
Volume A^{-3}	1692.11(15)	3123.7(5)
Z	4	1
Density [mg/m^3]	1.411	1.307
Crystal size [mm]	0.3 x 0.3 x 0.3	0.3 x 0.2 x 0.1
Refl. collected/unique	8253 / 3706	7369 / 3386
Refl. observed [I>2sigma(I)]	2864	1719
R1^a	0.0349	0.0450
wR2^a	0.0653	0.0810
Largest diff. peak / hole[e/ Å^{-3}]	0.146 / -0.198	0.223 / -0.301
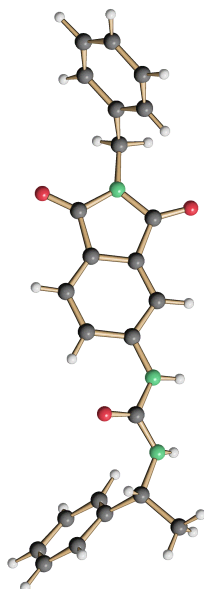
107 (Pydrs001a)

Crystal date	Pydrs001a
Empirical formula	$C_{24}H_{21}N_3O_3$
Formula weight	399.44
Temperature (°K)	100(2)
Crystal system	Triclinic
Space group	P1
a [Å]	4.7444(3)
b[Å]	6.5898(8)
c [Å]	16.224(2)
α [°]	78.946(4)
β [°]	88.347(7)
γ [°]	87.806(6)
Volume A^{-3}	497.34(9)
Z	1
Density [mg/m^3]	1.334
Crystal size [mm]	0.2 x 0.1 x 0.03
Refl. collected/unique	2930 / 2077
Refl. observed [I>2sigma(I)]	1446
R1^a	0.0442
wR2^a	0.0798
Largest diff. peak / hole[e/ Å^{-3}]	0.203 / -0.233

7 Literatur

[1]   A. Gilbert, and J. Baggott, *Essentials of Molecular Photochemistry*, **1991**, 1st edition, Blackwell Scientifics Publications, Oxford.

[2]   D. A. Skoog, and J. J. Leary, *Principles of Instrumental Analysis*, **1992**, 4th edition, Florida, United States.

[3]   http://www.ciba.com/index/ind-index/ind-paints_and_coatings/ind-pai_coa-tec-new/ind-paints_and_coatings_technologies_protection/ind-paints_and_coatings_technologies_protection_light-stabilizers.htm

[4]   N. J. Turro, *Modern Molecular Photochemistry*, **1991,** 1st edition, University Science Books, United States.

[5]   http://www.photobiology.info/Photochem.html

[6]   J.R. Lakowicz, *Principles of Fluorescence Spectroscopy*, **2006**, 3rd edition, Springer Science, New York, United States.

[7]   Sir J.F. W. Herschel, *Phil. Trans Poy Soc*, **1845**, 135, 143-145.

[8]   http://images.absoluteastronomy.com/images/encyclopediaimages/s/st/stokes_shift.png.

[9]   M. Kasha, *Disc. Faraday Soc.*, **1950**, 9, 14-19.

[10]   B. Valeur, *Molecular Fluorescence Principle and Applications,* **2002**, Wiley-VCH, Weinheim, Germany.

[11]   (a)R. Yang, W.-X. Liu, H. Shen, H.-H. Huang, Y.-B. Jiang, *J. Phys. Chem. B* **2008**, 112, 5105.(b) L. Nie, Z. Li, J. Han, X. Zhang, R. Yang, W.-X. Liu, F.-Y. Wu, J.-W. Xie, Y.-F. Zhao, Y.-B. Jiang, *J. Org. Chem.* **2004**, 69, 6449 (c) S. K. Kim, J. Yoon, *Chem. Commun.* **2002**, 770; (d) T. Gunnlaugsson, A. P. Davis, G. M. Hussey, J. Tierney, M. Glynn, *Org. Biomol. Chem.*, **2004**, 2, 1856; (e) T. Gunnlaugsson, A. P. Davis, J. O'Brien, M. Glynn, *Org. Lett.*, **2002**, 4, 2449; (f) T. Gunnlaugsson, A. P. Davis, M. Glynn, *Chem. Commun.*, **2001**, 2556; (g) V. Thiagarajan, P. Ramamurthy, D. Thirumalai, V. T. Ramakrishnan, *Org. Lett.*, **2005**, 7, 657.

[12]   (a) S. Nishizawa, H. Kaneda,, T. Uchida, N. Teramae, *J. Chem. Soc., Perkin Trans. 2.*, *1998*, 2325; (b) S. Nishizawa, Y. Kato, N. Teramae, *J. Am. Chem.* Soc., **1999**, 121, 946.

[13]   (a) A. Kovalchuk, J. L. Bricks, G. Reck, K. Rurack, B. Schulz, A. Szumna, H. Weibhoff, *Chem. Commun.*, **2004**, 1946; (b) F.-Y Wu, Y.-B. Jiang, *Chem. Phys. Lett.*, **2002**, 355, 438.

[14]   (a) X. Zhang, L. Guo, F.-Y Wu, Y.-B. Jiang, *Org. Lett.*, **2003**, 5, 2667; (b) K. Choi, A. D. Hamilton, *Angew. Chem.*, **2001**, 113, 4030; *Angew. Chem. Int. Ed.*, **2001**, 40, 3912.

[15]   I. Stanculescu, C. Mandravel, F. Delattre, D. Landy, P. Woisel, and G. Suspateanu, *J.Photochem. Photobiol. A: Chem.*, **2003**, 161, 79-85.

[16]   T. Gunnlaugsson, A. P. Davis, G. M. Hussey, J. Tierney, and M. Glynn, *Org. Biomol. Chem.*, **2004**, 2, 1856-183.

[17]   G-K. Li, Z-X. Xu, C-F. Chen, and Z-T. Huang, *Chem.Commun.*, **2008**, 1774-1776.

[18]   I. Oueslati, R. A. Sá Ferreira, L. D. Carlos, C. Baleizão, M. N. Berberan-Santos, B. de Castro, J. Vicens, and U. Pischel, *Inog. Chem.*, **2006,** 45, 2652-2660.

[19]   M. G. Choi, D. H. Ryu, H. L. Jeon, S. Cha, J. Cho, H. H. Joo, K.S. Hong, C. Lee, S. Ahn, and S-K. Chang, *Org. Lett.*, **2008**, 10, 17, 3717-3720.

[20]   S. S. Mallajosyula, H. Usha, A. Datta, and S. K. Pati, *J.Chem. Sci.*, **2008**, 120, 627-635.

[21]   R. Duke, and T. Gunnlaugsson, *Tetrahedron Lett.*, **2007**, 48, 8043-8047.

[22]   T-H. Kim, and T. M. Swager, *Angew. Chem. Int. Ed.*, **2003**, 42, 4803-4806.

[23]   D. H. Lee, J. H. Im, J-H. Lee, and J.-I. Hong, , **2002**, 43, 9637-9640.

[24]   J. Biwersi, B. Tulk, and A.S. Verkman, *Anal. Biochem.*, **1994**, 219, 139-143.

[25]   M. Shionoya, H. Futura, V. Lynch, A. Harriman, and J. L. Sessler, *J. Am. Chem. Soc.*, **1992**, 114, 5714-5722.

[26]   M. E. Huston, E. U. Akkaya, and A. W. Czarnik, *J. Am. Chem. Soc.*, **1989**, 111, 8735-8737.

[27]   T. Gunnlaugsson, A. P. Davis, and M. Glynn, *Chem.Commun.*, **2001**, 2556-2557.

[28]   X. Zhang, L. Guo, F-Y. Wu, and Y-B Jiang, *Org. Lett.*, **2003**, 5, 2667-2670.

[29]   G. Xu, and M. A. Tarr, *Chem. Commun.*, **2004**, 1050-1051.

[30]   T. Gunnlaugsson, A. P. Davis, J. E. O´Brien, and M. Glynn, *Org. Biomol. Chem.*, **2005**, 3, 48-56.

[31]   Z.-C. Wen, and Y-B. Jiang, *Tetrahedron*, **2004**, 60, 11109-11115.

[32]   D. E. Goméz, L. Fabbrizzi, M. Licchelli, and E. Monzani. *Org. Biomol Chem.*, **2005**, 3, 1495-1500.

[33]   C-L. Chen, T-P. Lin, Y-S, Chen, and S-S. Sun, *Eur. J. Org. Chem.*, **2007**, 3999-4010.

[34]   X-H. Huang, Y-B. He, Z-H. Chen, C-G. Hu, and G-Y. Qing, *Can. J. Chem.*, **2008**, 86, 170-176.

[35]   C. Hu, A. He, Z. Chen, and X. Huang, *Tetrahedrom: Asymmetry*, **2009**, 20, 104-110.

[36]   G-Y. Qing, F. W, Y-B. He, C-G. Hu, and X. Yang, *Supramol. Chem.*, **2008**, 20, 7, 635-641.

[37]   G-Y. Qing, T. Sun, Z.Chen, X. Yang, X. Wu, and Y. He, *Chirality*, **2009**, 21, 363-373.

[38]   X-H. Huang, Y-B. He, C-G. Hu, and Z-H. Chen, *J.Fluoresc.*, **2009**, 19, 97-104.

[39]   S. Liu, J. P. C. Pestano, and C. Wolf, *J. Org. Chem.*, **2008**, 73, 4267-4270.

[40]   L. Salem, X. Chapuisat, G. Segal, P. C. Hiberty, C. Minot, C. Leforestier, and P. Sautet, *J. Am. Chem. Soc.*,**1987**, 109, 2887.

[41]   L. Chi, J. Zhao, and T. D. James, *J.Org.Chem.*, **2008**, 73, 4684-4687.

[42]   A. E. Albers, V. s. Okreglak, and C. J. Chang, *J. Am.Chem. Soc.*, **2006**, 128, 9640-9641.

[43]   A. Mills, C. Tommons, R. T. Bailey. M. C. Tedford, and P. J. Crilly, *Analyst*, **2007**, 132, 566-571.

[44]   http://en.wikipedia.org/wiki/Hydrogen_peroxide

[45]   J. C. Sanchez, and W. C. Trogler, *J. Mater. Chem.*, **2008**, 18, 5134-5141.

[46]   G. J. Mohr, *Anal. Bioanal. Chem.*, **2006**, 386, 1201-1214.

[47]   M. Oelgemöller, A. G. Griesbeck, *J. Photochem. Photobiol. C.*, **2002**, 3, 109-127.

[48]   M. Sarkar, R. Yellampalli, B. Bhattacharya, R. K. Kanaparthi, and A. Samanta, *J. Chem. Sci.*, **2007**, 119, 2, 91-97.

[49]   S. Hübner, D. Michalik, H. Jiao, H. Neumann, S. Klaus, D. Strübing, A. Spannenberg, and M. Beller, *J Chem. Asian.*, **2007**, 2, 734-746.

[50]   A. Jacobi von Wangelin, Dissertation, Universität Rostock, 2002.

[51] H. Neumann, S. Klaus, M. Klawonn, D. Strübing, S. Hübner, D. Gördes, A.Jacobi von Wangelin, M. Lalk, and M. Beller, *Z. Naturforsch.*, **2004**, 59b, 431-438.

[52] R. B. Brundrett, and E. H. White, *J. Am. Chem. Soc.*, **1974**, 96:24, 7497-7502.

[53] A. Rose, and T. David Waite, *Anal. Chem.*, **2001**, 73, 5909-5920.

[54] T. Uzu, and S. Sasaki, *Org. Lett.*, **2007**, 9, 21, 4383-4386.

[55] W. R. Seitz, and D. M. Hercules, *Anal. Chem.*, **1972**, 44, 13, 2173-2149.

[56] A. Chihab-Eddine, A. Dafch, A. Jilate, and B. Decroix, *J. Heterocyclic Chem.* **2000**, 37,1543-1548.

[57] X. Collin, J-M. Robert, G. Wielgosz, G. Le Baut, C. Bobin-Dubigeon, N. Grimaud, and J-Y. Petit, *Eur. J. Med. Chem.*, **2001**, 36, 639.

[58] B. A. Pyrror, P. M. Palmer, P. M. Andrews, M. B. Berger, T. Troxler, and M. R. Topp, *Chem. Phys. Lett.*, **1997**, 271, 19-26.

[59] G-N. Ma, Y-P. Zhang, and M. Shi, *Synthesis*, **2007**, 2, 197-208.

[60] H. Suga, T. Kitamura, A. Kakehi and T. Baba, *Chem. Commun.*, **2004**, 1414-1415.

[61] C-J. Wang, and M. Shi, *J.Org. Chem.*, **2003**, 68, 6229-6237.

[62] Y-W. Wang, Y-T. Shi, Y. Peng, A-J. Zhang, T-H. Ma, W. Dou, and J-R. Zheng, *Spectrochim. Acta, A.*, **2009**, 72, 322-326.

[63] J. Wang, H. Li, X. Yu, L. Zu, and W. Wang, *Org.Lett*, **2005**, 7, 19, 4293-4296.

[64] Acetanilides are structural relatives to the powerful pharmaceutical Paracetamol [®] and Phenacetin [®].

[65] B. Joseph, H. Da Costa, J-Y. Mérour, and S. Léonce, *Tetrahedrom,* **2000**, 56, 3189-3196.

[66] A. Soldevilla, A.G. Griesbeck, *J. Am. Chem. Soc*, **2006**, 128, 16472-16473.

[67] K.-D, Warzecha, H. Görner, A. G. Griesbeck, *J. Phys. Chem. A*, **2006**, 110, 3356-3363.

[68] J. A. Blake, E. Gagnon, M. Lukeman and J. C. Scaiano, *Org. Lett.,* **2006**, 8, 1057

[69] H. Lebel, and O. Leogane, *Org. Letter*, **2006**, 8, 25, 5717-5720.

[70] H. G. Benesi, J. H. Hildebrand, *J. Am. Chem. Soc.*, **1949**, 71, 2703.

[71] R. Pérez-Ruiz, Y. Diaz, B. Goldfuss, D. Hertel, K. Meerholz, and A. Griesbeck, *Org. Biomol. Chem.,* **2009**, *7*, 3499-3504.

[72] (a) A. D. Becke, *J. Chem. Phys.*, **1993**, 98, 5648. Implementation: (b) P. J. Stephens, F. J. Devlin, C. F. Chabalowski, M. J. Frisch: *J. Phys. Chem.*, **1994**, 98, 11623. (c) C. Lee, W. Yang, R. G. Parr, *Phys. Rev. B.*, **1988**, 37, 785. (d) B. Miehlich, A. Savin, H. Stoll, H. Preuss, *Chem. Phys. Lett.*, **1989**, 157, 200.

[73] (a) V. Barone, M. Cossi, *J. Phys. Chem. A.*, **1998**, 102, 1995. (b) M. Cossi, N. Rega, G. Scalmani, V. Barone, *J. Comp. Chem.*, **2003**, 6, 669.

[74] K. Wolinski, J. F. Hilton, and P. Pulay, *J. Am. Chem. Soc.*, **1990**, 112, 8251.

[75] M. Sarkar, R. Yellampalli, B. Bhattacharya, R. K. Kanaparthi, and A. Samanta, *J. Chem. Sci.*, **2007**, 119, 91.

[76] S. J. Brooks, L. S. Evans, P. A. Gale, M. B. Hursthouse, and M. E. Light, *Chem. Commun.*, **2005**, 734.

[77] (a) J. M.Lehn., *Supramolecular Chemistry. In Concepts and Perspective*; VCH, Weinheim, **1995**. (b) X.X. Zhang, J. S. Bradshaw, R.M. Izatt, *Chem. Rev.,* **1997**, 97, 3313-3362. (c) M.G. Finn, *Chirality*, **2002**, 14, 534-540.

[78] A. L. Erwin, and E. C. Gostschlich, *J. Bacteriol.*, **1993**, 175, 6382-6391.

[79] L. Chan, J. Slater, J. Hasbargen, D. H. Herndon, R. L. Veech, and S. Wolf, *Integr Psych Behav.*, **1994**, 29, 383-394.

[80] J. Ballesta-Claver, M.C. Valencia-Mirón, and L.F. Capitán-Callvey, *Anal. Chim. Acta*, **2008**, 629, 136-144.

[81] A. G. Griesbeck, N. Hoffmann, and K-D. Warzecha, *Acc. Chem. Res.*, **2007**, 40, 128-140.

[82] J. G. Young, and W. Onyebuagu, *J. Org. Chem.*, **1990**, 55, 7, 2155-2159.

[83] J. H. Billman, and R. Vicent Cash, *J. Am. Chem. Soc.*, **1953**, 75, 10, 2499.

[84] J. Gawronski, M. Kwit, and P. Skowronek, *Org. Biomol. Chem.*, **2009**, 7, 1570.

[85] S. Mitra, R. Das, and S. Mukherjee, *J. Photochem. Photobiol A: Chem.*, **1995**, 87, 225-230.

[86] M. Voicescu, M. Vasilescu, T. Constantinescu, and A. Meghea, *J. Luminesc.*, **2003**, 13, 315-322.

[87] Y. Zhao, F. G. Bordwell, J-P. Cheng, and D. Wang, *J. Am. Chem. Soc.*, **1997**, 119, 9125–9129.

[88] T. S. Dobrolyubskaya, and L. I. Anikina, *J. Appl. Spectrosc.*, **1971**, 14, 402–404.

[89] P. B. Shevlin, and H. A. Neufeld, *J. Org. Chem.*, **1970**, 35, 2178.

[90] (a) R. B. Brundrett, and E. H. White, *J. Am. Chem. Soc.*, **1974**, 96, 7497. (b) R. B. Brundrett, D. F. Roswell, and E. H. White, *J. Am. Chem. Soc.*, **1972**, 94, 7536.

[91] Gaussian 03, Revision C.02, M. J. Frisch, G. W. Trucks, H. B. Schlegel, G. E. Scuseria, M. A. Robb, J. R. Cheeseman, J. A. Montgomery, Jr., T. Vreven, K. N. Kudin, J. C. Burant, J. M. Millam, S. S. Iyengar, J. Tomasi, V. Barone, B. Mennucci, M. Cossi, G. Scalmani, N. Rega, G. A. Petersson, H. Nakatsuji, M. Hada, M. Ehara, K. Toyota, R. Fukuda, J. Hasegawa, M. Ishida, T. Nakajima, Y. Honda, O Kitao, H. Nakai, M. Klene, X. Li, J. E. Knox, H. P. Hratchian, J. B. Cross, C. Adamo, J. Jaramillo, R. Gomperts, R. E. Stratmann, O. Yazyev, A. J. Austin, R. Cammi, C. Pomelli, J. W. Ochterski, P. Y. Ayala, K. Morokuma, G. A. Voth, P. Salvador, J. J. Dannenberg, V. G. Zakrzewski, S. Dapprich, A. D. Daniels, M. C. Strain, O. Farkas, D. K. Malick, A. D. Rabuck, K. Raghavachari, J. B. Foresman, J. V. Ortiz, Q. Cui, A. G. Baboul, S. Clifford, J. Cioslowski, B. B. Stefanov, G. Liu, A. Liashenko, P. Piskorz, I. Komaromi, R. L. Martin, D. J. Fox, T. Keith, M. A. Al-Laham, C. Y. Peng, A. Nanayakkara, M. Challacombe, P. M. W. Gill, B. Johnson, W. Chen, M. W. Wong, C. Gonzalez, and J. A. Pople, Gaussian, Inc., Wallingford CT, **2004**.

[92] J. Wang, H. Li, X. Yu, L. Zu, and W. Wang, *Adv. Synth. Catal.*, **2007**, 349, 11-12, 1182-1886.

[93] J. Kehler, and E. Breuer, *Synthesis.*, **1998**, 1419-1420.

[94] A. Mayr, M. Srisailas, Q. Zhao, Y. Gao, H. Hsieh, M. Hoshmand-Kochi, and N. St. Fleur, *Tetrahedrom*, **2007**, 63, 8206-8217.

[95] D. Shabashov, and O. Daugulis, *J. Org. Chem.*, **2007**, 72, 7720-7725.

[96] J. Gawroński, K. Gawroński, and K. Brzostowaska, *Tetrahedrom Lett.*, **1999**, 40, 1191.

[97] J. R. Casimir, G. Guichard, and J. -P. Briand, *J. Org. Chem.*, **2002**, 67, 3764.

[98] S-J. Wen, and Z-J. Yao, *Org. Lett.*, **2004**, 6, 16, 2721-2724.

[99] H. Ulrich, and R. Richter, *J. Org. Chem.*, **1973**, 38, 2557.

[100]   G. Wittmann, H.van Langenhove, and J.Dewulf, *J.Chromatogr. A*; **2000**, 874, 225.

[101]   S. Aich, C. Raha, and S. Basu, *J. Chem. Soc., Faraday trans*., **1997**, 93, 2991.

[102]   M. Cho, Dissertation, Universität zu Köln, 2009.

[103]   O. Höinck, Dissertation, Universität zu Köln, 2008.

[104]   P. R. Kym, A.J. Souers, T.J. Campbell, J. K. Lynch, A. S. Judd, R. Iyengar, A. Vasudevan, J. Gao, J C. Freeman, D. Wodka, M. Mulhem, G. Zhao, S. H. Wagaw, J. J. Napier, S. Brodjian, B. D. Dayton, R. M, Reilly, J. A. Segreti, R. M. Fryer, L. C. Preusser, G. A. Reinhart, L. Hernandez, K. C. Marsh, H. L. Sham, C. A. Collins, and J. S. Polakowski, *J.Med.Chem*, **2006**, 49, 2339-2352.

[105]   J. Jones, *The Chemical Synthesis of Peptides*, **1994**, International series of monographs on chemistry 23, Oxford-United States.

Erklärung

Ich versichere, dass ich die von mir vorgelegte Dissertation selbständig angefertigt, die benutzten Quellen und Hilfsmittel vollständig angegeben und die Stellen der Arbeit - einschließlich Tabellen, Karten und Abbildungen -, die anderen Werken im Wortlaut oder dem Sinn nach entnommen sind, in jedem Einzelfall als Entlehnung kenntlich gemacht habe; dass diese Dissertation noch keiner anderen Fakultät oder Universität zur Prüfung vorgelegen hat; dass sie - abgesehen von unten angegebenen Teilpublikationen - noch nicht veröffentlicht worden ist sowie, dass ich eine solche Veröffentlichung vor Abschluss des Promotionsverfahrens nicht vornehmen werde. Die Bestimmungen dieser Promotionsordnung sind mir bekannt.

Die von mir vorgelegte Dissertation ist von Prof. Dr. Axel. G. Griesbeck betreut worden.

…………………………………

Yrene Díaz Pérez

07. Dezember 2009.

List of Publications and Presentations

"Fluoride recognition by a chiral urea receptor linked to a phthalimide chromophore", Raúl Pérez-Ruiz, Yrene Díaz, Bernd Goldfuss, Dirk Hertel, Klaus Meerholz, and Axel G. Griesbeck, *Org. Biomol. Chem.***2009**, 7, 3499-3504.

"Synthesis of New Phthalimides as Fluorescent Sensors and Switches", Y. Díaz, A.G. Griesbeck and A.Soldevilla. *XXIII International Conference on Photochemstry*, **29 July-3 August 2007**, Cologne, Germany. *Poster*

"Synthesis of New Phthalimides as Fluorescent Sensors and Decarboxylative Photorelease coupled with Fluorescent Reporter Function based on the Aminophthalimide-Serine System", Y. Díaz, A.Soldevilla and A.G. Griesbeck. *Central European Conference on Photochemistry*, **10-14 February, 2008**, Bad Hofgastein, Austria. *Poster*

"Novel urea-activated phthalimide chemosensor: selective sensing fluoride", Yrene Díaz, Raúl Pérez-Ruiz, and Axel G. Griesbeck. *21. Lecture Conference*, **6-8 October**, **2008**, Bielefeld, Germany. *Poster and oral communication*

Lebenslauf

Persönliche Daten

Name:	Yrene Hortencia Díaz Pérez
Anschrift:	Melatengürtel 101
	50825 Köln
Tel.:	0177 / 2198763
E-Mail:	idiazper@uni-koeln.de
geboren:	18.09.1982 in Caracas
Familienstand	verheiratet

Schulbindung

1988 – 1994	Grundschule in Caracas
1994 – 1997	Gymnasium San Marco Evangelista, Caracas
1997 – 1999	Abschluss: Abitur am Gymnasium Esteban Gil Borges, Caracas

Hochschulausbildung

Okt. 1999 – Jul. 2004	Studium im Studiengang Chemie, Diplom an der Universidad Central de Venezuela
Jul. 2004 – Mai. 2005	Diplomarbeit im Bereich organische Chemie „Estudio de metabolitos secundarios de *Phyllanthus tenellus Roxb*.(Euphorbiaceae) y su actividad biológica"
Sep. 2005 – Mai. 2006	Magister Studium an der I.V.I.C (Instituto Venezolano de Investigaciones Cientificas).
Okt. 2006 Feb. 2010	Beginn Promotionsstudium an der Universität zu Köln Institut für Organische Chemie; im Arbeitskreis von Prof. Dr. A. G. Griesbeck , gefördert durch ein Doktoranden Stipendium des Deutscher Akademischer Austauschdiensts (DAAD)

Köln, den 07. Dezember 2009

Yrene Hortencia Díaz Pérez